Synthesis and Investigation on Water Soluble Mono(aquated) and Bis(aquated) Gd(III) and Mn(II) Complexes as Potential MRI Contrast Agents

A Dissertation Submitted in Partial Fulfilment of the Requirement for the Degree of Doctor of Philosophy at IIT Guwahati

by

Bedika Phukan

Roll No. 126122013

Department of Chemistry

Indian Institute of Technology Guwahati

Guwahati–781039, Assam

India

June 2017

To my loving family

Progress is made by trial and failure; the failures are generally a hundred times more numerous than the successes; yet they are usually left unchronicled

– William Ramsay

Indian Institute of Technology Guwahati

Department of Chemistry

Declaration

I do hereby declare that the research work embodied in this thesis entitled "***Synthesis and Investigation on Water Soluble Mono(aquated) and Bis(aquated) Gd(III) and Mn(II) Complexes as Potential MRI Contrast Agents***" has been carried out by me under the supervision of **Dr. Chandan Mukherjee**, Department of Chemistry, Indian Institute of Technology Guwahati, Assam–781039, India. The research works have been carried out in the period of August, 2012 to June, 2017.

In keeping with the general practice of reporting scientific observations, due acknowledgements have been made wherever the work described is based on the findings of other investigators.

IIT Guwahati — Bedika Phukan

June, 2017 — Roll No. 126122013

Dr. Chandan Mukherjee
Associate Professor
Department of Chemistry
Indian Institute of Technology Guwahati
Guwahati, 781039, Assam, India

Phone no. +91-361-258-2327(O)
Fax no. +91-361-258-2349
Email: cmukherjee@iitg.ernet.in

CERTIFICATE

This is to certify that the research work presented in this thesis entitled "***Synthesis and Investigation on Water Soluble Mono(aquated) and Bis(aquated) Gd(III) and Mn(II) Complexes as Potential MRI Contrast Agents***" is an authentic record of the results obtained from the research work carried out by **Mrs Bedika Phukan** (**Roll No. 126122013**) under my supervision in Department of Chemistry, Indian Institute of technology Guwahati, India. This work is original and has not been submitted elsewhere for a degree or award.

Place: IIT Guwahati
Date: 16/06/2017

Dr. Chandan Mukherjee
(Thesis Supervisor)

Acknowledgement

This thesis owes its existence to the help, support and inspiration of several people. I would like to thank all the people who contributed in some way to the work described in this thesis.

- First and foremost, I would like to express my sincere gratitude and appreciation to my supervisor **Dr. Chandan Mukherjee**, for his constant guidance during my research work. As a supervisor, he constantly forced me to remain focused on achieving my goal. I appreciate all his contributions of time, ideas, and funding to make my Ph.D. experience productive and stimulating.
- I am highly indebted to "**Indian Institute of Technology Guwahati**" for the doctoral fellowship.
- I would like to express my sincere thanks to **Dr. Ankona Datta** (TIFR, Mumbai) for generously sharing her time and knowledge in the field of MRI contrast agents. I am highly thankful to her for giving me the opportunity to work in her laboratory and providing excellent research facilities.
- I am highly obliged to **Prof. Anant B. Patel** (CCMB, Hyderabad) for allowing me to measure the relaxivity values at higher fields.
- I would like to thank my doctoral committee members **Prof. A. K. Saikia** (IIT Guwahati), **Prof. S. S. Ghosh** (IIT Guwahati), and **Dr. Sumana Dutta** (IIT Guwahati) for their valuable suggestions and showing interest in my work.
- I would like to acknowledge SAIF (IIT Bombay), CIF (IIT Guwahati), and Department of Chemistry (IIT Guwahati) for the instrument facilities.
- Thanks to **Dr. Baijayanta Saharia** (Director, Department of Radiology and Imaging, GNRC, North Guwahati) and the entire team of that department for MRI image measurement at 1.5 T.
- Thanks to the members of **Datta Group** (TIFR, Mumbai): **Samsuzzoha**, **Anindita**, **Ananya**, **Subha**, **Sayani**, and **Shafali**, for providing a friendly and cooperative atmosphere at work and helping me all the way.
- Thanks to **Dr. Babulal Das**, **Mr. Imdadul Islam**, and **Mr. Kh. Kesho Singh** for their help at instrumental laboratory during the research work.

- I express my sincere thanks to my lab mates (**Dr. Samir Ghorai**, **Dr. Manas Kumar Mondal**, **Richa Rakshit**, **Mahmuda Khannam**, **Ganesh Chandra Paul**, **Prasenjit Sarkar**, **Ujjal Ghosh**) and some of my friends (**Nirmali**, **Dhriti**, **Ravindra**, **Hemanta**, **Sujit**, **Gaurangi**, **Upashi**, **Murchana**, **Priyakhee**, **Protiti**, **Shikha**, **Gargi**, **Karuna**, and **Nibedita**) for their well wishes, encouragement, and constant support during the research period at IIT Guwahati.
- I would also like to say a heartfelt thank to my **parents** and my **brother** for always believing in me and encouraging me to follow my dreams. And finally to **Jitul**, who has been by my side throughout this journey, and without his patience and sacrifice, I could not have completed this thesis.

Bedika Phukan

Thesis Title:

"***Synthesis and Investigation on Water Soluble Mono(aquated) and Bis(aquated) Gd(III) and Mn(II) Complexes as Potential MRI Contrast Agents"***

Date of Submission of Thesis:

16–06–2017

List of Publications:

1. A Water–Soluble and Water–Coordinated Mn(II) Complex: Synthesis, Characterization and Phantom MRI Image Study, **Bedika Phukan**, A. B. Patel, and Chandan Mukherjee, *Dalton Trans.*, 2015, **44**, 12990.
2. Salen ligand complexes as electrocatalysts for direct electrochemical reduction of gaseous carbon dioxide to value added products, Surya Singh, **Bedika Phukan**, Chandan Mukherjee and Anil Verma, *RSC Adv.*, 2015, **5**, 3581.
3. Interactions of Alkali and Alkaline-Earth Metals in Water-Soluble Heterometallic FeIII/M (M = Na^{+}, K^{+}, Ca^{2+})-Type Coordination Complex, **Bedika Phukan**, Samir Ghorai, Kashmiri Deka, Pritam Deb, and Chandan Mukherjee, *Cryst. Growth Des.* 2018, **18**, 531.
4. A new heptadentate picolinate-based ligand and its corresponding Gd(III) complex: the effect of pendant picolinate versus acetate on complex properties, **Bedika Phukan**, Raunak Varshney, and Chandan Mukherjee, *Dalton Trans.*, 2018, **47**, 135.
5. A New Bis(aquated) High Relaxivity Mn(II) Complex as an Alternative to Gd(III)-Based MRI Contrast Agent, **Bedika Phukan**, Chandan Mukherjee*, Upashi Goswami, Amrit Sarmah, Subhajit Mukherjee, Suban K. Sahoo, and Sankar Ch. Moi, *Inorg. Chem.*, DOI: 10.1021/acs.inorgchem.7b03039.
6. A Bishydrated, Eight–Coordinate Gd(III) Complex with Very Fast Water Exchange: Synthesis, Characterization, and Phantom MR Imaging, **Bedika Phukan**, Patrick K.

Malikidogo, Célia S. Bonnet, Éva Tóth, Samsuzzoha Mondal, and Chandan Mukherjee, *Manuscript Submitted.*

List of Conferences/Symposiums

1. ChemConvene 2015, Department of Chemistry, Indian Institute of Technology Guwahati (poster presentation).
2. 18th CRSI National Symposium in Chemistry, 2016, Institute of Nano Science and Technology and Punjab University (poster presentation).
3. Frontiers in Chemical Sciences (FICS), 2016, Department of Chemistry, Indian Institute of Technology Guwahati (poster presentation).
4. ACS on Campus, One Day Symposium, 2017, Indian Institute of Technology Guwahati (oral presentation).
5. 19th CRSI–RSC National Symposium in Chemistry, 2017, Gauhati University, Guwahati (oral presentation).

Doctoral Committee:

Prof. Anil Kumar Saikia (Chairman)

Prof. Siddartha Shankar Ghosh (Member)

Dr. Sumana Dutta (Member)

Dr. Chandan Mukherjee (Supervisor)

Abstract

Chapter I

General Introduction and Motivation

Magnetic Resonance Imaging (MRI) is the most widely used non–invasive modern technique for detecting physical abnormalities without using any harmful radiation. The practice of generating images with MRI was developed from the same principles which govern routine Nuclear Magnetic Resonance (NMR) spectroscopy commonly used as a characterisation technique in organic synthesis. However, being the sensitivity of MRI relatively low, to enhance the image contrast, ~ 50% of all MRI experiments are accompanied by administration of contrast agents (CAs) prior to imaging. Among different paramagnetic (*e.g.*, Gd(III), Mn(II), Fe(III)) and superparamagnetic (*e.g.*, iron ixide nanoparticle) CAs, Gd(III)–based MRI CAs are the most popular due to the presence of seven unpaired electrons and long electronic relaxation time of Gd(III) ion.

The discovery of the disease Nephrogenic Systemic Fibrosis (NSF) has prompted a new research area to develop safer MRI contrast agents as some of the Gd(III)–based MRI contrast agents are known to cause this disease in patients having severe kidney diseases or following liver transplantation. With five unpaired electrons, fast water exchange rate and being an essential element in human biological system, Mn(II) is the best candidate in place of Gd(III).

The majority of clinical MRI operates at 1.5 T or 3 T, and nowadays the trend in MRI is moving towards higher magnetic field due to high signal–to–noise ratio and reduced acquisition time. The main drawback associated with commercially available MRI CAs is their lower relaxivity at higher field. Hence, development of CAs that will have high relaxivity value at high field seeks special attention.

Chapter II

A New Picolinate–Based High Relaxivity Gd(III) Complex as MRI Contrast Agent

In order to impose stability as well as water solubility, ligand H_4peada and its corresponding Gd(III) complex, **2A** were synthesised (**Scheme 1**). The facile funtionalisation of

the picolinate group present in the ligand backbone makes these types of ligands attractive candidates for potential MRI contrast agents. Ligand H_4peada, being hepta–coordinated, would allow maximum two water molecules to bind with the Gd(III) centre and consequently higher relaxivity value could be obtained. The number of coordinated water molecules (q) was found to be 1.4±0.1 from the luminescence life time measurements of the Tb(III) congener of the complex in H_2O and D_2O, which implied coexistence of both mono and bis(aquated) Gd(III) complex of ligand H_4peada in solution state (pH = 7.4, 25 °C)

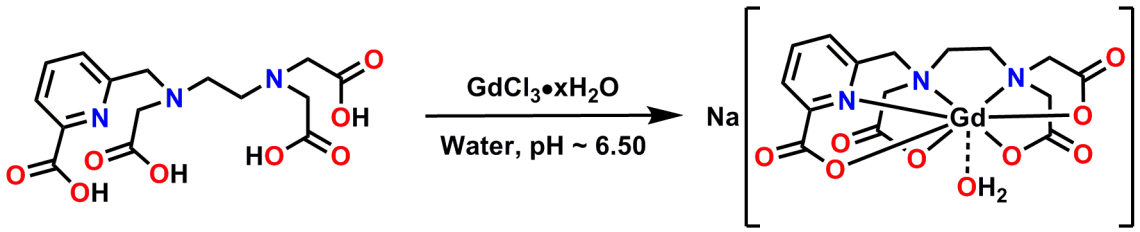

Scheme 1. Synthesis of complex **2A**.

With pGd value of 18.4 (at pH = 7.4 and 25 °C), ligand H_4peada showed comparable stability to that of the commercially available DTPA (pGd_{DTPA} = 19.1) and better stability than that of the previously reported Gd(III) complexes of picolinate based ligands. Complex **2A** showed r_1 relaxivity value of 6.08 $mM^{-1}s^{-1}$ at 1.41 T, 25 ºC and pH ~ 7.4, which was almost constant through pH range 4–10. The affinity of the complex for phosphate (PO_4^{3-}), bicarbonate (HCO_3^-), and fluoride (F^-) ions whose concentrations in blood serum may be of toxicity concern was investigated by measuring r_1 relaxivity value of the complex in the presence of 100 equivalents of the respective anions (experimental conditions: 1.41 T, 25 °C, pH ~ 7.4, [complex **2A**] = 0.5 mM, [anions] = 50 mM). These anions can form ternary adducts by replacing the inner sphere water molecules of the complex resulting in sharp decrease in relaxivity value. The r_1 relaxivity values of complex **2A** remained same in case of phosphate and bicarbonate, whereas in case of fluoride ion, the value dropped to 4.6 $mM^{-1}s^{-1}$ (Δr_1 = –1.48 $mM^{-1}s^{-1}$) which was due to a binding interaction of fluoride ion replacing inner sphere water molecules of the complex. The selectivity of ligand H_4peada for Gd(III) over Zn(II) and Cu(II) was investigated by measuring pZn and pCu value of the ligand, and a higher selectivity of the ligand towards Gd(III) over Cu(II) (pGd – pCu = 1.3) and comparable selectivity over Zn(II) (pGd – pZn = 3.6) was

observed in comparison to that of the commercially available ligand DTPA (for DTPA, pGd – pCu = 1.1, pGd – pZn = 3.7).

T_1–weighted phantom MR images of complex **2A** at four different concentrations of the complex at 1.5 T are shown in **Figure 1**.

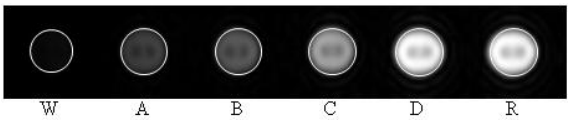

Figure 1. T_1–weighted phantom MR images of complex **2A** at 1.5 T, 25 °C, and pH ~ 7.4 (W = Water, A = 0.25 mM, B = 0.50 mM, C = 0.70 mM, D = 1.00 mM, R = Reference = Rezogad®).

Chapter III

A Bis(aquated) High Relaxivity Gd(III) Complex for High Field (14.1 T) MRI Study

MRI at high magnetic fields facilitates higher signal–to–noise ratio with better spatial resolution and reduced acquisition time. However, the effectiveness of clinically used Gd(III)–based MRI contrast agents are limited to 1.5–3.0 T and longitudinal relaxivity value, r_1 drastically decreases as the field strength increases. In search of developing a new MRI contrast agent which can show high relaxivity at higher magnetic field, ligand H_4bedik and its corresponding Gd(III) complex, **3A** were synthesised. From luminescence life time measurements of the corresponding Tb(III) complex of ligand H_4bedik in H_2O and D_2O, the number of coordinated water molecules (*q*) was found to be 2.22±0.1.

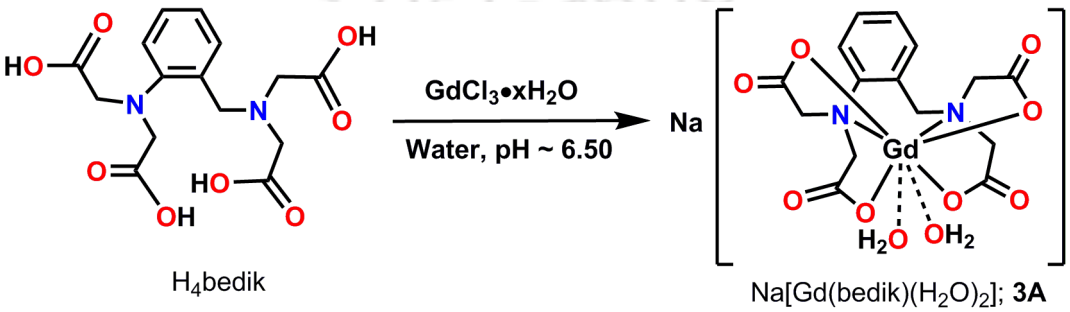

Scheme 2. Synthesis of complex **3A**.

Complex **3A** showed higher thermodynamic stability (pGd_{H_4bedik} = 19.9, at pH = 7.4, 25 °C) compared to the clinically approved ligand DTPA (pGd_{DTPA} = 19.1). At 14.1 T, 25 ºC and pH ~ 7.4, the longitudinal relaxivity, r_1 was measured and a higher relaxivity value of 12.40 $mM^{-1}s^{-1}$ per Gd(III) ion was obtained. Owing to the demand of a high relaxivity MRI contrast agent at high field, this complex showed significantly high r_1 value at 14.1 T.

The complex showed r_1 relaxivity value of 7.30 $mM^{-1}s^{-1}$ at 1.41 T, 25 °C, and pH ~ 7.4 which was found to be almost constant in the pH range 4–10. While r_1 relaxivity was measured in the presence of 100 equivalents of PO_4^{3-}, HCO_3^-, and F^- ions (experimental conditions: 1.41 T, 25 °C, pH ~ 7.4, [complex **3A**] = 0.5 mM, and [anions] = 50 mM), the complex did not show any interaction with PO_4^{3-} and HCO_3^-, whereas in case of F^- ion, lowering in the r_1 relaxivity value was observed (Δr_1 = – 1.14 $mM^{-1}s^{-1}$) due to the interaction of the F^- ion with complex **3A**. The pZn and pCu values of ligand H_4bedik implied more selectivity of the ligand towards Gd(III) over Zn(II) (pGd – pZn = 4.0) and Cu(II) (pGd – pCu = 2.9) in comparison to that of DTPA (pGd – pZn = 3.7, pGd – pCu = 1.1).

At 1.5 and 14.1 T, T_1–weighted phantom MR images of complex **3A** at four different concentrations were measured (at 25 °C, and pH ~ 7.4). Comparison of images with the commercially available MRI contrast agent MultiHance® at 1.5 T substantiated the complex as a better contrast agent even at very low concentration.

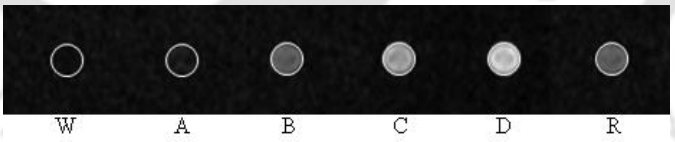

Figure 2. T_1–weighted phantom MR images of complex **3A** at 1.5 T, 25 °C, and pH ~ 7.4 (W = Water, A = 0.25 mM, B = 0.50 mM, C = 0.70 mM, D = 1.00 mM, R = Reference = MultiHance®).

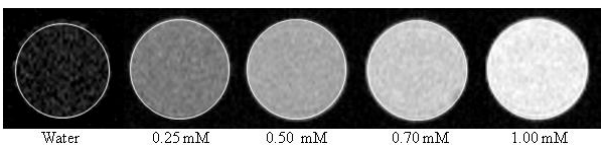

Figure 3. T_1–weighted phantom MR images of complex **3A** at four different concentration, at 14.1 T, 25 °C, and pH ~ 7.4.

Chapter IV

A New Water–Coordinated Seven–Coordinate Mn(II) Complex as T_1– and T_2– Dual Mode MRI Contrast Agent

The discovery of the disease Nephrogenic Systemic Fibrosis (NSF) has prompted new research to develop high spin Mn(II)–based MRI contrast agents as an alternative to classical Gd(III)–based MRI contrast agents. Being an essential element in human biological system, and with five unpaired electrons, slow electronic relaxation, and high water exchange rate on its complexes Mn(II) takes the place as the best alternative to Gd(III). Herein, in order to achieve water coordinated seven–coordinate Mn(II) complex, Mn(II) complex of ligand H_4bedik, **4A** was synthesized (**Scheme 3**), which contained a 2–amidobenzylamide backbone. The asymmetric coordination environment of the ligand favoured a water molecule to bind to the central Mn(II) metal ion and consequently, a seven–coordinate Mn(II) complex was achieved. Single crystal X–ray diffraction measurement at 293 K confirmed the presence of one coordinated water molecule in the complex.

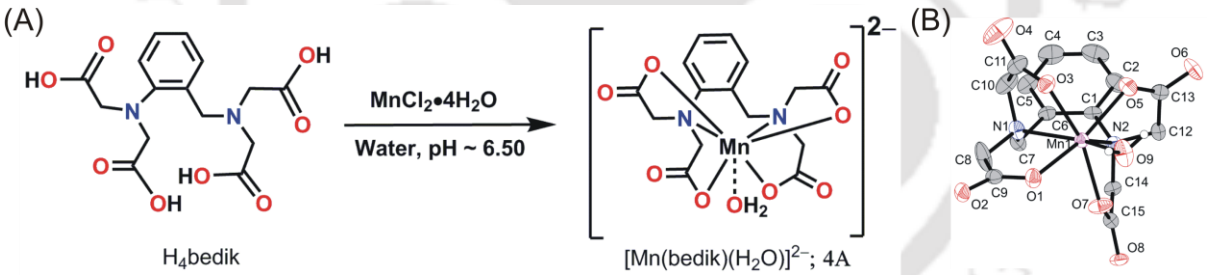

Scheme 3. (A) Synthesis of complex **4A**, (B) ORTEP presentation of the complex (dinegative unit).

A comparison of thermodynamic stability of the complex with $[Mn(EDTA)]^{2-}$ was done by determining the pMn value. pMn value for ligand H_4bedik was found to be 9.71 (at pH = 7.4, 25 °C) which was higher than the competing ligand EDTA (pMn_{EDTA} = 8.05). The r_1 relaxivity of the complex at 1.41 T, 25 ºC and pH ~ 7.4 was found to be 3.11 $mM^{-1}s^{-1}$ per Mn(II) which was significantly higher than that of the only commercially available Mn(II)–based MRI contrast agent, Teslascan® (r_1 = 2.1 $mM^{-1}s^{-1}$, at 1.5 T).

To note, complex **4A** exhibited high longitudinal relaxivity value of 6.29 $mM^{-1}s^{-1}$ per Mn(II) at higher magnetic field (14.1 T) as well as high transverse relaxivity value of 132.77 $mM^{-1}s^{-1}$ per Mn(II) at 25 °C and pH ~ 7.4. This indicated that the complex, in addition to T_1 contrast property also possessed excellent T_2 contrast property even at high field and can be used as a T_1– and T_2–dual mode contrast agent. Phantom MR images of complex **4A** measured at 1.5 T and 14.1 T consolidated its potential use as dual–mode MRI contrast agent.

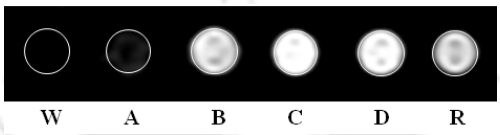

Figure 4. T_1–weighted phantom MR images of complex **4A** at 1.5 T, 25 °C, and pH ~ 7.4 (W = Water, A = 0.25 mM, B = 0.50 mM, C = 0.70 mM, D = 1.00 mM, R = Reference = MultiHance®).

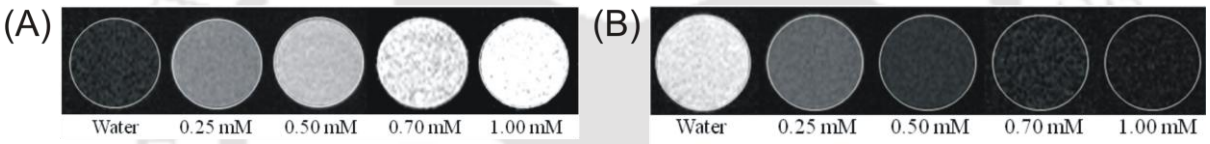

Figure 5. (A) T_1–weighted, and (B) T_2–weighted phantom MR images of complex **4A** at four different concentrations, at 14.1 T, 25 °C, and pH ~ 7.4.

Chapter V

A Bis(aquated) High Relaxivity Mn(II) Complex as Potential MRI Contrast Agent

Although Mn(II) has gained special attention as the best alternative in place of Gd(III)–based MRI contrast agents, due to the presence of only five unpaired electrons in Mn(II) as compared to the seven unpaired electrons in Gd(III), the main drawback of Mn(II)–based contrast agents is their low relaxivity as compared to Gd(III)–based contrast agents. An obvious strategy to increase the relaxivity is to increase the number of coordinated water molecules (q) of the complex keeping sufficient thermodynamic and kinetic stability. Ligand H_2pmpa and its corresponding Mn(II) complex, **5B** with two inner sphere water molecules were synthesised as

shown in **Scheme 4**. The incorporation of piperazine unit and pyridine unit in the ligand backbone were important concern regarding the stability of overall system. The theoretical calculations showed a significant enhancement in the structural stability of the complex with two water molecules.

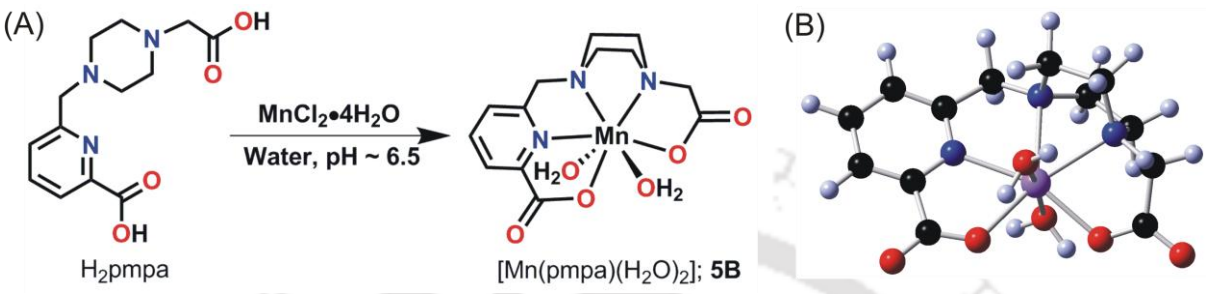

Scheme 4: (A) Synthesis of complex **5B**, (B) Optimised structure of the complex with two inner sphere water molecules.

Complex **5B** showed comparable stability (pMn_{H_2pmpa} = 7.88, at pH = 7.4, 25 °C) to that of $[Mn(EDTA)]^{2-}$ complex (pMn_{EDTA} = 8.05) and higher stability than previously reported bis(aquated) Mn(II) complexes. The r_1 relaxivity value of complex **5B** was found to be 5.88 $mM^{-1}s^{-1}$ (at 1.41 T, 25 °C and pH ~ 7.4) per Mn(II) which was higher compared to the commercially available MRI contrast agents and the higher value might be attributed due to the presence of two inner sphere water molecules. The relaxivity value was found to be fairly constant through a pH range of 5–10 (Δr_1 = ± 0.19 $mM^{-1}s^{-1}$, at 1.41 T and 25 ºC). Higher relaxivity value was observed at lower pH = 4 which was due to the dissociation of the complex and formation of aqua complex of Mn(II). While relaxivity measurements were performed in the presence of 200 equivalents of HCO_3^-, PO_4^{3-}, and F^- ions (experimental conditions: 1.41 T, 25 °C, pH ~ 7.4, [complex **5B**] = 0.5 mM, [anions] = 100 mM), no significant change in r_1 relaxivity value was observed in case of F^- and HCO_3^- ions. However, in case of PO_4^{3-}, an increase in realxivity value (Δr_1 = +1.43 $mM^{-1}s^{-1}$) was observed. This increment might be either due to release of free Mn(II) in solution or due to formation of a slowly tumbling system. To enlighten the fact, UV–vis spectra of complex **5B** was measured in the presence of various concentrations of phosphate anion at pH ~ 7.4, 25 °C. No significant change in the UV–vis spectrum of the complex in the presence of 200 fold excess of phosphate anion over ruled the decomposition of the complex and indicated the formation of a slowly tumbling system by

presumable intermolecular interactions in the presence of phosphate anion and/or complex–phosphate interaction.

T_1–weighted phantom MR images of complex **5B** at four different concentrations of the complex at 1.5 T are shown in **Figure 6**.

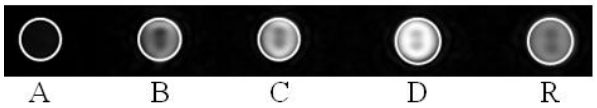

Figure 6. T_1–weighted phantom MR images of complex **5B** at 1.5 T, 25 ºC and pH ~ 7.4 (A = 0.25 mM, B = 0.50 mM, C = 0.70 mM, D = 1.00 mM, R = Reference = Rezogad®).

Contents

Chapter IV

A New Water–Coordinated Seven–Coordinate Mn(II) Complex as T_1– and T_2–Dual Mode MRI Contrast Agent

Chapter V

A Bis(aquated) High Relaxivity Mn(II) Complex as Potential MRI Contrast Agent

Abbreviations

Symbols:

m/z : mass per charge

λ : wavelength (nm)

δ : isomer shift

B : magnetic field

k_{ex} : water exchange rate

LD_{50} : lethal dose of a substance

T_1 : longitudinal relaxation time

R1 : longitudinal relaxation rate

r_1 : longitudinal relaxivity

T_2 : transverse relaxation time

R2 : transverse relaxation time

r_2 : transverse relaxivity

× : multiplication

E : total energy

Exp : experimental

Sim : simulated

J : coupling constant

S : electron spin

s : singlet

d : doublet

t : triplet

q : quartet

q : number of coordinated water molecules attached to the metal ion

τ : phosphorescence life time

Units:

Å : angstrom

cm : centimetre

amu : atomic mass unit

h : hour

K: kelvin

M : molar

min : minute

mm : millimetre

nm : nanometre

s : second

T : tesla

°C : degree centigrade

Hz : hertz

Solvents and reagents:

CH_2Cl_2 : dichloromethane

$CHCl_3$: chloroform

Et_2O : diethylether

Et_3N : triethylamine

KBr : potassium bromide

MeOH : methanol

CH_3CN : acetonitrile

THF : tetrahydrofuran

TFA : trifluroacetic acid

DMF : dimethylformamide

Boc : *tert*–butyloxycarbonyl

HEPES : 2–[4–(2–hydroxyethyl)–1–piperazinyl]ethanesulfonic acid)

Techniques:

NMR : nuclear magnetic resonance

ESI : electrospray ionisation

IR : infrared

MS : mass spectrometry

UV–vis : ultraviolet–visible spectroscopy

ICP–AES : inductively coupled plasma atomic emission spectroscopy

Latin expressions:

et al. : and co–workers
e. g. : for example
i. e. : that is
tert– : tertiary
vs. : versus, against
via : through
viz : namely

Chapter I

General Introduction and Motivation

1.1 Magnetic Resonance Imaging (MRI)

Magnetic Resonance Imaging (MRI) has become an indispensable medical technique since the pioneering work by Paul Lauterbur, the father of MRI, in the 1970s.[1] The idea of developing images from the Nuclear Magnetic Resonance (NMR) signals leads to the discovery of this very useful technique for non–invasively peering inside the body and allowing the detection of a variety of physical abnormalities. Unlike other imaging techniques, MRI does not use any harmful radiation that can be harmful to the tissues.[2] So, MRI is the best method to characterise and discriminate among the tissues using their physical and biochemical properties. Including cerebrospinal fluid and blood flow detection, contraction and relaxation of the organs, most of the physiological and pathological phenomena can be evaluated by using MRI which cannot be done by other imaging techniques like standard X–rays, Computed Tomography scan (CT scan), or Ultrasound.

The practice of generating images with MRI was developed from the same principles which govern routine Nuclear Magnetic Resonance (NMR) spectroscopy commonly used as a characterisation technique in organic synthesis.[3] A typical MRI scanner is comparable to that of a standard NMR spectrometer used for structural characterisation of a sample prepared in a relatively small tube. MRI, however, employs only the water proton signal in a much larger human 'sample' and relies on the abundant water distribution throughout tissue and magnetic field gradients in different directions to generate the image. **Figure 1.1** shows a basic setup of a typical MRI scanner.

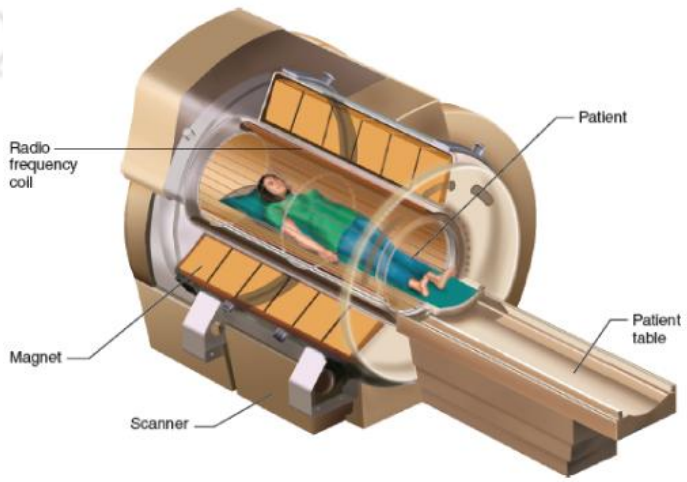

Figure 1.1. Basic setup of a typical MRI scanner.[4]

MRI scanner (**Figure 1.1**) consists of a super conducting magnet, which creates a homogeneous strong magnetic field, a radio frequency coil, and a gradient coil, surrounding the patient. A receiver coil is also present in the system, which is connected to an external computer. The computer receives the signals and processes the signals into images.

Human body is primarily consists of fat and water, which make the whole body approximately with 70% water.[5] MRI thus images the NMR signals of the hydrogen nuclei of these water molecules. The proton nuclear spins of these water molecules are constantly in spinning motion creating a magnetic field and they are randomly oriented in the absence an external magnetic field (**Figure 1.2**). Once they are placed in an external magnetic field (**Figure 1.2**), they align themselves either parallel or antiparallel to the magnetic field. The preferred state of alignment is the one that needs less energy. So, more protons are on the lower energy level, parallel to the external magnetic field. However, the difference in number is very small and depends on the strength of the applied magnetic field.

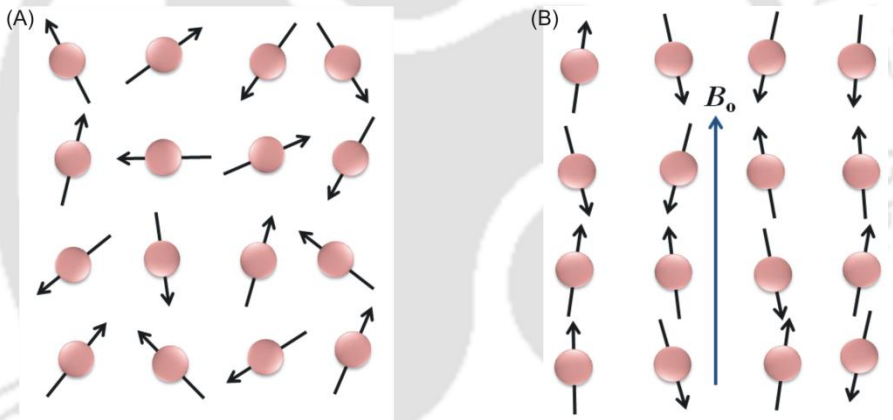

Figure 1.2. Protons in the (A) absence and (B) presence of magnetic field.

In addition to alignment of nuclei with a magnetic moment, application of an external magnetic field will produce a secondary spin or wobble of nuclei around the main or static magnetic field. This precessional path around the magnetic field is circular like a spinning top and the frequency is called Larmor frequency. This is the frequency with which the proton nuclear spin absorb the energy. When a radio frequency pulse at this Larmor frequency is applied, two things may happen: some of the proton spins flip to the opposite direction of the magnetic field, and the protons get synchronised, start to precess in phase. When the external radiofrequency signal is turned off, the protons which are in opposite direction of the magnetic field, return to their equilibrium positions with the loss of energy to the surrounding nuclei; and

the protons which precess in phase, lose phase coherence and they get out of phase. These phenomena are called relaxation.

Two ways of returning back to the equilibrium positions are:

1) Longitudinal relaxation or T_1 relaxation, and
2) Transverse relaxation or T_2 relaxation

Longitudinal relaxation is also called spin–lattice relaxation where relaxation takes place along the direction of the magnetic field or this is the relaxation time for the magnetization to return to 63% of its original value. The net magnetization M_z along the *z*–axis after time 't' is given by the equation:

$$M_{z(t)} = M_{z(0)} \left(1 - e^{-t/T_1}\right)$$

where T_1 is the longitudinal relaxation time.

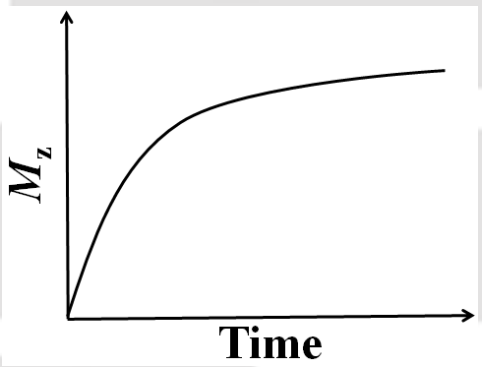

Figure 1.3. Change in magnetization along *z*–axis.

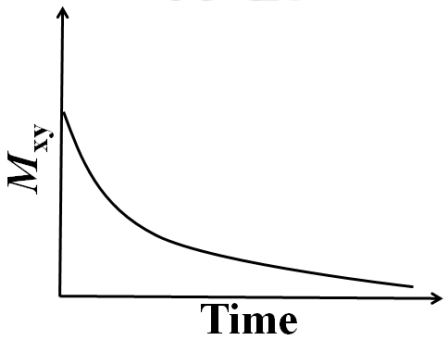

Figure 1.4. Decay in magnetization along *xy*–plane.

Transverse relaxation is also called spin–spin relaxation which is the time taken to disappear 69% of the magnetization along its transverse plane. The decay of the transverse magnetization along *xy*–plane is given by the equation:

$$M_{xy(t)} = M_{xy(0)}\, e^{-t/T_2}$$

where $M_{xy(t)}$ is the transverse magnetization after time 't', and T_2 is the transverse relaxation time.

The T_1 and T_2 relaxation times are dependent on the local environment of the water molecules. The discovery of the fact; different types of biological tissues have different relaxation times, led to design the MRI machine, which can detect the internal malignancies.

Table 1.1. T_1 Relaxation times of some malignant and normal tissues:[6]

Tissue	T_1 Tumar (s)	T_1 Normal (s)
Liver	0.832	0.570
Spleen	1.113	0.701
Lung	1.110	0.788
Skin	1.047	0.616
Stomach	1.238	0.765
Breast	1.080	0.367
Bone	1.027	0.554

Tissues which have shorter T_1 values provide brighter image intensity as the magnetization along *z*–axis becomes high with the faster relaxation process. On the other hand, short T_2 values are always associated with lower signal intensity since it diminishes the net transverse magnetization available for detection.

1.2 MRI Contrast Agents

Mostly, while doing MRI experiments, the contrast obtained between the normal tissues and the diseased tissues are not sufficient to detect the early stage of abnormalities. In this case, the duration of the experiment may be painful and to enhance the image contrast, an external agent needs to apply. This external agent is called MRI contrast agent (CA). The main

aim of the contrast agent is to accelerate the relaxation time of nearby water protons, allowing the reduction of experiment time, hence improving the contrast (**Figure 1.5**).[8]

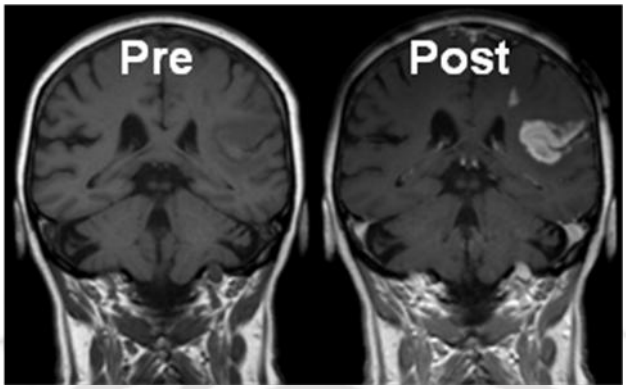

Figure 1.5. MRI of human brain before and after injection of contrast agent.[7]

Currently, ~ 50% of MRI studies are performed in the presence of MRI CAs.[9] They are injected into the patient's body to enhance the contrast between normal and diseased–tissues. The objective for using contrast agent, to accelerate the relaxation rate of nearby water protons, can be achieved by paramagnetic substances. The unique magnetic properties of lanthanides (in particular gadolinium) make these metal ions ideal for the purpose.[10] Other paramagnetic metal ions like Mn(II), Mn(III), Fe(III) and Cu(II) are also been studied (**Table 1.2**).[11]

Table 1.2. Paramagnetic metal ions used in the synthesis of MRI CAs:

Metal ion	No. of unpaired electrons	Magnetic moment
Mn(II)	5	5.92
Mn(III)	4	4.90
Fe(III)	5	5.92
Cu(II)	1	1.73
Gd(III)	7	7.94

For relaxation, water protons need to encounter a fluctuating magnetic field. Protons have Brownian motions and generate small fluctuating magnetic field. An electron has ~ 700 times more potent local magnetic field than a proton. So, the paramagnetic metal ions with higher number of unpaired electrons can be used as MRI CAs. With seven unpaired *f*–shell electrons

and large magnetic moment, Gd(III) ion is the most commonly used CA in clinical practice. Owing to the symmetric *S*–state, which is an hospitable environment for electron spins, Gd(III) possesses a high spin paramagnetism and slow electronic relaxation rate than other lanthanides.[12]

However, free Gd(III) ion is highly toxic in nature with LD_{50} ~ 0.5 $mmolkg^{-1}$ and cannot be injected to living system directly.[13] To use it as MRI CA in living system, it must be encapsulated by a strong multidentate ligand. Since lanthanide ions are classified as hard acids, multidentate ligands having hard σ–donor atoms *e.g.* nitrogen and oxygen are favoured.[14] Poly(aminocarboxylate) ligands are most widely used as the chelating ligand for commercially available MRI CAs. This chelation enhances both thermodynamic and kinetic stability of the complex.[15]

Contrast agents are divided into two large groups on the basis of their relaxation properties: T_1 contrast agent or positive contrast agent and T_2 contrast agent or negative contrast agent. T_1 relaxation time reflects the length of time it takes for regrowth of Mz back toward its initial maximum value (Mz(o)). Tissues with short T_1 recover more quickly than those with long T_1. Their Mz values are larger, producing stronger signals. On the other hand, T_2 reflects the length of time it takes for the MR signal to decay in the transverse plane. A short T_2 means rapid lose of spin phase coherence. Since T_1 relaxation is associated with reappearance of its longitudinal magnetisation, T_1 contrast agents are also termed as positive contrast agents. Alternatively, T_2 relaxation is associated with decrease in transverse magnetisation and T_2 contrast agents are also termed as negative contrast agents. Till date, superparamagnetic iron oxide nanoparticles are predominantly used as T_2 contrast agents. The iron oxide nanoparticles are mainly divided into two groups depending on their dimensions:[17]

1) Superparamagnetic iron oxide (SPIO), with diameter, $d > 40$ nm
2) Ultrasmall superparamagnetic iron oxide (USPIO), with diameter, $d < 40$ nm

Some commercially available CAs based on superparamagnetic iron oxide nanoparticles are Feridex/Endorem®, Resovist®, Lumirem® etc. Although these CAs were successfully applied in some instances for liver tumour imaging but their use has been discontinued due to safety concern.[18]

The paramagnetic contrast agents of mostly Gd(III)–based metal complexes. In this context, Mn(II)– and Fe(III)–based complexes are not frequently used as commercial T_1 MRI

CAs due to the fact that both Mn(II) and Fe(III) ion generate low fluctuating magnetic field owing five unpaired electrons compared to seven unpaired electrons in Gd(III) ion. **Scheme 1.1** shows some of the commercially available Gd(III)–based MRI CAs.[9a,10b]

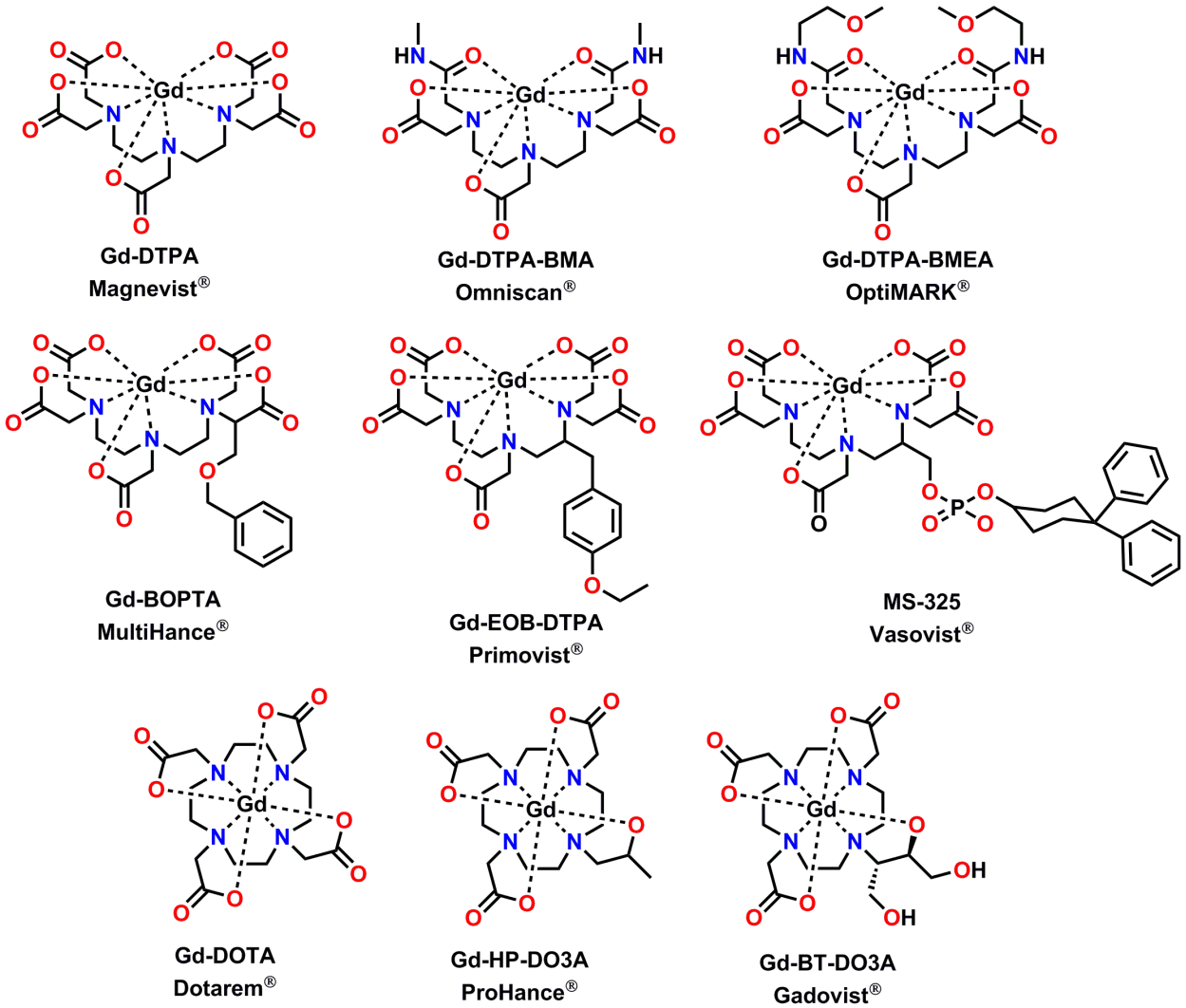

Scheme 1.1. Commercially available Gd(III)–based MRI CAs. The number of coordinated water molecule in all cases is one.

All these Gd(III)–based contrast agents are nine–coordinate complexes, where a low molecular weight poly(aminocarboxylate) ligand occupies eight coordinating sites and the ninth coordination site is occupied by one water molecule. Two types of poly(aminocarboxylate) ligands are used till now in case of commercially available MRI CAs:

1) DTPA (Diethylenetriaminepentaacetic acid), which is a acyclic ligand system and
2) DOTA (1,4,7,10–tetraazacyclododecane–1,4,7,10–tetraacetic acid), which is a macrocyclic ligand system

Both these systems are proven to be the best ligand backbone for highly thermodynamically and kinetically stable Gd(III) complexes.[19] The contrast agents are not organ specific except the latest approved MRI CA MultiHance®,[20] which accumulates only in liver.

Although Gd(III)–based MRI CAs are considered to be very safe, the discovery of the disease Nephrogenic Systemic Fibrosis (NSF) in 2006 opens up a new research area where people are trying to synthesise an alternative to Gd(III)–based MRI CAs.[21] Patients having severe kidney diseases or who underwent liver transplantation, when exposed to Gd(III)–based CAs, are known to develop this disease which is devastating, often lead to disability, and even death. In these patients, lacking of proper excretion mechanism due to severe kidney dysfunction, small molecule contrast agents could not be excreted for several days or weeks, which leads to dissociate Gd(III)–based CAs, leaving the toxic ligands and free Gd(III) ions in the body. This Gd(III) has a high affinity for Ca(II) ion channels and has been associated with a thickening of organs and skin.

The development of safe alternative to Gd(III)–based MRI CAs for the patients with kidney disorder is one of the great challenges in the field of MRI CAs. These contrast agents should have sufficient thermodynamic and kinetic inertness along with its rapid elimination from the body. Nanoparticles, *e.g.* iron oxides, manganese oxides etc, have been synthesised extensively as an alternative to Gd(III)–based CAs. But due to their larger sizes, their uses are restricted for angiography, liver imaging, and targeting imaging of macrophages etc.[23] Also, these nanoparticles show some adverse effects when employed to the patients. Another imaging probe PARACEST, which contrasts the images *via* chemical exchange saturation transfer needs higher doses compared to Gd(III)–based CAs. Different metal ions such as Fe(III), Ni(II), Co(II), Co(III) etc have been successfully used for synthesising PARACEST MRI CAs.[24]

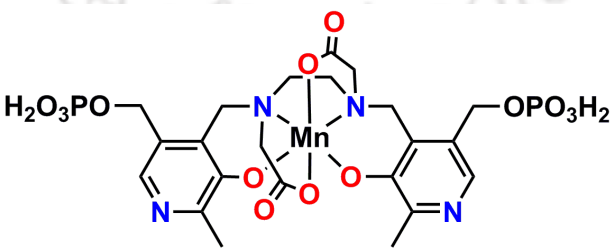

Figure 1.6. Commercially available Mn(II)–based MRI CA,Teslascan®.

Mn(II) ion with five unpaired electrons, slow electronic relaxation rate and high water exchange rate on its complexes takes the place as the best alternative to Gd(III).[25] Additionally,

Mn(II) is an essential element in human biological system and can be excreted from the body through bile also.[26] This excretion pathway along with renal excretion makes the Mn(II) complexes prime candidate for using them in the perspective of renal compromise. However, at higher concentrations, free Mn(II) shows significant toxicity ($MnCl_2$, LD_{50} = 0.22 mmol kg^{-1} in rat) and accumulation of Mn(II) in the brain has been proven. Overexposure to Mn(II) can also lead to a neurological disorders resulting in a form of parkinsonism termed as manganism. Due to this reason, chelating ligands are required to ensure the thermodynamic and kinetic stability of the Mn(II) complexes. The complex Manganese(II)–dipyridoxal diphosphate, $Mn(DPDP)^{4-}$, (Teslascan®) was commercially approved for human liver imaging, which fulfilled the criteria of stable Mn(II) chelate with enhanced image contrast.[27] Another one which is currently undergoing phase III clinical trials is a mixture of $MnCl_2$, alanine, and vitamin D_3 (CMC–001), and will be useful in the near future for evaluation of liver metastases.[28]

MRI CAs provide anatomical details with high spatial resolution. While T_1 based MRI CAs provide brightening in the MR images, T_2 CAs darken the images. The darker images are often confusing with the signals from blood clotting, hemorrhage, and calcification inside the body.[29] These phenomena mimic the MRI signals coming from contrast agents and lead to difficulty in discrimination between the contrast agents and the MRI artefacts. To overcome these disadvantages, various modified MRI techniques have been used.[30] Even then, these techniques are limited to only certain type of artefacts and cannot be eliminated completely. To deal with the problem, synthesis of dual mode contrast agents (DMCAs) by integrating both T_1 and T_2 CAs is gaining special attention.[31] Since each imaging technique has its own advantages and limitations, the DMCAs can overcome the limitations of each technique by combining both the modalities in a single contrast agent. The reported DMCAs are generally a combination of superparamagnetic nanoparticles and small Gd(III) species in a core–shell format. Superparamagnetic iron oxide and manganese oxide nanoparticles are widely used in this case.[32]

1.3 Relaxivity of Metal Complexes

The efficiency of a contrast agent is evaluated in terms of its relaxivity (r), the ability to enhance the relaxation rate of the nearby water protons to enhance the signal intensity. The presence of paramagnetic metal complex increases both longitudinal ($1/T_1$) and transverse ($1/T_2$)

relaxation rates of a NMR active solvent nucleus. The diamagnetic and paramagnetic contributions to the relaxation rates of such solutions are additive and is given by eq. (1).

$$(1/T_i)_{obs} = (1/T_i)_{diamagnetic} + (1/T_i)_{paramagnetic} \qquad i = 1, 2 \qquad (1)$$

where $(1/T_i)_{obs}$ is the observed relaxation rate of the solvent due to the presence of paramagnetic complex,

$(1/T_i)_{diamagnetic}$ is the relaxation rate in the absence of any paramagnetic substance, and

$(1/T_i)_{paramagnetic}$ is the relaxation rate in the presence of paramagnetic substance.

The observed relaxation rate is linearly dependent on the concentration of the paramagnetic substance ([M]), and in the absence of solvent–solvent interaction, eq. (1) becomes:

$$(1/T_i)_{obs} = (1/T_i)_{diamagnetic} + r_i[M] \qquad i = 1, 2 \qquad (2)$$

In eq. (2), **relaxivity, r_i** is defined as the slope of this dependence and expressed in the unit of $mM^{-1}s^{-1}$.

The relaxation pathway is provided by the paramagnetic centre by creating a large and fluctuating magnetic field around it. Each type of chemical interaction with the paramagnetic centre yields different relaxation efficiencies depending on the distance and time of interaction. Paramagnetic relaxation includes both inner sphere contribution from relaxation of a water molecule directly coordinated to the metal centre and an outer sphere contribution from relaxation of water molecule in the second coordination sphere and the bulk solvent. The classification of the water molecules with respect to different types of interactions are shown in **Figure 1.7**. However, current designing of the contrast agents mainly focuses on attaining higher inner sphere longitudinal relaxivity, r_{1p}, from protons of water molecules in the first coordination sphere of the paramagnetic metal. A clear understanding of the outer sphere water molecule contribution is still under investigation despite its high importance in contrast agent design and in understanding second coordination sphere effects in chemical reactions and electron transfer.[7a]

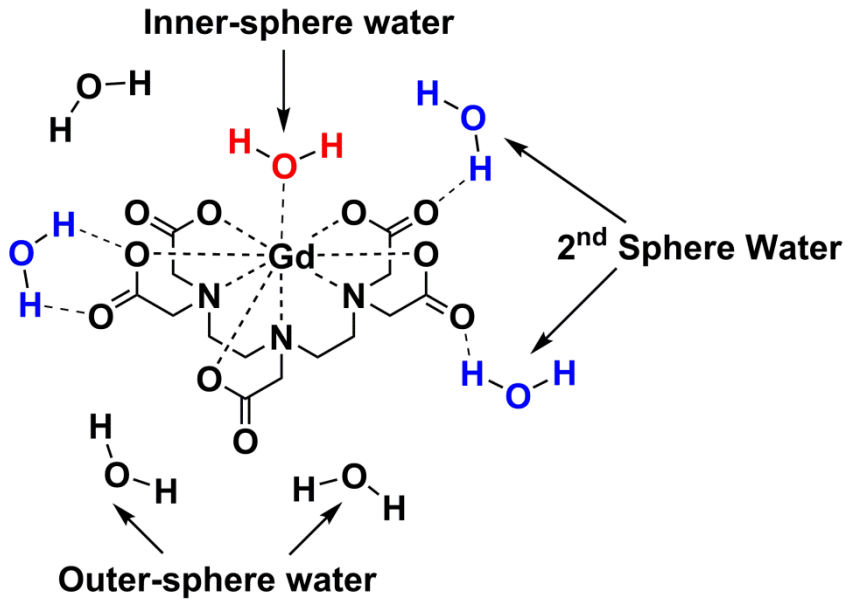

Figure 1.7. Different types of water molecules yielding different relaxation efficiency.

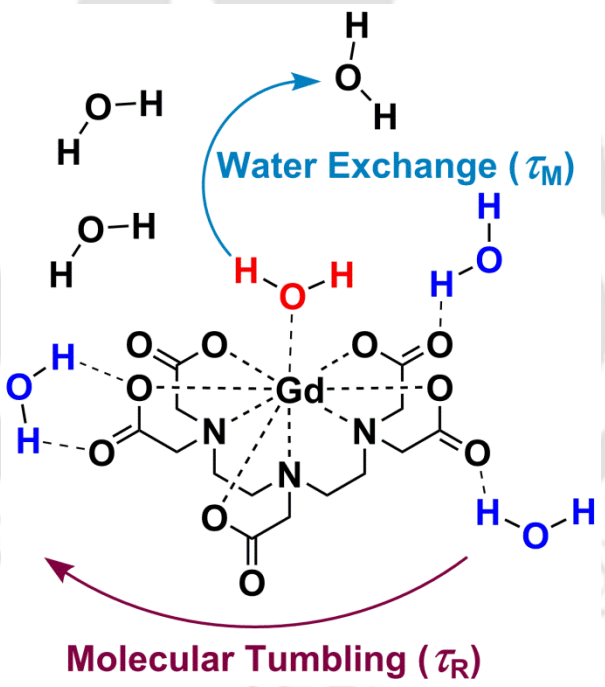

Figure 1.8. Schematic representation of the factors affecting proton relaxivity.

A chemical exchange between the inner sphere water molecules (or any water molecule in the primary coordination site) and the bulk solvent results in proton relaxation. The longitudinal component of relaxation is given by eq. (3):

$$(1/T_i)^{IS} = qP_M[1/(T_{1M} + \tau_M)] \qquad (3)$$

where $(1/T_i)^{IS}$ is the relaxation time,

q is the number of water molecule bound to the metal centre,

P_M is the mole fraction of bound water,

T_{1M} is the relaxation time of bound water, and

τ_M is the mean water residence time

The eq. (3) implies that if water exchange at the paramagnetic metal centre is fast enough (small values of τ_M), then the paramagnetic relaxation enhancement experienced by the bulk solvent will come from the increase in the relaxation rate of the coordinated solvent molecule (T_{1M}).

The inner sphere relaxivity results from dipolar contribution through–space interactions due to random fluctuations of the electronic field arising from the unpaired spin on metal ion and can be described by Solomon–Bloembergen–Morgan (SBM) equations (4) and (5).[33]

$$\frac{1}{T_{1M}^{DD}} = \frac{2}{15}\frac{\gamma^2 g^2 S(S+1)\mu_B^2}{r_{Gd-H}^6}\left[\frac{3\tau_{C1}}{1+\omega_H^2\tau_{C1}^2} + \frac{7\tau_{C2}}{1+\omega_S^2\tau_{C2}^2}\right] \quad (4)$$

$$1/\tau_{ci} = 1/\tau_R + 1/T_{ie} + 1/\tau_M \qquad i = 1, 2 \quad (5)$$

Here, γ is the proton gyromagnetic ratio,

g is the electronic g–factor,

S is the total electron spin of the metal ion,

μ_B is the Bohr magneton,

r is the metal–proton distance (Gd–H),

τ_{ci} is the correlation time that defines dipole–dipole relaxation,

ω_S and ω_H are the electronic and proton Larmor precession frequencies respectively,

T_{ie} is the electronic relaxation time, and

τ_R is the rotational tumbling time of the entire metal water unit.

The SBM equations show the field–dependency of the relaxivity. The equations also show the importance of the correlation time τ_c. All the factors given in the equation become critical if one is to obtain the high relaxivities predicted by theory.

According to SBM theory, the relaxivity of a contrast agent can be enhanced by the following:

1. increasing the number of water molecules coordinated to the metal centre (q),
2. reducing the tumbling rate of the contrast agent ($1/\tau_R$), and
3. keeping the water exchange rate ($1/\tau_M$) optimum ($\tau_M \sim 10$ ns).

Relaxivities of current commercially available contrast agents based on poly(aminocarboxylate) ligands are small (r_1 = 4.4–5.2 $mM^{-1}s^{-1}$) compared to what is theoretically possible.[10b] Theory reveals that by increasing the number of coordinated water molecules one can attain higher relaxivity irrespective of field strength. Relative to commercial agents, it is necessary to increase water exchange rates[34] and slow molecular tumbling,[35] with higher number of inner sphere water molecules[36] as possible to achieve high relaxivities predicted by theory. The electronic relaxation time of the metal centre also has an important role to play while designing a chelate. Once all the other parameters are optimised, still this parameter remains as a limiting factor in achieving high relaxivity values. While it is the most difficult parameter to rationally influence, theory says that longer T_{1e} values can be achieved through increasing the symmetry at the metal centre, as well as rigidity of the complex.[37]

1.4 High Relaxivity at High Field Strength

The trend in MRI is nowadays moving towards higher magnetic fields, as higher fields result in high signal resolution and short acquiring time.[38] The majority of clinical MRI machine operates at 1.5 T and 3 T. It is found that at high fields, the benefits of commercially available contrast agents are less because of their lower relaxivity.[39] Theory says that higher relaxivities at higher magnetic field can still be achieved by judicious ligand designing. Unlike low field parameters, an intermediate correlation time is desired (0.5–4 ns) to attain high relaxivity at high field. Also, in case of high field, the water exchange rate is not a crucial factor as it is in the low field. A simulation to attain higher relaxivity at higher field by P. Caravan and his co–workers[38a] showed that even r_1 relaxivity value of 80, 45 and 18 $mM^{-1}s^{-1}$ at 1.5, 3 and 9.4 T can be obtained respectively for Gd(III) and Mn(II) complexes.

References

1. (*a*) P. C. Lauterbur, *Nature*, 1973, **242**, 190; (*b*) M. J. Dawson, *Paul Lauterbur and the Invention of MRI*, The MIT Press, 2013.
2. R. Salzer, *Biomedical Imaging: Principles and Applications*, a Jhon Wiley and Sons, Inc., 2012.
3. (*a*) R. A. Pooly, *RadioGraphics*, 2005, **25**, 1087; (*b*) S. Currie, N. Haggard, I. J. Craven, M. Hadjivassiliou and I. D. Wilkinson, *Postgrad. Med. J.*, 2013, **89**, 209; (*c*) K. L. Mcmahon, G. Cowin and G. Galloway, *J. Orthop. Sports Phys. Ther*., 2011, **41**, 806.
4. http://mgh-images.s3.amazonaws.com/9780077824976/11940-6-1ICS1.png
5. H. H. Mitchell, T. S. Hamilton, F. R. Steggerda and H. W. Bean, *J. Biol. Chem*., 1945, **158**, 625.
6. R. Damadian, K. Zaner, D. Hor and T. DrMaio, *Proc. Nat. Acad. Sci. USA*, 1974, **71**, 1471.
7. https://goo.gl/images/b8cl1w
8. (*a*) R. B. Lauffer, *Chem. Rev*., 1987, **87**, 901; (*b*) M. H. Mendonça-Dias, E. Gaggelli and P. C. Lauterbur, *Semin. Nucl. Med*., 1983, **13**, 364.
9. (*a*) P. Caravan, *Chem. Soc. Rev*., 2006, **35**, 512; (*b*) P. Hermann, J. Kotek, V. Kubíček and I. Lukeš, *Dalton Trans*., 2008, **23**, 3027; (*c*) S. Laus, R. Ruloff, E. Tóth and A. E. Merbach, *Chem. Eur. J*., 2003, **9**, 3555; (*d*) K. N. Raymond and V. C. Pierre, *Bioconjugate Chem*., 2005, **16**, 3; (*e*) J. M. Major and T. J. Meade, *Acc. Chem. Res*., 2009, **42**, 893; (*f*) E. J. Werner, A. Datta, C. J. Jocher and K. N. Raymond, *Angew. Chem., Int. Ed.*, 2008, **47**, 8568; (*g*) E. L. Que and C. J. Chang, *Chem. Soc. Rev.*, 2010, **39**, 51.
10. (*a*) G. J. Strijkers, W. J. Mulder, G. A. F. van Tilborg and K. Nicolay, *Anticancer Agents Med. Chem*., 2007, **7**, 291; (*b*) A. Merbach, L. Helm and É. Toth, *The Chemistry of Contrast Agents in Medical Magnetic Resonance Imaging*, Second Edition. Wiley, New York, 2001.
11. (*a*) B. Drahoš, I. Lukeš and E. Tóth, *Eur. J. Inorg. Chem*., 2012, 1975; (*b*) S. Aime, M. Botta, M. Fasano and E. Terreno, *Chem. Soc. Rev*., 1998, **27**, 19; (*c*) A. J. L. Villaraja, A. Bumb, M. W. Brechbiel. *Chem. Rev*., 2010, **110**, 2921.
12. (*a*) P. Caravan, J. J. Ellison, T. J. McMurry and R. B. Lauffer, *Chem. Rev.*, 1999, **99**, 2293; (*b*) M. Bottrill, L. Kwok and N. J. Long, *Chem. Soc. Rev*., 2006, **35**, 557.
13. Zheng-R. Lu, A. M. Mohs, Y. Zong and Y. Feng, *Int. J. Nanomedicine*, 2006, **1**, 31.
14. A. D. Sherry, P. Caravan and R. E. Lenkinski, *J. Magn. Reson. Imaging*, 2009, **30**, 1240.

15. (*a*) K. Wai-Y. Chan, S. Barra, M. Botta and Wing-T. Wong, *J. Inorg. Biochem*., 2004, **98**, 677; (*b*) S. Gu, Hee-K. Kim, G. H. Lee, Bong-S. Kang, Y. Chang and Tae-J. Kim, *J. Med. Chem*., 2011, **54**, 143; (*c*) A. Takács, R. Napolitano, M. Purgel, A. C. Bényei, L. Zékány, E. Brücher, I. Tóth, Z. Baranyai and S. Aime, *Inorg. Chem.*, 2014, **53**, 2858; (*d*) B. Jebasningh and V. Alexander, *Inorg. Chem*., 2005, **44**, 9434.
16. (*a*) S. Laurent, Jean-L. Bridot, L. V. Elst and R. N. Muller, *Future Med. Chem*., 2010, **2**, 427; (*b*) N. Lee and T. Hyeon, *Chem. Soc. Rev*., 2012, **41**, 2575; (*c*) F. Sousa, B. Sanavio, A. Saccani, Y. Tang, I. Zucca, T. M. Carney, A. Mastropietro, P. H. J. Silva, R. P. Carney, K. Schenk, A. O. Omrani, P. Huang, L. Yang, H. M. Ronnow, F. Stellacci and S. Krol, *Bioconjugate Chem*., 2017, **28**, 161; (*d*) Z. Zhen and J. Xie, *Theranostics*, 2012, **2**, 45.
17. R. Qiao, C. Yang and M. Gao, *J. Mater. Chem*., 2009, **19**, 6274.
18. C. C. Hanot, Y. S. Choi, T. B. Anani, D. Soundarrajan and A. E. David, *Int. J. Mol. Sci*., 2016, **17**, 54.
19. A. Bianchi, L. Calabi, F. Corana, S. Fontana, P. Losi, A. Maiocchi, L. Paleari and B. Valtancoli, *Coord. Chem. Rev*., 2000, **204**, 309.
20. A. L. Baert, *Encyclopedia of Imaging*, Springer, 2008, **2**, 481.
21. T. Grobner, *Nephrol. Dial. Transplant*., 2006, **21**, 1104.
22. (*a*) H. S. Thomsen, *Eur. Radiol*., 2007, **17**, 2692; (*b*) N. Nainani and M. Panesar, *Am. J. Nephrol*., 2009, **29**, 1; (*c*) D. R. Martin, *Pediatr. Radiol*., 2008, **38**, S125; (*d*) E. A. Sadowski, L. K. Bennet, M. R. Chan, A. L. Wentland, A. L. Garrett, R. W. Garrett and A. Djamali, *Radiology*, 2007, **243**, 148; (*e*) M. Sieber, P. Lengsfeld, J. Walter, H. Schirmer, T. Frenzel, F. Siegmund, H. Weinmann and H. Pietsch, *J. Magn. Reson. Imaging*, 2008, **27**, 955; (*f*) D. J. Todd and J. Kay, *Curr. Rheumatol. Rep*., 2008, **10**, 195; (*g*) S. E. Cowper, *Adv. Dermatol*., 2007, **23**, 131.
23. M. R. Bashir, L. Bhatti, D. Marin and R. C. Nelson, *J. Magn. Reson. Imaging*, 2015, **41**, 884.
24. S. Aime, D. D. Castelli, S. Geninatti, E. Gianolio and E. Terreno, *Acc. Chem. Res.*, 2009, **42**, 822.
25. (*a*) B. Drahoš, M. Pniok, J. Havlíčková, J. Kotek, I. Císařová, P. Hermann, I. Lukeš and É. Tóth, *Dalton Trans*., 2011, **40**, 10131; (*b*) J. S. Troughton, M. T. Greenfield, J. M. Greenwood, S. Dumas, A. J. Wiethoff, J. Wang, M. Spiller, T. J. McCurry and P. Caravan, *Inorg. Chem.*, 2004, **43**, 6313.
26. D. W. Christianson, *Prog. Biophys. Mol. Biol*., 1997, **67**, 217.

27. S. M. Rocklage, W. P. Cacheris, S. C. Quay, F. E. Hahn and K. N. Raymond, *Inorg. Chem*., 1989, **28**, 477.
28. J. T. Jorgensen, M. Rief, T. B. Brismar, M. Wagner and N. Albeiin, *Acta Radiol*., 2012, **53**, 707.
29. (*a*) H. U. Ahmed, A. Kirkham, M. Arya, R. Illing, A. Freeman, C. Allen and M. Emberton, *Nat. Rev. Clin. Oncol*., 2009, **6**, 197; (*b*) J. W. M. Bulte and D. L. Kraitchman, *NMR Biomed*., 2004, **17**, 484.
30. C. A. Helms, *Am. J. Roentgenol*., 1999, **173**, 234.
31. (*a*) T. H. Sin, J. S. Choi, S. Yun, I. S. Kim, H. T. Song, Y. Kim, K. I. Park and J. Cheon, *ACS Nano*., 2014, **8**, 3393; (*b*) N. A. Keasberry, M. Banobre-López, C. Wood, G. J. Stasiuk, J. Gallo and N. J. Long, *Nanoscale*, 2015, **7**, 16119.
32. (*a*) H. Yang, Y. Zhuang, Y. Sun, A. Dai, X. Shi, D. Wu, F. Li, H. Hu and S. Yang, *Biomaterials*, 2013, **32**, 4584; (*b*) A. Szpak, S. Fiejdasz, W. Prendota, T. Straczek, C. Kapusta, J. Szmyd, M. Nowakowska and S. Zapotoczny, *J. Nanopart. Res*., 2014, **16**, 2678; (*c*) G. H. Im, S. M. Kim, Dong-G. Lee, W. J. Lee, J. H. Lee and I. S. Lee, *Biomaterials*, 2013, **34**, 2069.
33. I. Solomon and N. Bloembergen, *J. Chem. Phys.*, 1956, **25**, 261.
34. (*a*) M. F. Ferreira, A. F. Martins, J. A. Martins, P. M. Ferreira, É. Tóth and C. F. G. C. Geraldes, *Chem. Commun.*, 2009, 6477; (*b*) M. Woods, S. Aime, M. Botta, J. A. K. Howard, J. M. Moloney, M. Navet, D. Parker, M. Port and O. Rousseaux, *J. Am. Chem. Soc*., 2000, **122**, 9781; (*c*) N. Iki, E. Boros, M. Nakamura, R. Baba and P. Caravan, *Inorg. Chem*., 2016, **55**, 4000.
35. (*a*) P. Caravan, *Acc. Chem. Res*., 2009, **42**, 851; (*b*) A. Datta and K. N. Raymond, *Acc. Chem. Res*., 2009, **42**, 938.
36. (*a*) E. M. Gale, N. Kenton and P. Caravan, *Chem. Commun*., 2013, **49**, 8060; (*b*) V. C. Pierre, M. Botta, S. Aime and K. N. Raymond, *Inorg. Chem*., 2006, **45**, 8355; (*c*) D. T. Puerta, M. Botta, C. J. Jocher, E. J. Warner, S. Avendano, K. N. Raymond and S. M. Cohen, *J. Am Chem. Soc*., 2006, **126**, 2222.
37. (*a*) P. H. Fries, C. Gateau and M. Mazzanti, *J. Am Chem. Soc*., 2005, **127**, 15801; (*b*) A. Nonat, M. Giraud, C. Gateau, P. H. Fries, L. Helm and M. Mazzanti, *Dalton Trans*., 2009, 8033; (*c*) N. Chatterton, C. Gateau, M. Mazzanti, J. Pécaut, A. Borel, L. Helm and A. Merbach, *Dalton Trans*., 2005, 1129.
38. (*a*) P. Caravan, C. T. Farrar, L. Frullano and R. Uppal, *Contrast Media Mol. Imaging*, 2009, **4**, 89; (*b*) M. Takahashi, H. Uematsu and H. Hatabu, *Eur. J. Radiol*., 2003, **46**, 45;

(*c*) P. Marzola, F. Osculi and A. Sbarbati, *Eur. J. Radiol.*, 2003, **48**, 165; (*d*) K. Uğurbil, G. Adriany, P. Andersen, W. Chen, M. Garwood, R. Gruetter, Pierre-G. Henry, Seong-G. Kim, H. Lieu, I. Tkac, T. Vaughan, Pierre-F. V. D. Moortele, E. Yacoub and Xiao-H. Zhu, *Magn. Reson. Imaging*, 2003, **21**, 1263.

39. M. Rohrer, H. Bauer, J. Mintorovitch, M. Requardt and H. J. Weinmann, *Invest. Radiol.*, 2005, **40**, 715.

Chapter II

A New Picolinate–Based High Relaxivity Gd(III) Complex as MRI Contrast Agent

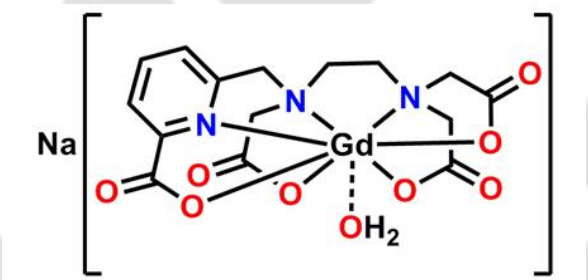

Na[Gd(peada)(H_2O)]; **2A**

r_1 = 6.08 $mM^{-1}s^{-1}$ per Gd(III)

2.1 Introduction

MRI is the most widely used non–invasive modern technique for imaging anatomical details. It exempts from ionising radiation by utilising ^{1}H NMR signal of water molecules present inside the body. The images are obtained from the differences in relaxation times developed in different environment of the tissues. The unique properties of Gd(III) ion with its high magnetic moment (S = 7/2) and long electronic relaxation time make it ideal for enhancing the image contrast by significantly decreasing the T_1 relaxation time. Currently, approximately 50% of all MRI scans are made after administration of a Gd(III)–based CA. To date, Gd(III) complexes of poly(aminocarboxylate) based ligands such as DTPA (diethylenetriaminepentaacetic acid) and DOTA (1,4,7,10–tetraazacyclododecane–1,4,7,10–tetraacetic acid) having one coordinated water molecule are most widely used.[1] However, relative to the theoretically attainable maximum, these CAs show lower relaxivity values. On the basis of well established SBM theory of contrast agents, this lower relaxivity is due to the difference in real and optimal values of the parameters determining relaxivity enhancement. Hence, a continuing research area of interest remains for the development of contrast agents with higher relaxivity value. Although large efforts have been made in optimising the parameters that enhance relaxivity, the mechanisms and coordination properties underlying the electronic relaxation of Gd(III) complexes still remain poorly understood.[2]

Higher relaxivity value, irrespective of field strength can be achieved by increasing the number of inner sphere water molecules (q). A few Gd(III) complexes with $q > 1$ have been reported till now as the increase in inner sphere water molecules may lead to decrease in thermodynamic stability which could in turn lead to *in vivo* toxicity. Gd(III) complexes containing picolinate group(s) have shown interesting properties to use them as MRI contrast agents.[3] Different polydentate ligands having picolinate groups are shown in **Scheme 2.1**. The Gd(III) complexes of these ligands with $q \geq 1$ have already been investigated with sufficient thermodynamic stability and better relaxivity values.[4] The picolinate groups present in the ligand backbone have important concern regarding the increased relaxivity on its Gd(III) complexes. Also, the facile funtionalisation of the picolinate group made these ligands attractive candidates for potential MRI contrast agents.[5]

The Gd(III) complexes of picolinate group containing ligands showed higher relaxivity values in the range 4.55–13.30 $mM^{-1}s^{-1}$ (20–60 MHz, at 25 ºC).[3,4] In fact, without having coordinated water molecule, the Gd(III) complex of nonadentate ligand H_3tpatcn showed a

relaxivity value of 5.3 $mM^{-1}s^{-1}$ at low field (< 1 MHz) which had been interpreted in terms of a favourable electronic relaxation rate.[4b] However, due to lower water solubility of some of the complexes, thorough investigation on the properties of the complexes is still under progress. Also, the Gd(III) complexes of picolinate based ligands are known to cause very high water exchange rate which in turn is responsible for showing high relaxivity values of the complexes. This high water exchange rate is related to the presence of a very flexible inner coordination sphere around the metal centre.[4a]

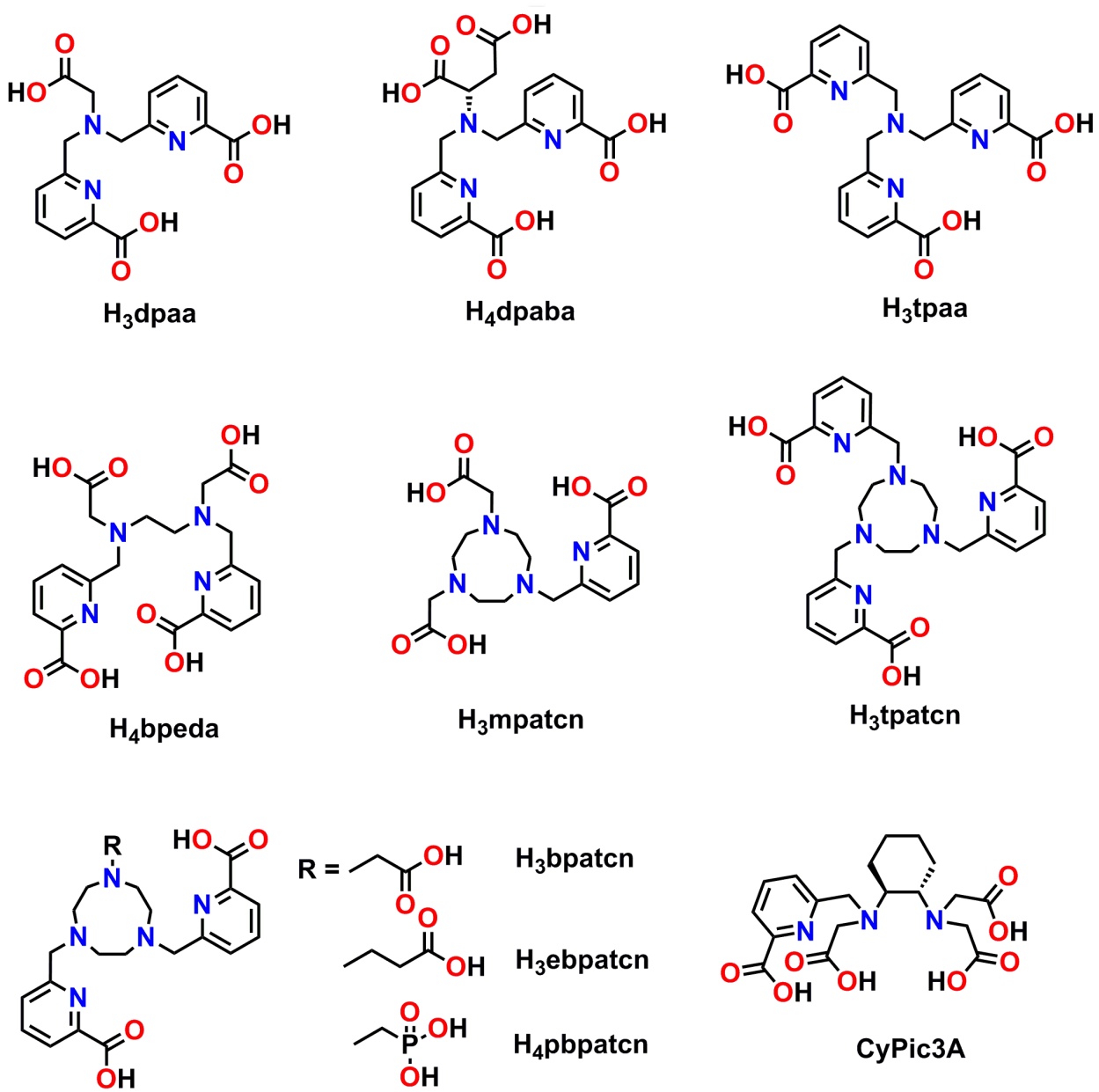

Scheme 2.1. Ligands containing picolinate group(s).

In 2005, Chatterton *et al*. reported a picolinate based ligand H_4bpeda (**Scheme 2.1**), which showed relatively lower stability of its Gd(III) complex in comparison to that of EDTA ligand.[4g] In spite of the presence of two pyridine units in ligand H_4bpeda, the lower stability was explained as a result of lower contribution of the metal–nitrogen bond to complex stability. However, it has also been investigated that the presence of picolinate moiety in the ligand backbone can modulate the water exchange rate on its Gd(III) complexes and the highest water exchange rate (k_{ex}^{298} = 8.8 × 10^8 s^{-1}) was measured for the Gd(III) complex of picolinate containing ligand *N*,*N*′–bis(6–carboxy–2–pyridylmethyl)ethylenediamine–*N*,*N*′–methyl–enephosphonic acid.[4c]

Herein, in order to impose water solubility, as well as to attain higher relaxivity value, a new ligand H_4peada having one picolinate group and carboxylate pendants, and its corresponding Gd(III) complex, **2A** were synthesised. The ligand being hepta–coordinated, would allow maximum two water molecules to bind to the Gd(III) centre and consequently higher relaxivity values could be obtained. Also, due to the fact that Gd(III) complexes of hexa– or hepta–coordinate ligands have fast water exchange rates than the complexes with octa–coordinate ligands, a higher relaxivity value was expected for complex **2A**.

2.2 Synthesis and Characterisation of Ligand H_4peada, $C_{15}H_{19}N_3O_8$

A schematic representation for the synthesis of ligand H_4peada is shown in **Scheme 2.2**.

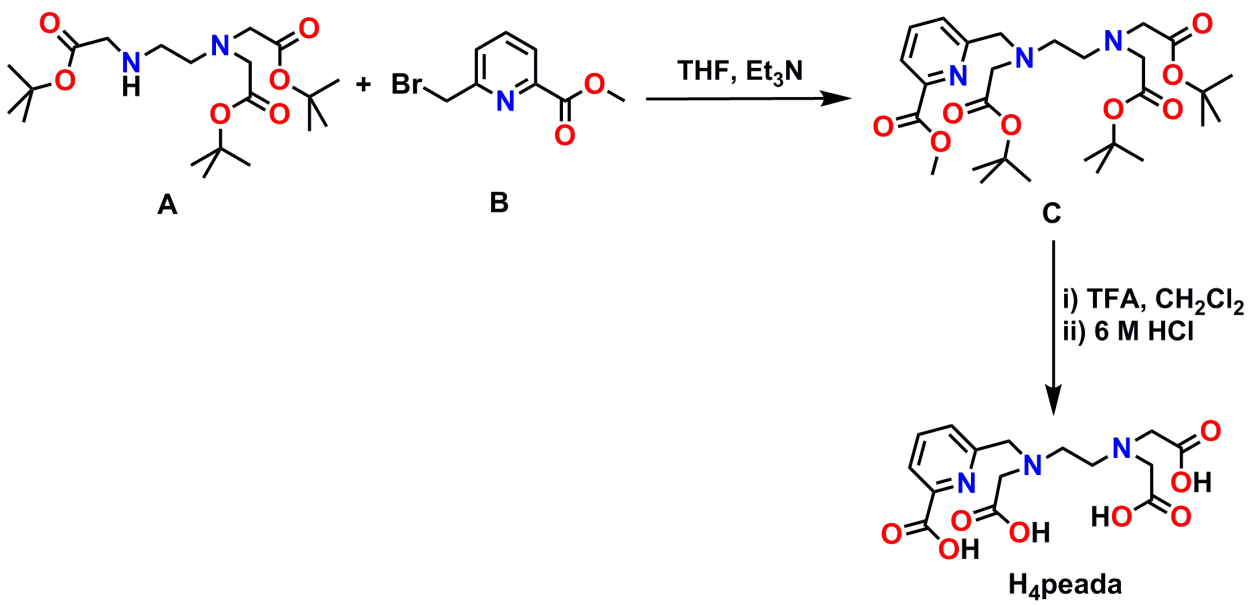

Scheme 2.2. Synthetic route of ligand H_4peada.

N,*N*′,*N*′–tris(*tert*–butyloxycarbonylmethyl)ethylenediamine (**A**) and 6–(bromomethyl) pyridine–2–carboxylate (**B**) were prepared by slightly modified procedures comparison to the previously reported procedures.[6] A reaction between ethylenediamine and *tert*–butylbromoacetate (1:2) in the presence of Et_3N, provided (**A**), which upon reacting with equimolar amount of 6–(bromomethyl)pyridine–2–carboxylate (**B**) in the presence of Et_3N provided **C.** The ligand H_4peada was obtained as a pale yellow solid after successive treatment of compound **C** with trifluoroacetic acid and 6 M HCl. The ligand was characterised by using FTIR spectroscopy, mass spectrometry, and NMR spectroscopy techniques.

Infrared (IR) spectrum of ligand H_4peada is shown in **Figure 2.1**. It showed a band at 3392 cm^{-1} due to *ν*(O–H) stretching.[7a] The bands appeared in the region around 3000 cm^{-1} was due to aromatic and aliphatic C–H stretching.[7b] The observed band ~ 2600 cm^{-1} was due to the H–bonded O–H of the carboxylic acid group.[7c] The stretching frequency for C=O group appeared as a sharp band at 1735 cm^{-1}.[7a] The band observed at 1414 cm^{-1} was due to in plane O–H bending.[7d] The *ν*(C–O) stretching band appeared at 1262 cm^{-1}.[7c]

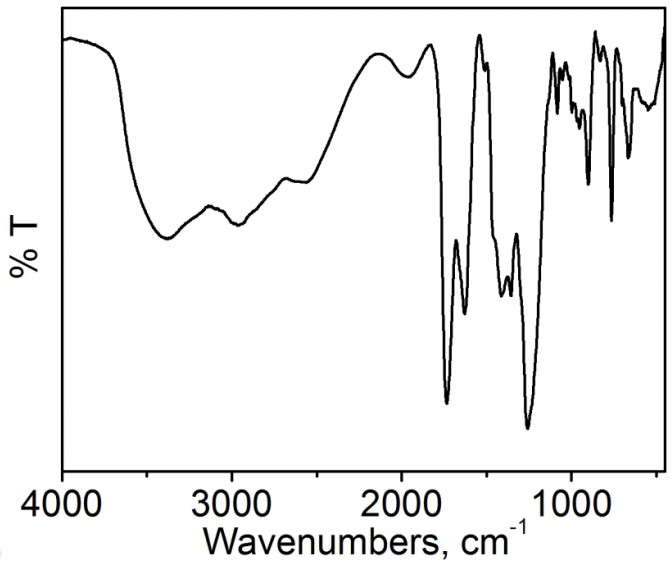

Figure 2.1. FTIR spectrum of ligand H_4peada.

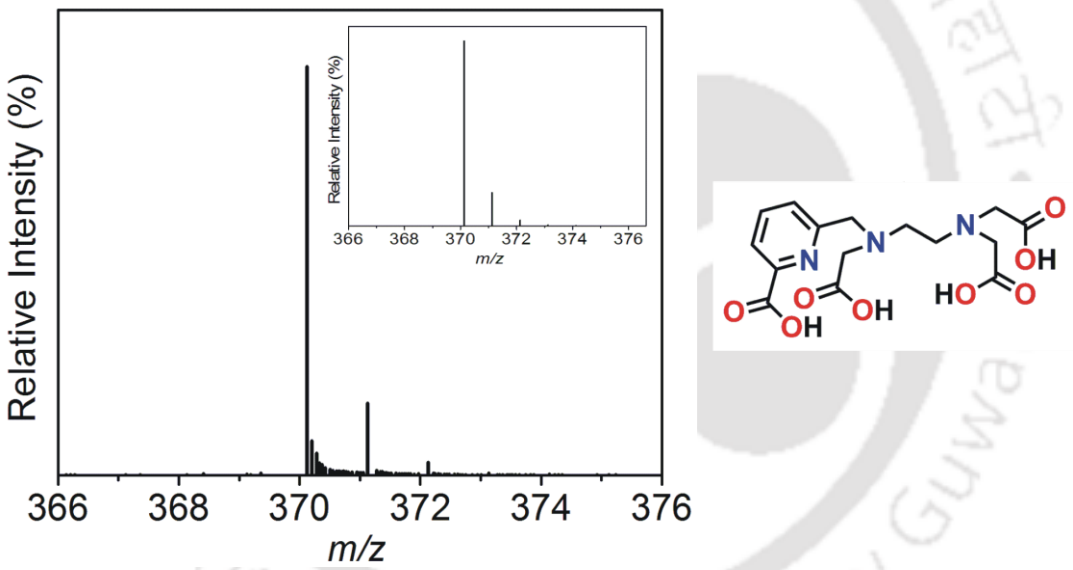

Figure 2.2. ESI–MS spectrum of ligand H_4peada. Simulated spectrum is shown as inset.

The electrospray ionisation mass spectrum measurement of the ligand in the positive mode in HPLC grade MeOH, provided a 100% molecular ion peak at *m/z* = 370.1258 amu. The peak corresponded to the composition $[C_{15}H_{19}N_3O_8 + H]^+$ (*m/z* = 370.1244 amu) as evident by isotope pattern distribution analysis (**Figure 2.2**).

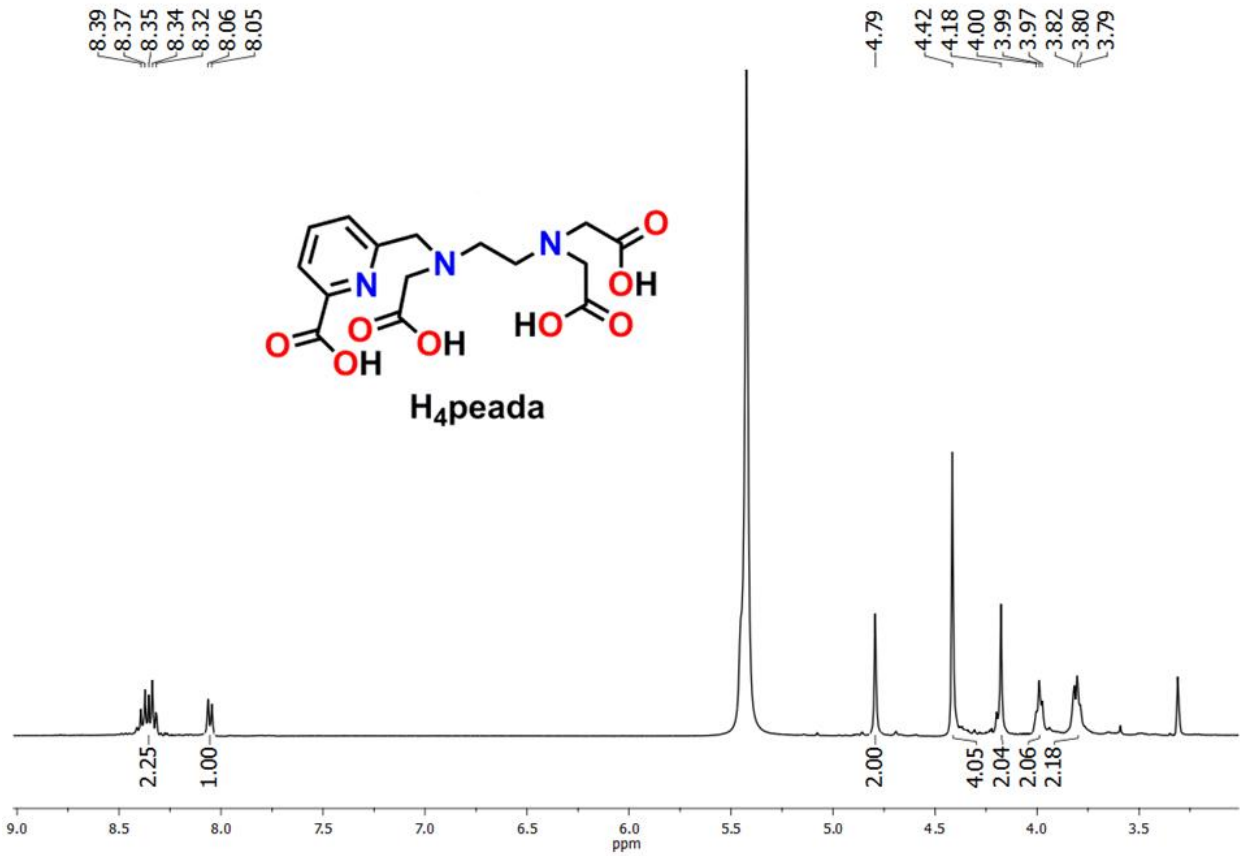

Figure 2.3. ^{1}H NMR spectrum of ligand H_4peada.

^{1}H NMR spectrum of ligand H_4peada is shown in **Figure 2.3**. The signals in the region 8.39–8.05 ppm were due to three aromatic protons present in the pyridine unit. The singlets at 4.79, 4.42, and 4.18 ppm were due to eight hydrogen atoms attached to ethylenediamine moiety. The multiplets in the region 4.00–3.79 ppm were because of four –CH_2 protons present in the ligand backbone. ^{13}C NMR spectrum (**Figure 2.4**) of the ligand showed 13 characteristic peaks for 13 different kinds of carbon atoms.

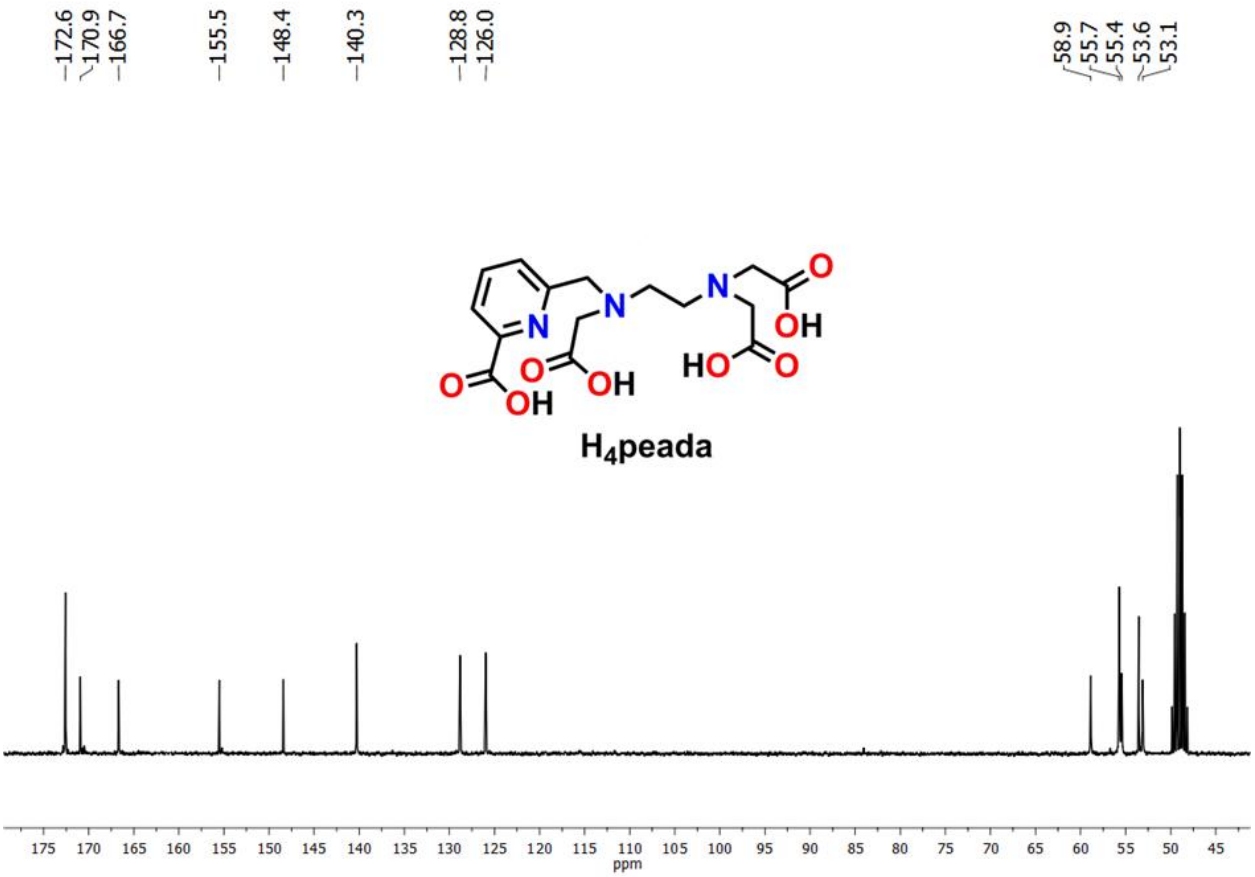

Figure 2.4. ^{13}C NMR spectrum of ligand H_4peada.

2.3 Synthesis and Characterisation of Gd(III) Complex of Ligand H_4peada, 2A

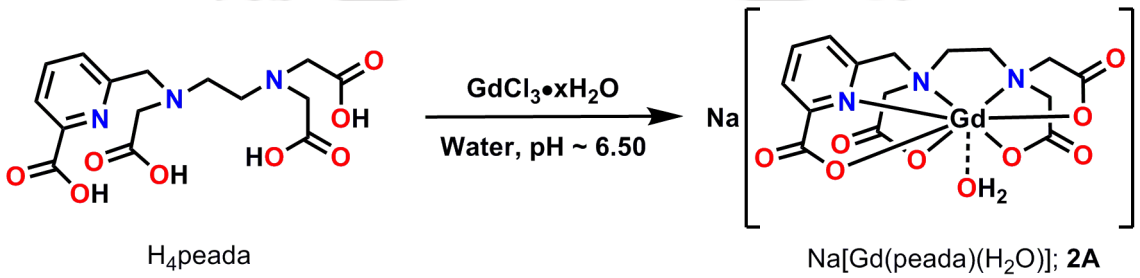

Scheme 2.3. Synthesis of complex **2A**, $[C_{15}H_{17}GdN_3O_9Na]$.

To a solution of ligand H_4peada in water, $GdCl_3 \bullet xH_2O$ was added and stirred the reaction mixture at room temperature (25 °C) until complete dissolution. The pH was then adjusted to ~ 6.50 by adding aq. NaOH solution drop wise. After stirring the reaction mixture at room

temperature for another 24 h, the resultant solution was kept at room temperature for slow evaporation of water. The white solid obtained was then washed several times with MeOH and formation of the complex was confirmed by using mass spectrometry and FTIR spectroscopy.

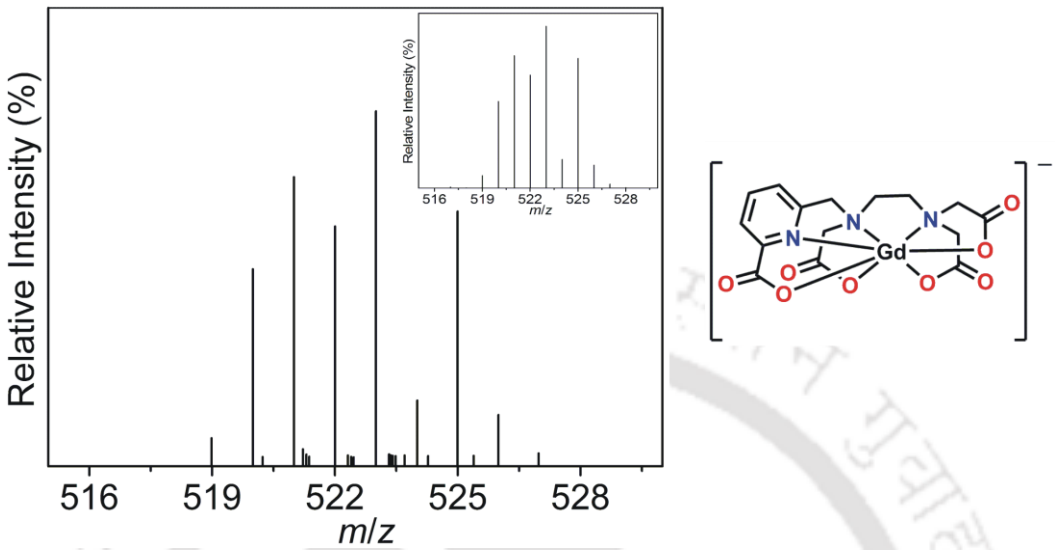

Figure 2.5. ESI–MS spectrum of complex **2A**. Simulated spectrum is shown as inset.

The electrospray ionisation mass spectrum measurement in negative mode of complex **2A** in Mili Q water, provided a 100% molecular ion peak at *m/z* = 523.0028 amu. The peak corresponded to the composition $[C_{15}H_{15}GdN_3O_8]^-$, (*m/z* = 523.0057 amu) as evident from isotope pattern distribution analysis (**Figure 2.5**).

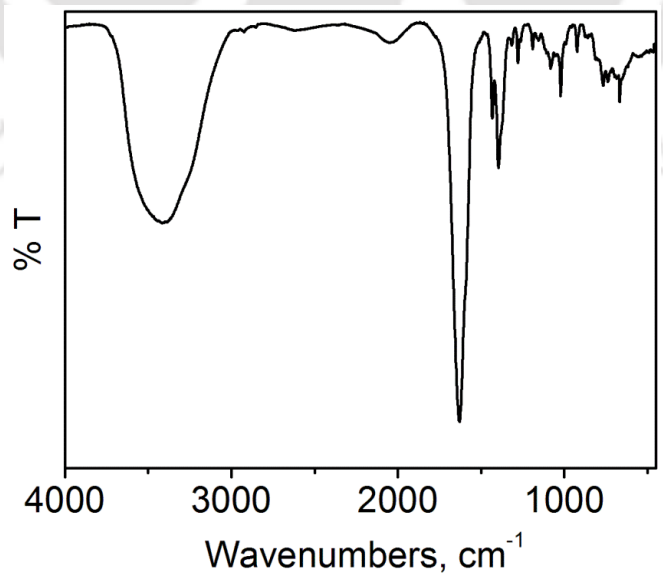

Figure 2.6. FTIR spectrum of complex **2A**.

Infrared (IR) spectrum (**Figure 2.6**) of complex **2A** showed a sharp band at 3396 cm^{-1} due to *ν*(O–H) stretching. The formation of the complex was confirmed from the *ν*(C=O) stretching frequency, which appeared as a sharp band at 1630 cm^{-1} for the complex whereas that of the ligand was observed at 1735 cm^{-1}.

2.4 Xylenol Orange Test for Determination of Free Gd(III) in Complex 2A

Free Gd(III) ion is highly toxic for living organism. With similar size to that of Ca(II), it can bind to Ca(II) binding enzymes and affects voltage–gated calcium channels, and therefore, lead to adverse biological effects. Also, Gd(III) is neurotoxic in nature and it inhibits mitochondrial functions and induces oxidative stress.[8] For these reasons it is very important to determine the amount of free Gd(III) ion present in the complex before using it as MRI contrast agent.

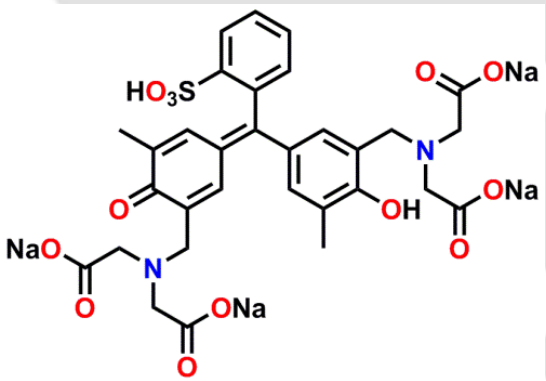

Figure 2.7. Stucture of xylenol orange (XO).

The amount of free Gd(III) ion in a solution can be conveniently determined by using complexometric indicator, xylenol orange, which shows different colour in the presence of different concentrations of free Gd(III).[9] Due to the lower thermodynamic stability of Gd(III)–xylenol orange complex (log K = 5.8)[10] compared to the commercially available Gd(III)–based MRI CAs and their derivatives, xylenol orange can only form chelate with the free Gd(III) ions.

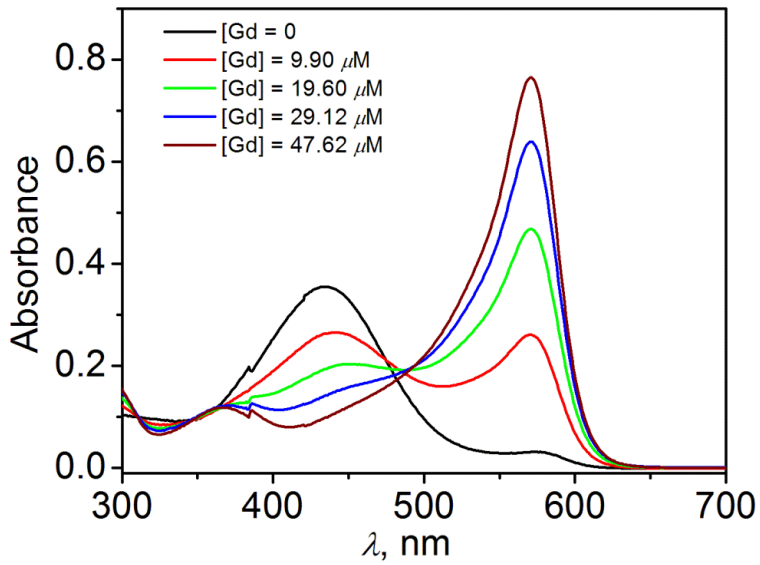

Figure 2.8. UV–vis spectra of xylenol orange solutions in acetate buffer (pH = 5.8) in the presence of varied concentrations of free Gd(III) ions, from zero to 47.62 μM.

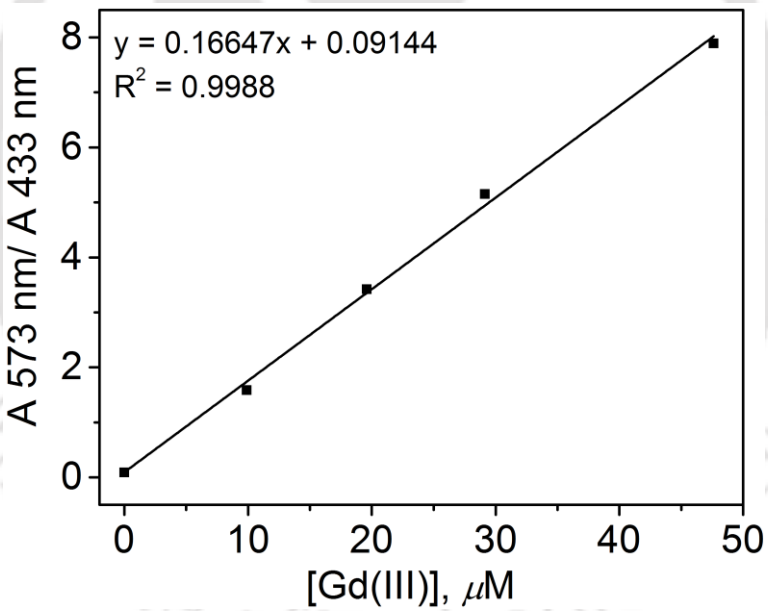

Figure 2.9. Calibration curve obtained from the spectrophotometric changes of xylenol orange (in acetate buffer pH = 5.8) absorptions in the presence of varied concentrations of Gd(III) ions.

The colour of aqueous solution of xylenol orange varies with change in pH of the solution. In acidic or neutral pH, the colour is yellow whereas in basic medium, the colour of the solution is violet. The coordination of Gd(III) ion takes place through the involvement of two iminodiacetic acid moiety and the phenolic oxygen (**Figure 2.7**). At higher pH also, deprotonation of the phenolic –OH group leads to an extended delocalisation which in turn

changes the colour from yellow to violet. So, during the whole experiment it is very important to control the pH of the solution at slightly acidic, as at basic condition, xylenol orange itself shows violet colour even in the absence of Gd(III) ion.

Figure 2.8 shows the UV–vis spectra of xylenol orange solutions in acetate buffer (pH = 5.8) in the presence of different concentrations of Gd(III) ion from zero to 47.62 μM. The acetate buffer solution of xylenol orange showed two absorption maxima at 433 nm and 573 nm, respectively. The increasing concentration of Gd(III) caused a decrease in the band at 433 nm, whereas the band at 573 nm got increased. A linear calibration curve was obtained from the ratio of the absorbance values at 573 and 433 nm *vs.* Gd(III) ion concentration (**Figure 2.9**). In order to estimate free Gd(III) ion in complex **2A**, 50 μL of the complex solution (concentration = 27.5 mM) was added to 2.0 mL of the xylenol orange solution (pH = 5.8). The inclusion of the ratio of absorbance values at 573 and 433 nm of complex **2A** (A_{573}/A_{433} = 0.0987) in the calibrated curve showed 0.04 μM concentration of the free Gd(III) ion in the solution, which was in negligible amount. This experimental fact indicated the presence of very low concentration of free Gd(III) ion in the complex solution.

2.5 Determination of Number of Coordinated Water Molecules (q)

Several attempts to grow single crystal of complex **2A,** suitable for X–ray diffraction analysis from various organic solvents and from water were not successful. So, in order to find out the number of metal coordinated water molecules (*q*) in the complex, its Tb(III) congener (complex **2B**) with luminescence property was synthesised by reacting an equimolar amount of ligand H_4peada and $TbCl_3$•$6H_2O$ in water at pH ~ 6.5 under refluxing condition.

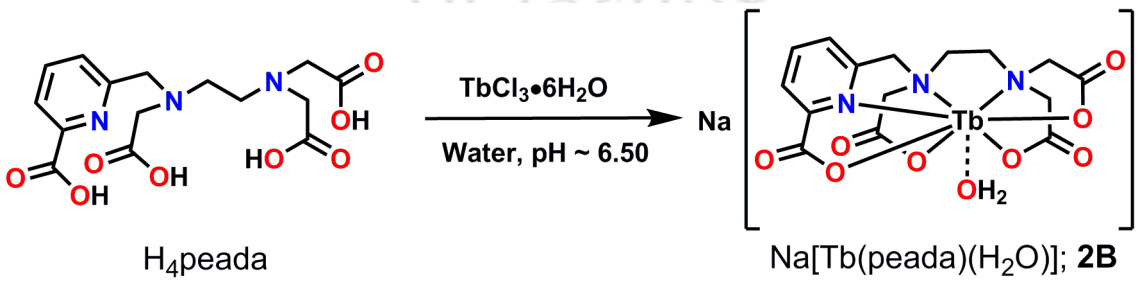

Scheme 2.4. Synthesis of complex **2B**, $Na[C_{15}H_{17}TbN_3O_9]$.

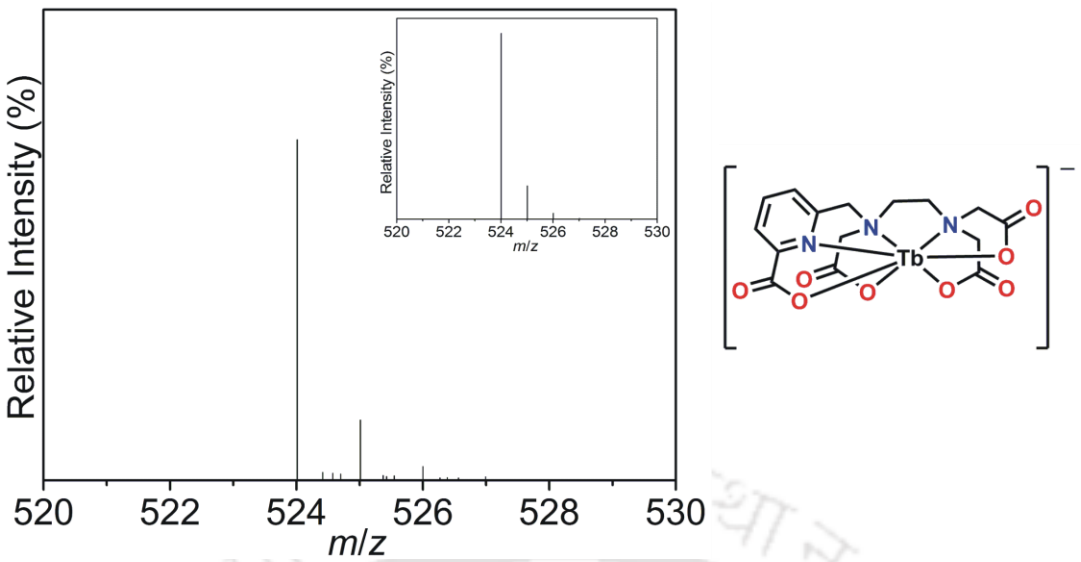

Figure 2.10. ESI–MS spectrum of complex **2B**. Simulated spectrum is shown as inset.

A 100% molecular ion peak was found at 524.0112 amu (**Figure 2.10**) in the ESI mass spectrum of complex **2B**, which corresponded to $[C_{15}H_{15}TbN_3O_8]^-$ composition (*m/z* = 524.0113 amu) and supported the formation of the complex.

The quenching of the lanthanide excited states through non–radiative energy transfer takes place where an abundance of O–H oscillators are present.[11] O–H oscillators are found to be the most efficient quenchers of metal–centred luminescence both in solution and in the solid state. Other vibrational overtones of N–H, C–H and C=O can also quench the luminescence of lanthanide ions, but not to that extent as O–H oscillators. The extent of this quenching is also related to the energy gap between the emissive state and the ground state of the metal ion and with respect to the energy gap requirement, the $^7F_0 \rightarrow {}^5D_0$ transition in Eu(III) and the $^7F_6 \rightarrow {}^5D_4$ in Tb(III) analogues of Gd(III) chelates permits the determination of number of coordinated water molecules (*q*) *via* time dependent luminescence lifetime decay. When O–H oscillator is replaced by O–D one in deuterated solvent, it results in less efficient quenching of the lanthanide excited states. Hence, in D_2O, the luminescence lifetimes of Eu(III) and Tb(III) are much longer than those in H_2O. This difference in luminescence lifetimes of the excited state is related to the number of coordinated water molecules by modified Horrock's equation,[12]

$$q = A\,(1/\,\tau_{H_2O} - 1/\,\tau_{D_2O} - B)$$

where A and B are constants specific to each individual lanthanide (**Table 2.1**), and τ_{H_2O} and τ_{D_2O} are the lifetime of the lanthanide complex in H_2O and D_2O respectively.

Table 2.1. A and B values for different lanthanides[12e]

Ln(III)	A (ms)	B (ms^{-1})
Eu(III)	1.2	(0.25 + 0.075*x*) *x* = the number of exchangeable N–H oscillators
Tb(III)	5	0.06

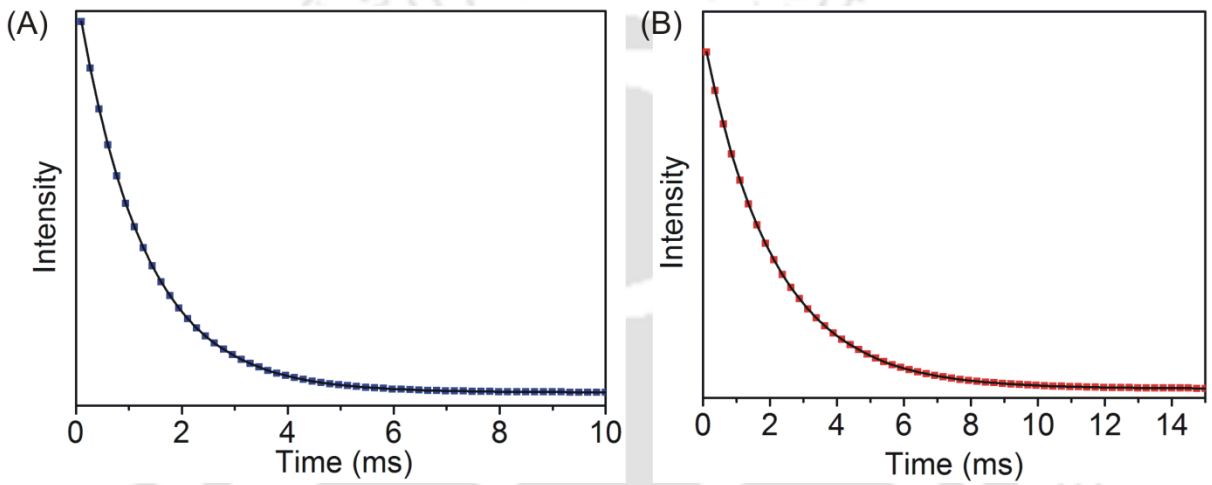

Figure 2.11. Lifetime measurements of complex **2B** in (A) H_2O, and (B) D_2O.

A 10 μM solution of complex **2B** prepared in 10 mM HEPES buffer (pH = 7.4, and at 25 °C) was used for the luminescence lifetime measurements. To determine the luminescence lifetime decay in H_2O, first the solution was excited at 270 nm and emission was recorded at 544 nm. The same solution was then evaporated completely by spin concentration under reduced pressure and addition of equal volume of D_2O to the completely dry residue resulted in solution of same concentration of the complex in D_2O buffer. The luminescence lifetimes of the complex, τ_{H_2O} = 1.24 ms and τ_{D_2O} =2.10 ms were then obtained by fitting decay curves with single exponential model using non–linear least square method and goodness of the fits were determined by minimizing the reduced Chi^2 values. The *q* value was found to be **1.4±0.1**; which implied the coexistence of both mono(aquated) and bis(aquated) complexes almost in equal quantity in solution state at pH = 7.4 and temperature 25 °C (**Figure 2.12**).

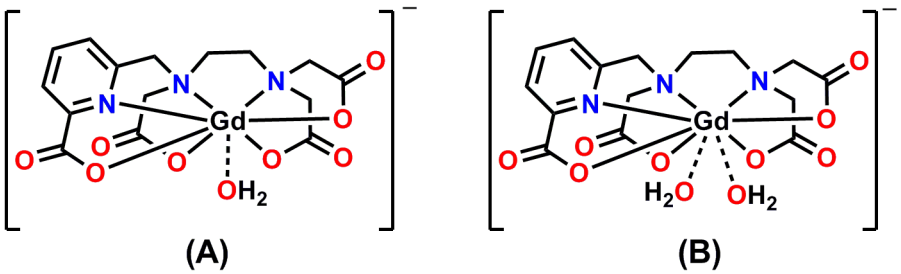

Figure 2.12. (A) Mono(aquated) and (B) bis(aquated) Gd(III) complexes of ligand H_4peada exist in aqueous solution at pH = 7.4 and 25 °C.

2.6 Stability of Complex 2A

To avoid toxicity related to free Gd(III) ion, the Gd(III) complexes need to be thermodynamically stable. When used under physiological conditions, pM value of a metal–ligand complex is considered to be the accurate method for describing the stability of the complex, where pM is $-\log[M^{n+}]_{free}$ at pH = 7.4, 25 ºC having [M] = 1 μM and $[L]_{total}$ = 10 μM.[5f,13]

At constant pH = 7.4, the protonation equilibria of the ligand can be neglected and under equilibrium condition,

$M + L \longleftrightarrow ML$

$M + C \longleftrightarrow MC$

where M is the metal ion, L is the ligand and C is the competing ligand used.

The formation constants for the above reactions are given by,

$\beta_{ML} = [ML]/[M][L]$ and $\beta_{MC} = [MC]/[M][C]$

Since standard conditions are used at pH 7.4, these formation constants can be considered as conditional stability constants. The difference in the logarithimic values of formation constants will now equivalent to the difference in pM values.

Now, $pM_{ML} - pM_{MC} = \log \beta_{ML} - \log \beta_{MC}$

$= \log ([ML]/[M][L]) - \log ([MC]/[M][C])$

$= \log ([ML][C] /[MC][L])$

$= \log ([ML]/[MC]) + \log ([C]/[L])$

This equation is primarily used to determine the pM value of the ligand and can be rearranged to:

$$-\log ([ML]/[MC]) = \log ([C]/[L]) - (pM_{ML} - pM_{MC})$$

or $\log ([MC]/[ML]) = \log ([C]/[L]) + \Delta pM$

where $\Delta pM = pM_{MC} - pM_{ML}$

Now the plot of log ([MC]/[ML]) *vs.* log ([C]/[L]) directly gives the difference in pM value between the ligand and the competing ligand (ΔpM), when log ([MC]/[ML]) = 0 or when the concnetration of the competing ligand generates a equal partition of the metal between the ligand and the competing ligand.

A competition batch titration method was used to determine the pGd value of ligand H_4peada by using DTPA (diethylenetriaminepentaacetic acid) as the competing ligand. DTPA was used as a competing ligand as this ligand is easily accessible, and $[Gd(DTPA)(H_2O)]^-$ complex, Magnevist® has been successfully used as a commercial MRI CA. Throughout the experiment, the pH of all solutions was kept constant at 7.4 by using 10 mM HEPES buffer. Different volumes of DTPA were added to constant concentrations of ligand H_4peada and Gd(III), and all the solutions were kept for 24 h at 25 ºC to ensure thermodynamic equilibrium. The concentrations of the free and complexed ligand in each solution were then determined by using UV–vis spectroscopy.

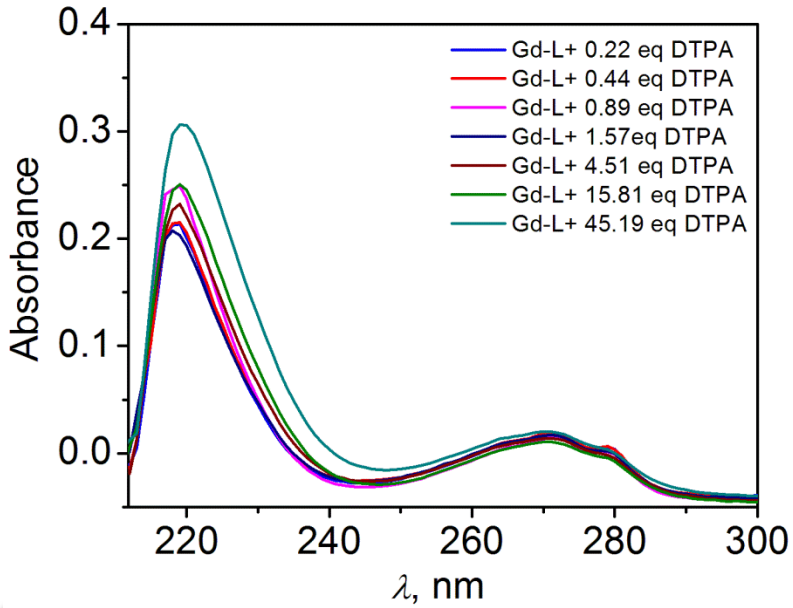

Figure 2.13. Spectral changes during the competition titration of ligand H_4peada against DTPA, (L in the figure represents ligand H_4peada).

The spectral changes during competition batch titration of ligand H_4peada against DTPA is shown in **Figure 2.13**. The uv–visible spectrum of Gdpeada with 0.22 equivalent of DTPA showed absorption at 272 nm along with another small peak at 279 nm. This trend in uv–visible spectra was observed till the addition of 4.51 equivalent of DTPA. Upon addition of 15.81 equivalent of DTPA, the small peak at 279 nm was found to be less intense and was almost diminished upon addition of 45.19 equivalent of DTPA.

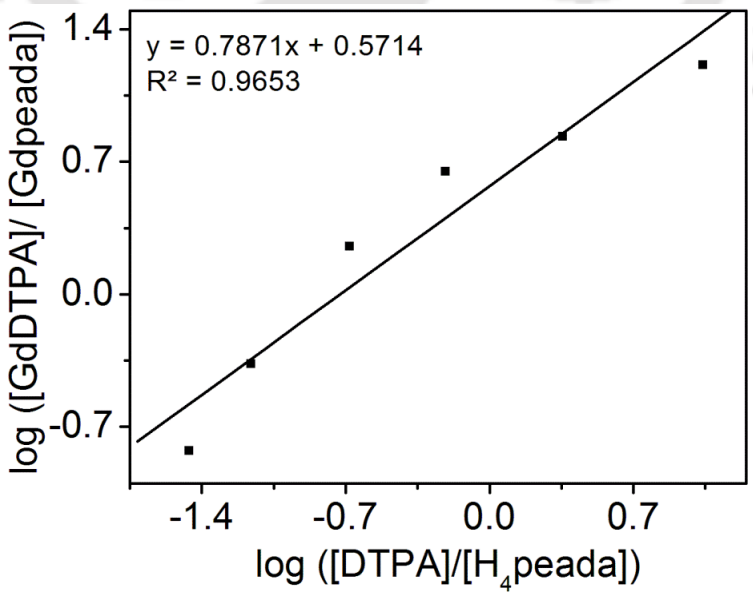

Figure 2.14. Competition titration of ligand H_4peada against DTPA.

From the plot of log ([DTPA]/[H_4peada]) *vs*. log ([GdDTPA]/[Gdpeada]), the difference in pGd value of ligand H_4peada and that of DTPA (ΔpGd) was found. This difference was the value of log ([DTPA]/[H_4peada]) when log ([GdDTPA]/[Gdpeada]) = 0 or when the concentration of DTPA generates an equal partition of Gd(III) between the ligand H_4peada and DTPA. Using the known value of pGd of DTPA 19.1,[13g] the pGd value of ligand H_4peada was found to be 18.4. Although this value was slightly less than that of the commercially available DTPA, yet complex **2A** showed better stability than the previously reported Gd(III) complexes of picolinate based ligands. **Table 2.2** shows pGd values of some of the picolinate based ligands at pH = 7.4 and 25 ºC.

Table 2.2. pGd values calculated for picolinate based ligands.[4f]

Ligand	pGd (pH = 7.4, 25 ºC)
H_3tpatcn	14.9
H_4pbpatcn	14.1
H_4dpaba	13.3
H_4peada	**18.4**

2.7 Longitudinal Relaxivity Measurement of Complex 2A at 1.41 T

The longitudinal relaxivity, r_1 of complex **2A** was measured at 1.41 T in a BRUKER minispec mq60 NMR analyzer.

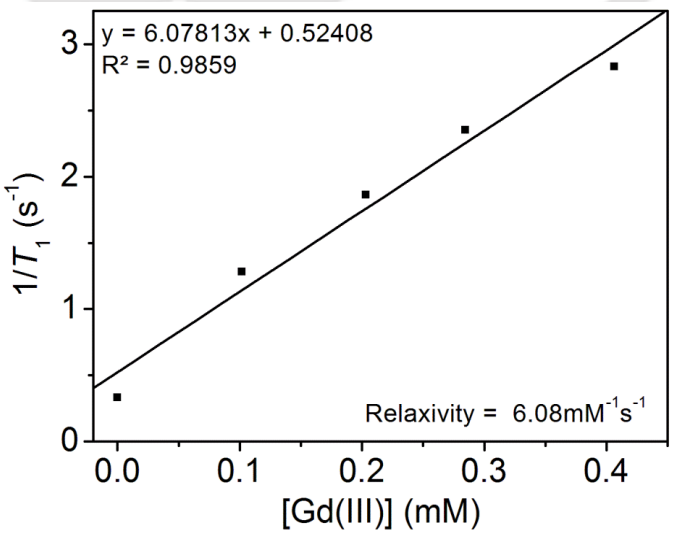

Figure 2.15. $1/T_1$ *vs.* [Gd(III)] plot. Measurements were performed using complex **2A** at 1.41 T, 25 °C, and pH ~ 7.4.

By using inversion recovery method, at four different concentrations of the complex, the longitudinal relaxation times (T_1) were measured. From the slope of the plot of longitudinal relaxation rate, $1/T_1$ *vs.* [Gd(III)], the r_1 relaxivity of the complex was found to be 6.08 $mM^{-1}s^{-1}$ (at 25 ºC and pH ~ 7.4) per Gd(III) ion. The exact Gd(III) ion concentration was determined by ICP–AES method.

While the r_1 relaxivity of the commercially available MRI CAs are in the range 4.4–5.2 $mM^{-1}s^{-1}$, the value obtained from complex **2A** was better to use it as an efficient MRI contrast agent. It has been found that for small ploy(aminocarboxylate) based Gd(III) complexes, one inner sphere water molecule contributes around 3.0 $mM^{-1}s^{-1}$ of its r_1 relaxivity value. So, the presence of two inner sphere water molecules in complex **2A** accounted for its increased relaxivity value. Also, the presence of picolinate group in the ligand backbone, creating a flexible coordination environment in the system and the fast water exchange rate of the complex (as picolinate based Gd(III)–based complexes are known to have highest water exchange rate)[3,4] were important factors for enhancing the r_1 relaxivity value.

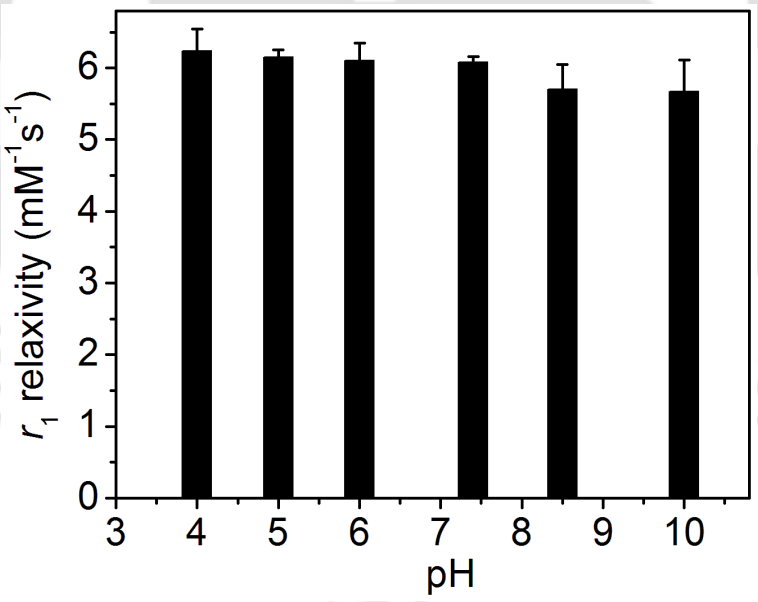

Figure 2.16. Longitudinal relaxivity measurement of complex **2A** in pH range 4–10, at 1.41 T and 25 °C.

In pH range 4–10, at different pH, the r_1 relaxivity values of complex **2A** were measured (at 1.41 T, and 25 ºC) to know its behaviour besides physiological pH 7.4. The results are depicted in **Figure 2.16**. A slight increase in r_1 relaxivity value was observed towards lower pH (at pH = 4, Δr_1 = +0.16 $mM^{-1}s^{-1}$), while at higher pH, r_1 relaxivity value decreased to 5.17 mM^{-}

$^{1}s^{-1}$ (at pH = 10) from 6.08 $mM^{-1}s^{-1}$. This decrease in relaxivity could be due to the formation of hydroxy species at higher pH by replacing one inner sphere water molecule.[4a]

2.8 Affinity for Physiological Anions

A potential drawback of Gd(III) complex having coordinated water molecule is the replacement of the water molecule by endogenous anions in serum which are present in non–negligible concentrations. This replacement of water molecule results in sharp decrease in relaxivity value with the formation of ternary adducts. Previous investigations on picolinate based Gd(III) complexes showed decrease in the r_1 relaxivity values due to the formation of adducts with the endogenous anions phosphate (PO_4^{3-}) and bicarbonate (HCO_3^-), whose concentrations in serum are 0.38 mM and 24.5 mM respectively.[2f] Because of the strong affinity of serum fluoride ion for lanthanides and formation of stable complex, fluoride ion (F^-) is also included in this study.[14]

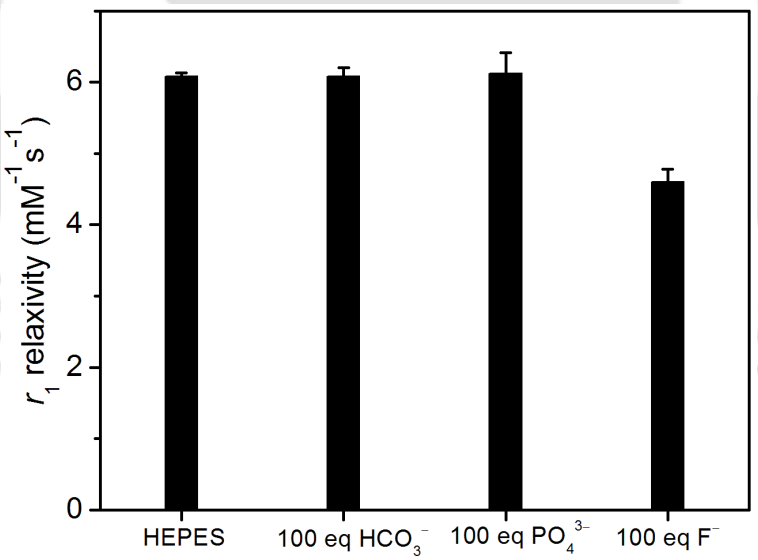

Figure 2.17. Relaxivity measurements of complex **2A** in the presence of 100 equivalents of different anions **(**at 1.41 T, 25 °C, pH ~ 7.4, [complex **2A**] = 0.5 mM, and [physiological anions] = 50 mM).

The affinity of PO_4^{3-}, HCO_3^-, and F^- ions for complex **2A** was investigated by r_1 relaxivity measurements in the presence of 100 equivalents of the respective anions (experimental conditions: 1.41 T, 25 °C, pH ~ 7.4, [complex **2A**] = 0.5 mM, [physiological

anions] = 50 mM). The result showed that in case of phosphate and bicarbonate ions, r_1 relaxivity values remained same, whereas in case of fluoride ion, r_1 relaxivity value dropped to 4.6 $mM^{-1}s^{-1}$ (Δr_1 = –1.48 $mM^{-1}s^{-1}$) which was due to a binding interaction of F^- ion replacing inner sphere water molecule of the complex. The results are summarized in **Figure 2.17**.

2.9 Affinity for Physiological Cations

Another important parameter for determining toxicity of Gd(III) complexes is their selectivity over other endogenous metal ions. Being very labile in nature, transmetallation can also occur very easily in these complexes with the ions, which are present in non–negligible concentrations in blood serum in non–complexed form. The chemical instability of the Gd(III) chelate can lead to exchange with these metal ions, which in turn can have biological consequences such as accumulation of Gd(III) in bones, interaction with metal dependent biological systems such as metalloenzymes, etc.[15] The selectivity of ligand H_4peada for Gd(III) over Zn(II) and Cu(II) (whose concentrations in serum are 50 μM and 1 μM respectively)[16] was included in this study.

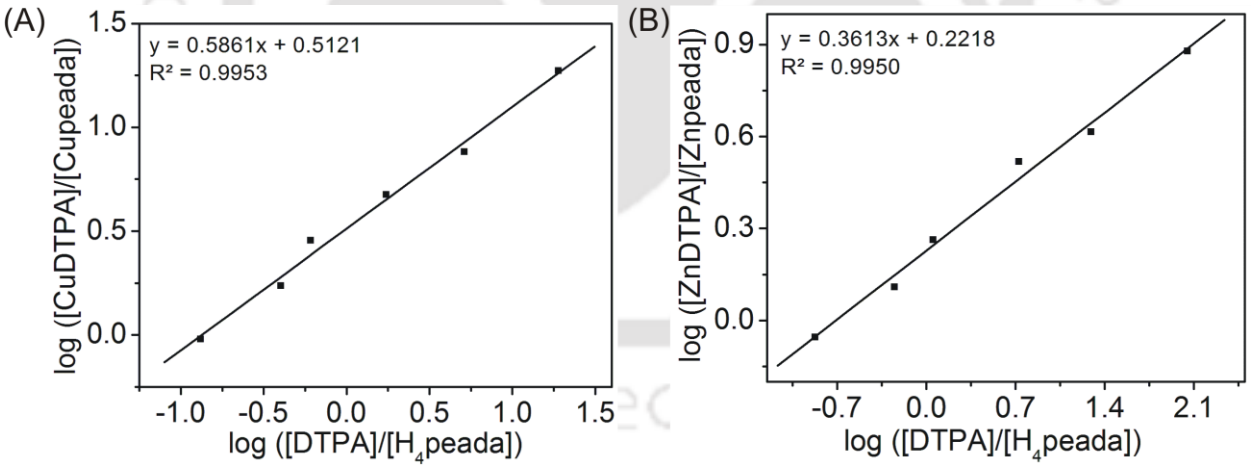

Figure 2.18. Competition batch titrations for determining (A) pCu, and (B) pZn of ligand H_4peada against DTPA. The *x*–intercepts indicated the differences in pM between H_4peada and DTPA.

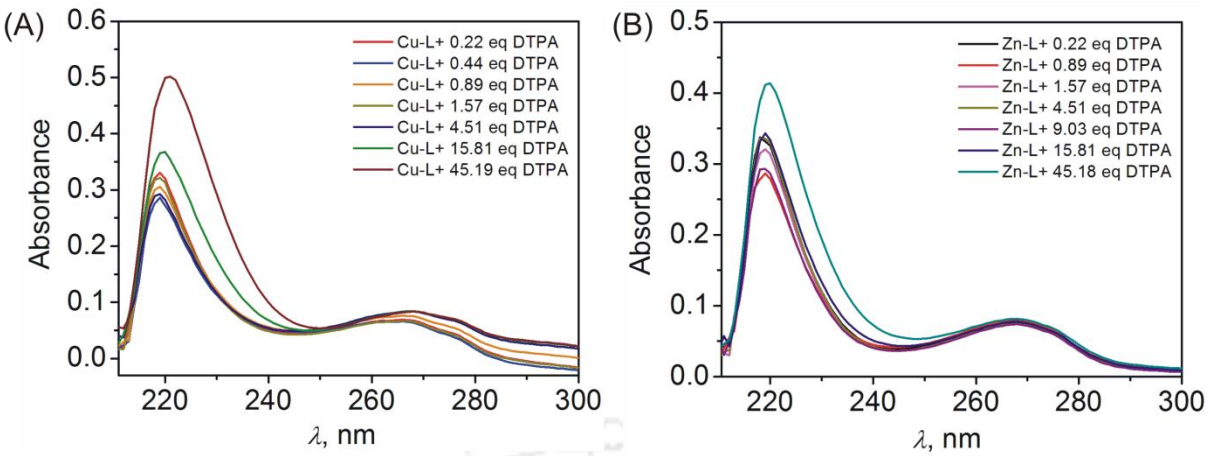

Figure 2.19. Spectral changes during competition batch titration of ligand H_4peada against DTPA for determining (A) pCu, and (B) pZn. (L in the figures represents ligand H_4peada)

Spectral changes during competition batch titration of ligand H_4peada against DTPA for determining pCu and pZn are shown in Figure 2.19. In Figure 2.19(A), the spectrum obtained for Cupeada upon addition of 0.22 equivalent of DTPA showed absorption at 269 nm with ashoulder at 276 nm. Upon addition of higher equivalent of DTPA, the trend in the corresponding spectra remained almost same. In Figure 2.19(B), the spectrum obtained for Znpeada upon addition of 0.22 equivalnet of DTPA showed absorption peak at 269 nm with a shoulder at 274 nm. However, the absortion bands were found to be consistent upon addition of higher concentrations of DTPA implied almost similar affinity of H_4peada towards Zn in comparison to DTPA.

The selectivity was measured by relative stability measurement in terms of pM of the different metal complexes formed by ligand H_4peada. Using commercially available DTPA as the competing ligand, following the same protocol used for determining pGd value of ligand H_4peada, pZn and pCu value of the ligand H_4peada were determined at pH = 7.4 and 25 ºC. From the titration curves (**Figure 2.18**), pZn and pCu values of the ligand H_4peada were found to be 14.8 and 16.1, respectively. The ligand with a difference in pGd and pZn value of **3.6**, showed comparable selectivity for Zn(II) as that of DTPA (pGd – pZn = 3.7 for DTPA), whereas it showed better selectivity towards Gd(III) over Cu(II) (pGd – pCu = **1.3**) in comparison to that of DTPA (pGd – pCu = 1.1 for DTPA).[13g] These pZn and pCu values implied the usefulness of complex **2A** as MRI contrast agent.

2.10 Phantom MR Images of Complex 2A at 1.5 T

At 1.5 T, by using clinical MRI scanner BRIVO MR355, T_1–weighted phantom MR images of complex **2A** at four different concentrations *viz*. 0.25, 0.50, 0.70, and 1.00 mM were measured (at 25 °C, and pH ~ 7.4) (**Figure 2.20**).

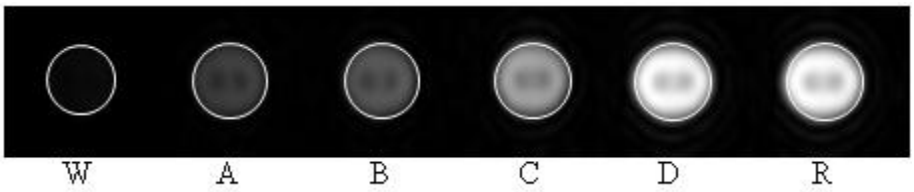

Figure 2.20. T_1–weighted phantom MR images of complex **2A** at 1.5 T, 25 °C, and pH ~ 7.4 (W = Water, A = 0.25 mM, B = 0.50 mM, C = 0.70 mM, D = 1.00 mM, R = Reference = Rezogad®).

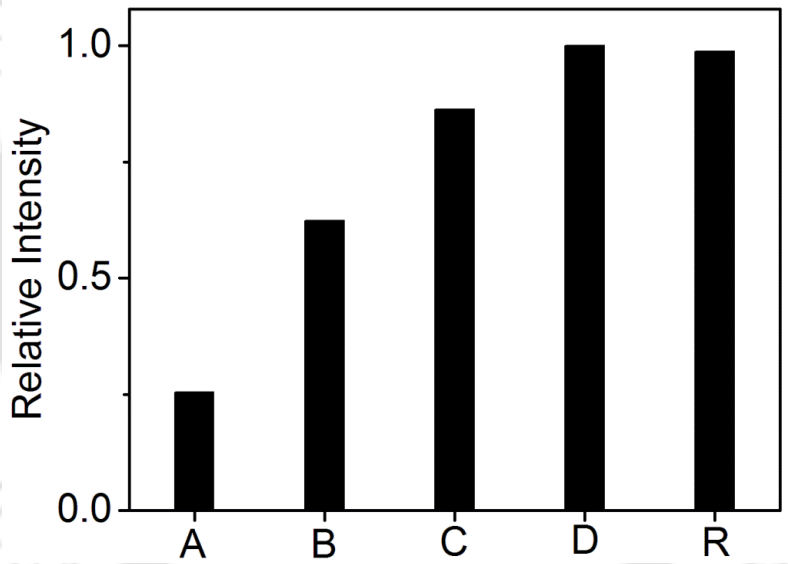

Figure 2.21. Comparison of T_1–weighted phantom MR images of complex **2A** (A = 0.25 mM, B = 0.50 mM, C = 0.70 mM, D = 1.00 mM, R = Reference = Rezogad®) at 1.5 T, 25 °C, and pH ~ 7.4.

The complex concentrations were compared with a commercially available MRI contrast agent Rezogad®, and the comparison of image intensities by using ImageJ Software under the same area of the images substantiated the complex as a good contrast agent even at low concentration (**Figure 2.21**).

2.11 Conclusion

- The ligand H_4peada and its corresponding aquated–Gd(III) complex, **2A** were synthesised.
- The complex with a pGd value of 18.4 (at pH = 7.4 and 25 ºC), showed comparable stability as that of the commercially availble $[Gd(DTPA)(H_2O)]^-$ complex and better stability than that of the previously reported Gd(III) complexes of picolinate based ligands.
- Complex **2A** showed higher r_1 relaxivity value of 6.08 $mM^{-1}s^{-1}$ at 1.41 T, 25 °C and pH ~ 7.4 compared to commercially available Gd(III)–based MRI CAs.
- The ligand H_4peada showed better selectivity for Gd(III) over Cu(II) (pGd – pCu = 1.3) and comparable selectivity over Zn(II) (pGd – pZn = 3.6) than the commercially available ligand DTPA (pGd – pCu = 1.1, pGd – pZn = 3.7).
- The complex showed no affinity for phosphate and bicarbonate ions even in the presence of 100 fold excess of the respective ions, but showed modest affinity for fluoride ion.
- Phantom MR images of complex **2A** at 1.5 T under a clinical MRI imager also support its candidature as a potential MRI contrast agent.

References

1. *(a)* P. Caravan, J. J. Ellison, T. J. McMurry and R. B. Lauffer, *Chem. Rev*., 1999, **99**, 2293; *(b)* S. Aime, M. Botta, M. Fasano and E. Terreno, *Chem. Soc. Rev.*, 1998, **27**, 19; *(c)* C. S. Bonnet and É. Tóth, *Adv. Inorg. Chem*., 2016, **68**, 43; *(d)* S. Aime, S. G. Crich, E. Gianolio, G. B. Giovenzana, L. Tei and E. Terreno, *Coord. Chem. Rev.*, 2006, **250**, 1562; *(e)* S. Aime, M. Botta and E. Terreno, *Adv. Inorg. Chem.*, 2005, **57**, 173; *(f)* R. Artali, M. Botta, C. Cavallotti, G. B. Giovenzana, G. Palmisano and M. Sisti, *Org. Biomol. Chem.*, 2007, **5**, 2441.
2. *(a)* P. Caravan, *Chem. Soc. Rev*., 2006, **35**, 512; *(b)* J. Costa, É. Tóth, L. Helm and A. E. Merbach, *Inorg. Chem*., 2005, **44**, 4747; *(c)* P. Verwilst, S. Park, B. Yoon and J. S. Kim, *Chem. Soc. Rev*., 2015, **44**, 1791; *(d)* P. Hermann, J. Kotek, V. Kubíček and I. Lukeš, *Dalton Trans*., 2008, 3027; (*e*) Z. Zhang, M. T. Greenfield, M. Spiller, T. J. McMurry, R. B. Lauffer and P. Caravan, *Angew. Chem. Int. Ed*., 2005, **44**, 6766; (*f*) A. Merbach, L. Helm and É. Toth, *The Chemistry of Contrast Agents in Medical Magnetic Resonance Imaging*, Second Edition. Wiley, New York, 2001.
3. (*a*) E. Balogh, M. Mato-Iglesias, C. Platas-Iglesias, É. Toth, K. Djanashvili, J. A. Peters, A. de Blas and T. R. Blas, *Inorg. Chem*., 2006, **45**, 8719; (*b*) P. H. Fries, C. Gateau and M. Mazzanti, *J. Am. Chem. Soc*., 2005, **127**, 15801; (*c*) Y. Bretonnière, M. Mazzanti, F. A. Dunand, A. E. Merbach and J. Pècaut, *Chem. Commun*., 2001, 621; (*d*) A. Borel, H. Kang, C. Gateau, M. Mazzanti, R. B. Clarkson and R. L. Belford, *J. Phys. Chem. A*, 2006, **45**, 110.
4. (*a*) A. Nonat, P. H. Fries, J. Pècaut and M. Mazzanti, *Chem. Eur. J*., 2007, **13**, 8489; (*b*) A. Nonat, C. Gateau, P. H. Fries and M. Mazzanti, *Chem. Eur. J*., 2006, **12**, 7133; (*c*) M. Mato-Iglesias, C. Platas-Iglesias, K. Djanashvili, J. A. Peters, É. Toth, E. Balogh, R. N. Muller, L. V. Elst, A. de Blas and T. Rodríguez-Blas, *Chem. Commun*., 2005, 4729; (*d*) A. Nonat, M. Giraud, C. Gauteau, P. H. Fries, L. Helm and M. Mazzanti, *Dalton Trans*., 2009, 8033; (*e*) C. Platas-Iglesias, M. Mato-Iglesias, K. Djanashvili, R. N. Muller, L. V. Elst, J. A. Peters, A. de Blas and T. Rodríguez-Blas, *Chem. Eur. J.*, 2004, **10**, 3579; (*f*) A. Nonat, C. Gateau, P. H. Fries, L. Helm and M. Mazzanti, *Eur. J. Inorg. Chem.*, 2012, 2049; (*g*) N. Chatterton, C. Gateau, M. Mazzanti, J. Pècaut, A. Borel, L. Helm and A. Merbach, *Dalton Trans*., 2005, 1129.

5. (*a*) Md. N. Khan, S. Pal, T. Parvinb and L. H. Choudhury, *RSC Adv.*, 2012, **2**, 12305; (*b*) G. Bringmann, Y. Reichert, V. V. Kane, *Tetrahedron*, 2004, **60**, 3539; (*c*) B. B. Fredholm, A. P. Izerman, K. A. Jacobson, K. N. Klotz and J. Linden, *Pharmacol. Rev*., 2001, **53**, 527.
6. (*a*) T. Storr, B. R. Cameron, R. A. Gossage, H. Yee, R. T. Skerlj, M. C. Darkes, S. P. Fricker, G. J. Bridger, N. A. Davis, M. T. Wilson, K. P. Maresca and J. Zubieta, *Eur. J. Inorg. Chem*., 2005, 2685. (*b*) Yuan-Y. Zhu, Chang-W. Liu, J. Yin, Zhao-S. Meng, Q. Yang, J. Wang, T. Liu and S. Gao, *Dalton Trans*., 2015, 20906; (*c*) V. Chandrasekhar, S. Hossain, S. Das, S. Biswas and Jean-P. Sutter, *Inorg. Chem*., 2013, **52**, 6346; (*d*) E. W. Price, J. F. Cawthray, G. A. Bailey, C. L. Ferreira, E. Boros, M. J. Adam and C. Orvig, *J. Am. Chem. Soc*., 2012, **134**, 8670.
7. (*a*) J. Wang, G. R. Gao, Z. H. Zhang, X. D. Zhang, X. Z. Liu, Y. M. Kong and Y. Li, *Russ. J. Coord. Chem*., 2007, **33**, 258; (*b*) E. S. G. Choo, X. Tang, Y. Sheng, B. Shuter and J. Xue, *J. Mater. Chem*., 2011, **21**, 2310; (*c*) J. Coates, *Interpretation of Infrared Spectra: A Practical Approach*, John Wiley & Sons Ltd, Chichester, 2000; (*d*) B. C. Smith, *Infrared Spectral Interpretation: A Systematic Approach*, CRC press, 1998.
8. (*a*) M. A. Sieber, T. Steger-Hartmann, P. Lengsfeld and H. Pietsch, *J. Magn. Reson. Imaging*, 2009, **30**, 1268; (*b*) C. Cabella, S. G. Crich, D. Corpillo, A. Barge, C. Ghirelli, E. Bruno, V. Lorusso, F. Uggeri and S. Aime, *Contrast Med. Mol. Imaging*, 2006, **1**, 23; (*c*) M. E. Bartolinia, J. Pekara, D. R. Chettlea, F. McNeilla, A. Scottb, J. Sykesc, F. S. Pratoc and G. R. Morana, *Magn. Reson. Imaging*, 2003, **21**, 541; (*d*) A. D. Sherry, P. Caravan and R. E. Lenkinski, *J. Magn. Reson. Imaging*, 2009, **30**, 1240.
9. (*a*) A. Barge, G. Cravotto, E. Gianolio and F. Fedeli, *Contrast Med. Mol. Imaging*, 2006, **1**, 184; (*b*) S. W. Kang, C. M. Park, K. H. Cho and H. S. Han, *Bull. Korean Chem. Soc*., 1993, **14**, 59; (*c*) S. Zhang, Z. Jiang, X. H. Liu, L. Zhou and W. Peng, *Nanoscale*, 2013, **5**, 8146.
10. K. V. Yatsimirsky, N. A. Kostromina, Z. A. Seka, N. K. Davidenko, E. E. Kriss and V. J. Ermolenko, *Khimya komplexnikh redkozemel' nikh elementov*. Naukova Dumka: Kiev, 1966.
11. (*a*) G. R. Choppin and D. R. Peterman, *Coord. Chem. Rev*., 1998, **174**, 283; (*b*) J. G. Bünzli and C. Piguet, *Chem. Soc. Rev*., 2005, **34**, 1048; (*c*) W. D. Horrocks Jr. and D. R. Sudnick, *Acc. Chem. Res*., 1981, **14**, 384; (*d*) L. M. Manus, R. C. Strauch, A. H. Hung, A. L. Eckermann and T. J. Meade, *Anal. Chem*., 2012, **84**, 6278; (*e*) S. Faulkner, S. J. A. Pope and B. P. Burton-Pye, *Appl. Spectrosc. Rev*., 2005, **40**, 1.

12. A. Beeby, I. M. Clarkson, R. S. Dickins, S. Faulkner, D. Parker, L. Royle, A. S. de Sousa, J. A. G. Williams and M. Woods, *J. Chem. Soc. Perk. T. 2*, 1999, 493.
13. (*a*) D. M. J. Doble, M. Melchior, B. O'Sullivan, C. Siering, J. Xu, V. C. Pierre and K. N. Raymond, *Inorg. Chem.*, 2003, **42**, 4930; (*b*) C. J. Jocher, , M. Botta, S. Avedano, E. G. Moore, J. Xu, S. Aime and K. N. Raymond, *Inorg. Chem.*, 2007, **46**, 4796; (*c*) C. J. Jocher, E. G. Moore, J. Xu, S. Avedano, M. Botta, S. Aime and K. N. Raymond, *Inorg. Chem.*, 2007, **46**, 9182; (*d*) E. J. Werner, J. Kozhukh, M. Botta, E. G. Moore, S. Avedano, S. Aime and K. N. Raymond, *Inorg. Chem.*, 2009, **48**, 277; (*e*) D. T. Puerta, M. Botta, C. J. Jocher, E. J. Werner, S. Avedano, K. N. Raymond and S. M. Cohen, *J. Am. Chem. Soc.*, 2006, **128**, 2222; (*f*) K. N. Raymond and V. C. Pierre, *Bioconjugate Chem.*, 2005, **16**, 3; (*g*) V. C. Pierre, M. Botta, S. Aime and K. N. Raymond, *Inorg. Chem.*, 2006, **45**, 8355.
14. M. Botta, S. Aime, A. Barge, G. Bobba, R. S. Dickins, D. Parker and E. Terreno, *Chem. Eur. J.*, 2003, **9**, 2102.
15. Jean-M. Idée, M. Port, I. Raynal, M. Schaefer, S. L. Greneur and C. Corot, *Fundam. Clin. Pharmacol*., 2006, **20**, 563.
16. W. P. Cacheris, S. C. Quay and S. M. Rocklage, *Magn. Reson. Imaging*, 1990, **8**, 467.

Chapter III

A Bis(aquated) High Relaxivity Gd(III) Complex for High Field (14.1T) MRI Study

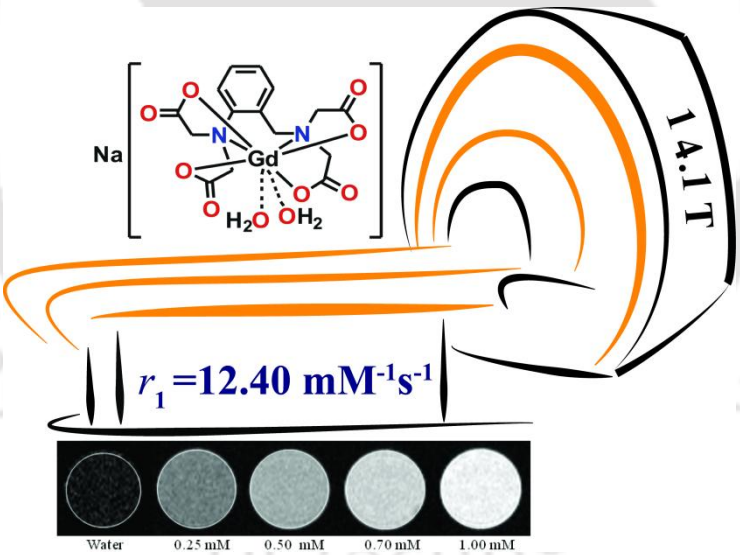

3.1 Introduction

MRI at stronger magnetic fields facilitates higher signal–to–noise ratio with better spatial resolution and reduced acquisition time.[1] The highest field strength of current clinically available MRI scanner is 3 T. MRI scanner with field strength 7 T or 9.4 T are expected to be available in the market very soon, and at the highest magnetic field of 9.4 T, safe and successful human MRI has been reported in last few years.[2] The best achievement in MRI technology is by National High Magnetic Field Laboratory in successful construction of 21.1 T MRI magnet.[3] However, the effectiveness of clinically used Gd(III)–based MRI contrast agents (CAs) are limited to 1.5–3.0 T and their longitudinal relaxivity value, r_1 decreases as the field strength increases and less than theoretically attainable maximum. Relaxivity values (r_1) of some of the commercially available MRI CAs at different magnetic fields are summarized in **Table 3.1**.[4]

Table 3.1. r_1–relaxivity values ($Lmmol^{-1}s^{-1}$) in water at 37 °C:

Trade name	0.47 T	1.5 T	3 T	4.7 T
Magnevist	3.4	3.3	3.1	3.2
MultiHance	4.2	4.0	4.0	4.0
ProHance	3.1	2.9	2.8	2.8
Dotarem	3.4	2.9	2.8	2.8
Resovist	20.6	8.7	4.6	2.8
Fexidex/ Endorem	27.0	4.7	4.1	2.3

The trend associated with the decrease in r_1 relaxivity with increasing field strength lead to a new research interest to design some new contrast agents, which can show high r_1 relaxivities even at high fields. This can be achieved if the parameters, which are responsible for enhancing relaxivity *viz.* water exchange rate (τ_M), molecular tumbling (τ_R), and hydration state (q) etc., are tuned by judicious ligand design.[1d,5] Solomon–Bloembergen–Morgan (SBM) theory indicates that by optimising these parameters, up to 20 times higher relaxivity value can be attained. The theory also predicts that at lower field, r_1 relaxivity is proportional to the rotational correlation time, τ_R whereas at field above ~ 200 MHz, r_1 relaxivity varies inversely with τ_R.[1e]

The number of coordinated water molecules (q) plays an important role in the r_1 relaxivity value of a complex irrespective of field strength. Commercially available Gd(III)–based MRI CAs have nine–coordinated Gd(III) centre bound by octadentate ligand with one

inner sphere water molecule. Several complexes bound by hexa and heptadentate poly(aminocarboxylate) ligands with $q > 1$ have been reported with higher relaxivity values without reducing the complex stability. Raymond *et al*. reported a series of HOPO (hydroxypyridinonate) based ligands and their corresponding Gd(III) chelates having two or three coordinated water molecules at their metal centres.[6] Owing to the presence of higher number of coordinated water molecules, these complexes have been considered as high relaxivity next generation MRI CAs without disturbing the chelate stability. Caravan *et al*. also reported a heptadentate ligand CyPic3A, and its corresponding bis(aquated) Gd(III) complex with high thermodynamic stability.[7] These results indicated that an appropriate choice of the coordination environment could lead to high relaxivity as well as sufficient thermodynamic stability. **Scheme 3.1** shows some examples of high relaxivity Gd(III) complexes with $q > 1$.[6a,7]

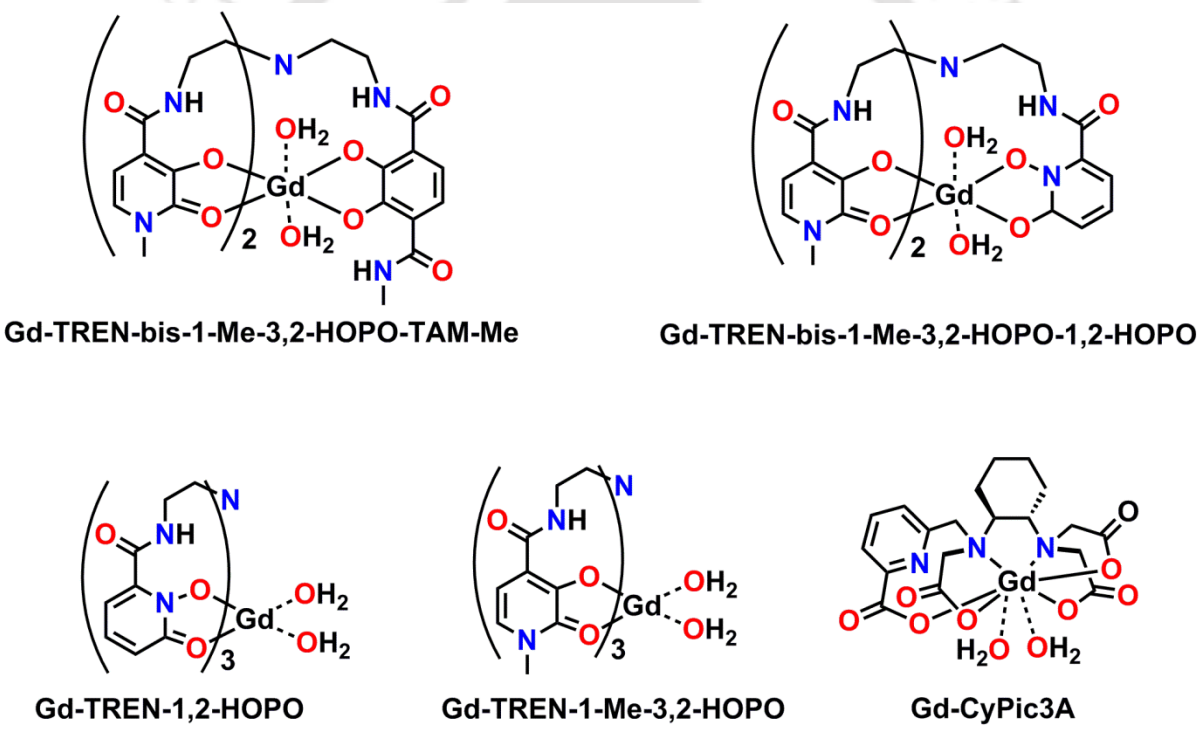

Scheme 3.1. Examples of Gd(III) complexes having two inner sphere water molecules.

However, synthesis of water soluble suitable contrast agents for high field MRI study is still challenging. Livramento *et al.* reported a self–assembled, metallostar–structured Gd(III)–based MRI CA, which showed remarkably higher relaxivity at high field (r_1 = 15.8 $mM^{-1}s^{-1}$ at 200 MHz, 37 ºC, in H_2O). This high relaxivity value at higher magnetic field was explained due to its small molecular space, which in turn increased the rotational correlation time, τ_R.[1e]

In search of developing a new MRI CA, which can show high relaxivity at higher magnetic field, small poly(aminocarboxylate) based ligand H_4bedik and its corresponding Gd(III) complex were synthesised. Since Gd(III) complexes are either eight–coordinate or nine–coordinate; this hexadentate ligand was expected to allow maximum coordination of three water molecules, *i.e.*, q_{max} would be 3. Furthermore, the asymmetric nature of the ligand would create an asymmetric coordination–environment around the metal centre, which in turn would facilitate coordination of water molecules due to less steric effect. A 2–aminobenzylamine moiety was incorporated in the ligand backbone and all the four –H atoms of the two amine groups were replaced by four acetic acid groups. Thus, in addition to three water molecules, the primary coordination environment of Gd(III) ion would be comprised of two strong σ–donating sp^3 N atoms and four strong σ–donating carboxylate oxygen ($–COO^-$) atoms. Gd(III) ion being oxophilic in nature would coordinate very strongly with carboxylate oxygen atoms and thus would form stable complex. Furthermore, the coordination of four carboxylate oxygen atoms to the Gd(III) ion will diminish the Lewis acidic character of Gd(III) and thus, water exchange rate would be enhanced.

3.2 Synthesis and Characterisation of Ligand H_4bedik, $C_{15}H_{18}N_2O_8$

A schematic representation for the synthesis of ligand H_4bedik is shown in **Scheme 3.2**.

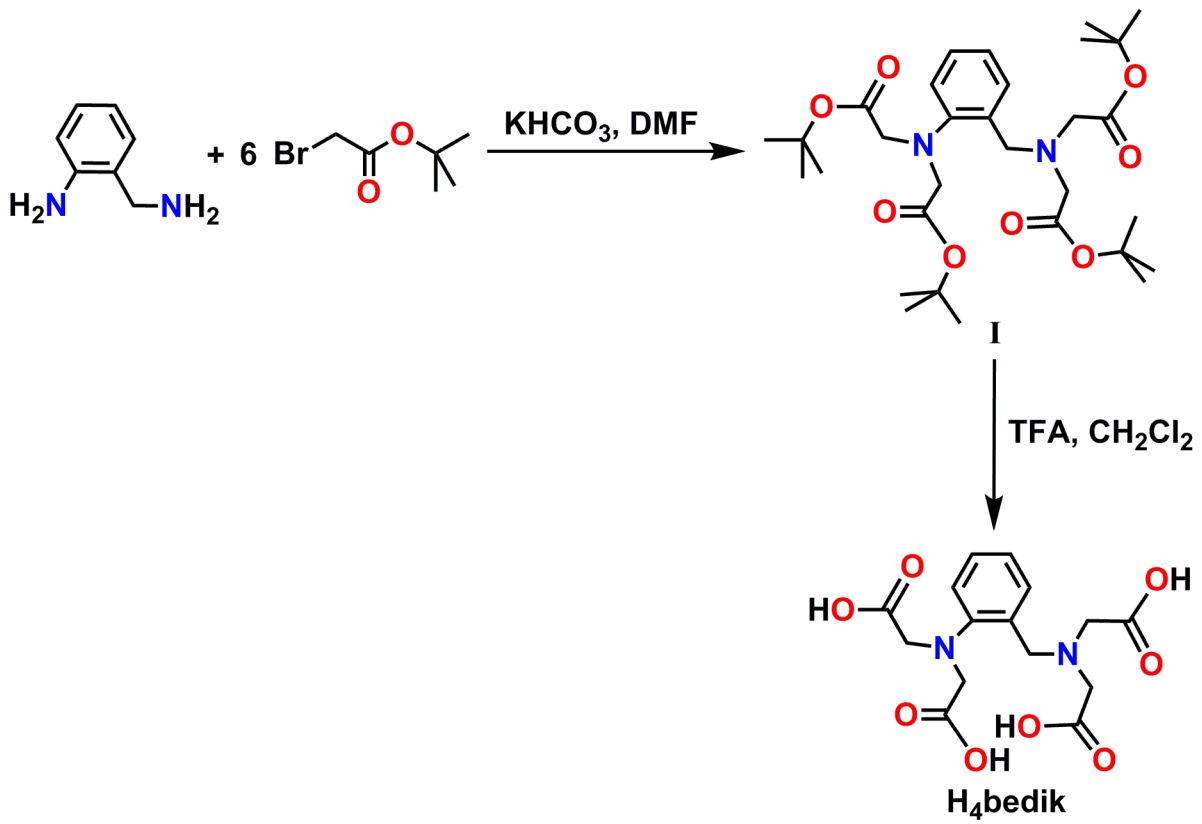

Scheme 3.2. Synthetic route of ligand H_4bedik.

A reaction between 1:6 2–aminobenzylamine and *tert*–butylbromoacetate mixture in DMF in the presence of $KHCO_3$ provided **I**, which upon reaction with trifluoroacetic acid provided ligand H_4bedik as a white solid. The ligand was characterised by using FTIR spectroscopy, mass spectrometry and NMR spectroscopy technique.

Infrared (IR) spectrum (**Figure 3.1)** of ligand H_4bedik showed a sharp band at 3450 cm^{-1} due to ν(O–H) stretching.[8a] Aromatic and aliphatic C–H stretching bands appeared in the region from 3013 to 2925 cm^{-1}.[8b] The band at 2534 cm^{-1} was due to H–bonded O–H of the carboxylic acid group.[8c] The stretching frequency for C=O group appeared as a sharp band at 1726 cm^{-1}.[8a] The band at 1406 cm^{-1} was attributed to in plane O–H bending.[8d]. The ν(C–O) stretching band appeared at 1210 cm^{-1}.[8c]

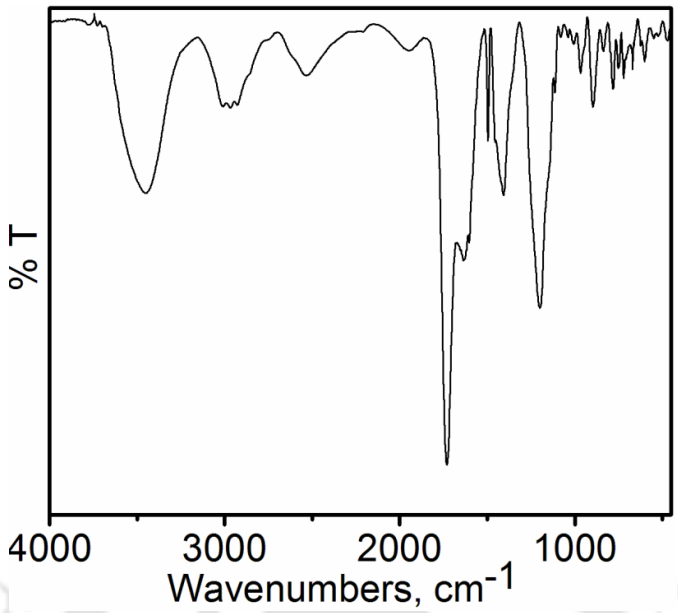

Figure 3.1. FTIR spectrum of ligand H_4bedik.

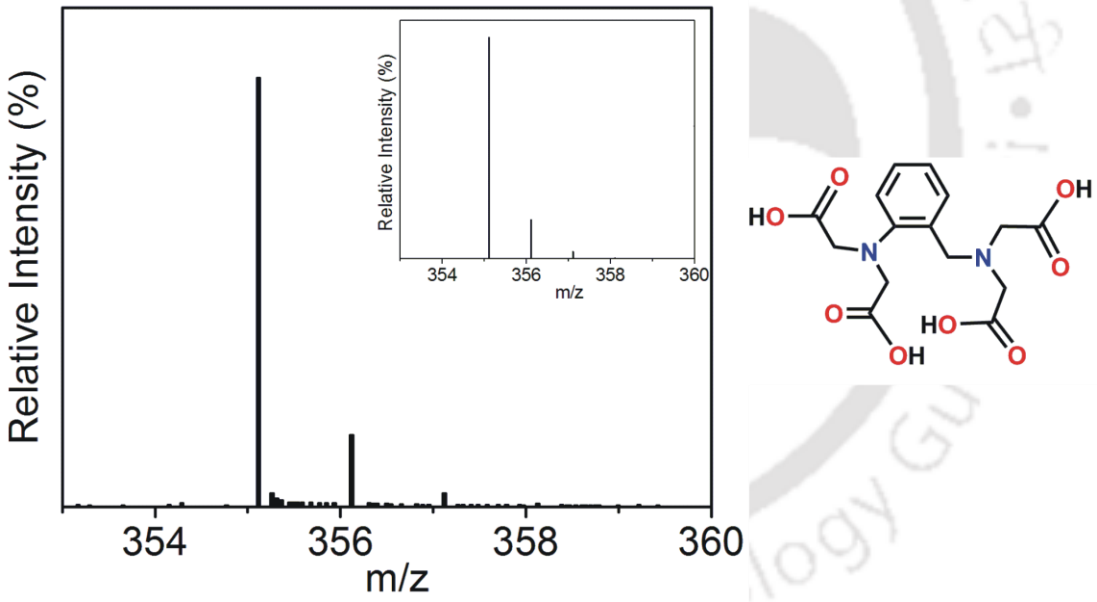

Figure 3.2. ESI–MS spectrum of ligand H_4bedik. Simulated spectrum is shown as inset.

The ESI mass spectrum measurement of the ligand in the positive mode in HPLC grade MeOH, provided a 100% molecular ion peak at *m/z* = 355.1175 amu. The peak corresponded to the composition $[C_{15}H_{18}N_2O_8 + H]^+$ (*m/z* = 355.1136 amu) as evident by isotope pattern distribution analysis (**Figure 3.2**).

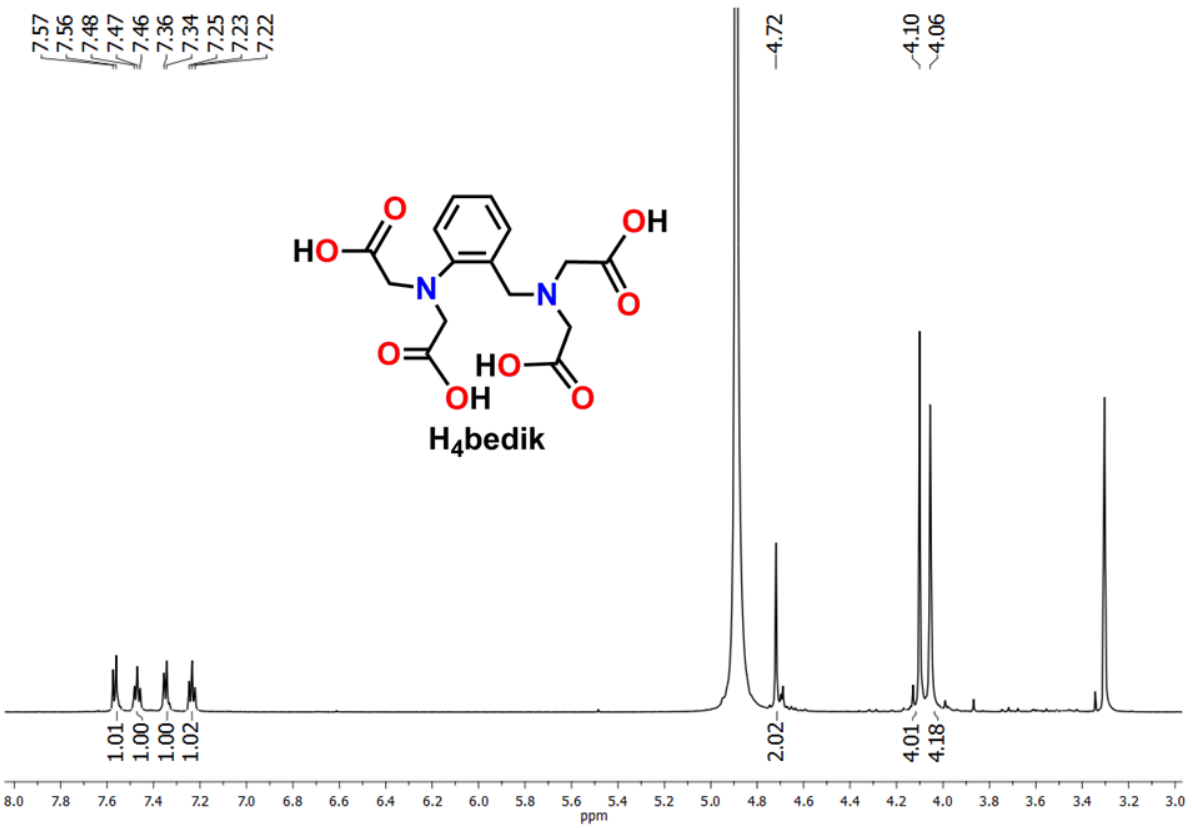

Figure 3.3. ^{1}H NMR spectrum of ligand H_4bedik.

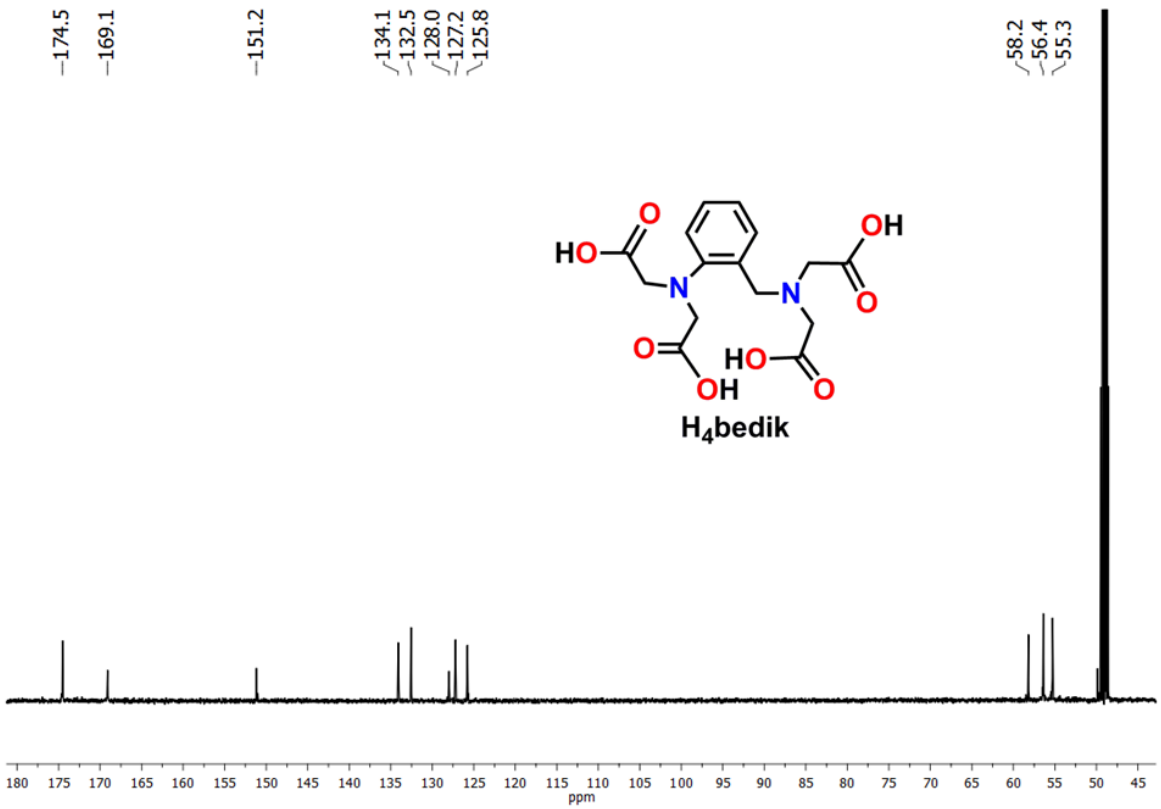

Figure 3.4. ^{13}C NMR spectrum of ligand H_4bedik.

^{1}H NMR spectrum of ligand H_4bedik is shown in **Figure 3.3**. The signals in the region 7.57–7.22 ppm were due to four aromatic protons of the benzene ring in the ligand backbone. The singlet appeared at 4.72 ppm was due to two protons in the methylene unit. The two singlet signals at 4.10 and 4.06 ppm were due to eight hydrogen atoms attached to four carboxylic acid groups. The ^{13}C NMR spectrum (**Figure 3.4**) of the ligand showed 11 characteristic peaks for 11 different kinds of carbon atoms.

3.3 Synthesis and Characterisation of Bis(aquated) Gd(III) Complex of Ligand H_4bedik, 3A

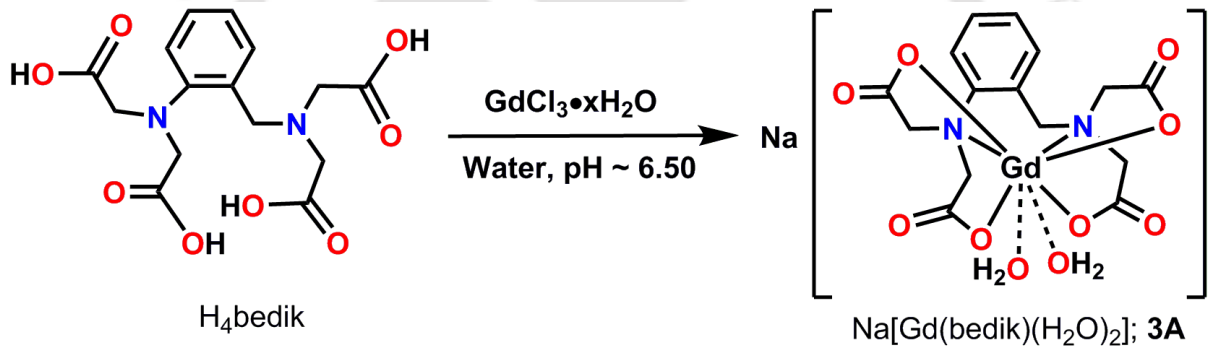

Scheme 3.3. Synthesis of complex **3A**, $Na[C_{15}H_{18}GdN_2O_{10}]$.

To a solution of H_4bedik in water, $GdCl_3$•xH_2O was added and stirred the reaction mixture for 10 minutes. The solution became transparent and then pH was adjusted to ~ 6.5 by dropwise addition of aq. NaOH solution. Stirring was continued at room temperature (25 °C) for 24 h and kept the reaction mixture at room temperature for slow evaporation of water. The white solid obtained was washed thoroughly with MeOH and formation of the complex was confirmed by using mass spectrometry and FTIR spectroscopy.

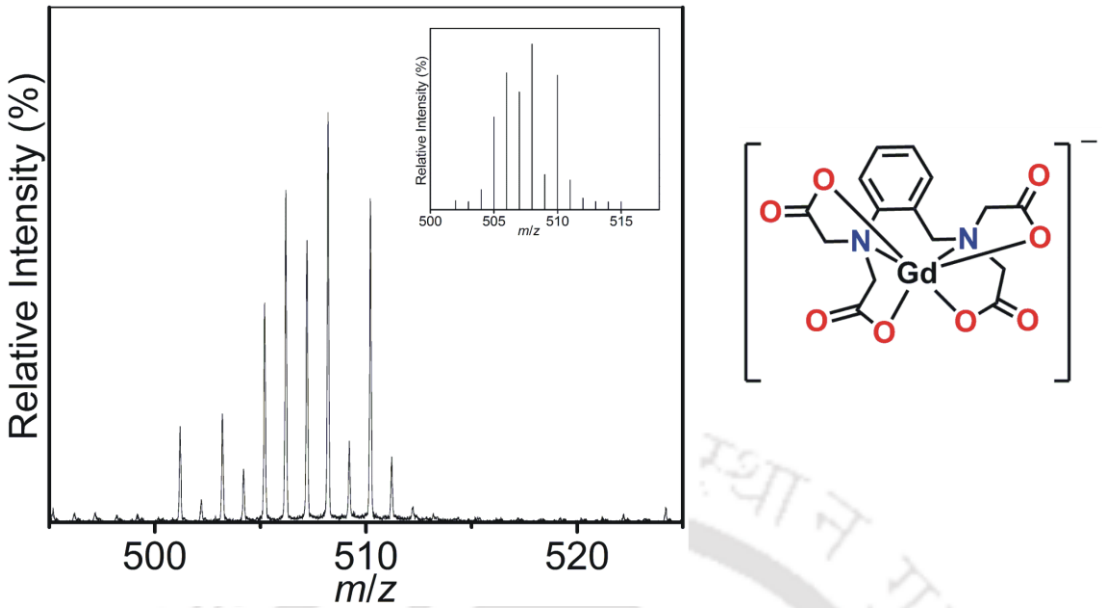

Figure 3.5. ESI–MS spectrum of complex **3A**. Simulated spectrum is shown as inset.

The electrospray ionisation mass spectrum measurement in negative mode of complex **3A** in Mili Q water, provided a 100% molecular ion peak at *m/z* = 508.23 amu. The peak corresponded to the composition $[C_{15}H_{14}GdN_2O_8]^-$ (*m/z* = 507.99 amu) as evident by isotope pattern distribution analysis (**Figure 3.5**).

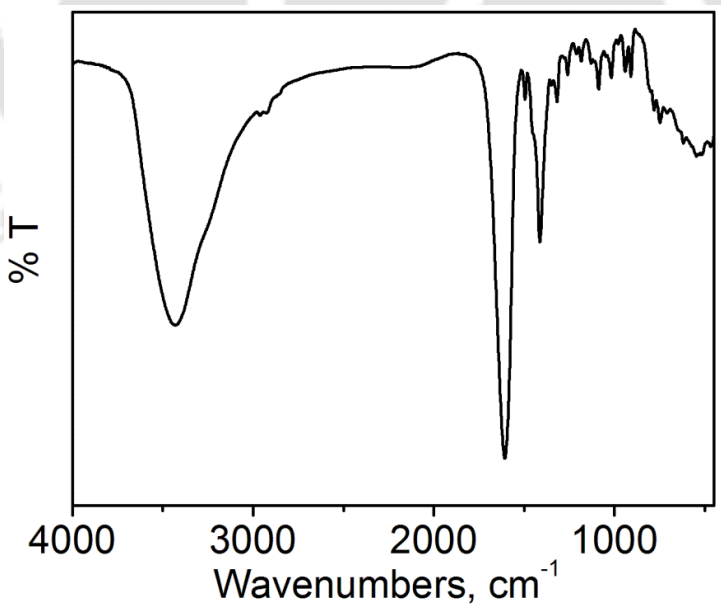

Figure 3.6. FTIR spectrum of complex **3A**.

Infrared (IR) spectrum (**Figure 3.6**) of complex **3A** showed a sharp band at 3431 cm^{-1} due to *ν*(O–H) stretching. The formation of the complex was confirmed from the change in

ν(C=O) stretching frequency, which appeared as a sharp band at 1606 cm^{-1} for the complex whereas that of the ligand was observed at 1726 cm^{-1}.

3.4 Xylenol Orange Test for Determination of Free Gd(III) in Complex 3A

Free Gd(III) ion is highly toxic in nature. It precipitates in different tissues of the body, obstructs Ca(II) ion passage through muscle cells and nerve tissue cells, and interferes with intracellular enzymes and cell membranes by the process of transmetallation.[9] So, to prevent the toxicity of free Gd(III) ion, it is very important to determine the amount of free Gd(III) ion present in the complex.

Arsenazo III (2,7–bis(arsonophenylazo)–1,8–dihydroxy–naphthalene–3,6–disulfonic acid) and xylenol orange are two complexometric indicators, which are used to determine the amount of free lanthanide ion concentration in a solution.[10]

Xylenol orange indicator is known to be more convenient as it shows different colour in the presence of different concentrations of Gd(III). Since the thermodynamic stability of Gd(III) complex of xylenol orange (log K = 5.8)[11] is lower than that of the commercially available Gd(III)–based MRI CAs and their derivatives, it is expected that xylenol orange would only form chelate with the free Gd(III) ions present in the complex solution.

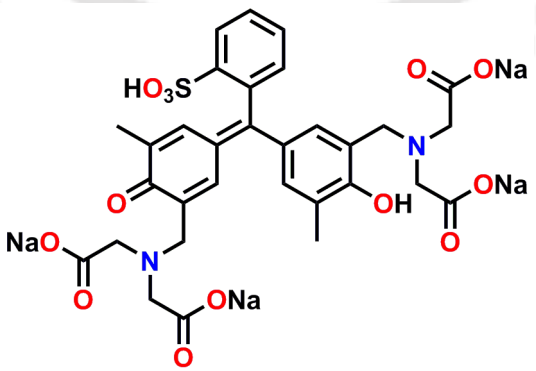

Figure 3.7. Structure of xylenol orange (XO).

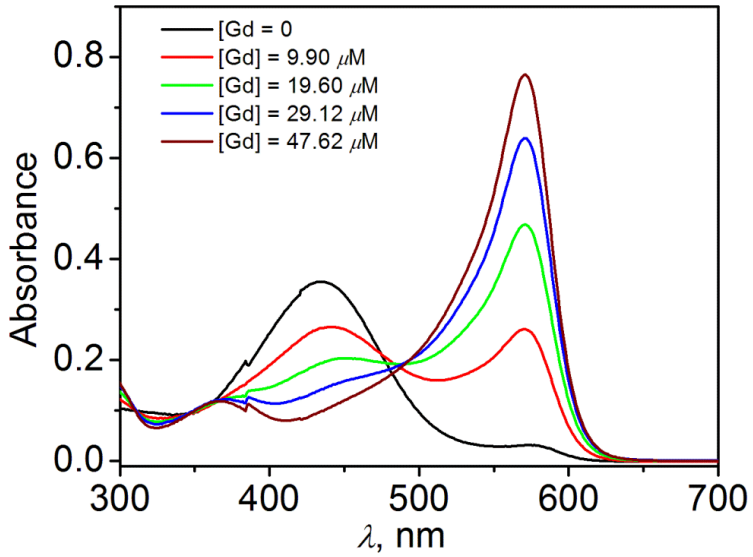

Figure 3.8. UV–vis spectra of xylenol orange solutions in acetate buffer (pH = 5.8) in the presence of varied concentrations of Gd(III) ions, from zero to 47.62 μM.

Figure 3.8 shows the UV–vis spectra of xylenol orange solutions in acetate buffer (pH = 5.8) in the presence of different concentrations of Gd(III) ion in the range 0 to 47.62 μM. During the whole experiment, the pH of xylenol orange solution was kept constant at 5.8 by using acetate buffer, as the colour of xylenol orange itself varies at different pH even in the absence of Gd(III) ion. Xylenol orange in acetate buffer solution showed two absorption maxima at 433 nm and 573 nm respectively. With the increase in concentration of Gd(III), the band at 433 nm decreases, whereas the band at 573 nm increases progressively.

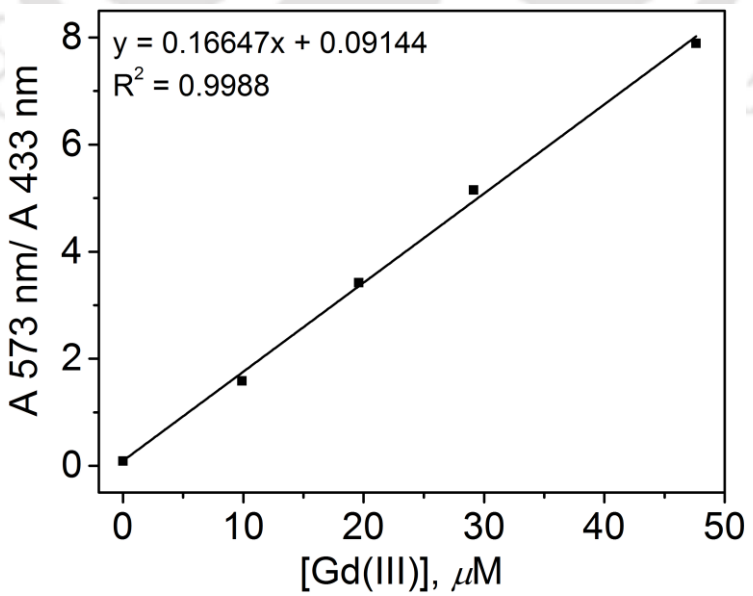

Figure 3.9. Calibration curve obtained from the spectrophotometric changes of xylenol orange (in acetate buffer pH = 5.8) in the presence of varied concentrations of Gd(III) ions.

A linear calibration curve was obtained from the ratio of absorbance values at 573 and 433 nm *vs*. Gd(III) ion concentration (**Figure 3.9**). 50 μL of complex **3A** (concentration = 29.1 mM) was then added to 2.0 mL of xylenol orange solution (pH = 5.8) and inclusion of the ratio of absorbance at 573 and 433 nm in the calibration curve, the percentage of free Gd(III) ion in the complex was found to be < 0.005 %.

3.5 Determination of Number of Coordinated Water Molecules (q)

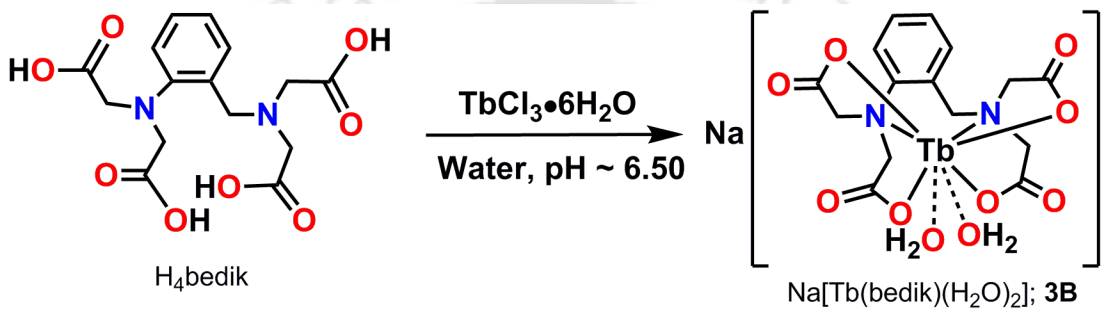

Scheme 3.4. Synthesis of complex **3B**, $Na[C_{15}H_{18}TbN_2O_{10}]$.

Several attempts to grow single crystal suitable for X–ray diffraction analysis were not successful. Therefore, in order to find out indirectly the number of Gd(III)–coordinated water molecules (*q*) in complex **3A**, its surrogate complex **3B** with luminescence lanthanide Tb(III) ion was synthesized. Here, complex **3B** was synthesised by reacting an equimolar amount of ligand H_4bedik and $TbCl_3$•$6H_2O$ in water at pH ~ 6.5 under refluxing condition.

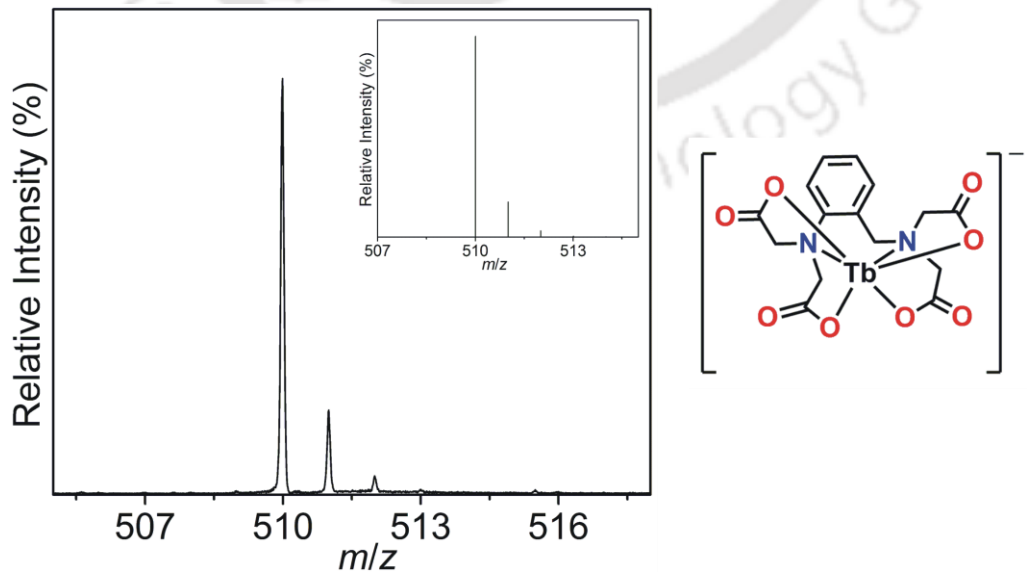

Figure 3.10. ESI–MS spectrum of complex **3B**. Simulated spectrum is shown as inset.

The ESI mass spectrum of complex **3B** showed a 100% molecular peak at 509.09 amu in the negative mode (**Figure 3.10**), which corresponded to $[C_{15}H_{14}TbN_2O_8]^-$ composition (*m/z* = 509.00 amu) and supported the formation of complex **3B**.

The hydration state of complex **3A** was confirmed by preparing its Tb(III) congener and then measuring the luminescence life time of Tb(III) complex, **3B** in H_2O and D_2O. Gd(III) cannot be sensitised by UV-visible absorbing chromophores and is not a very useful luminescent probe as its luminescence interferes with either emission or absorption processes in the organic part of the complex molecules.[12] A 50 μM solution of complex **3B** in 10 mM HEPES buffer (pH = 7.4), 25 °C was used for the lifetime measurements. Solution was excited at 270 nm and emission was recorded at 544 nm. The same solution was then evaporated completely by spin concentration under reduced pressure and addition of equal volume of D_2O to the completely dry residue resulted in solution of same concentration of the complex in D_2O buffer. The *q*–value was calculated from the decay constants τ_{H_2O} and τ_{D_2O} by using modified Horrock's equation,[13]

$$q = 5\,(1/\tau_{H_2O} - 1/\tau_{D_2O} - 0.06)$$

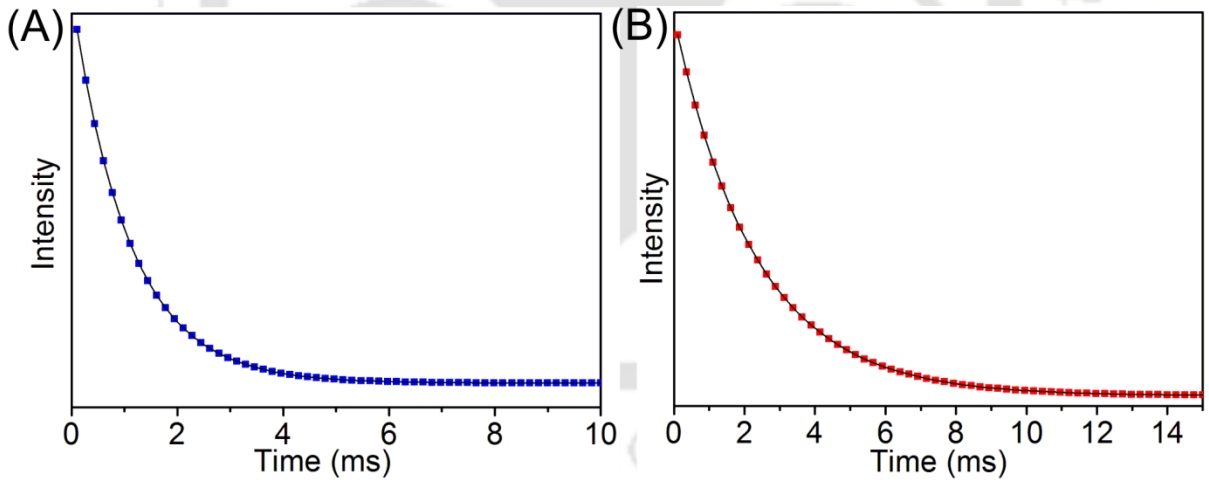

Figure 3.11. Lifetime measurements of complex **3B** in (A) H_2O and (B) D_2O.

The correlation between τ and *q* results from the efficient energy transfer from the excited state of Tb(III) to O–H oscillator of the coordinated water molecule.[14] When O–H is replaced by O–D, the luminescence lifetime of the complex increases because of less efficient energy transfer. τ_{H_2O} = 1.08 ms and τ_{D_2O} =2.33 ms were obtained by fitting decay curves with single exponential model using non–linear least square method and goodness of the fits were

determined by minimizing the reduced Chi^2 values. The q value was found to be **2.22±0.1** by putting these values in the modified Horrock's equation. The value indicated that the majority of the complex (~80%) present in the solution was in bis(aquated) form.

3.6 Stability of complex 3A

Complex stability plays an important role while using Gd(III) chelates as MRI CAs. To understand the stability of complex **3A** in comparison to the commercially available MRI CAs, spectrophotometric titration method was used to determine pM value of the ligand. pM is analogous to pH and is defined as –log of free metal ion concentration in solution *i.e.* pM = $-\log[M^{n+}]_{free}$ at some specific conditions (typically [M] = 1 μM, ligand concentration [L] = 10 μM, pH = 7.4 and temperature 25 °C).[6a,6c,15]

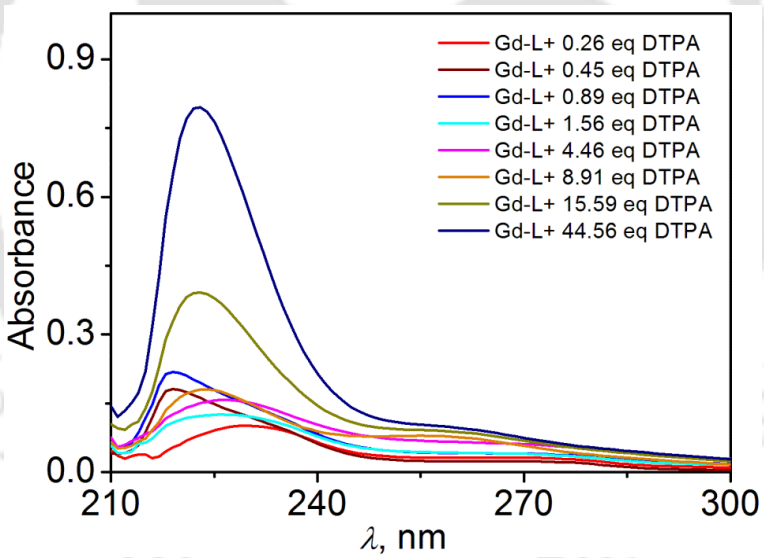

Figure 3.12. Spectral changes during the competition titration of ligand H_4bedik against DTPA. (L in the figure represents the ligand H_4bedik)

A competition batch titration was performed using DTPA (diethylenetriaminepentaacetic acid) as the competing ligand. During the experiment, concentrations of ligand H_4bedik and Gd(III) were kept constant while the concentration of DTPA was gradually increased. The pH of all the solutions was kept constant at 7.4 by using 10 mM HEPES buffer. After keeping the solutions for 24 h, the concentrations of the free and complexed ligand were determined by using UV–vis spectroscopy. Figure 3.12 shows the UV-visible spectra of Gdbedik upon addition of

increased equivalents of DTPA. No significant changes were observed in the spectral trend upon addition of higher concentrations of DTPA.

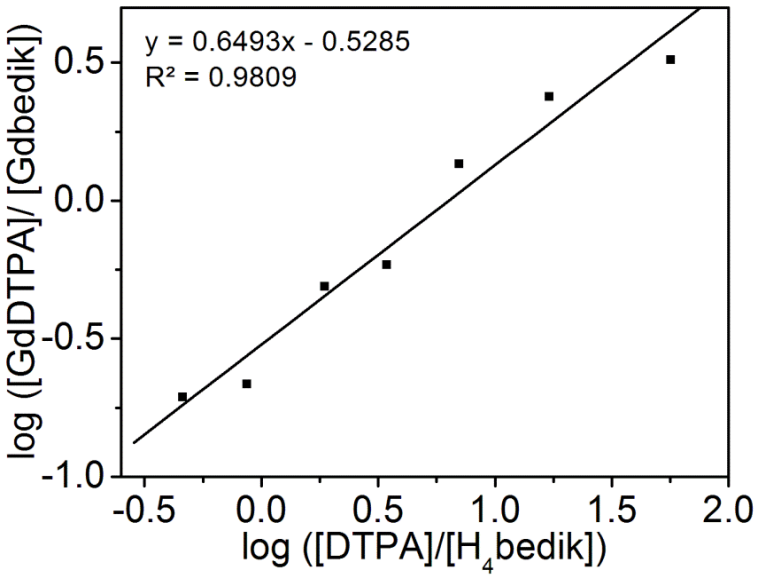

Figure 3.13. Competition titration of ligand H_4bedik against DTPA.

From the *x*–intercept of the plot of log ([DTPA]/[H_4bedik]) *vs.* log ([GdDTPA]/[Gdbedik]), the difference in pGd value of the ligand and that of DTPA was found. This difference was the value of log ([DTPA]/[H_4bedik]) when log ([GdDTPA]/[Gdbedik]) = 0 or when the concentration of DTPA generated an equal partition of Gd(III) between ligand H_4bedik and DTPA. Using the known value of pGd of DTPA 19.1,[15a] pGd value of ligand H_4bedik was found to be 19.9. This pGd value of 19.9 at pH = 7.4 suggested a better thermodynamic stability of complex **3A** than the commercially available MRI CAs under physiological conditions.

Table 3.2. pGd values calculated for ligands having bis(aquated) Gd(III) complexes.[15,16]

Ligand	pGd (pH = 7.4, 25 ºC)
TREN–MOE–3,2–HOPO	19.8
TREN–Me–3,2–HOPO	20.1
TREN–1,2–HOPO	19.3
TRENMAM	19.3
TREN–Me–MAM	19.0
H_3mpatcn	11.8

H_2dpaba	12.5
H_4bedik	**19.9**

3.7 Relaxivity Measurements of Complex 3A at 1.41 T and 14.1 T

Using inversion recovery method, the r_1 relaxivity of complex **3A** was measured at 1.41 T in a BRUKER minispec mq60 NMR analyzer.

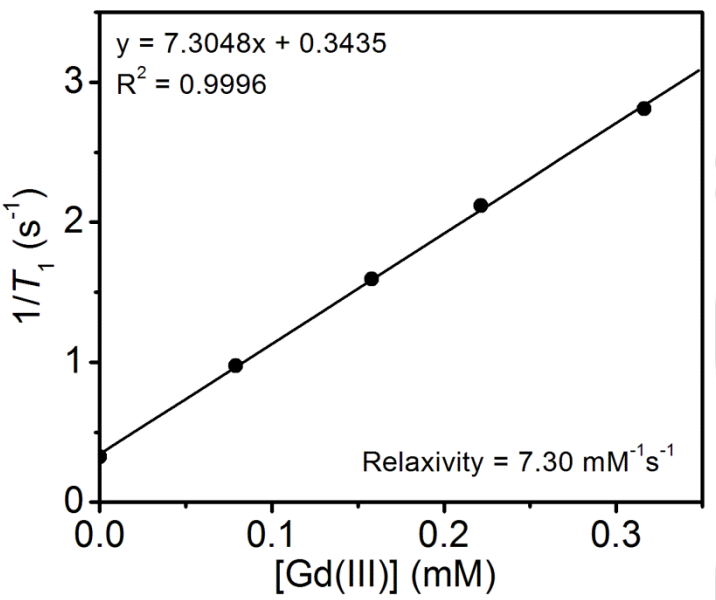

Figure 3.14. $1/T_1$ *vs.* [Gd(III)] plot for determining longitudinal relaxivity of complex **3A** at 1.41 T, 25 °C, and pH ~ 7.4.

At four different concentrations of complex **3A**, the longitudinal relaxation times (T_1) were measured. From the slope of the curve of longitudinal relaxation rate (R1 = $1/T_1$) *vs.* [Gd(III)], the r_1 relaxivity of the complex was found to be 7.30 $mM^{-1}s^{-1}$(at 25 ºC and pH ~ 7.4). The exact Gd(III) ion concentration was determined by ICP–AES method.

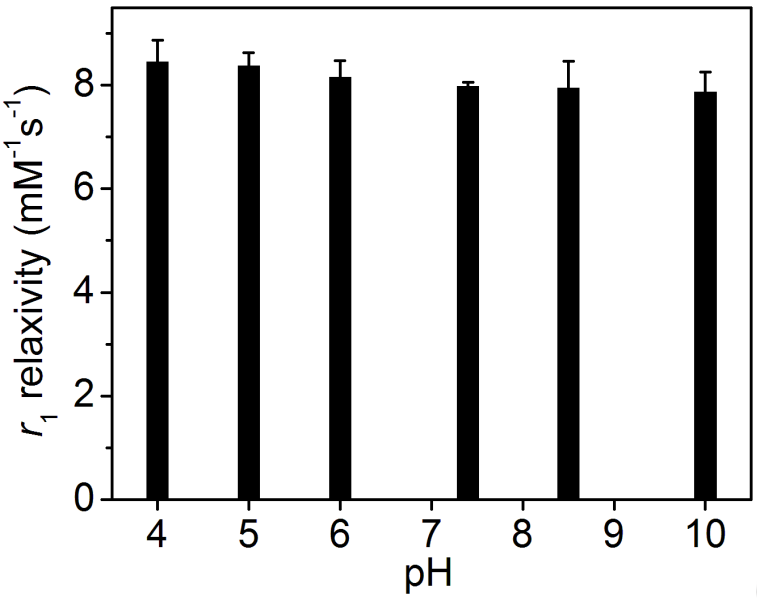

Figure 3.15. Longitudinal relaxivity measurement of complex **3A** in pH range 4–10, at 1.41 T and 25 °C.

The r_1 relaxivity value of the complex was found to be significantly higher than that of the commercially available MRI CAs, and the presence of two inner sphere water molecules could be considered as the key factor for attaining this higher value. While measured in a pH range 4–10, the r_1 relaxivity values of complex **3A** were found to be almost constant (Δr_1 = ±0.47 $mM^{-1}s^{-1}$) and the results are depicted in **Figure 3.15**.

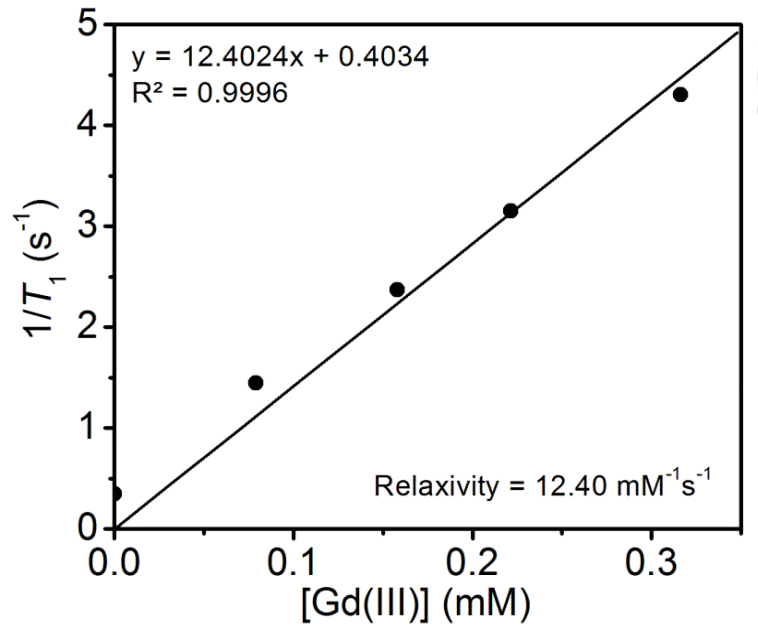

Figure 3.16. $1/T_1$ *vs.* [Gd(III)] plot for determining r_1 relaxivity at 14.1 T, 25 °C and pH ~ 7.4.

To attain greater spatial resolution and also to reduce acquisition time, the r_1 relaxivity of complex **3A** was measured at higher frequency. At 14.1 T, longitudinal relaxation times were measured at four different concentrations of the complex, and from the slope of the curve of longitudinal relaxation rate $1/T_1$ *vs.* [Gd(III)], the r_1 relaxivity of the complex was determined. Owing to the demand of a high relaxivity MRI CA at higher field, complex **3A** showed significantly high r_1 value of 12.40 $mM^{-1}s^{-1}$ (at 25 ºC and pH ~ 7.4) at 14.1 T.

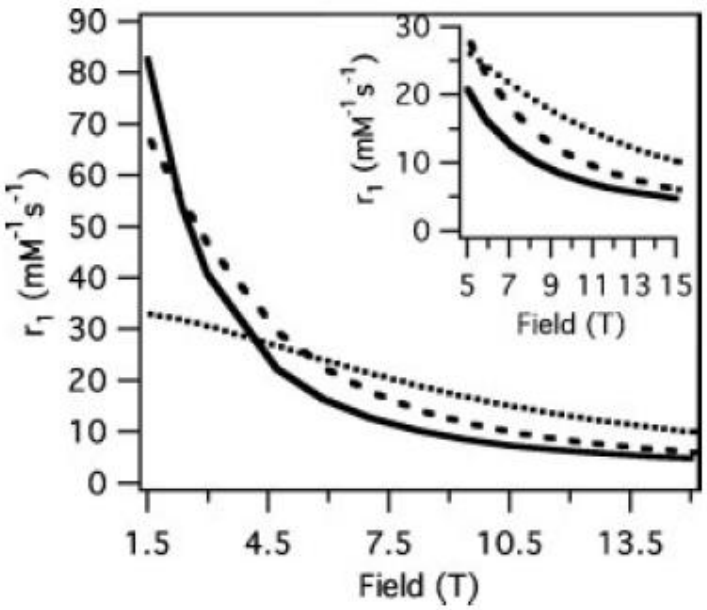

Figure 10. Simulated r_1 for a Gd^{3+} complex with two rapidly exchanging ($\tau_m = 50$ ns) inner-sphere waters and one water with $r'_{GdH} = 3.5$ Å, $\tau'_m = 1$ ns for three different isotropic rotational correlation times: $\tau_R = 0.5$ ns (●●●), 1.6 ns (---) or 4.6 ns (—).

Figure 3.17. Simulated result described by Caravan *et al.* for attaining high field relaxivity even at high field.[1d]

This unconventional increase in relaxivity with increase in field strength could be due to a shorter correlation time (τ_R) of the compound. An understanding of this high relaxivity gain at high field was well explained by Caravan *et al.*[1d] The simulated result (**Figure 3.17**) of a bis(aquated) Gd(III) complex with fast water exchange rate (τ_m = 50 ns) and a long lived water (τ_m'= 1 ns) showed that the rotational correlation time in the range 0.5–4.6 ns gave the excellent high field relaxivity.

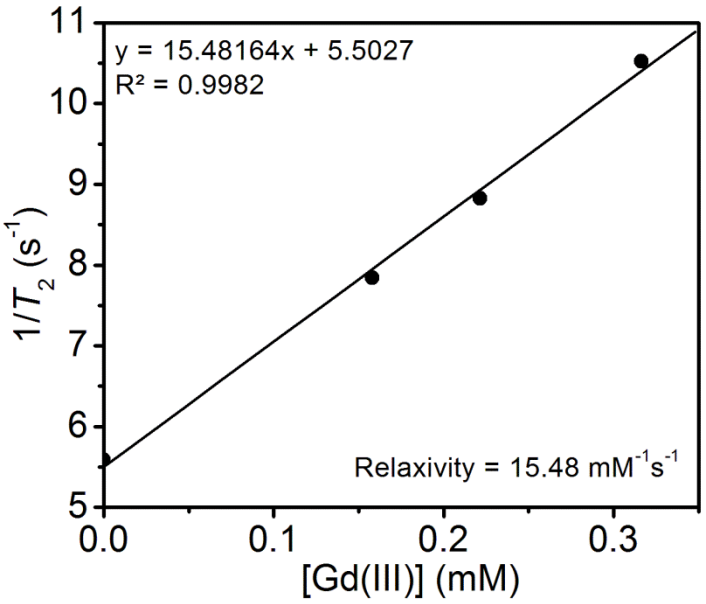

Figure 3.18. $1/T_2$ *vs.* [Gd(III)] plot for determining r_2 relaxivity of complex **3A** at 14.1 T, 25 °C and pH ~ 7.4.

In addition to this, transverse relaxivity of complex **3A** was also measured at 14.1 T. Similar to longitudinal relaxivity, at four different concentrations of the complex, the transverse relaxation times were measured and from the slope of transverse relaxation rate (R2 = $1/T_2$) *vs.* [Gd(III)], the transverse relaxivity, r_2 of the complex was found to be 15.48 $mM^{-1}s^{-1}$ (at 25 ºC and pH ~ 7.4) (**Figure 3.18**). The r_2/r_1 = 1.25 value was not high enough to designate the complex as a T_2 contrast agent. Rather, the complex was best described as a T_1 contrast agent.

3.8 Affinity for Physiological Anions

Physiological anions, which are present in sufficient concentration in blood plasma, may be of toxicity concern, as they can easily bind to the metal centre by replacing the inner sphere water molecules. The concentrations of bicarbonate (HCO_3^-) and phosphate (PO_4^{3-}) ions in blood plasma are 24.5 mM and 0.38 mM, respectively, which could be potentially problematic.[17] The affinity of phosphate (PO_4^{3-}), bicarbonate (HCO_3^-), and fluoride (F^-) ions for complex **3A** was evaluated by relaxivity measurements in the presence of 100 equivalents of the respective anions (experimental conditions: 1.41 T, 25 °C, pH ~ 7.4, [complex **3A**] = 0.5 mM,

[physiological anions] = 50 mM). Because of the strong affinity of fluoride ion for lanthanides and formation of stable complex, F^- ion was also included in this study.[18]

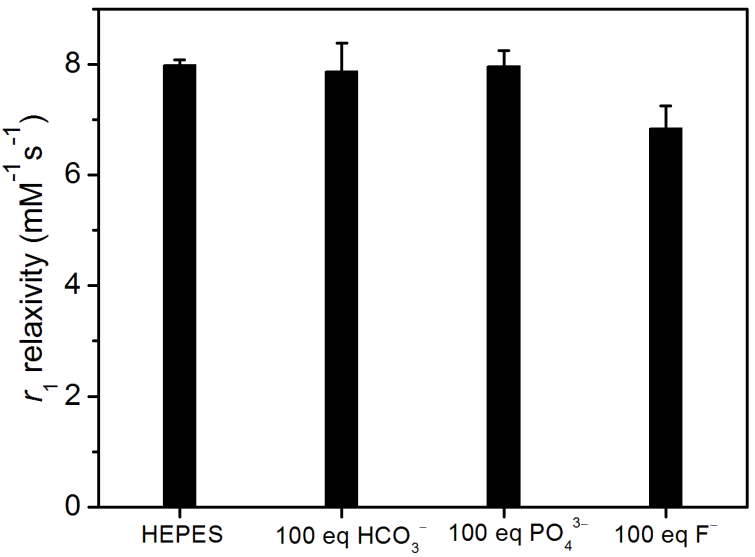

Figure 3.19. Relaxivity measurements of complex **3A** in the presence of 100 equivalents of different anions **(**at 1.41 T, 25 °C, pH ~ 7.4, [complex **3A**] = 0.5 mM, and [physiological anions] = 50 mM).

The result showed that the ions phosphate and bicarbonate did not interact with complex **3A,** whereas in case of fluoride ion, slight decrease in r_1 relaxivity value was observed (Δr_1 = –1.14 $mM^{-1}s^{-1}$) due to the interaction of fluoride ion with the complex.

3.9 Affinity for Physiological Cations

The toxicity of a MRI CA is not only controlled by its high thermodynamic stability but also its selectivity over other metal ions, which are present in blood serum in non–negligible amount. The selectivity of ligand H_4bedik for Gd(III) over Zn(II) and Cu(II) (whose concentrations in serum are 50 μM and 1 μM respectively)[19] was determined by measuring the conditional stability constants pZn and pCu. Following the same protocol used for measuring pGd, competition batch titrations against commercially available DTPA were employed to determine the stability of both Zn(II) and Cu(II) complexes of ligand H_4bedik. From the titration curves (**Figure 3.20**), pZn and pCu values of ligand H_4bedik were found to be 15.9 and 17.0

respectively. The results implied more selectivity of ligand H_4bedik towards Gd(III) over Zn(II) (pGd – pZn = 4.0) and Cu(II) (pGd – pCu = 2.9) in comparison to that of DTPA (for DTPA, pGd – pZn = 3.7, pGd – pCu = 1.1).[15e]

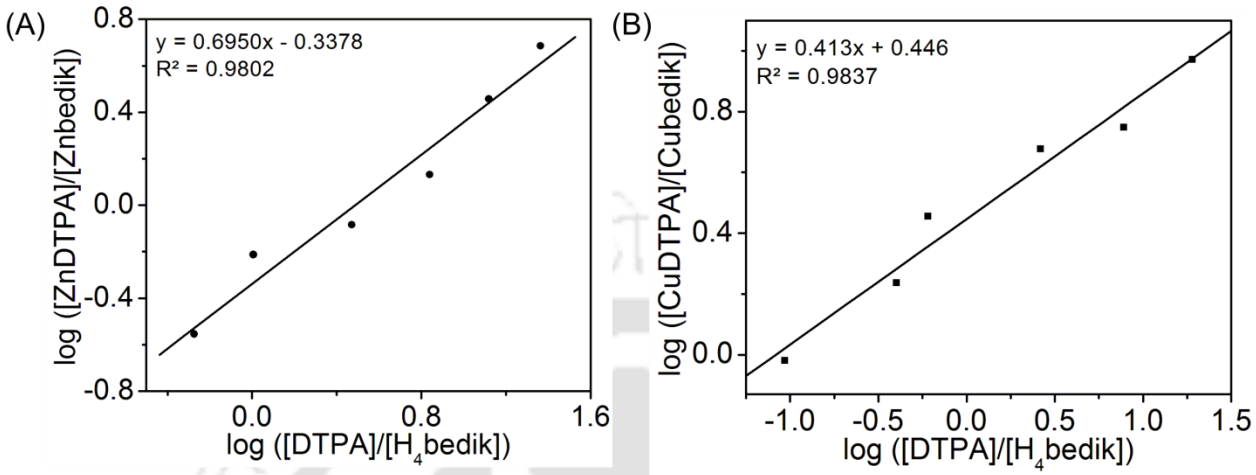

Figure 3.20. Competition batch titrations for determining (A) pZn, and (B) pCu of ligand H_4bedik against DTPA. The *x*–intercepts indicated the differences in pM between H_4bedik and DTPA.

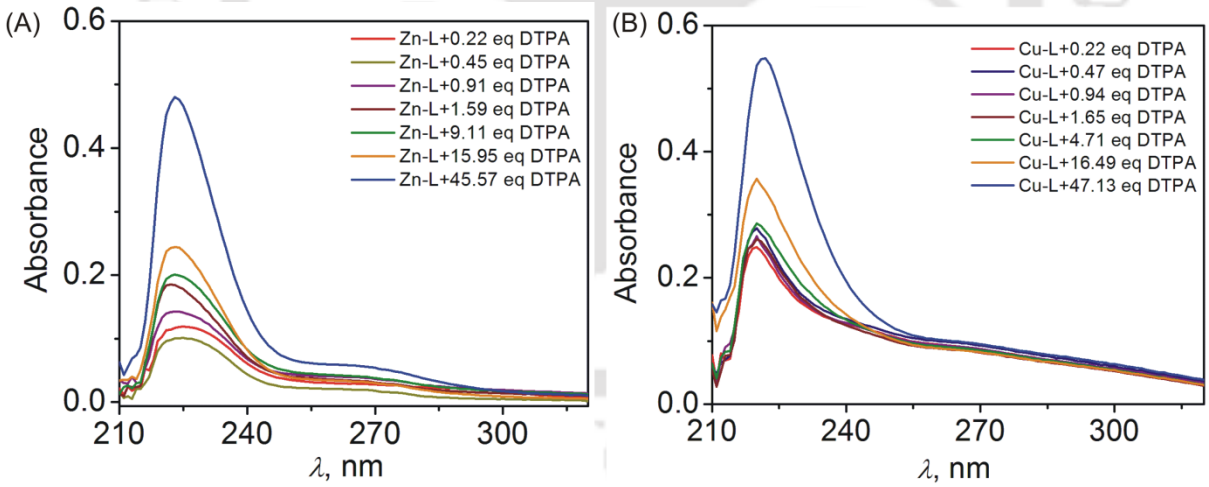

Figure 3.21. Spectral changes during competition batch titration of ligand H_4bedik against DTPA for determining (A) pZn, and (B) pCu. (L in the figures represents ligand H_4bedik)

3.10 Phantom MR Images of Complex 3A at 1.5 T

At 1.5 T, by using clinical MRI scanner BRIVO MR355, T_1–weighted phantom MR images of complex **3A** at four different concentrations 0.25, 0.50, 0.70, and 1.00 mM were measured (at 25 °C, and pH ~ 7.4) (**Figure 3.22**).

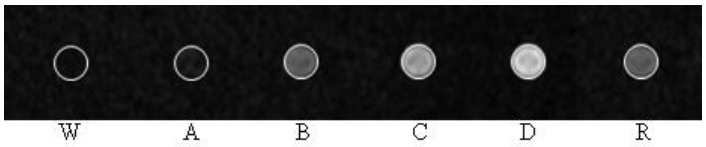

Figure 3.22. T_1–weighted phantom MR images of complex **3A** at 1.5 T, 25 °C, and pH ~ 7.4 (W = water, A = 0.25 mM, B = 0.50 mM, C = 0.70 mM, D = 1.00 mM, R = Reference = MultiHance® = 0.5 M).

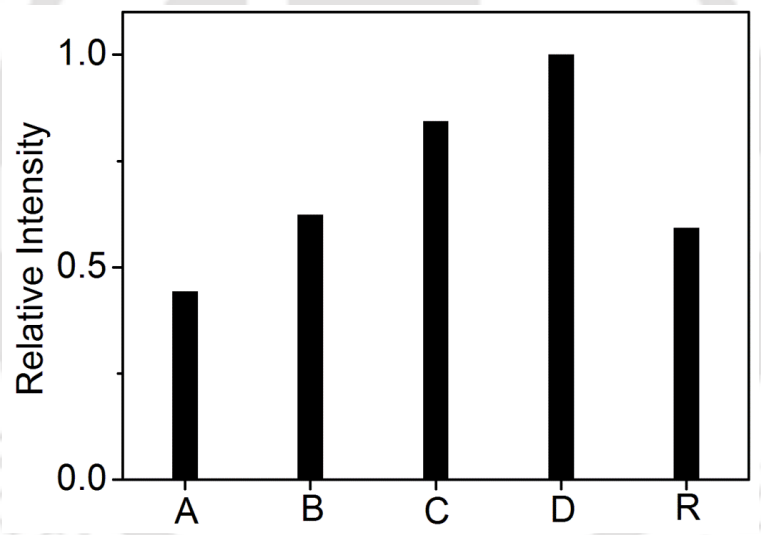

Figure 3.23. Comparison of T_1–weighted phantom MR images of complex **3A** (A = 0.25 mM, B = 0.50 mM, C = 0.70 mM, D = 1.00 mM, R = Reference = MultiHance®) at 1.5 T, 25 °C, and pH ~ 7.4.

When the images were compared with a commercially available MRI contrast agent MultiHance®, complex **3A** showed better image intensity compared to the commercially available one. The comparison of image intensities by using ImageJ Software under the same area of the images also substantiated the complex as a better contrast agent even at very low concentration (**Figure 3.23**).

3.11 Phantom MR Images of Complex 3A at 14.1 T

In a BRUKER NMR microimager at 14.1 T, T_1 and T_2–weighted phantom MR images of complex **3A** were measured by maintaining the complex concentrations 0.25, 0.50, 0.70, and 1.00 mM.

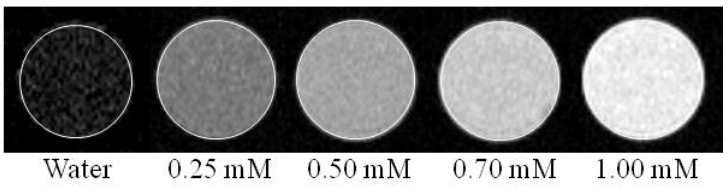

Figure 3.24. T_1–weighted phantom MR images of complex **3A** at four different concentrations, at 14.1 T, 25 °C, and pH ~ 7.4.

It was observed that in case of T_1–weighted images (**Figure 3.24**), with increase in complex concentration, the MR image intensity of the corresponding images increased. Comparison of image intensities by using ImageJ software under the same area of the images is as shown in **Figure 3.25**.

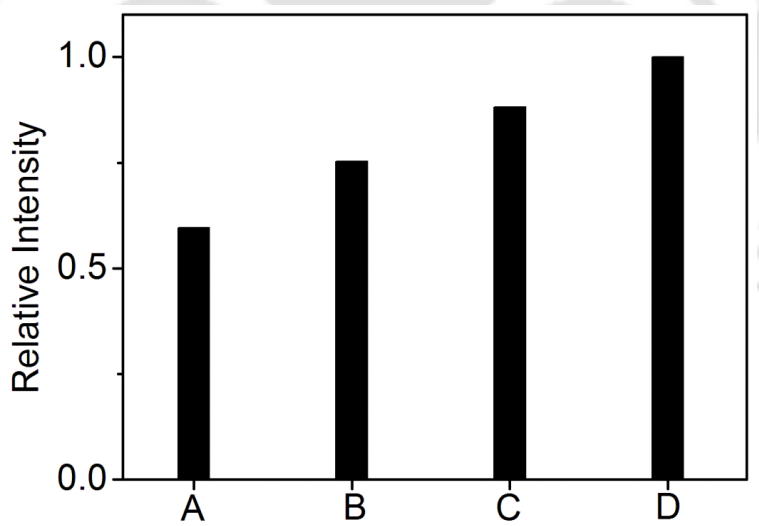

Figure 3.25. Comparison of T_1–weighted phantom MR images of complex **3A** at four different concentrations, at 14.1 T, 25 °C, and pH ~ 7.4 (A = 0.25 mM, B = 0.50 mM, C = 0.70 mM, D = 1.00 mM).

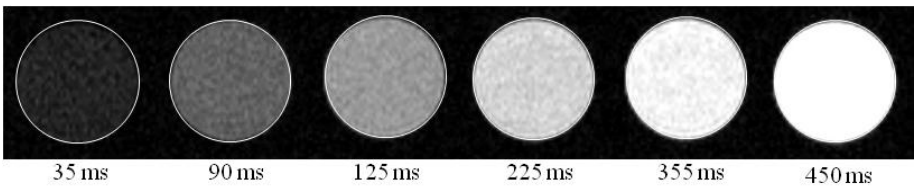

Figure 3.26. Phantom MR images of 1.00 mM concentration of complex **3A** at different repetation time (TR).

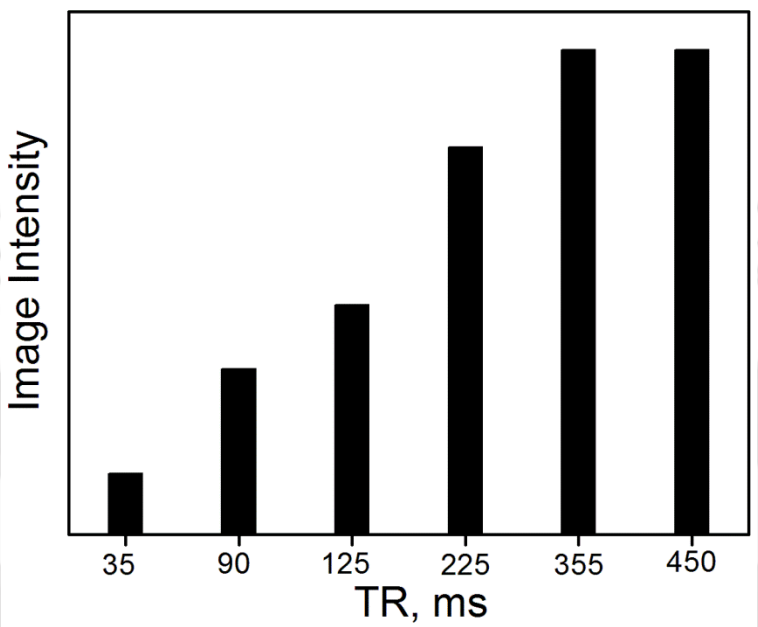

Figure 3.27. T_1–weighted phantom MR images of complex **3A** at different repetition time (TR), at 14.1 T, 25 °C, and pH ~ 7.4.

The phantom MR images of 1.00 mM concentration of complex **3A** at different repetition times (TR) are shown in **Figure 3.26**. **Figure 3.27** shows the comparison of image intensities by ImageJ software. It shows increased image intensity with the repetition time. It was observed that, with increase in TR, the image intensity gradually increased and attained maximum intensity at 355 ms.

The variation of T_1–weighted MRI signal intensity with repetition time (TR) at four different concentrations of the complex (0.25, 0.50, 0.70, and 1.00 mM) is shown in **Figure 3.28**.

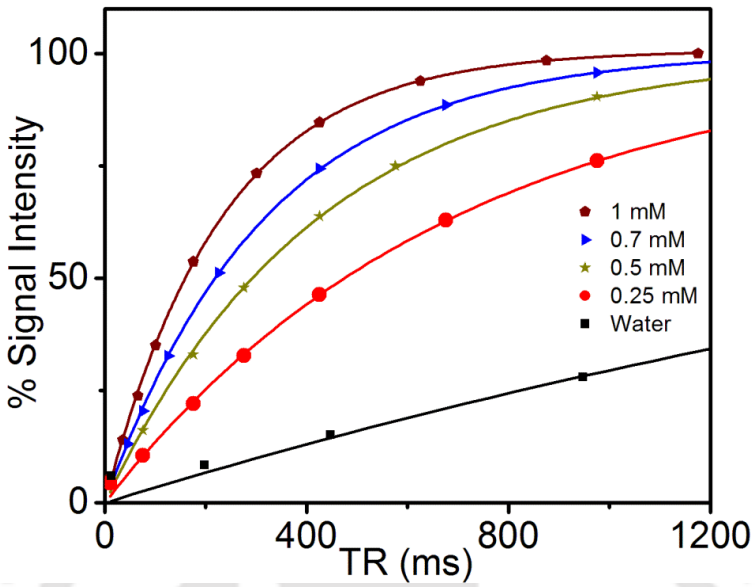

Figure 3.28. Variation of MRI signal intensity with repetition time (TR) at different concentrations of complex **3A**.

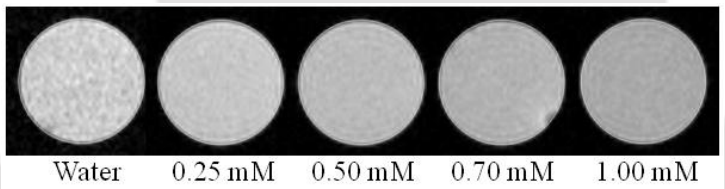

Figure 3.29. T_2–weighted phantom MR images of complex **3A** at four different concentration, at 14.1 T, 25 °C, and pH ~ 7.4.

However, in case of T_2–weighted images, with increase in concentration of complex **3A** from 0.25 mM to 1.00 mM, the T_2–weighted MR image signal intensity remained almost constant as shown in **Figure 3.29**. The comparison of image intensities were done by using ImageJ software and are shown in **Figure 3.30**. The comparison showed that even at the concentration of 1 mM, the image intensity of complex **3A** only dropped to ~ 20 % in comparison to that of water. This decrease in intensity was due to the small r_2 relaxivity value obtained for the complex 15.48 $mM^{-1}s^{-1}$ (at 14.1 T, 25 ºC and pH ~ 7.4).

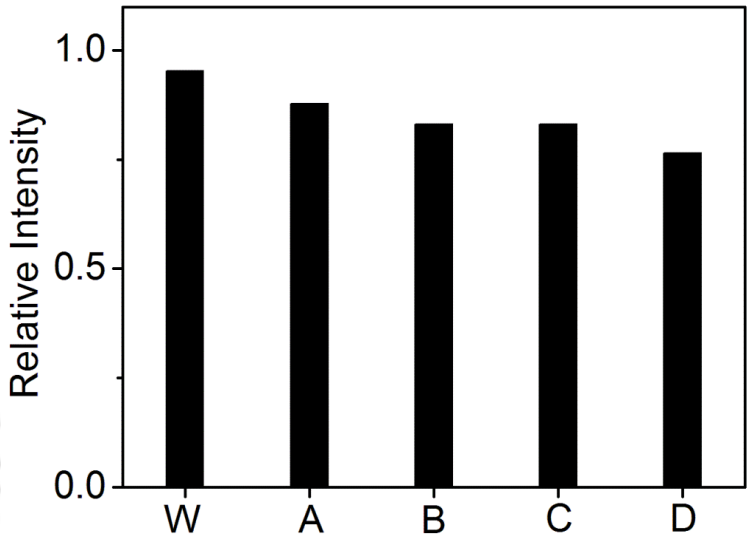

Figure 3.30. Comparison of T_2–weighted phantom MR images of complex **3A** at four different concentrations (W = water only, A = 0.25 mM, B = 0.50 mM, C = 0.70 mM, D = 1.00 mM), at 14.1 T, 25 °C, and pH ~ 7.4.

3.12 Conclusion

- A hexadentate ligand H_4bedik and its corresponding water soluble and bis(aquated) complex, **3A** were synthesised.
- The complex showed better stability than that of commercially available Gd(III) complex of DTPA.
- At 1.41 T, complex **3A** showed r_1 relaxivity value of 7.30 $mM^{-1}s^{-1}$, at pH ~ 7.4 and 25 °C.
- Complex **3A** also showed a higher r_1 relaxivity value of 12.40 $mM^{-1}s^{-1}$, at pH ~ 7.4 and 25 °C; which is an exceptional case in the trend of MRI CAs.
- The ligand H_4bedik was found to be more selective for Gd(III) over Cu(II) and Zn(II), (pGd – pZn = 4.0, pGd – pCu = 2.9) than the commercially available ligand DTPA (pGd – pZn = 3.7, pGd – pCu = 1.1).
- The complex also showed no affinity for biologically available oxyanions, bicarbonate and phosphate, and a little affinity for fluoride ion.
- Phantom MR images of complex **3A** both at 1.5 T (under a clinical MRI scanner) and at 14.1 T (under BRUKER NMR microimager) implicit the usefulness of the complex as a high field MRI CA.
- The investigations on finding out the parameters which could be responsible for this unusual higher relaxivity of the complex are under process.

References

1. (*a*) P. Marzola, F. Osculi and A. Sbarbati, *Eur. J. Radiol.*, 2003, **48**, 165; (*b*) B. Sana, C. L. Poh and S. Lim, *Chem. Commun.*, 2012, **48**, 862; (*c*) M. Takahashi, H. Uematsu and H. Hatabu, *Eur. J. Radiol.*, 2003, **46**, 45; (*d*) P. Caravan, C. T. Farrar, L. Frullano and R. Uppal, *Contrast Media Mol. Imaging*, 2009, **4**, 89; (*e*) J. B. Livramento, C. Weidensteiner, M. I. M. Prata, P. R. Allegrini, C. F. G. C. Geraldes, L. Helm, R. Knuer, A. E. Merbach, A. C. Santos, P. Schmidt and É. Tóth, *Contrast Media Mol. Imaging*, 2006, **1**, 30.
2. T. Vaughan, L. DelaBarre, C. Snyder, J. Tian, C. Akgun, D. Shrivastava, W. Liu, C. Olson, G. Adriany, J. Strupp, P. Andersen, A. Gopinath, P. F. van de Moortele, M. Garwood and K. Ugurbil, *Magn. Reson. Med*., 2006, **56**, 1274.
3. (*a*) V. D. Schepkin, F. C. Bejarano, T. Morgan, S. Gower-Winter, M. Ozambela Jr. and C. W. Levenson, *Magn. Reson. Med*., 2012, **67**, 1159; (*b*) R. Fu, W. W. Brey, K. Shetty, P. Gor'kov, S. Saha, J. R. Long, S. C. Grant, E. Y. Chekmenev, J. Hu, Z. Gan, M. Sharma, F. Zhang, T. M. Logan, R. Brüschweller, A. Edison, A. Blue, I. R. Dixon, W. D. Markiewicz and T. A. Cross, *J. Magn. Reson.*, 2005, **177**, 1.
4. M. Rohrer, H. Bauer, J. Mintorovitch, M. Requardt and H. J. Weinmann, *Invest. Radiol.*, 2005, **40**, 715.
5. (*a*) P. Hermann, J. Kotek, V. Kubíček and I. Lukeš, *Dalton Trans.*, 2008, 3027; (*b*) E. Boros, E. M. Gale and P. Caravan, *Dalton Trans.*, 2005, **44**, 4804; (*c*) V. C. Pierre, M. J. Allen and P. Caravan, *J. Biol. Inorg. Chem*., 2014, **19**, 127.
6. (*a*) E. J. Werner, J. Kozhukh, M. Botta, E. G. Moore, S. Avedano, S. Aime and K. N. Raymond, *Inorg. Chem.*, 2009, **48**, 277; (*b*) J. Xu, S. J. Franklin, D. W. Whisenhunt Jr. and K. N. Raymond, *J. Am. Chem. Soc.*, 1995, **117**, 7245; (*c*) C. J. Jocher, M. Botta, S. Avedano, E. G. Moore, J. Xu, S. Aime and K. N. Raymond, *Inorg. Chem.*, 2007, **46**, 4796; (*d*) E. J. Werner, S. Avedano, M. Botta, B. P. Hay, E. G. Moore, S. Aime and K. N. Raymond, *J. Am. Chem. Soc.*, 2007, **129**, 1870.
7. E. M. Gale, M. Kenton and P. Caravan, *Chem. Commun.*, 2013, **49**, 8060.
8. (*a*) J. Wang, G. R. Gao, Z. H. Zhang, X. D. Zhang, X. Z. Liu, Y. M. Kong and Y. Li, *Russ. J. Coord. Chem.*, 2007, **33**,258; (*b*) E. S. G. Choo, X. Tang, Y. Sheng, B. Shuter and J. Xue, *J. Mater. Chem*., 2011, **21**, 2310; (*c*) J. Coates, *Interpretation of Infrared Spectra: A Practical Approach*, John Wiley & Sons Ltd, Chichester, 2000; (*d*) B. C. Smith, *Infrared Spectral Interpretation: A Systematic Approach*, CRC press, 1998.

9. (*a*) M. Rogosnitzky and S. Branch, *Biometals*, 2016, **29**, 365; (*b*) A. D. Sherry, P. Caravan, , R. E. Lenkinski, *J. Magn. Reson. Imaging*, 2009, **30**(6), 1240; (*c*) M. Panesar, F. Boateng, S. S. Patel, S. F. Massod, P. Mahajan, N. Patel and B. Murray, *Hemodial. Int*., 2010, **14**, 289.
10. (*a*) E. Hvaltum, P. T. Normamm, G. C. Jamieson, J. J. Lai and T. Skotland, *J. Pharm. Biomed. Anal.*, 1995, **13**, 927; (*b*) S. W. Kang, C. M. Park, K. H. Cho, H. S. Han, *Bull. Korean Chem. Soc.*, 1993, **14**, 59; (*c*) A. Barge, G. Cravotto, E. Gianolio, F. Fedeli, *Contrast Med. Mol. Imaging*, 2006, **1**, 184.
11. K. V. Yatsimirsky, N. A. Kostromina, Z. A. Seka, N. K. Davidenko, E. E. Kriss, V. J. Ermolenko, *Khimya komplexnikh redkozemel' nikh elementov*. Naukova Dumka: Kiev, 1966.
12. J. G. Bünzli and C. Piguet, *Chem. Soc. Rev*., 2005, **34**, 1048.
13. A. Beeby, I. M. Clarkson, R. S. Dickins, S. Faulkner, D. Parker, L. Royle, A. S. de Sousa, J. A. G. Williams and M. Woods, *J. Chem. Soc. Perk. T. 2*, 1999, 493.
14. (*a*) G. R. Choppin and D. R. Peterman, *Coordin. Chem. Rev*., 1998, **174**, 283; (*b*) W. D. Horrocks Jr. and D. R. Sudnick, *Acc. Chem. Res.*, 1981, **14**, 384; (*c*) L. M. Manus, R. C. Strauch, A. H. Hung, A. L. Eckermann and T. J. Meade, *Anal. Chem*., 2012, **84**, 6278.
15. (*a*) D. M. J. Doble, M. Melchior, B. O'Sullivan, C. Siering, J. Xu, V. C. Pierre and K. N. Raymond, *Inorg. Chem.*, 2003, **42**, 4930; (*b*) C. J. Jocher, E. G. Moore, J. Xu, S. Avedano, M. Botta, S. Aime and K. N. Raymond, *Inorg. Chem.*, 2007, **46**, 9182; (*c*) D. T. Puerta, M. Botta, C. J. Jocher, E. J. Werner, S. Avedano, K. N. Raymond and S. M. Cohen, *J. Am. Chem. Soc.*, 2006, **128**, 2222 (*d*) K. N. Raymond and V. C. Pierre, *Bioconjugate Chem.*, 2005, **16**, 3; (*e*) V. C. Pierre, M. Botta, S. Aime and K. N. Raymond, *Inorg. Chem.*, 2006, **45**, 8355.
16. A. Nonat, C. Gateau, P. H. Fries, L. Helm and M. Mazzanti, *Eur. J. Inorg. Chem.*, 2012, 2049.
17. A. Merbach, L. Helm and É. Toth, *The Chemistry of Contrast Agents in Medical Magnetic Resonance Imaging*, Second Edition, Wiley, New York, 2001.
18. M. Botta, S. Aime, A. Barge, G. Bobba, R. S. Dickins, D. Parker, E. Terreno, *Chem. Eur. J.*, 2003, **9**, 2102.
19. W. P. Cacheris, S. C. Quay and S. M. Rocklage, *Magn. Reson. Imaging*, 1990, **8**, 467.

Chapter IV

A New Water–Coordinated Seven–Coordinate Mn(II) Complex as T_1– and T_2– Dual Mode MRI Contrast Agent

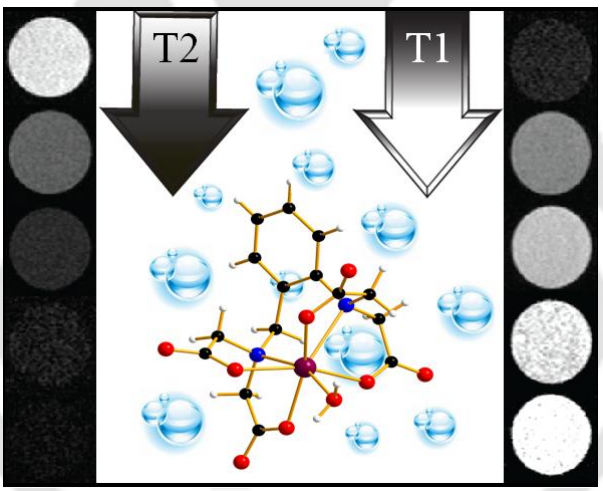

*Published in *Dalton Trans.*, 2015, **44**, 12990.

4.1 Introduction

The discovery of the disease Nephrogenic Systemic Fibrosis (NSF) has prompted new research to develop safer MRI contrast agents (CAs). NSF is a systemic disorder which characteristically exhibits fibrosis (formation of scar tissue) of the skin and the connective tissues and till now there is no effective treatment of NSF.[1] Some of the Gd(III)–based MRI CAs are known to cause this disease in patients having severe kidney diseases or following liver transplantation.[2] In these patients, lacking of proper excretion mechanism due to severe kidney dysfunction, small molecule contrast agents could not be excreted for several days or weeks, which leads to dissociate Gd(III)–based CAs, leaving the toxic ligands and free Gd(III) ions in the body. This Gd(III) has a high affinity for Ca(II) ion channels and has been associated with a thickening of organs and skin. In this regard, the requirements were for an alternative to Gd(III)–based contrast agents with high water solubility and high relaxivity that could be rapidly eliminated from the body after administration of the CAs. The metal complexes of some other paramagnetic metal ions with large number of unpaired electrons, such as Fe(III) [$3d^5$, S = 5/2], and Mn(II) [$3d^5$, S = 5/2], have obtained special attention in this field.

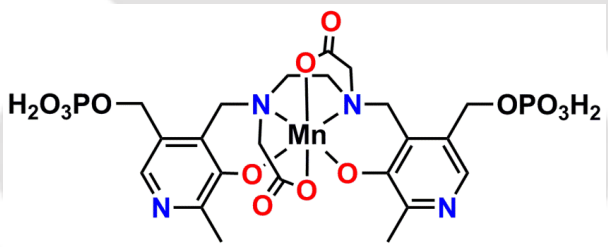

Figure 4.1. Commercially available Mn(II)–based MRI CA, Teslascan®.

Mn(II) ion became the best alternative to Gd(III) ion because of five unpaired electrons, slow electronic relaxation and high water exchange rate.[3] Additionally, Mn(II) is an essential element in human biological system and acts as a cofactor in enzymes, *e. g.*, manganese superoxide dismutase, arginase, and glutamine synthetase.[4] In the history of MRI, manganese has played an important role since $MnCl_2$ was the first contrast agent proposed by Paul Lauterbur while describing the first MRI image.[5] Later, the relaxation effects of $MnCl_2$ were studied in different animals. A very special technique related to manganese ion is the Manganese–Enhanced MRI (MEMRI), which is an interesting combination of high relaxivity value and unique biology of $[Mn(H_2O)_6]^{2+}$.[6] MEMRI relies on the facts that Mn(II) is a Ca(II) analogue and can be taken up by the activated neurons in the brain. Mn(II) ion then migrates along neuronal

processes, and finally gets eliminated by neurons. CMC–001, which is a mixture of $MnCl_2$, alanine, and vitamin D_3, is employed for visualization of liver and bile.[7] In phase I and phase II studies of CMC–001, in total 196 patients and healthy volunteers have been exposed to it and no serious adverse events related to the administration of the compound have been reported so far. Presently, CMC–001 is undergoing final clinical evaluation in phase III, where a large number of patients with liver metastases are being exposed to the compound to know how to use this contrast agent in the most optimal way in the clinical setting. Although several Mn(II)–based contrast agents have been investigated over the past decade, but so far, only one is commercially available, Teslascan®, $Mn(DPDP)^{4-}$, {($DPDP^{6-}$ = *N*,*N*′–dipyridoxylethylenediamine–*N*,*N*′–diacetate–5,5′–bisphosphate) (**Figure 4.1**)} used for human liver imaging.[8] The complex $Mn(DPDP)^{4-}$ itself contains no inner–sphere water molecule, and the observed relaxivity arises from the release of free Mn(II) ion in the body. Although bare Mn(II) ion is very efficient in understanding the detailed brain structure; achieving high quality image of liver lesions, a large dose of Mn(II) can cause neurological disorder in human being called 'Manganism', a Perkinson–like symptom, which is due to accumulation of Mn(II) ion in the brain.[9] Therefore, the MEMRI technique is limited to small animals imaging only.

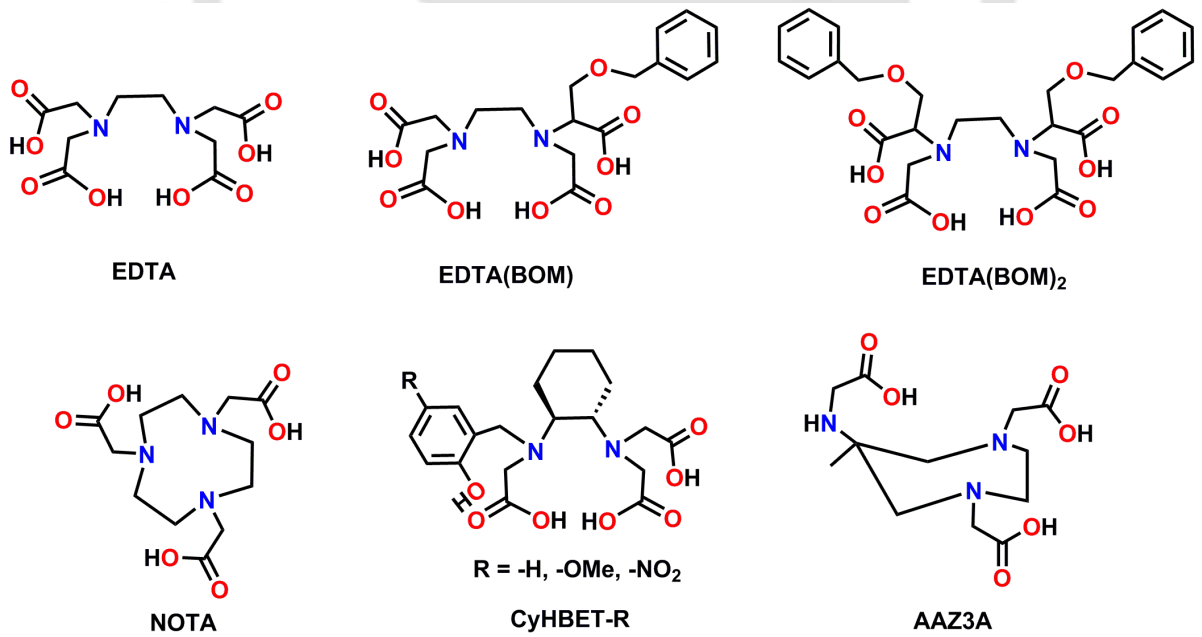

Scheme 4.1. Ligands studied for synthesising mono(aquated) seven–coordinate Mn(II) complex.

In this context, synthesis of stable and water–soluble Mn(II) complexes as MRI CAs have been demanding considerable attention.[10] A good Mn(II)–based MRI CA requires coordination of at least one water molecule to the Mn(II) centre. Most of the stable Mn(II) complexes are

mainly six–coordinate with no coordinated–water molecule. In search of water–coordinated seven–coordinate complexes, Mn(II) complexes of linear polydentate ligands (EDTA[3a], EDTA(BOM)[10b], $EDTA(BOM)_2$[10b], CyHBET–R[10k] etc.) and macrocyclic ligands (NOTA[3a], AAZ3A[10a] etc.) have been studied (**Scheme 4.1**). It has been recently suggested that the rigidified backbone of a ligand with complementary cavity for metal ion is helpful for increasing the complex stability, and favourable for improving longitudinal relaxivity. E. Tóth *et al*. reported a series of 12/15–membered pyridine based macrocyclic pentadentate ligands (12–pyDO1R, 15–pyN_5, 15–pyN_3O_2), which provide Mn(II) complexes with one or two inner–sphere water molecules.[11]

In order to improve diagnosis accuracy, there is a growing interest for developing dual mode contrast agents (DMCAs).[12] DMCAs are combination of both T_1 and T_2 MRI CAs and can simultaneously provide images of both modes (brightening and darkening). Employment of DMCAs would eliminate the confusion arises due to the same darker signals from T_2 contrast agents, and calcification or internal blood clotting. Most of the reported DMCAs generally consist of two parts: one is Gd(III) or Mn(II)–based materials for T_1–weighted MR imaging and the other is Fe(III)–based or Mn(II)–based nanoparticles for T_2–weighted MR imaging.[13] However, it is very challenging to develop a strong DMCA. When both T_1 and T_2 contrast agents come in close proximity, they interfere with each other, and as a result, the T_1 relaxivity decreases. Thus, developing DMCAs with single component (Fe(III)–, Mn(II)– or Gd(III)–based) without any conflicting effect is still a great challenge.

Herein, in order to achieve water coordinated seven–coordinate Mn(II) complex, ligand H_4bedik was synthesized (**Scheme 4.2**), which contained a 2–amidobenzylamide backbone. In the ligand, the presence of sp^3 methylene unit in the backbone created an asymmetric environment and a difference in the coordination capability of the two backbone–belonging nitrogen atoms. This asymmetric coordination environment favoured water molecule to bind to the central Mn(II) metal ion and consequently, a seven–coordinate Mn(II) complex was achieved. In order to impose water solubility of the ligand as well as the corresponding Mn(II) complex, all the H–atoms of the backbone–belonging two amine units were substituted by four acetic acid units.

4.2 Synthesis and Characterisation of Ligand H_4bedik, $C_{15}H_{18}N_2O_8$

A schematic representation for the synthesis of ligand H_4bedik is shown in **Scheme 4.2**.

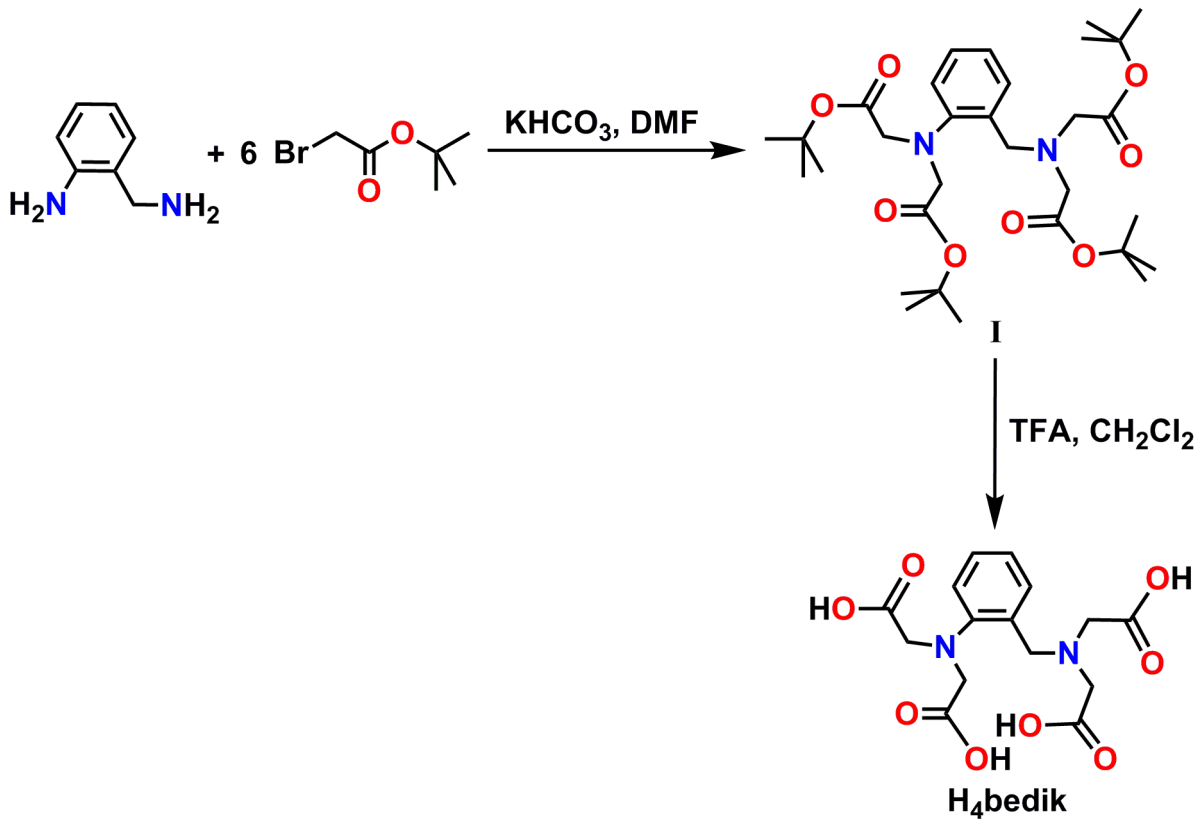

Scheme 4.2. Synthetic route of ligand H_4bedik.

A reaction between 1:6 2–aminobenzylamine and *tert*–butylbromoacetate mixture in DMF in the presence of $KHCO_3$ provided **I**, which upon reaction with trifluoroacetic acid provided ligand H_4bedik as a white solid. The characterisation of ligand H_4bedik by using FTIR spectroscopy, NMR spectroscopy and mass spectrometry technique has already been discussed in **Chapter III**.

4.3 Synthesis and Characterisation of Water Coordinated Mn(II) Complex of Ligand H_4bedik, 4A

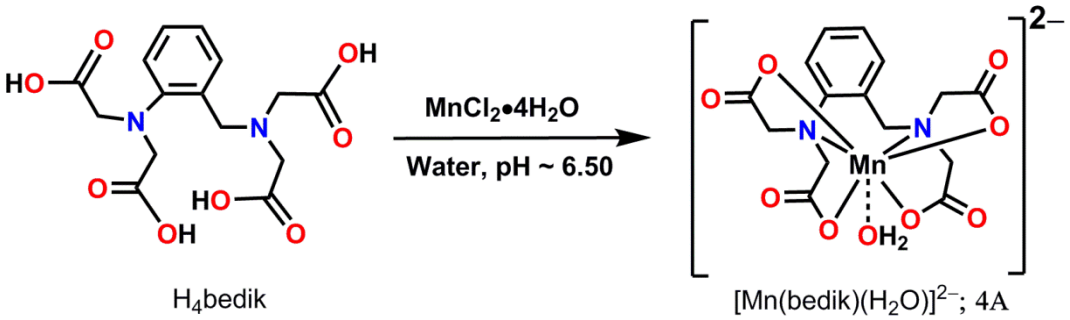

Scheme 4.3. Synthesis of complex **4A**, $[C_{15}H_{16}MnN_2O_9]^{2-}$.

To a solution of H_4bedik in water, $MnCl_2$•$4H_2O$ was added and stirred the reaction mixture for 10 minutes. The solution became transparent and then pH was adjusted to ~ 6.5 by dropwise addition of aq. NaOH solution. Stirring was continued at room temperature (25 °C) for 24 h and the clear solution was kept at room temperature for crystallisation. Colourless crystals were obtained suitable for single crystal X–ray study.

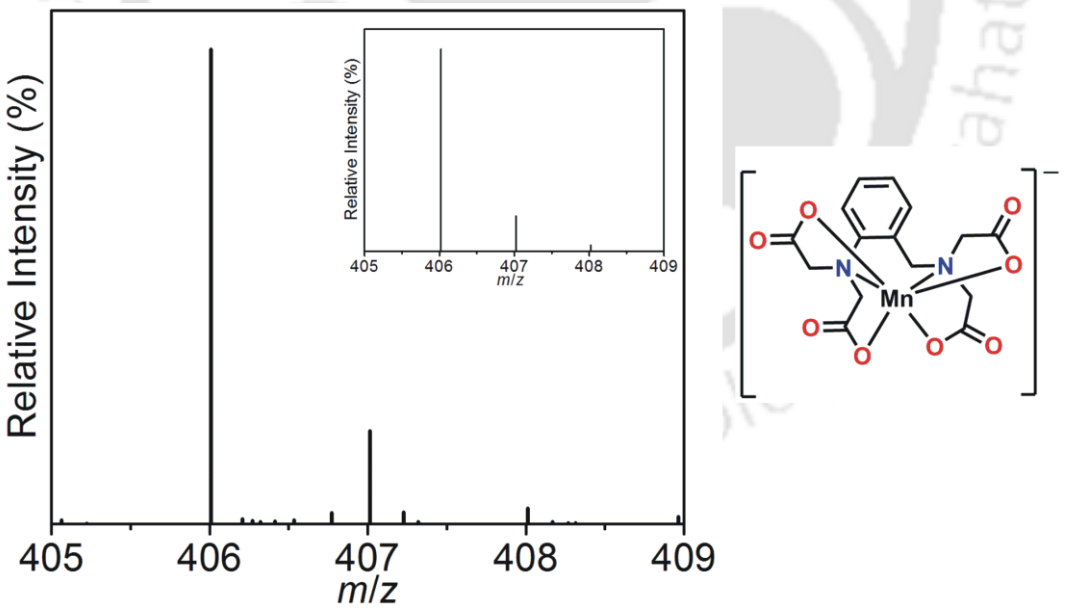

Figure 4.2. ESI–MS spectrum of complex **4A**. Simulated spectrum has been given as inset.

Electrospray ionisation mass spectrum of complex **4A** (**Figure 4.2**) in Mili Q water provided a 100% ion peak at 406.0095 amu in the negative mode. Simulated isotope distribution

pattern indicated a composition of $[C_{15}H_{14}MnN_2O_8 + H]^-$ (*m/z* = 406.0209 amu) for the observed peak.

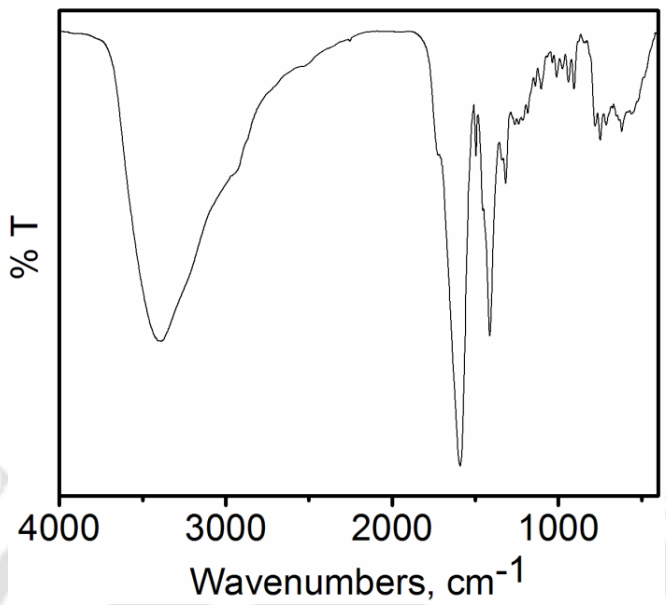

Figure 4.3. FTIR spectrum of complex **4A**.

Infrared (IR) spectrum (**Figure 4.3**) of complex **4A** showed a sharp band at 3391 cm^{-1} due to *ν*(O–H) stretching.[14a] The *ν*(C=O) stretching frequency of the complex appeared as a sharp band at 1591 cm^{-1} whereas that of the ligand was observed at 1726 cm^{-1}.[14b]

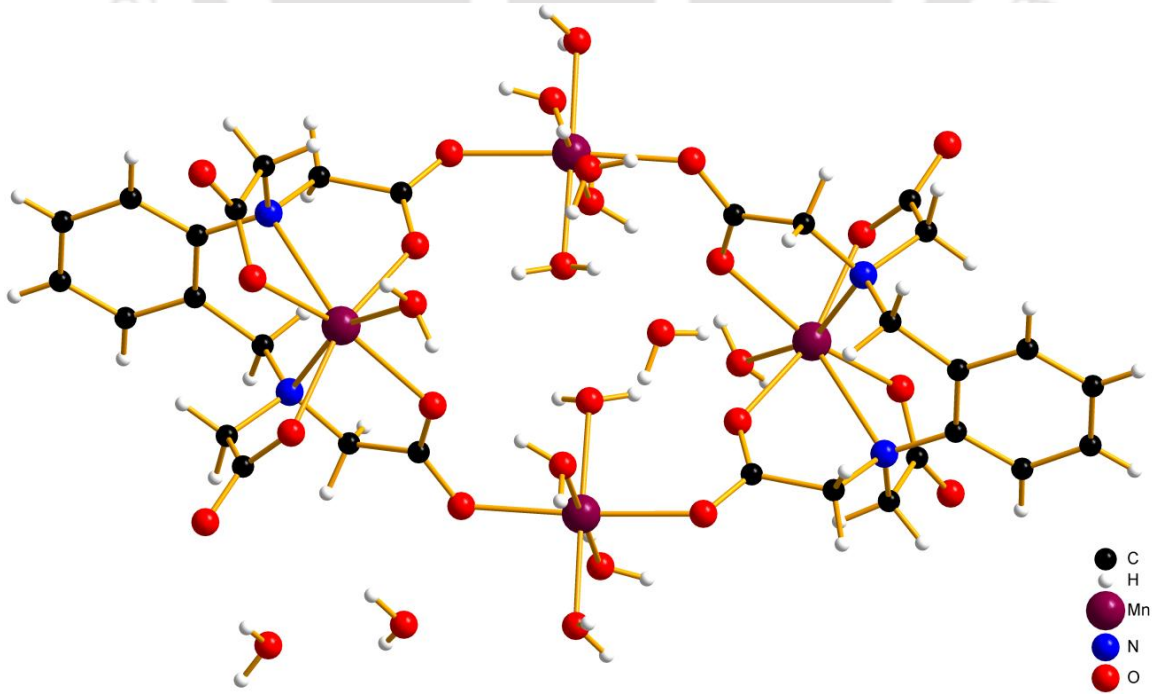

Figure 4.4. Showing a unit cell in the crystal structure of complex **4A**.

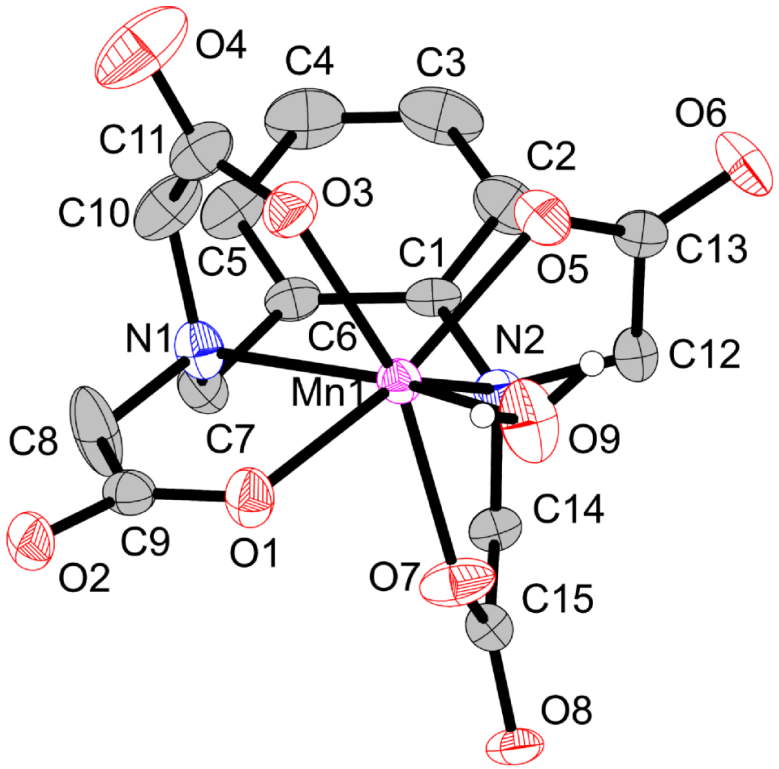

Figure 4.5. ORTEP representation of complex **4A** (dinegative unit); thermal ellipsoids were drawn at 50% probability level, all hydrogen atoms except the bound water, and solvent molecules were omitted for clarity.

Single crystal X–ray diffraction measurement for complex **4A** was performed at 293 K. The complex crystallized in the triclinic *P*–1 space group. Molecular structure (only the dinegative unit) is shown in **Figure 4.5**. Selected bond distances and bond angles are given in **Table 4.1**.

In the crystal structure, it has been found that a unit cell was comprised of two neutral molecules (**Figure 4.4**). Each asymmetric unit, *i.e.*, each neutral molecule, was composed of two Mn(II) ion–containing units, which were different in terms of coordination environment and formal charge. Mn1 was seven–coordinate and was encapsulated by the six–coordinate tetranegative ligand, $[bedik]^{4-}$, and a neutral water molecule. This unit was formally dinegative. The other Mn(II) centre, Mn2, was octahedrally coordinated by four water molecules and two neutral keto oxygen atoms (O2, and O8) from two dinegative units, hence, the overall dipositive formal charge prevailed in this unit.

In the dinegatively charged unit, the Mn1–O1 = 2.228(2), Mn2–O3 = 2.257(3), Mn–O5 = 2.201(2), Mn–O7 = 2.197(2), Mn1–N1 = 2.339(3), and Mn1–N2 = 2.650(3) Å bond distances

indicated that the geometry around Mn1 centre was asymmetric and the asymmetric environment was mainly caused by Mn–N coordination linkages. The presence of sp^3 methylene unit (C7) between C6 and N1 promoted more flexibility in the C6–C7–N1 arm than that of C1–N2 arm. Hence, N1 experienced a closer exposure to Mn1 than that of N2. The coordinated water molecule was tightly bound with the Mn(II) centre with Mn–O bond distance of 2.184(2) Å.

Table 4.1. Selected bond distances (Å) and bond angles (º) for complex **4A**:

Mn1–O1	2.228(2)	O1–Mn1–O3	81.19(10)
Mn1–O5	2.201(2)	O1–Mn1–N1	76.86(9)
Mn1–O3	2.257(3)	O5–Mn1–O1	155.67(10)
Mn1–O9	2.184(2)	O5–Mn1–O3	79.63(10)
Mn1–O7	2.197(3)	O5–Mn1–N1	111.36(10)
Mn1–N1	2.339(3)	O3–Mn1–N1	73.26(10)
Mn1–N2	2.650(3)	O9–Mn1–O1	83.33(9)
O8–C15	1.247(4)	O9–Mn1–O5	83.45(10)
O1–C9	1.257(4)	O9–Mn1–O3	94.68(10)
O4–C11	1.250(5)	O9–Mn1–O7	84.92(11)
O2–C9	1.265(4)	O9–Mn1–N1	158.08(10)
O6–C13	1.246(4)	O7–Mn1–O1	81.66(10)
O5–C13	1.260(4)	O7–Mn1–O5	117.33(10)
O3–C11	1.253(4)	O7–Mn1–O3	62.78(9)
O7–C15	1.258(4)	O7–Mn1–N1	101.19(11)

Table 4.2. Crystallographic data for complex **4A**:

Empirical formula	$C_{30}H_{64}Mn_4N_4O_{34}$
Formula weight	1244.61
Crystal habit, colour	Plates/ colourless
Crystal size, mm^3	0.30 × 0.28 × 0.24
Temperature, T(K)	293(2)
Wavelength, λ (Å)	0.71073
Crystal system	Triclinic
Space group	*'P*–1*'*
Unit cell dimensions	a = 10.4029(8) Å b =11.7222(8) Å c = 11.8865(7) Å α = 71.602(6) ° β = 64.303(7) ° γ = 77.400(6) °
Volume, V ($Å^3$)	1233.77(15)
Z	1
Calculated density, $mg \cdot mm^{-3}$	1.675
Absorption coefficient, μ (mm^{-1})	1.106
F(000)	644.0
θ range for data collection	2.99 to 25.00°
Limiting indices	$-12 \le h \le 12, -13 \le k \le 13, -14 \le l \le 11$
Reflection collected / unique	6911/3840
Completeness to θ	88.3% (θ = 25.00°)
Max. and min. transmission	0.767/0.725
Refinement method	'SHELXL–97 (Sheldrick, 1997)'
Data / restraints / parameters	3840/0/324
Goodness–of–fit on F^2	1.074
Final R indices [I>2sigma(I)]	R_1 = 0.0423, wR_2 = 0.0890
R indices (all data)	R_1 = 0.0583, wR_2 = 0.1012
Largest diff. peak and hole	0.451/–0.385 e $Å^{-3}$

4.4 Stability of Complex 4A

To use any complex as MRI CA, one practical concern associated with it is its stability. Spectrophotomeric titration method was used to determine the conditional stability constant, pM[15] of ligand H_4bedik with Mn(II), where pM is defined as:

$$pM = -\log [M^{n+}]_{free}$$

i.e., –log of the concentration of free metal ion typically at the condition when metal ion concentration, [M] = 1 μM and ligand concentration, [L] = 10 μM at pH = 7.4 and temperature 25 °C.

A competition batch titration was performed with EDTA (ethylenediaminetetraacetic acid) as the competing ligand to determine the pMn value of the ligand H_4bedik at 25 °C. In case of Mn(II)–based MRI CAs, EDTA serves as a reference, as $[Mn(EDTA)]^{2-}$ derivatives have been successfully employed in *in vivo* MRI studies.[3b,10b]

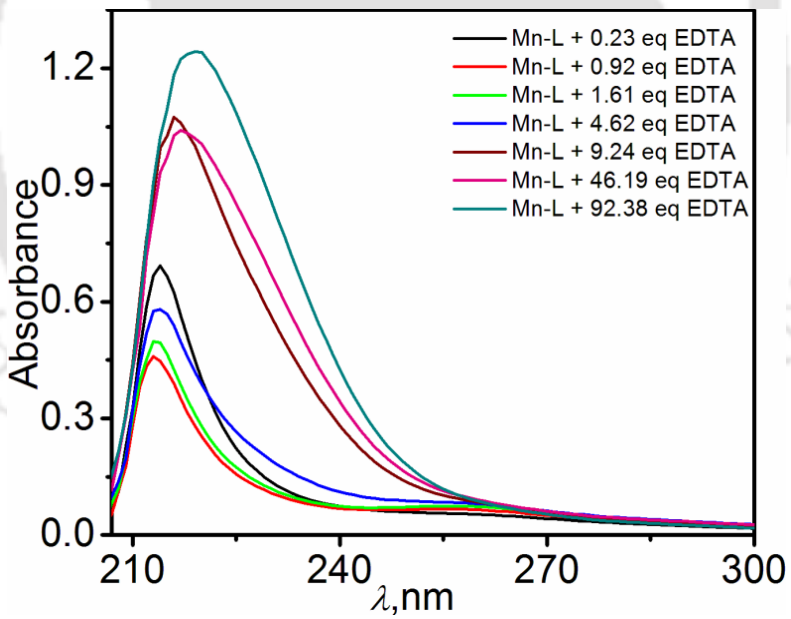

Figure 4.6. Spectral changes during competition titration of ligand H_4bedik against EDTA. (L in the figure represents ligand H_4bedik)

In this method, different volumes of EDTA stock solutions were added to the solutions of constant concentrations of ligand H_4bedik and Mn(II). pH was kept constant at 7.4 by using 10 mM HEPES buffer. The solutions were kept for 24 h to ensure thermodynamic equilibrium. The

concentration of the free and the complexed ligand in each solution were then determined by UV–vis spectroscopy.

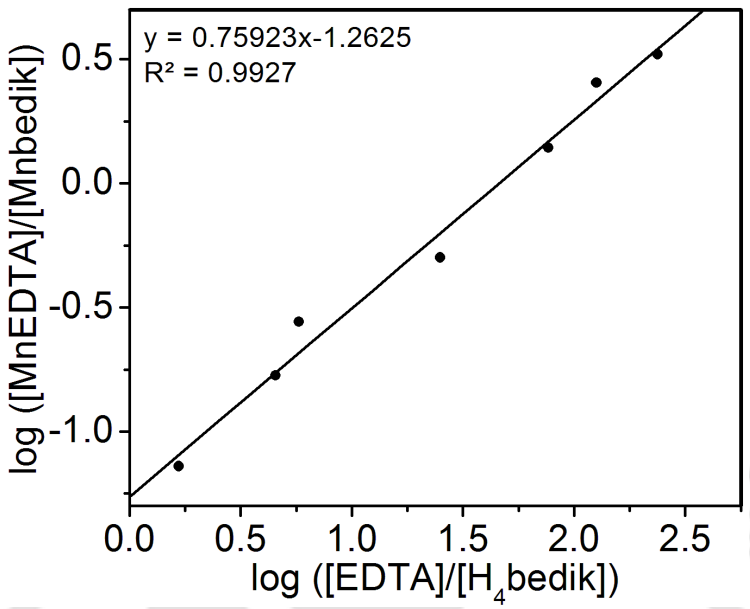

Figure 4.7. Competition titration of H_4bedik against EDTA.

From the *x*–intercept of the plot of log ([MnEDTA]/[Mnbedik]) *vs.* log ([EDTA]/[H_4bedik]), the difference in pMn between the ligand and EDTA was obtained (**Figure 4.7**). This difference was the value of log ([EDTA]/[H_4bedik]) when log ([MnEDTA]/[Mnbedik]) = 0 or when the concentration of EDTA generates an equal partition of Mn(II) between ligand H_4bedik and EDTA. Using the value 8.05 for pMn of EDTA,[11] the pMn of ligand was found to be 9.71 which implied the usefulness of complex **4A** as a thermodynamically stable alternative to Gd(III)–based MRI CA.

4.5 Relaxivity Measurements of Complex 4A at 1.41 and 14.1 T

Having confirmed adequate stability, the longitudinal relaxivity, r_1 of complex **4A** was measured at 1.41 T in a BRUKER minispec mq60 NMR analyzer. By using inversion recovery method, the longitudinal relaxation times, T_1 were measured at four different concentrations of the complex, and the slope of the plot of longitudinal relaxation rate (R1 = $1/T_1$) *vs.* [Mn(II)] provided longitudinal relaxivity, r_1 (**Figure 4.8**). The exact Mn(II) concentration was measured

by ICP–AES method. It was observed that with the increase in concentration of the complex, R1 increased linearly.

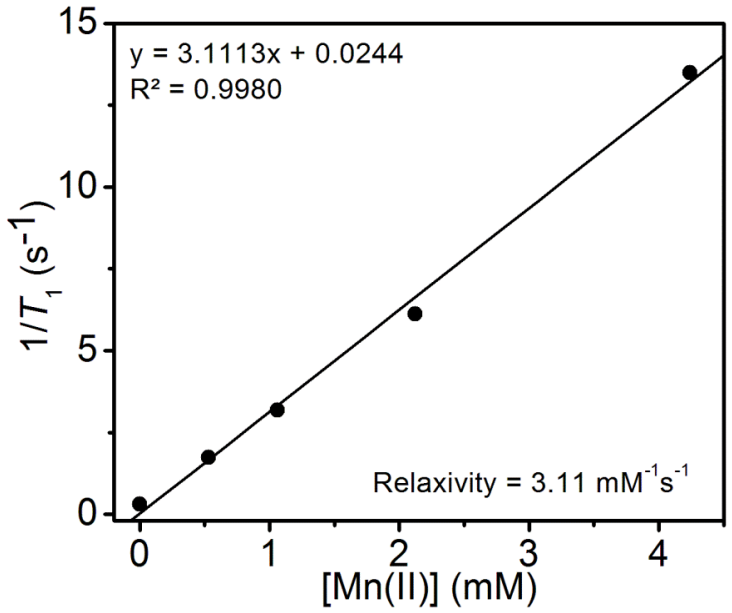

Figure 4.8. $1/T_1$ *vs.* [Mn(II)] plot. Measurements were performed using complex **4A** at 1.41 T, 25 °C, and pH ~ 7.4.

The r_1 value of the complex was found to be 3.11 $mM^{-1}s^{-1}$ (at 25 °C and pH ~ 7.4) per Mn(II), which was higher than that of the commercially available Mn(II)–based MRI CA, Teslascan® (r_1 = 2.1 $mM^{-1}s^{-1}$, at 1.5 T).[16]

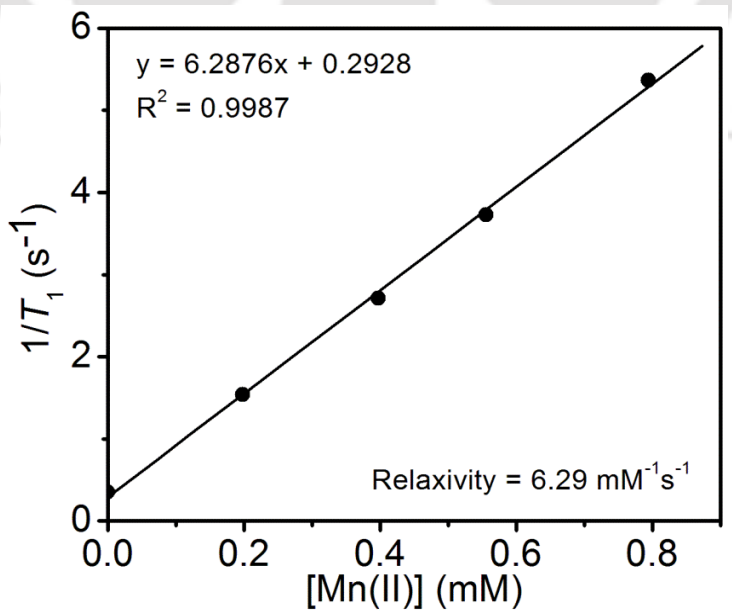

Figure 4.9. $1/T_1$ *vs.* [Mn(II)] plot. Measurements were performed using complex **4A** at 14.1 T, 25 °C, and pH ~ 7.4.

MRI at stronger magnetic fields provides higher signal–to–noise ratio with better spatial resolution and reduced acquisition times.[17] In this regard, relaxivity measurements were performed at a high field (14.1 T) by using saturation recovery method. Similar to 1.41 T, longitudinal relaxation time, T_1 was measured at four different concentrations of complex **4A**, at 25 °C, and pH ~ 7.4 and the slope of the plot of longitudinal relaxation rate (R1 = $1/T_1$) *vs.* [Mn(II)] provided longitudinal relaxivity, r_1 at 14.1 T (**Figure 4.9**).

To note, a higher r_1 relaxivity value of 6.29 $mM^{-1}s^{-1}$ per Mn(II) was found at 14.1 T. This indicated that unlike other MRI CA, r_1 was unconventionally increasing for complex **4A** with increase in field strength. A multimeric nature of the complex and intermediate correlation time (0.5–4 ns) have been suggested for such behaviour.[18]

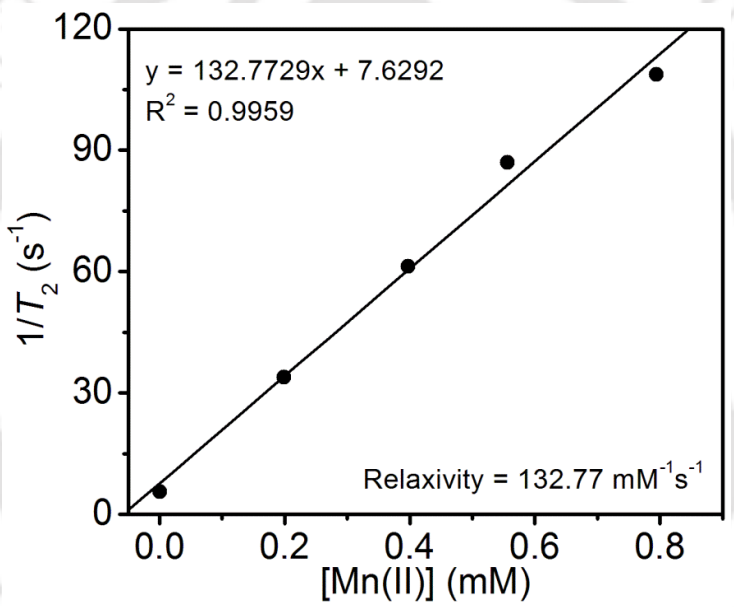

Figure 4.10. $1/T_2$ *vs.* [Mn(II)] plot. Measurements were performed using complex **4A** at 14.1 T, 25 °C, and pH ~ 7.4.

In addition to longitudinal relaxation time, the transverse relaxation time measurements at four different concentrations of complex **4A** were performed at 14.1 T, 25 °C, and pH ~ 7.4. The slope of the plot of transverse relaxation rate (R2 = $1/T_2$) *vs.* [Mn(II)] provided transverse relaxivity, r_2 as 132.77 $mM^{-1}s^{-1}$ per Mn(II) ion at 25 °C, pH ~ 7.4 (**Figure 4.10**). This indicated that the complex, in addition to T_1 contrast property also possessed excellent T_2 contrast property even at high field. These phenomena reinforced the candidature of the complex as a T_1– and T_2–dual mode contrast agent.

4.6 Phantom MR Images of Complex 4A at 1.5 T

By using BRIVO MR355 clinical MRI scanner, at 1.5 T, T_1–weighted phantom MR images of complex **4A** were measured by maintaining the concentrations at 0.25, 0.50, 0.70, and 1.00 mM (**Figure 4.11**).

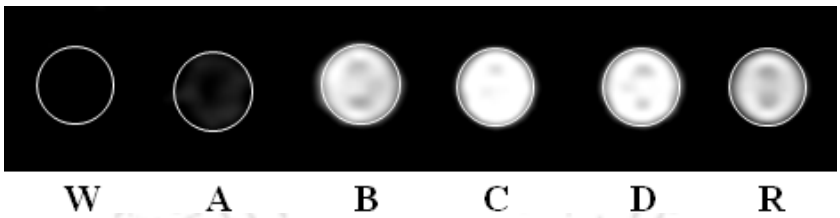

Figure 4.11. T_1–weighted phantom MR images of complex **4A** at different concentrations (W = Water, A = 0.25 mM, B = 0.50 mM, C = 0.70 mM, D = 1.00 mM, R = Reference = MultiHance®), at 1.5 T, 25 °C, and pH ~ 7.4.

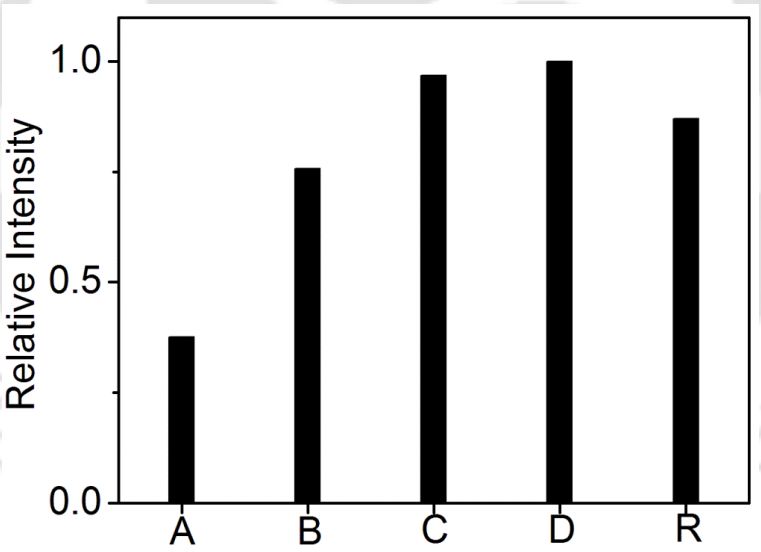

Figure 4.12. Comparison of T_1–weighted phantom MR images of complex **4A** at four different concentrations (A = 0.25 mM, B = 0.50 mM, C = 0.70 mM, D = 1.00 mM, R = Reference = MultiHance®), at 1.5 T, 25 °C, and pH ~ 7.4.

Here, a comparative MR image intensity study was also performed with a commercially available Gd(III)–based MRI CA, MultiHance®, and when the image intensities were compared by using ImageJ software by maintaining the constant area under the images, it was found that the image intensity with 0.5 mM concentration of complex **4A** was similar to that of the

commercially available MultiHance® (**Figure 4.12**). Hence, a lower dose was expected for complex **4A**.

4.7 Phantom MR Images of Complex 4A at 14.1 T:

T_1– and T_2–weighted phantom MR images of aqueous solutions of complex **4A** were measured at 14.1 T in a BRUKER microimager by maintaining the complex concentrations 0.25, 0.50, 0.70, and 1.00 mM.

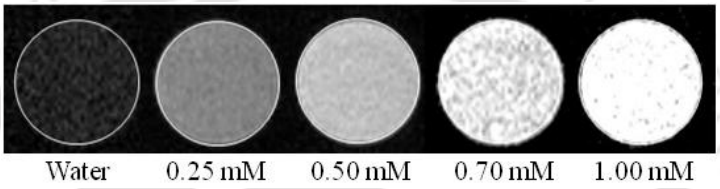

Figure 4.13. T_1–weighted phantom MR images of complex **4A** at four different concentrations, at 14.1 T, 25 °C, and pH ~ 7.4.

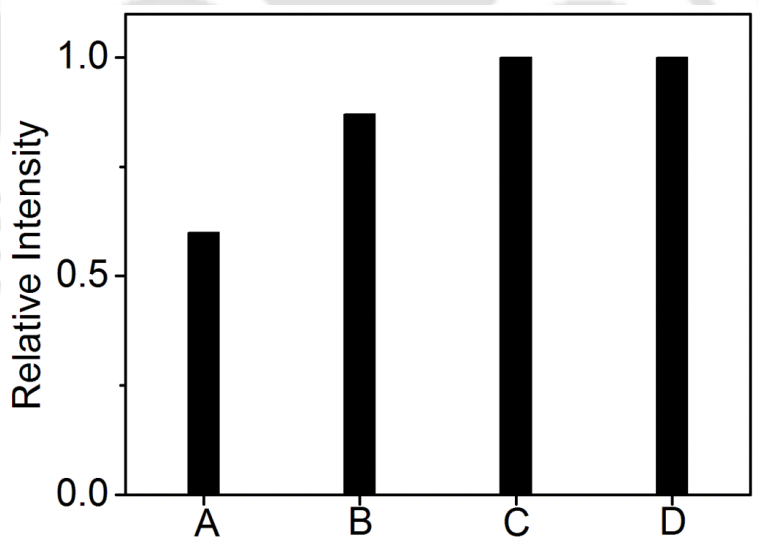

Figure 4.14. Comparison of T_1–weighted phantom MR images of complex **4A** at four different concentrations (A = 0.25 mM, B = 0.50 mM, C = 0.70 mM, D = 1.00 mM), at 14.1 T, 25 °C, and pH ~ 7.4.

It was observed that in case of T_1–weighted images (**Figure 4.13**), with increase in complex concentration, the MR image intensity of the corresponding image increases. This is

supported by the relative image intensity plot, while comparing the images by using ImageJ software under the same area of the images (**Figure 4.14**).

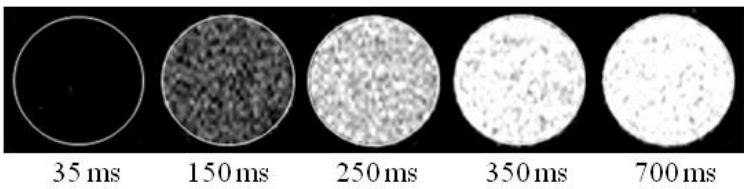

Figure 4.15. T_1–weighted phantom MR images of complex **4A** at different repetition time (TR), at 14.1 T, 25 °C, and pH ~ 7.4.

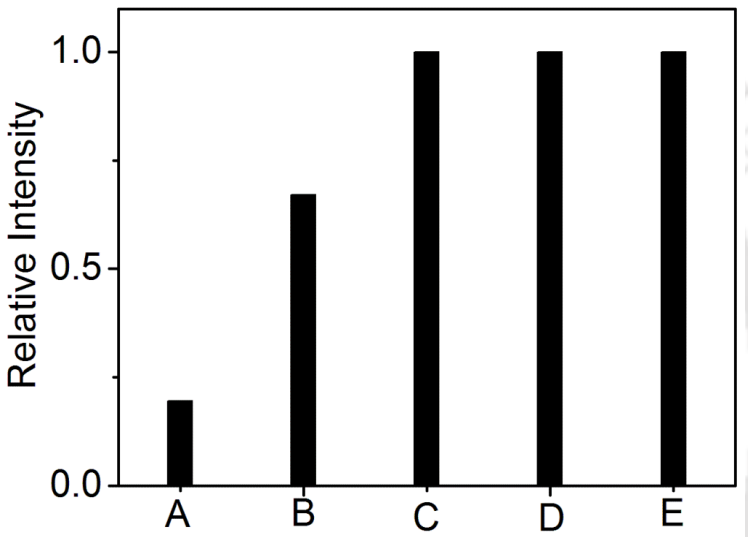

Figure 4.16. Comparison of T_1–weighted phantom MR images of complex **4A** at different repetition time (TR) (A = 35 ms, B = 150 ms, C = 250 ms, D = 350 ms, E = 700 ms), at 14.1 T, 25 °C, and pH ~ 7.4.

The phantom MR images of 1.00 mM concentration of complex **4A** at different repetition times (TR) are shown in **Figure 4.15**. The images when compared by ImageJ software, it was observed that with increase in TR, image intensity gradually increased and attained maximum intensity even at TR = 350 ms (**Figure 4.16**). The variation of T_1–weighted MRI signal intensity with repetition time (TR) at four different concentrations of complex **4A** (0.25, 0.50, 0.70, and 1.00 mM) is shown in **Figure 4.17**.

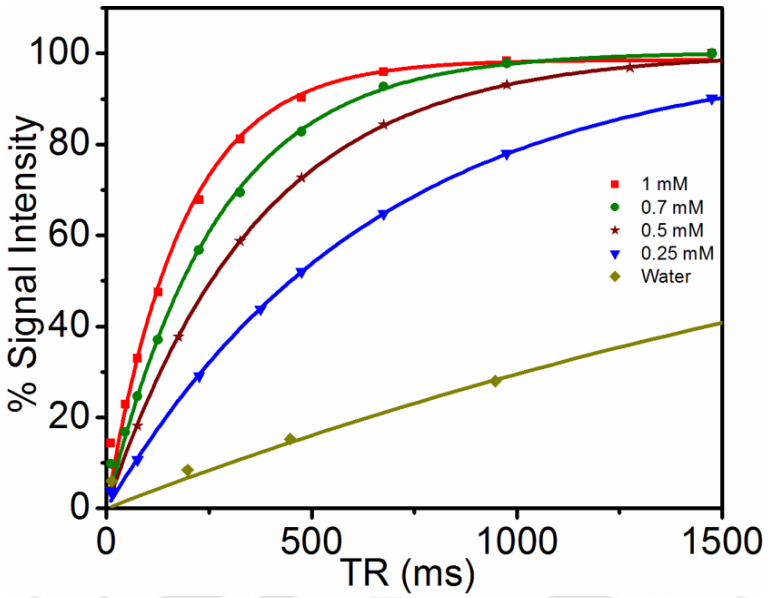

Figure 4.17. Variation of MRI signal intensity with repetition time (TR) at different concentrations of complex **4A** at 14.1 T.

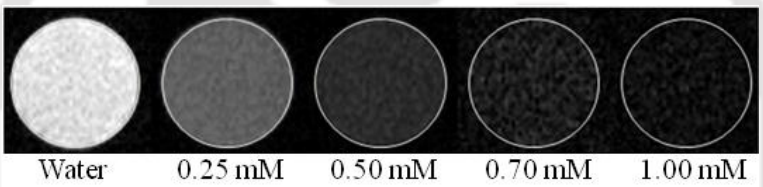

Figure 4.18. T_2–weighted phantom MR images of complex **4A** at four different concentrations, at 14.1 T, 25 °C, and pH ~ 7.4.

In case of T_2–weighted images, it was observed that with increase in concentration of the complex from 0.25 mM to 1.00 mM the T_2–weighted MR images signal intensity decreased gradually and became almost nil at 1.00 mM concentration. **Figure 4.18** shows how images were getting darker in comparison to that of water. The comparison of the image intensities were done by using ImageJ software and are as shown in **Figure 4.19**.

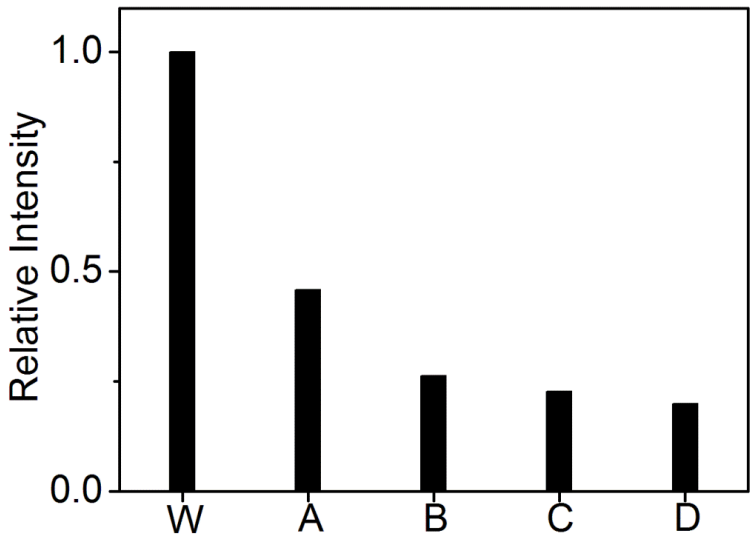

Figure 4.19. Comparison of T_2–weighted phantom MR images of complex **4A** at four different concentrations (W = Water, A = 0.25 mM, B = 0.50 mM, C = 0.70 mM, D = 1.00 mM), at 14.1 T, 25 °C, and pH ~ 7.4.

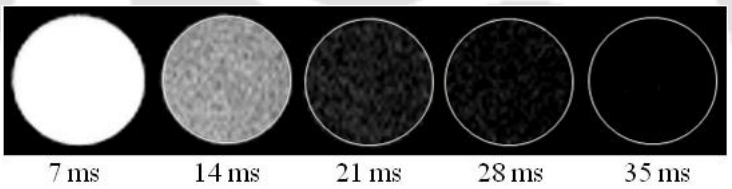

Figure 4.20. T_2–weighted phantom MR images of complex **4A** at different echo time, at 14.1 T, 25 °C, and pH ~ 7.4.

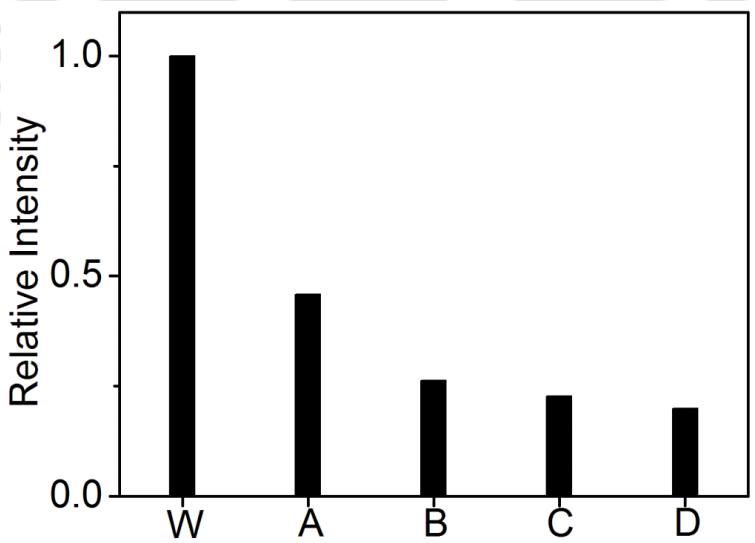

Figure 4.21. Comparison of T_2–weighted phantom MR images of complex **4A** at different echo time (TE) (W = Water, A = 7 ms, B = 14 ms, C = 21 ms, D = 28 ms, E = 35 ms), at 14.1 T, 25 °C, and pH ~ 7.4.

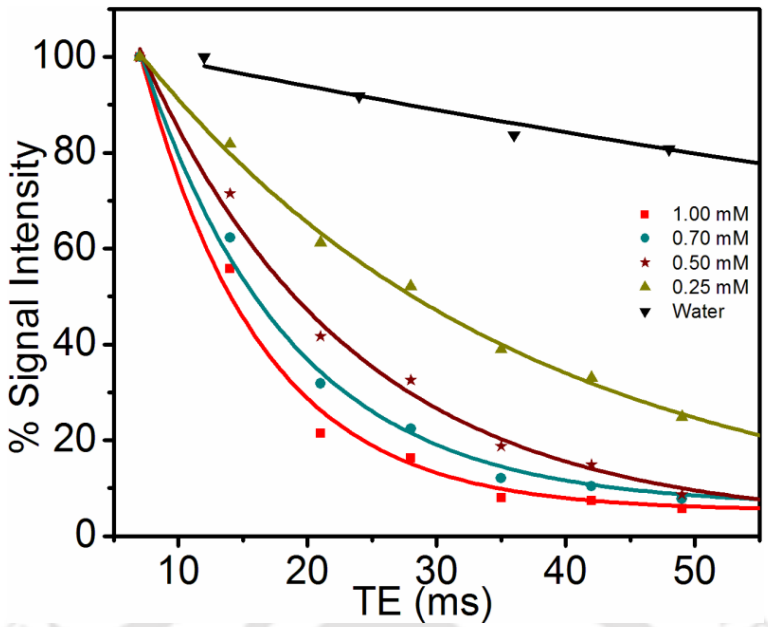

Figure 4.22. Variation of MRI signal intensity with echo time (TE) at different concentrations of complex **4A**.

The phantom MR images of 1.00 mM concentration of the complex at selected echo times are also depicted in **Figure 4.20**. It was observed that with the increase in echo time, the image intensity decreased and almost became nil at TE = 35 ms (**Figure 4.21**). The variation of T_2–weighted MRI signal intensity with echo time (TE) at four different concentrations of the complex (0.25, 0.50, 0.70, and 1.00 mM) is shown in **Figure 4.22**.

4.8 Conclusion

- Hexadentate, asymmetric, water soluble, ligand H_4bedik was synthesized. The ligand reacted with $MnCl_2 \bullet 4H_2O$ at pH ~ 6.50 and provided a seven–coordinate Mn(II)–complex, **4A,** which contained one coordinated water molecule.
- The complex showed better thermodynamic stability than that of EDTA complex of Mn(II).
- Complex **4A** exhibited high longitudinal relaxivity value, r_1 = 3.11 $mM^{-1}s^{-1}$ per Mn(II) at 1.41 T, 25 °C and pH ~ 7.4, which was significantly higher than that of the commercially available Mn(II)–based MRI CA, Teslascan® (r_1 = 2.1 $mM^{-1}s^{-1}$, at 1.5 T, and 37 °C).
- In addition to it, the complex also exhibited high longitudinal relaxivity value of 6.29 $mM^{-1}s^{-1}$ per Mn(II) at higher magnetic field (14.1 T) as well as high transverse relaxivity value of 132.77 $mM^{-1}s^{-1}$ per Mn(II) at 25 °C and pH ~ 7.4.
- Phantom MR images of complex **4A** measured at 1.5 T and 14.1 T consolidated its potential use as dual–mode MRI CA.
- Hence, complex **4A** opens up an alternative of using nanomaterials for dual–mode MRI CA.

References

1. *(a)* R. Kaewlai and H. Abujudeh, *AJR Am. J. Roentgenol.*, 2012, **199**, W17; (*b*) T. A. Hope, R. J. Herfkens, K. S. Denianke, P. E. leBoit, Yun–Y. Hung and E. Weil, *Invest. Radiol.*, 2009, **44**, 135; (*c*) P. Marckmann, L. Skov, K. Rossen, A. Dupont, M. Damholt, J. Heaf and H. Thomsen, *J. Am. Soc. Nephrol.*, 2006, **17**, 2359; (*d*) C. Thakral, J. Alhariri and J. Abraham, *Contrast Media Mol. Imaging 2*, 2007, 199.
2. (*a*) E. A. Sadowski, L. K. Bennet, M. R. Chan, A. L. Wentland, A. L. Garrett, R. W. Garrett and A. Djamali, *Radiology*, 2007, **243**, 148; (*b*) M. Sieber, P. Lengsfeld, J. Walter, H. Schirmer, T. Frenzel, F. Siegmund, H. Weinmann and H. Pietsch, *J. Magn. Reson. Imaging*, 2008, **27**, 955; (*c*) D. J. Todd and J. Kay, *Curr. Rheumatol. Rep*., 2008, **10**, 195; (d) S. E. Cowper, *Adv. Dermatol*., 2007, **23**, 131.
3. (*a*) B. Drahoš, I. Lukeš and E. Tóth, *Eur. J. Inorg. Chem.*, 2012, 1975; (*b*) J. S. Troughton, M. T. Greenfield, J. M. Greenwood, S. Dumas, A. J. Wiethoff, J. Wang, M. Spiller, T. J. McCurry and P. Caravan, *Inorg. Chem*., 2004, **43**, 6313.
4. D. P. Kessissoglou, *Manganese–Protiens and Enzymes and Relevant Trinuclear Synthetic Complexes, in Bioinorganic Chemistry: An Inorganic Perspective of Life*, Springer, 1995, 299.
5. P. C. Lauterbur, *Nature*, 1973, **242**, 190.
6. (*a*) A. Bertin, J. Steibel, Anne-I. Michou-Gallani, Jean–L. Galllani and D. Felder–Flesch, *Bioconjugate Chem*., 2009, **20**, 760; (*b*) A. C. Silva, J. H. Lee, I. Aoki and A. P. Koretsky, *NMR Biomed*., 2004, **17**, 532.
7. (*a*) J. T. Jorgensen, M. Rief, T. B. Brismar, M. Wagner and N. Albeiin, *Acta Radiol.*, 2012, **53**, 707; (*b*) N. Albin, N. Kartalis, A. Bergquist, B. Sadigh and T. B. Brismer, *Magn. Reson. Mater. Phy*., 2012, **25**, 361.
8. S. M. Rocklage, W. P. Cacheris, S. C. Quay, F. E. Hahn and K. N. Raymond, *Inorg. Chem*., 1989, **28**, 477.
9. (*a*) R. G. Lucchini, C. J. Martin and B. C. Doney, *Neuromol. Med*., 2009, **11**, 311; (*b*) J. Crossgrove and W. Zheng, *NMR Biomed*., 2004, **17**, 544.
10. (*a*) L. Tei, G. Gugliotta, M. Fekete, F. K. Kálmán and M. Botta, *Dalton Trans*., 2011, **40**, 2025; (*b*) S. Aime, P. L. Anelli, M. Botta, M. Brocchetta, S. Canton, F. Fedeli, E. Gianolio and E. Terreno, *J. Biol. Inorg. Chem*., 2002, **7**, 58; (*c*) B. K. Wagnon and S. C. Jackels, *Inorg. Chem*., 1989, **28**, 1923; (*d*) B. Drahoš, M. Pniok, J. Havlíčková, J. Kotek, I. Císařová, P. Hermann, I. Lukeš and É. Tóth, *Dalton Trans*., 2011, **40**, 10131; (*e*) E.

Balogh, Z. He, W. Hsieh, S. Liu and É. Tóth, *Inorg. Chem.*, 2007, **46**, 238; (*f*) Q. Zhang, J. D. Gorden, R. J. Beyers and C. R. Goldsmith, *Inorg. Chem.*, 2011, **50**, 9365; (*g*) H. Su, C. Wu, J. Zhu, T. Miao, D. Wang, C. Xia, X. Zhao, Q. Gong, B. Song and H. Ai, *Dalton Trans.*, 2012, **41**, 14480; (*h*) E. Molnár, N. Camus, V. Patinec, G. A. Rolla, M. Botta, G. Tircsó, F. K. Kálmán, T. Fodor, R. Tripier and C. P. Iglesias, *Inorg. Chem.*, 2014, **53**, 5136; (*i*) E. Wiener, K. Woertler, G. Weirich, E. J. Rummeny and M. Settles, *Eur. J. Radiol.*, 2007, **63**, 110; (*j*) K. H. Chuang, A. P. Koretsky and C. H. Sotak, *Magn. Reson. Med.*, 2009, **61**, 1528; (*k*) E. M. Gale, S. Mukherjee, C. Liu, G. S. Loving and P. Caravan, *Inorg. Chem.*, 2014, **53**, 10748.

11. B. Drahoš, J. Kotek, P. Hermann, I. Lukeš and E. Tóth, *Inorg. Chem.*, 2010, **49**, 3224.
12. (*a*) N. A. Keasberry, M. Banobre–López, C. Wood, G. J. Stasiuk, J. Gallo and N. J. Long, *Nanoscale*, 2015, **7**, 16119; (*b*) J. Schnorr, S. Wagner, C. Abramjuk, R. Drees, T. Schink, E. A. Schellenberger, H. Pilgrim, B. Hamm and M. Taupitz, *Radiology*, 2006, **240**, 90; (*c*) A. Szpak, S. Fiejdasz, W. Prendota, T. Strączek, C. Kapusta, J. Szmyd, M. Nowakowska and S. Zapotoczny, *J. Nanopart. Res.*, 2014, **16**, 2678; (*d*) N. A. Keasberry, M. Banobre-López, C. Wood, G. J. Stasuik, J. Gallo and N. J. Long, *Nanoscale*, 2015, **7**, 16119; (*e*) H. Yang, Y. Zhuang, Y. Sun, A. Dai, X. Shi, D. Wu, F. Li, H. Hu and S. Yang, *Biomaterials*, 2011, **32**, 4584.
13. (*a*) T. Courant, V. G. Roullin, C. Cadiou, M. Callewaert, M. C. Andry, C. Protefaix, C. Hoeffel, M. C. de Goltstein, M. Port, S. Laurent, L. V. Elst, R. Muller, M. Molinari and F. Chuburu, *Angew. Chem. Int. Ed.*, 2012, **51**, 9119; (*b*) T. H. Sin, J. S. Choi, S. Yun, I. S. Kim, H. T. Song, Y. Kim, K. I. Park and J. Cheon, *ACS Nano.*, 2014, **8**, 3393; (*c*) G. H. Im, S. M. Kim, Dong-G. Lee, W. J. Lee, J. H. Lee and I. S. Lee, *Biomaterials*, 2013, **34**, 2069.
14. (*a*) J. Wang, G. R. Gao, Z. H. Zhang, X. D. Zhang, X. Z. Liu, Y. M. Kong and Y. Li, *Russ. J. Coord. Chem.*, 2007, **33**, 258; (*b*) B. C. Smith, *Infrared Spectral Interpretation: A Systematic Approach*, CRC press, 1998.
15. (*a*) C. J. Jocher, E. G. Moore, J. Xu, S. Avedano, M. Botta, S. Aime and K. N. Raymond, *Inorg. Chem.*, 2007**,** **46**, 9182; (*b*) E. J. Werner, J. Kozhukh, M. Botta, E. G. Moore, S. Avedano, S. Aime and K. N. Raymond, *Inorg. Chem.*, 2009**,** **48**, 277; (*c*) K. N. Raymond and V. C. Pierre, *Bioconjugate Chem.*, 2005, **16**, 3; (*d*) D. M. J. Doble, M. Melchior, B. O'Sullivan, C. Siering, J. Xu, V. C. Pierre and K. N. Raymond, *Inorg. Chem.*, 2003, **42**, 4930; (*e*) V. C. Pierre, M. Botta, S. Aime and K. N. Raymond, *Inorg. Chem.*, 2006**,** **45**, 8355.

16. E. Wiener, K. Woertler, G. Weirich, E. J. Rummeny and M. Settles, *Eur. J. Radiol.*, 2007, **63**, 110.

17. (*a*) B. Sana, C. L. Poh and S. Lim, *Chem. Commun*., 2012, **48**, 862; (*b*) K. Ugurbil, G. Adriany, P. Anderson, W. Chen, M. Garwood, R. Gruetter, Pierre-G. Henry, Seong-G. Kim, H. Lieu, I. Tkac, T. Vaughan, Pierre-F. V. de Moortele, E. Yacoub and Xiao-H. Zhu, *J. Magn. Reson. Imagimg*, 2003, **21**, 1263; (*c*) M. Takahashi, H. Uematsu and H. Hatabu, *Eur. J. Radiol*., 2003, **46**, 45; (*d*) P. Marzola, F. Osculati and A. Sbarbati, *Eur. J. Radiol.*, 2003, **48**, 165.

18. P. Caravan, C. T. Farrar, L. Frullano and R. Uppal, *Contrast Media Mol. Imaging*, 2009, **4**, 89.

Chapter V

A Bis(aquated) High Relaxivity Mn(II) complex as Potential MRI Contrast Agent

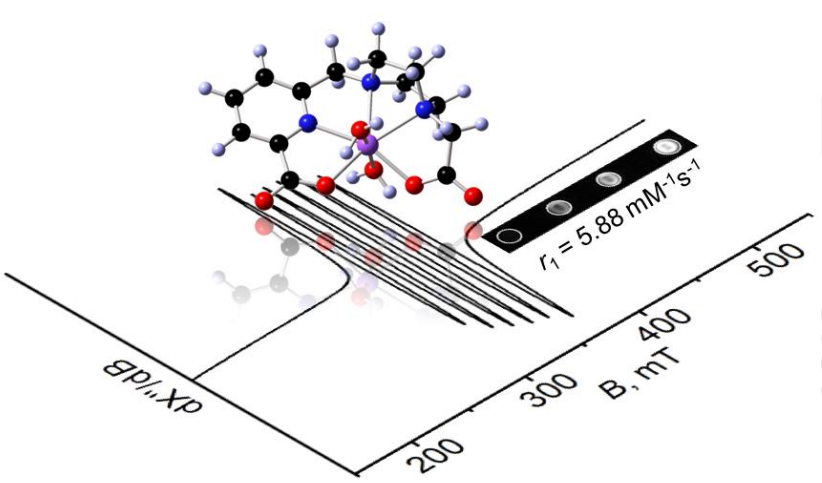

5.1 Introduction

In the history of MRI contrast agents (CAs), although the majority of clinically approved MRI CAs are still based on Gd(III) complexes,[1] the recent concerns on Nephrogenic Systemic Fibrosis (NSF), raising new questions about the safety of Gd(III)–based CAs available in the market.[2] NSF is a disease related to Gd(III) deposition in patients suffering from severe renal disease or who underwent liver transplantation. Very recent review also showed that certain Gd(III)–based CAs may cause problems for patients even with normal renal function.[3] These results are triggering new research in order to design safer CAs. Stable complexation of other paramagnetic metal ions such as Fe(III) and Mn(II) have gained special attention due to their five unpaired electrons. These ions have important biological roles[4] and are less toxic than Gd(III). Mn(II) ion with its five unpaired electrons, slow electronic relaxation rate and fast water exchange rate is the best candidate in place of Gd(III)–based MRI CAs.[5]

However, the relaxivity value of Mn(II)–based complexes are lower than that of Gd(III) complexes. This lower relaxivity of Mn(II) complexes is due to 5 unpaired electrons in Mn(II) than 7 unpaired electrons in Gd(III)). Thus, Gd(III)–based contrast agents are more effective than Mn(II)–containing contrast agents. The only commercially available Mn(II)–based MRI CA is Teslascan®, and is used for liver imaging. This complex is lack of inner sphere water molecule and the enhanced contrast is obtained in by the *in vivo* release of the free Mn(II) ion from the chelate.[6] More recently, another Mn(II)–based oral contrast agent CMC–001 has been developed which is a mixture of $MnCl_2$, alanine and vit D_3.[7] The relaxivity in this case is due to free Mn(II) ion. However, long term exposure to Mn(II) can lead to 'Manganism', a disease due to deposition of Mn(II) in the brain.[8] Therefore, care must be taken before administrating a large dose of these contrast agents.

To minimise the release of free Mn(II) ion, it is very important to synthesise new Mn(II)–based CAs having coordinated water molecule, and with sufficient stability. Literature demonstrate the synthesis of Mn(II) chelates having at least one inner sphere water molecule.[9] However, at 0.47 T and 25 ºC, while the Gd(III)–based commercially available MRI CAs have the relaxivity value in the range 4.4–5.2 $mM^{-1}s^{-1}$, the reported relaxivity of the Mn(II)–based complexes containing one water molecule are 2.1–3.7 $mM^{-1}s^{-1}$ only.[9e, 1b]

From well established Solomon–Bloembergen–Morgan (SBM) theory of contrast agents, it is found that r_1 relaxivity increases with the increase in number of coordinated water molecules

(*q*) irrespective of magnetic field strength. This idea has already been found useful in case of Gd(III)–based CAs for obtaining high relaxivity value.[10] However, bis(aquated) Mn(II) complexes are less investigated till now. Furthermore, the relaxivity value has been achieved for the reported Mn(II)–complexes is low compared to the potential Gd(III)–based MRI CAs. For example, bis(aquated) Mn(II) complexes of ligand with 15–membered triaza–dioxa–crown(15–pyN_3O_2) and pentaaza–crown ether macrocycles(15–pyN_5) showed relaxivity values of 4.48 $mM^{-1}s^{-1}$ and 3.56 $mM^{-1}s^{-1}$ respectively at 20 MHz and 25 °C.[11] More recently, another series of ligands containing pentadentate 6,6′–((methylazanediyl)bis(methylene))dipicolinic acid binding units were reported which form mono–, bi– and trinuclear Mn(II) complexes containing two and three coordinated water molecules per Mn(II) ions. These complexes showed remarkably high relaxivity values and showed high affinity for human serum albumin (HSA).[12]

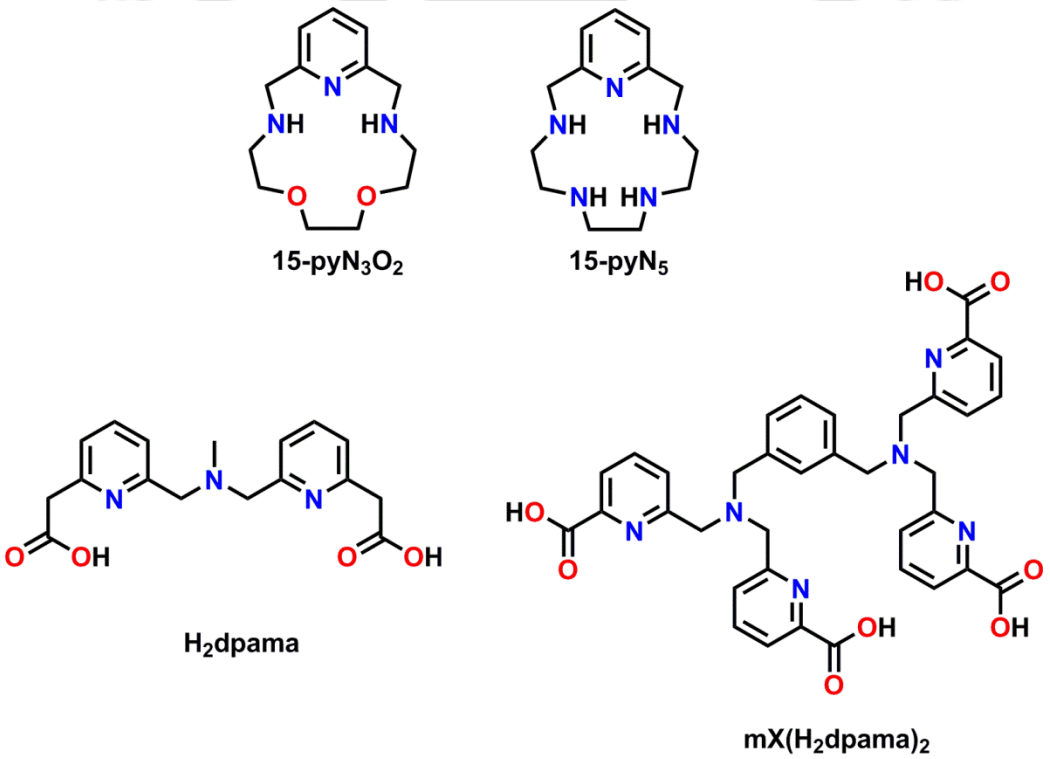

Scheme 5.1. Ligands coordinating with Mn(II), and have two inner sphere water molecules.

Herein, in order to achieve high relaxivity with sufficient thermodynamic stability, we have reported a ligand H_2pmpa and its corresponding Mn(II) complex with two inner sphere water molecules. A picolinate unit was incorporated in the ligand backbone, as the presence of this group in a Mn(II) complex rigidify the chelate structure and provides an additional lipophilic character to the overall system. Mn(II) complex of ligand PyC3A containing one pyridine unit

was found to be one of the most thermodynamically stable complex with one inner sphere water molecule.[13] Previous investigations also revealed the increased kinetic inertness of Mn(II) complexes having pyridine moiety, which is an important concern regarding enhanced stability. Moreover, the pyridine unit can be easily functionalized with groups able to conjugate with biological material.[14] The piperazine group with a puckered ring structure introduces a great deal of structural strain to the system. Due to the cyclic and boat structure of the piperazine unit, it was expected that the N–substituted groups would be in the same plane as that of the two N–atoms of the piperazine moiety in the complex. Hence, a disc–shaped ligand chelation could be achieved where the two axial positions would be available for coordination of water molecules.

5.2 Synthesis and Characterisation of Ligand H_2pmpa, $C_{13}H_{17}N_3O_4$

A schematic representation for the synthesis of ligand H_2pmpa is shown in Scheme **5.2**.

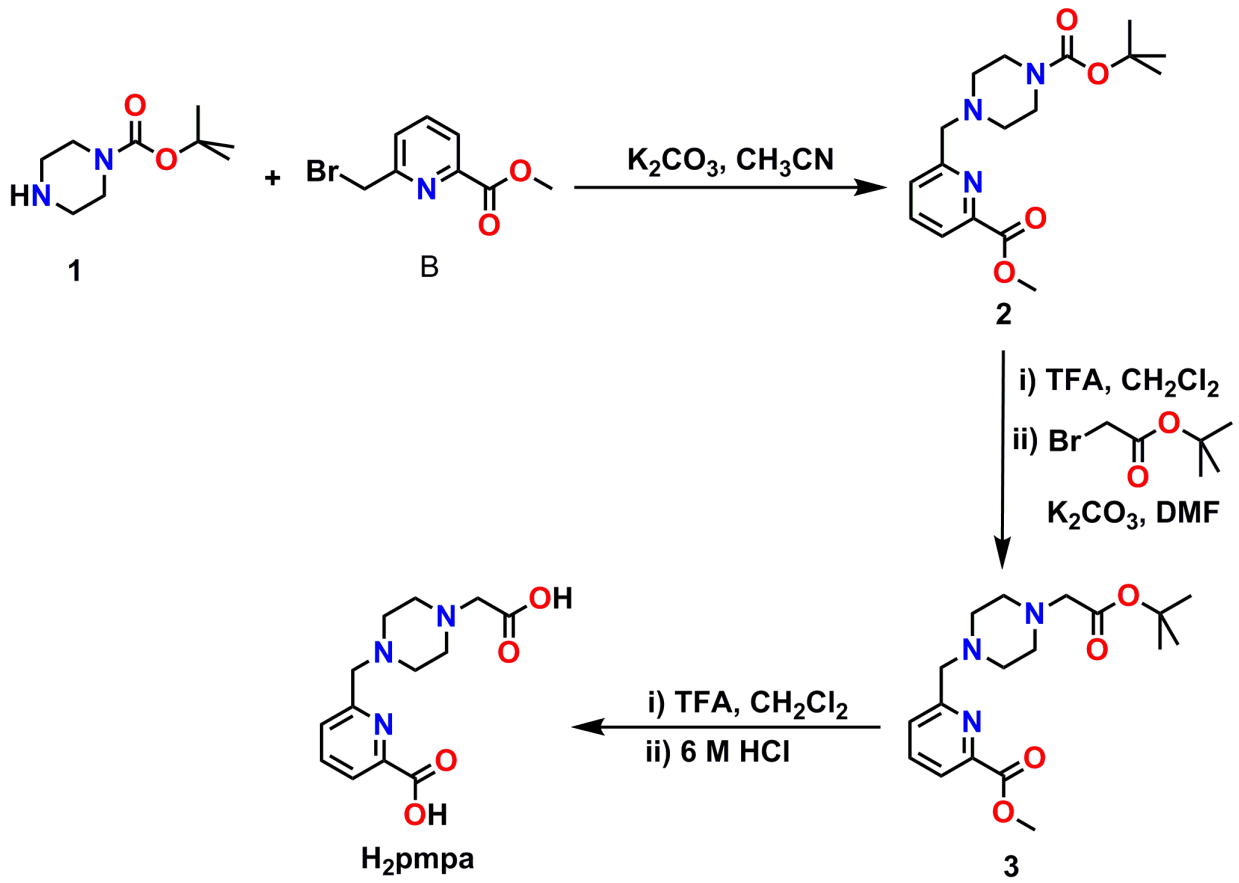

Scheme 5.2. Synthetic route of ligand H_2pmpa.

N–Boc piperazine and 6–(bromomethyl)pyridine–2–carboxylate were prepared by using reported procedures.[15] A reaction between 1:1 N–Boc piperazine with 6–(bromomethyl)pyridine–2–carboxylate in CH_3CN in the presence of K_2CO_3 gave **2**. Deprotection of **2** with trifluoroacetic acid followed by addition of *tert*–butyl bromoacetate in DMF in the presence of K_2CO_3 produced the O–protected ligand **3**. The ligand H_2pmpa was obtained as a pale brown solid by successive deprotection of **3** using trifluoroacetic acid and 6 M HCl. The ligand was characterised by using FTIR spectroscopy, mass spectrometry, and NMR spectroscopy technique.

Infrared (IR) spectrum of ligand H_2pmpa is shown in **Figure 5.1**. The sharp band observed at 3434 cm^{-1} was due to ν(O–H) stretching.[16a] The bands appeared at 2976, and 2927

cm^{-1} were due to ν(C–H) stretching.[16b] The stretching frequency for C=O group appeared as a sharp band at 1724 cm^{-1}.[16a] The stretching bands at 1443 cm^{-1} was due to the in plane O–H bending.[16c] The ν(C–O) stretching band appeared at 1263 cm^{-1}.[16d]

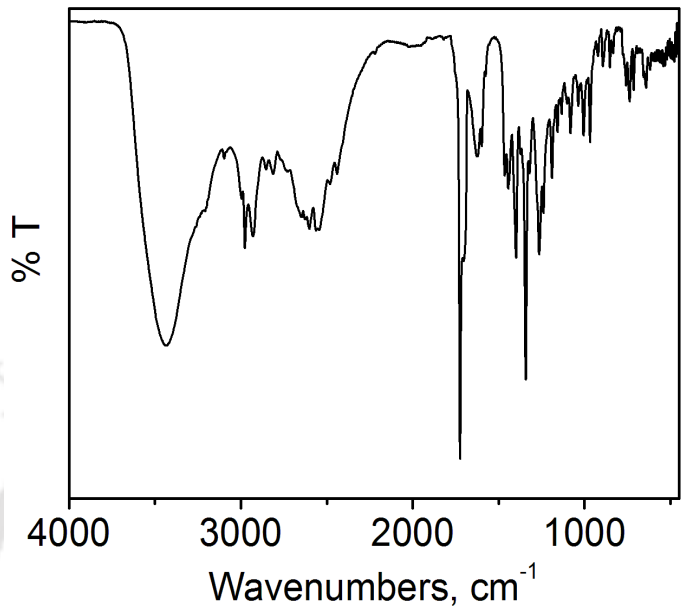

Figure 5.1. FTIR spectrum of ligand H_2pmpa.

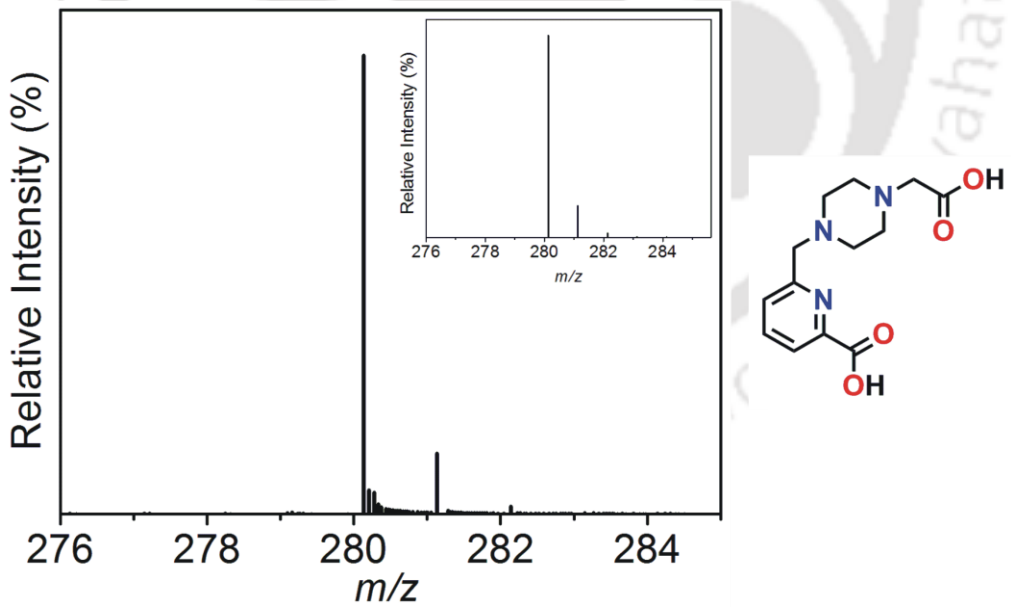

Figure 5.2. ESI–MS spectrum of ligand H_2pmpa. Simulated spectrum is shown as inset.

The electrospray ionisation mass spectrum measurement of ligand H_2pmpa in the positive mode in HPLC grade MeOH, provided a 100% molecular ion peak at *m/z* = 280.1333 amu. The

peak corresponded to the composition $[C_{13}H_{17}N_3O_4 + H]^+$ (*m/z* = 280.1292 amu) as evident by isotope pattern distribution analysis (**Figure 5.2)**.

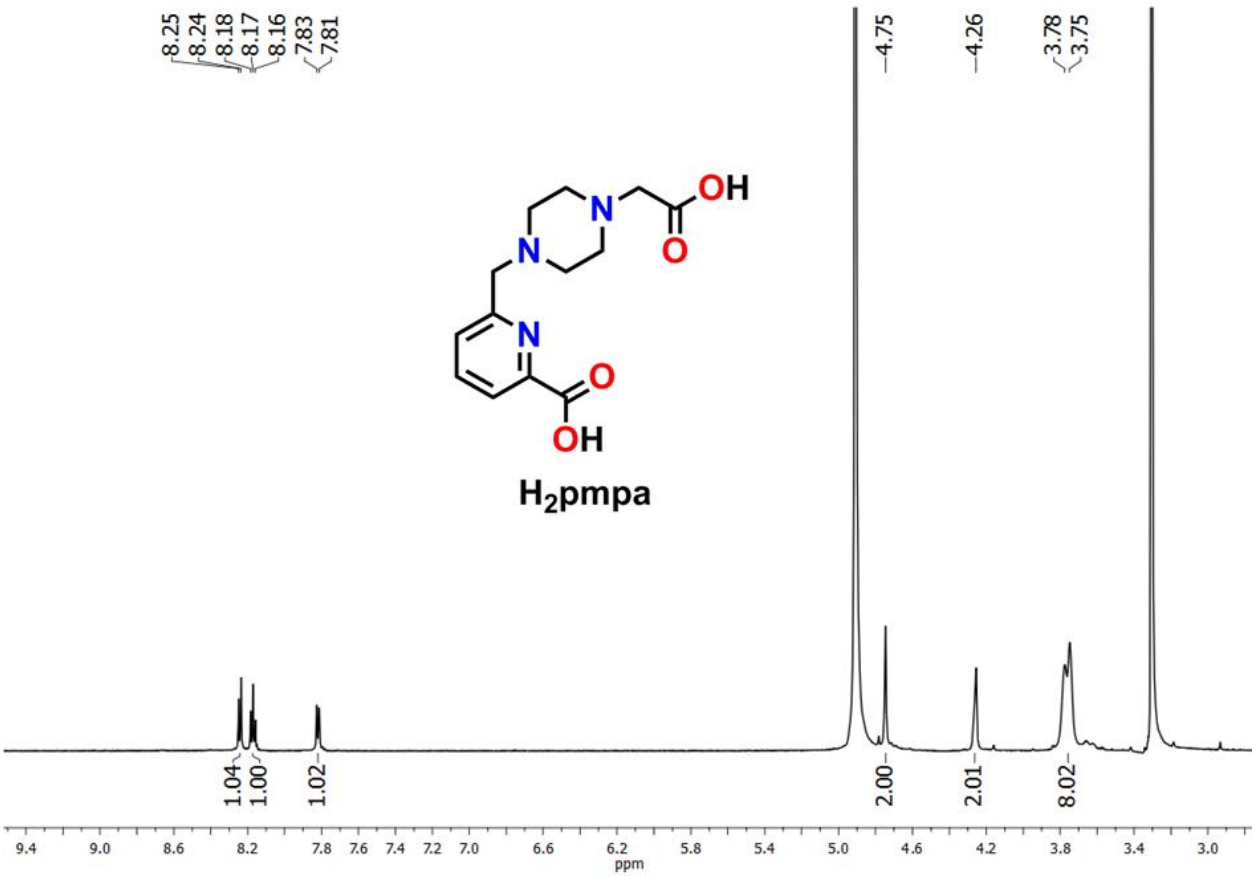

Figure 5.3. ^{1}H NMR spectrum of ligand H_2pmpa.

^{1}H NMR spectrum (**Figure5.3**) of the ligand showed signals in the region 8.25–7.81, which were due to three aromatic protons. The singlet peaks at 4.75 and 4.26 ppm were due to four hydrogen atoms attached to the piperazine moiety. The multiplet in the region 3.78–3.75 ppm was due to eight protons present in the piperazine ring. ^{13}C NMR spectrum (**Figure 5.4**) of the ligand showed 11 characteristic peaks for 11 different kinds of carbon atoms.

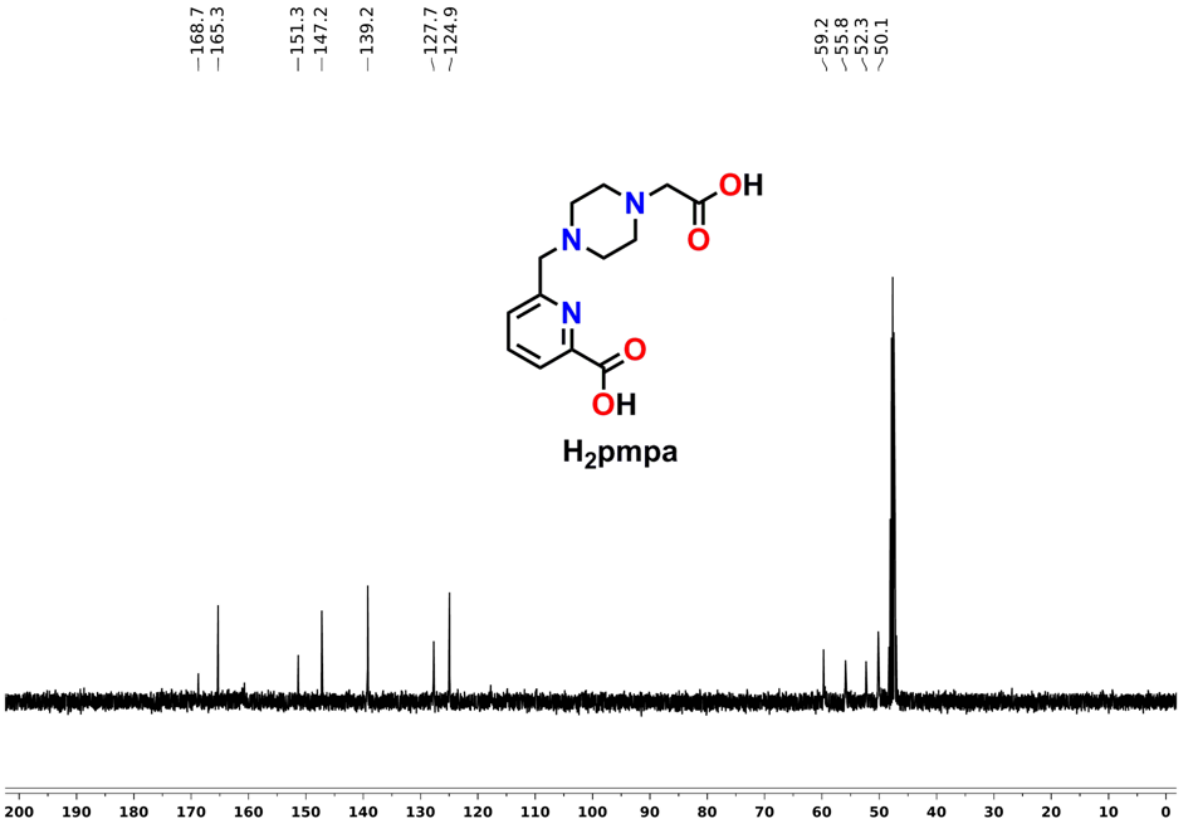

Figure 5.4. ^{13}C NMR spectrum of ligand H_2pmpa.

5.3 Synthesis and Characterisation of Bis(aquated) Mn(II) Complex of Ligand H_2pmpa, 5B

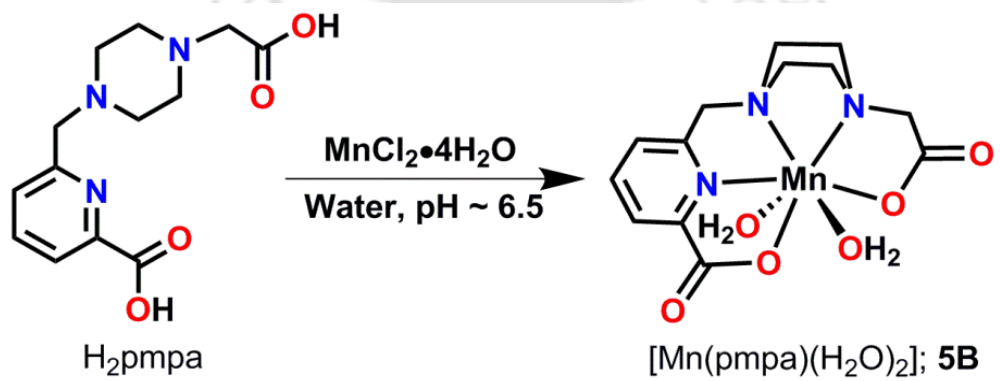

Scheme 5.3. Synthesis of complex **5B**, $[C_{13}H_{19}MnN_3O_6]$.

To a solution of ligand H_2pmpa in water, $MnCl_2 \cdot 4H_2O$ was added and stirred the reaction mixture for 10 minutes. The solution became transparent and then pH was adjusted to ~ 6.5 by dropwise addition of aq. NaOH solution. Stirring was continued at room temperature (25 °C) for 24 h and the clear solution was kept at room temperature for solvent evaporation. However, several attempts to grow single crystal suitable for X–ray diffraction analysis from pure water or other solvent mixtures were not successful.

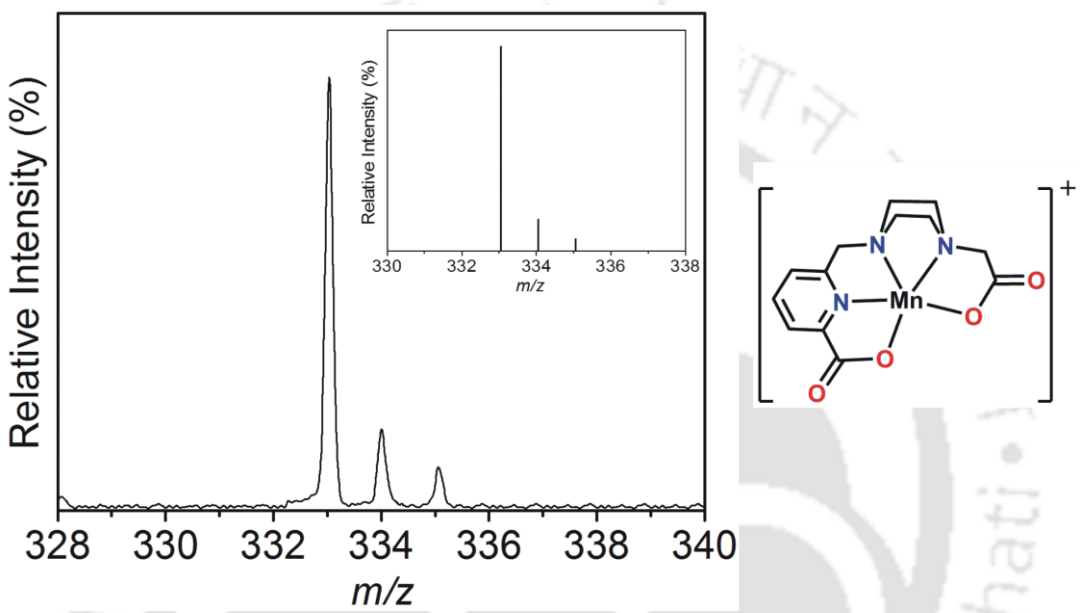

Figure 5.5. ESI–MS spectrum of complex **5B**. Simulated spectrum is shown as inset.

The electrospray ionisation mass spectrum measurement in positive mode of complex **5B** in Mili Q water, provided a 100% molecular ion peak at *m/z* = 333.03 amu. The peak corresponded to the composition $[C_{13}H_{15}N_3O_4Mn + H]^+$ (*m/z* = 333.05 amu) as evident by isotope pattern distribution analysis (**Figure 5.5**).

Infrared (IR) spectrum (**Figure 5.6)** of complex **5B** showed a sharp band at 3406 cm^{-1} due to *ν*(O–H) stretching. The formation of the complex was confirmed from the change in *ν*(C=O) stretching frequency, which appeared as a sharp band at 1595 cm^{-1} for the complex whereas that of the ligand was observed at 1724 cm^{-1}.

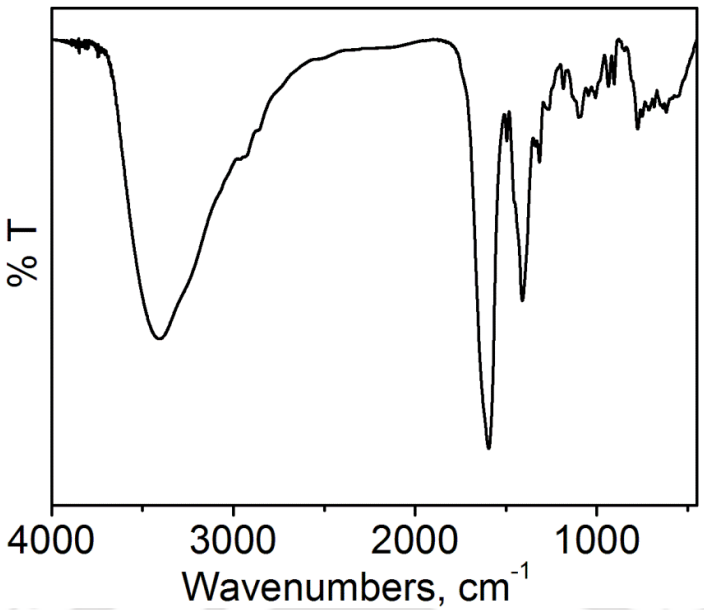

Figure 5.6. FTIR spectrum of complex **5B**.

For high relaxivity Mn(II) complexes, it is very important to have at least one coordinated water molecule that exchanges rapidly with bulk water molecules. From the literature it is found that Mn(II) ion can form either six– or seven–coordinated complexes, which can be used as MRI CAs.[8,10,11] The ligand H_2pmpa, being pentadentate, could form either six–coordinated Mn(II) complex with one inner sphere water molecule or seven–coordinated Mn(II) complex with two inner sphere water molecules.

Being unsuccessful to grow single crystal suitable for X–ray diffraction analysis, we performed high level DFT based calculations to understand the relative stability of both mono and bis(aquated) complexes. All the calculations were done by using Gaussian09 package.[17] Different DFT functionals were tested (both hybrid and meta–GGA) and based on the performance and earlier reports, M06–2x (Global hybrid functional containing 56% HF exchange)[18] was used for the entire calculations. Perhaps, M06–2x was found to be a good performer for main group thermochemistry, kinetics, noncovalent interactions, etc.[19] The initial geometries of the complexes were optimized at M06–2x/6–311+G(d,p) level. The solvent effect was taken care through SCRF (self consistent reaction field)[20] approach using CPCM[21] (polarizable conductor calculation model) formalism for water, as implemented in Gaussian09. Subsequent frequency calculations were performed on the optimized structures to ensure global minima in the energy landscape.

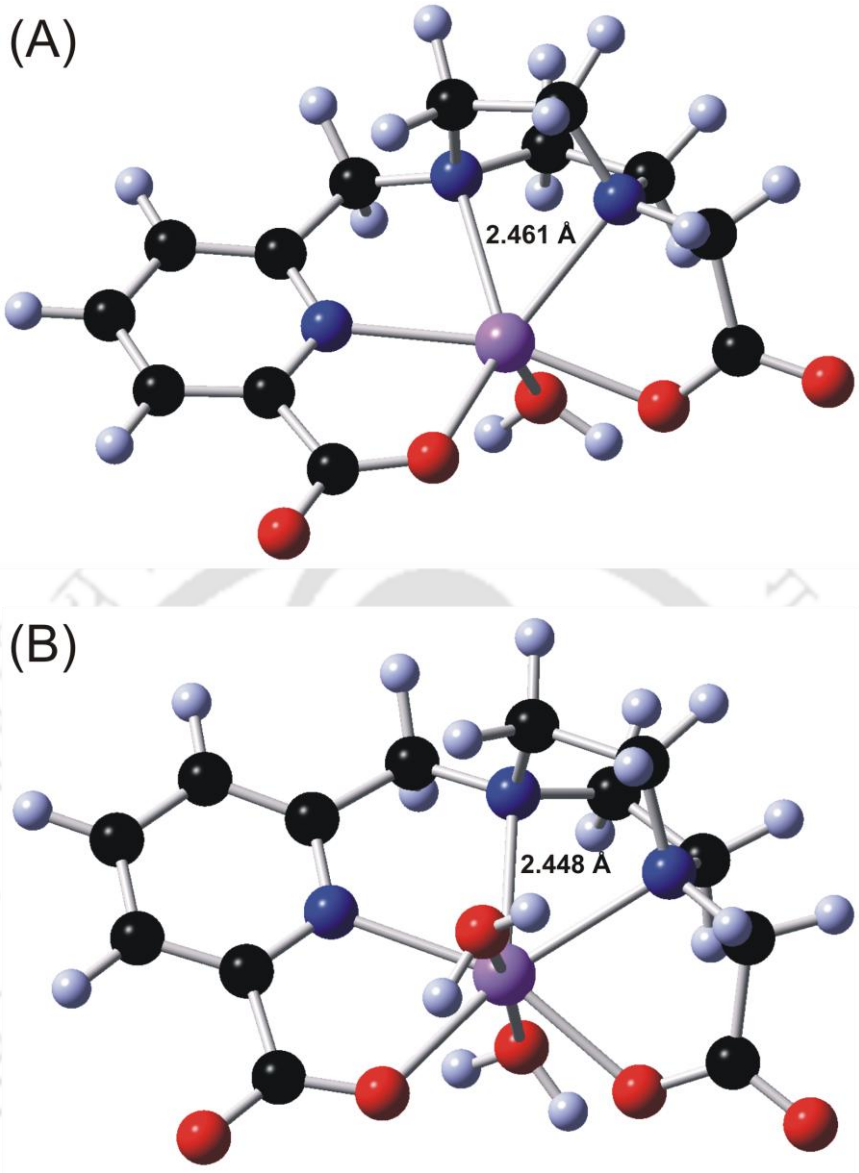

Figure 5.7. Optimized structures of (A) mono(aquated) complex, **5A**; and (B) bis(aquated) complex, **5B**. Optimized at M06–2x/6–311+G(d,p) level.

Optimized structures of mono and bis(aquated) complexes are reported in **Figure 5.7**. DFT based theoretical calculations provided some nice understanding on relative stability of both mono and bis(aquated) form of the Mn(II) complex. Both the structures were found to be stable after initial optimization. Interestingly, there was no significant distortion in the optimized structures. This also indicated that the structures were energetically favourable. It is important to note that optimization did not introduce some drastic changes in the geometrical parameters for the complexes. However, DFT based study predicted relatively higher thermodynamic stability for the bis(aquated) complex, **5B**. Taking the analogy from above discussion we assumed that the

Mn–N bond (as shown in **Figure 5.7**) was the key factor to the overall structural stability of the complexes. Here, the shorting of this particular bond in bis(aquated) complex, **5B** was the direct consequence of higher structural stability of the complex. The theoretical calculations showed a significant enhancement in the structural stability of the complex with two inner sphere water molecules. Computed DFT based formation energy for bis(aquated) complex was found to be –400.03 kcalmol^{-1} which was much higher than that of mono(aquated) complex (–12.54 kcalmol^{-1}).[22]

Thus, a pentagonal bipyramedal geometry was confirmed from the optimised structure of complex **5B**, where the two axial positions were occupied by two water molecules. The equatorial plane was constituted by two N atoms from the piperazine unit, one N atom from the pyridine unit and two O atoms from two carboxylate groups, making Mn(II) centre feasible for interacting with the surrounding water molecules. The obtained bond lengths, Mn–N (piperazine) = 2.357, 2.448, Mn–N (Py) = 2.282, Mn–O (carboxylate) = 2.221, 2.175, and Mn–O (water) = 2.254, 2.309 Å from the optimised structure of complex **5B** are in accordance with the previously reported similar Mn(II) complexes.[23]

Table 5.1. Optimized coordinates of mono(aquated) complex (at M06–2x/6–311+G(d,p) level):

C	0.24019000	-2.06677700	-1.38350900
C	1.60113200	-1.48634400	-1.84246700
C	2.50744500	-1.56843700	0.36329100
C	1.30051300	-2.46654600	0.72415600
N	2.12277700	-0.66858400	-0.74114400
N	0.12212800	-1.89335500	0.07258800
Mn	0.39410400	0.54705700	0.23669100
C	-4.00089600	0.71286800	-0.30326700
C	-2.63859300	0.93332800	-0.16678400
C	-2.22693100	-1.30667500	0.26367200
C	-3.57829500	-1.61455100	0.13533000
C	-4.47213500	-0.58753200	-0.14434300
H	-4.65700800	1.53999900	-0.53767300
H	-3.91647300	-2.63738000	0.24581200
H	-5.52880000	-0.80211000	-0.25062400
N	-1.79039100	-0.05670600	0.11813600
C	-1.16365400	-2.33867200	0.58824500
H	-1.08682700	-2.42390400	1.67674800
H	-1.46193600	-3.32209400	0.20141600
C	-1.98866700	2.30667500	-0.35217600
O	-0.72088900	2.32348500	-0.24306200
O	-2.72280900	3.26410000	-0.59190600
C	3.28672200	1.39134300	-0.03391900
O	2.23555800	1.60561300	0.65695200
O	4.34190300	2.02229000	0.03691100
O	0.68751300	0.13875100	2.41808200
H	1.37561700	0.75579200	2.70018000
H	0.00937000	0.13802300	3.10201200
C	3.19722500	0.25607400	-1.07639200
H	4.17172300	-0.23879400	-1.16065200
H	2.97342100	0.72429300	-2.03917100
H	1.14470700	-2.46609900	1.80224000
H	1.46595600	-3.50144400	0.39647000
H	2.79634500	-0.95419900	1.21823700
H	3.37202900	-2.17545000	0.06669600
H	0.15864600	-3.12785800	-1.65366100
H	-0.58325500	-1.52976400	-1.86068400
H	2.30715500	-2.28810600	-2.09432200
H	1.47059500	-0.85924500	-2.72420200

Table 5.2. Optimized coordinates of bis(aquated) complex (at M06–2x/6–311+G(d,p) level):

C	0.47096700	-2.17468900	-1.29857400
C	1.89714200	-1.65228200	-1.59166300
C	2.50323100	-1.56106500	0.71303400
C	1.28508700	-2.48335900	0.93721400
N	2.26673400	-0.75326200	-0.49450600
N	0.17771600	-1.96179500	0.12934900
Mn	0.36581600	0.47880700	0.15678300
C	-4.08036300	0.54713300	-0.16226300
C	-2.72513400	0.81181500	-0.03862800
C	-2.21549600	-1.43392100	0.19356700
C	-3.55606700	-1.78693900	0.05528100
C	-4.49602500	-0.78105800	-0.12387100
H	-4.77617300	1.36504300	-0.28972700
H	-3.84955200	-2.82893800	0.09397600
H	-5.54518800	-1.02924000	-0.23129600
N	-1.82447800	-0.16242100	0.12818600
C	-1.13926600	-2.45489300	0.50547400
H	-1.15027800	-2.61662000	1.58745700
H	-1.37950400	-3.41572400	0.03225300
C	-2.15558300	2.23151500	-0.07515000
O	-0.88679500	2.30454400	-0.01516400
O	-2.94872600	3.16835400	-0.16212000
C	3.26470600	1.40380900	0.18862500
O	2.12258100	1.63978200	0.70296200
O	4.28452400	2.07857200	0.34336500
O	0.41362000	0.30821600	2.40418700
H	1.04485700	0.98021200	2.69260500
H	-0.35373400	0.37376800	2.98248100
C	3.35596500	0.17708700	-0.74605700
H	4.34448900	-0.28544700	-0.64104600
H	3.27531300	0.55548100	-1.76921300
H	0.99570600	-2.46728200	1.98746000
H	1.51648700	-3.51993500	0.65800000
H	2.62838700	-0.87963400	1.55736600
H	3.42278600	-2.15078000	0.60406300
H	0.38954800	-3.23896100	-1.55547300
H	-0.26957200	-1.62193800	-1.88358900
H	2.61113900	-2.48266100	-1.67005300
H	1.91689300	-1.10954000	-2.53621100
O	0.31075100	1.05565500	-2.07826200
H	-0.07518200	1.93736000	-1.98191400
H	0.94574800	1.10708800	-2.79958700

5.4 Stability of Complex 5B

A comparison of thermodynamic stability of the complex with other reported complexes can be best understood by pM values of the ligand as it allows a straightforward comparison of complex stability at physiological conditions.[10(a–c),24] pM is defined as $-\log[M]_{free}$ at pH = 7.4, 25 °C, [M] = 1 μM and [L] = 10 μM.

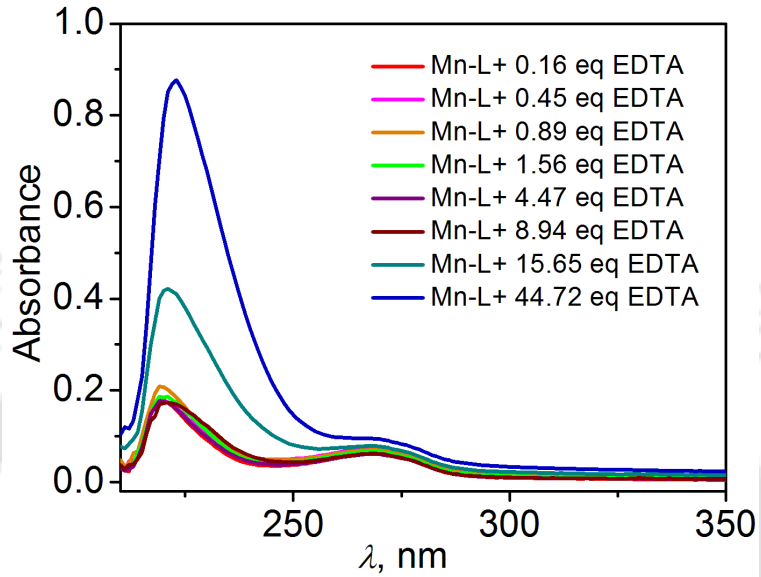

Figure 5.8. Spectral changes during the competition titration of ligand H_2pmpa against EDTA. (L in figure represents ligand H_2pmpa).

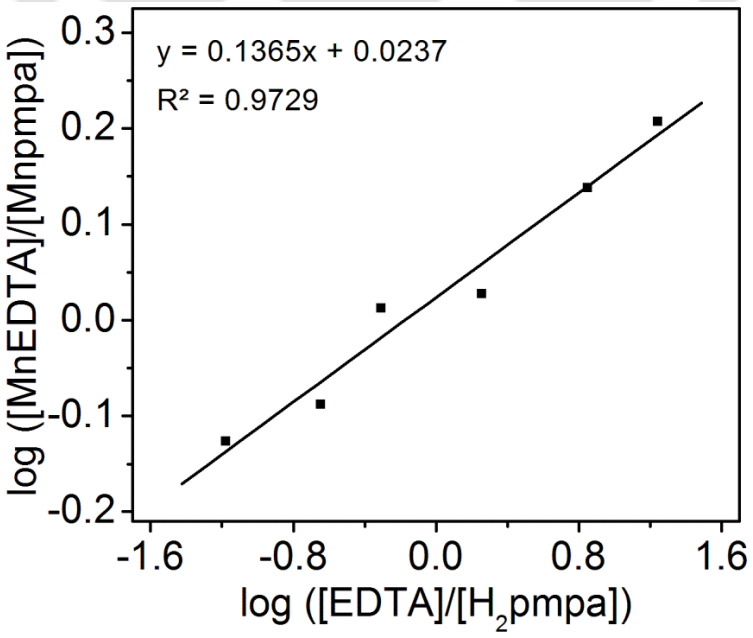

Figure 5.9. Competition batch titration of ligand H_2pmpa against EDTA.

A competition batch titration was performed using EDTA as the competing ligand to determine the pMn value of ligand H_2pmpa. Throughout the process, pH of all the solutions was kept constant at 7.4 by using 10 mM HEPES buffer. The concentration of ligand H_2pmpa and metal were kept constant while the concentration of the competing ligand was increased progressively during the process. Each solutions containing ligand H_2pmpa, metal and competing ligand EDTA were kept for 24 h to obtain thermodynamic equilibrium. The concentrations of the free and complexed ligand were then determined by using UV–vis spectroscopy. From the *x*–intercept of the plot log ([MnEDTA]/[Mnpmpa]) *vs.* log ([EDTA]/[H_2pmpa]), the difference in pMn between the ligand H_2pmpa and EDTA was obtained (**Figure 5.9**) (*i.e.* ΔpMn = pMn_{H_2pmpa} – pMn_{EDTA}). This difference was the value of log ([EDTA]/[H_2pmpa]) when log ([MnEDTA]/[Mnpmpa]) = 0 or when the concentration of EDTA generates an equal partition of Mn(II) between H_2pmpa and EDTA. Using the value 8.05 for pMn of EDTA, the pMn of ligand H_2pmpa was found to be 7.88 which is higher than the reported pMn values of ligand 15–pyN_3O_2, 15–pyN_5, H_2DPAPhA, and H_2DPAMeA (**Table 5.3**).[11]

Table 5.3. pMn values calculated for ligands having bis(aquated) Mn(II) complexes.

Ligand	pMn (pH = 7.4, 25 °C)
15–pyN_3O_2	5.28
15–pyN_5	6.37
H_2DPAPhA	7.37
H_2DPAMeA	7.38
H_2pmpa	**7.88**

5.5 Longitudinal Relaxivity Measurement of Complex 5B at 1.41 T

Longitudinal relaxivity r_1, is defined as the enhancement of relaxation rate of water protons by 1 mM paramagnetic metal ion concentration and provides a convenient way to express the efficiency of a paramagnetic complex as MRI CA. After confirming adequate stability of the complex, r_1 relaxivity of complex **5B** was measured at 1.41 T in a BRUKER minispec mq60 NMR analyzer. By using inversion recovery method, at four different

concentrations of the complex, the longitudinal relaxation time, T_1 was measured, and longitudinal relaxivity, r_1 (**Figure 5.10**) was obtained from the slope of the plot of longitudinal relaxation rate (R1 = $1/T_1$) *vs.* Mn(II) ion concentration, [Mn(II)]. The exact Mn(II) ion concentration was determined by ICP–AES method.

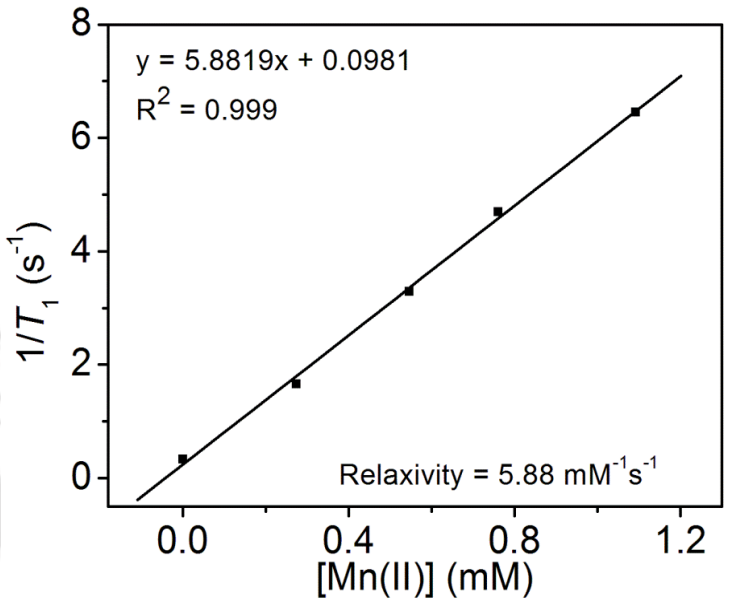

Figure 5.10. $1/T_1$ *vs.* [Mn(II)] plot. Measurements were performed using four different concentrations of complex **5B** at 1.41 T, 25 °C, and pH ~ 7.4.

The r_1 value was found to be 5.88 $mM^{-1}s^{-1}$ (at 1.41 T, 25 °C and pH ~ 7.4) per Mn(II). This value was significantly higher compared to the commercially available Mn(II)–based MRI CA, Teslascan® and even higher than the commercially available Gd(III)–based contrast agents (r_1 = 4.5–5.2 $mM^{-1}s^{-1}$).[1b] The two inner sphere water molecules in complex **5B** accounted for this higher r_1 relaxivity value. Thus, with two inner sphere water molecules and keeping the thermodynamic stability intake, complex **5B** is a good candidate as a safer MRI CA for the patients having renal problems.

Besides physiological pH, the relaxivity values were checked for a wide range of pH. It is one of the important concerns to have a constant relaxivity value of the complex below physiological pH also, as pH in the renal system is known to be lower than the physiological pH (~ 5.5–6.5).[25]

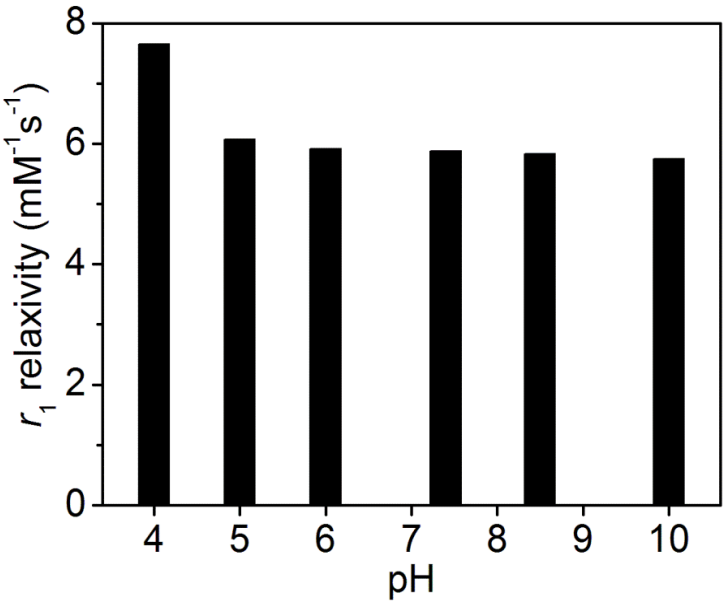

Figure 5.11. Longitudinal relaxivity measurement of complex **5B** in pH range 4–10, at 1.41 T, 25 °C.

The relaxivity value of the complex was found to be fairly constant through a pH range of 5–10 ($\Delta r_1 = \pm 0.19$ $mM^{-1}s^{-1}$, at 1.41 T and 25 ºC). However, high relaxivity value was observed at lower pH = 4, which was due to the partial dissociation of the complex and formation of aqua complex of Mn(II).

5.6 Longitudinal Relaxivity of Complex 5B at 1.41 T in the Presence of Physiological Anions

The anions like bicarbonate (HCO_3^-), phosphate (PO_4^{3-}), and fluoride (F^-) which are present in sufficient concentrations in blood serum, can replace the inner sphere water molecules of the complex if the complex is not stable enough. As a result, the r_1 relaxivity values sharply decrease due to the formation of ternary adducts. To investigate the affinity of complex **5B** towards phosphate, bicarbonate, and fluoride anions, relaxivity measurements were performed in the presence of 200 equivalents of the respective anions (experimental conditions: 1.41 T, 25 °C, pH ~ 7.4, [complex **5B**] = 0.5 mM, [physiological anions] = 100 mM).

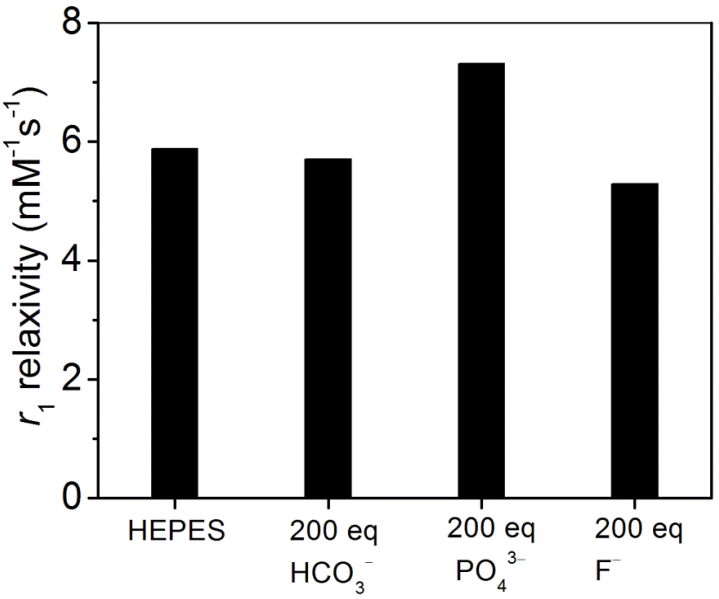

Figure 5.12. Relaxivity measurements of complex **5B** in the presence of 200 equivalents of different anions **(**at 1.41 T, 25 °C, pH ~ 7.4, [complex **5B**] = 0.5 mM, and [physiological anions] = 100 mM).

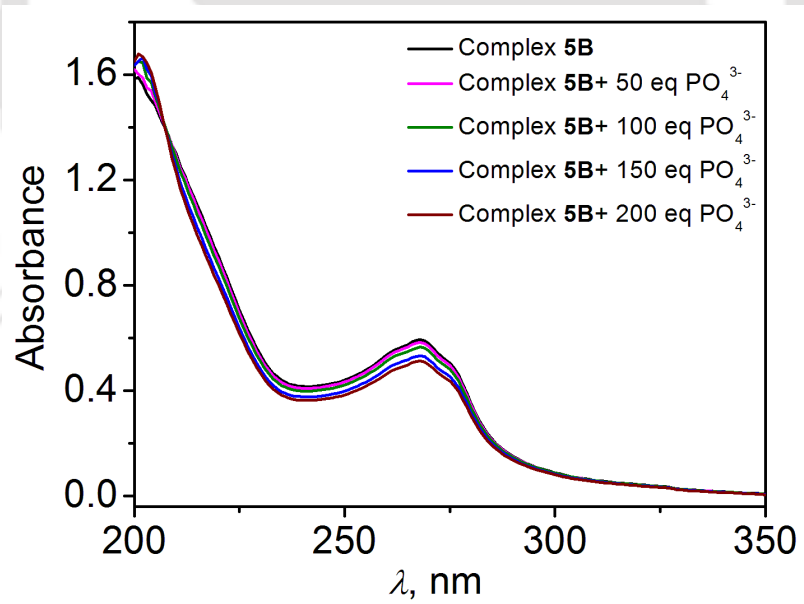

Figure 5.13. Change in UV–visible spectra of complex **5B** in the presence of 200 equivalents of phosphate anion **(**at 25 °C and pH ~ 7.4).

The results implied no significant decrease in r_1 relaxivity value in case of fluoride and bicarbonate ions, (Δr_1 = –0.18 $mM^{-1}s^{-1}$ for HCO_3^- and Δr_1 = –0.59 $mM^{-1}s^{-1}$ for F^-). The optimized structure of complex **5B** was also supportive of this result, where the two coordinated

water molecules were in axial positions on the opposite side of the molecular plane, which was not favorable for anion binding.[11a]

However, in case of phosphate anion, an increase in realxivity value (Δr_1 = +1.43 $mM^{-1}s^{-1}$) was observed, which may be due to the release of free Mn(II) ion or a molecular aggregation. The increase in relaxivity due to dissociation of the complex and formation of aqua complex of Mn(II) ion in the presence of phosphate anion could be discarded from UV–visible spectra of the complex (**Figure 5.13**). The spectra did not show any change even in the presence of 200 equivalents of phosphate ion concentration. Hence, the increase in relaxivity could be due aggregation of the complex by its interaction with the phosphate without replacing the inner sphere water molecules. The aggregation then lowered the tumbling rate and consequently relaxivity was being increased. Notably, a contribution from the outer sphere water molecules to the relaxivity due to ion-pairing interaction cannot be ignored.[26] A similar type of increased relaxivity value was also observed for the bis(aquated) Mn(II) complex of the ligand 15–pyN_3O_2 in the presence of 100 fold excess of phosphate ion.[11a]

5.7 Phantom MR Images of Complex 5B at 1.5 T

T_1–weighted phantom MR images of the complex at four different concentrations 0.25, 0.50, 0.70, and 1.00 mM were measured at 1.5 T, 25 °C and pH ~ 7.4 by using clinical MRI scanner BRIVO MR355 (**Figure 5.14)**.

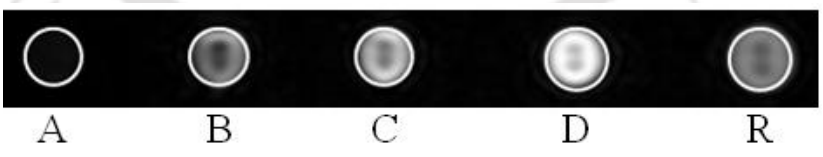

Figure 5.14. T_1–weighted phantom MR images of complex **5B** at different concentrations (A = 0.25 mM, B = 0.50 mM, C = 0.70 mM, D = 1.00 mM, R = Reference = Rezogad®) at 1.5 T, 25 °C, and pH ~ 7.4.

It was observed that with the increase in complex concentration, the image intensity increases. The images were also compared with the commercially available MRI CA Rezogad®. When the image intensities were compared by using ImageJ Software under the same area of the

images, the complex showed good image intensity compared to the commercially available one (**Figure 5.15**). So, a lower dose is expected for this complex.

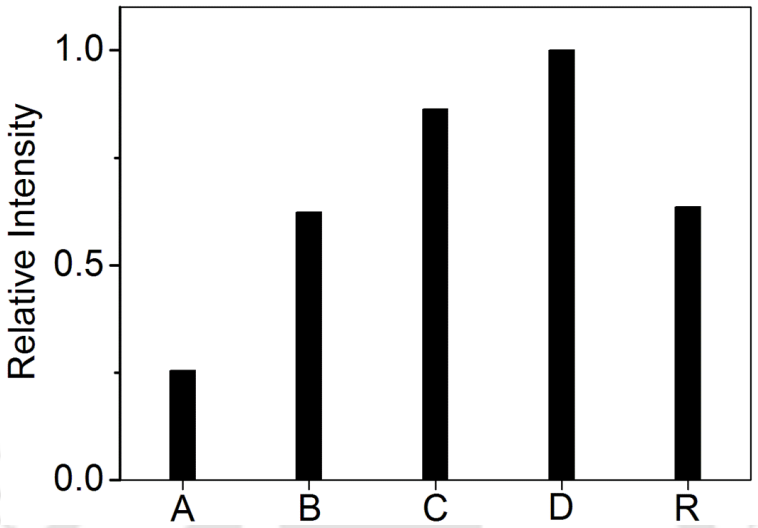

Figure 5.15. Comparison of T_1–weighted phantom MR images of complex **5B** (A = 0.25 mM, B = 0.50 mM, C = 0.70 mM, D = 1.00 mM, R = Reference = Rezogad®) at 1.5 T, 25 °C, and pH ~ 7.4.

5.8 Conclusion

- To develop safer MRI probes with enhanced efficacy, ligand H_2pmpa and its corresponding bis(aquated) Mn(II) complex, **5B**, have been investigated.
- DFT–based structural optimisation of the complex implied its pentagonal bipyramidal geometry having two inner sphere water molecules in the axial positions and the coordinating ligand in the equatorial plane.
- The complex showed comparable stability to that of $[Mn(EDTA)]^{2-}$ complex and better stability in comparison to the previously reported bis(aquated) Mn(II) complexes.
- The two bound waters afforded high r_1 relaxivity value of 5.88 $mM^{-1}s^{-1}$ at 1.41 T, pH ~ 7.4 and at 25 °C, which was almost constant in the pH range 5–10.
- T_1–weighted phantom MR images of complex **5B** under clinical MRI scanner showed good image intensity to use it as MRI CA with a lower dose than the commercially available one.
- The complex holds promise regarding the development of highly efficient Mn(II)–based MR imaging probes as an alternative to Gd(III)–based CAs.

References

1. (*a*) P. Hermann, J. Kotek, V. Kubíček and I. Lukeš, *Dalton Trans*., 2008, 3027; (*b*) A. Merbach, L. Helm and É. Toth, *The Chemistry of Contrast Agents in Medical Magnetic Resonance Imaging*, Second Edition. Wiley, New York, 2001; (*c*) A. D. Sherry, P. Caravan and R. E. Lenkinski, *J. Magn. Reson. Imaging*, 2009, **30**, 1240; (*d*) B. Drahoš, I. Lukeš and É. Tóth, *Eur. J. Inorg. Chem*., 2012, 1975; (*e*) J. S. Troughton, M. T. Greenfield, J. M. Greenwood, S. Dumas, A. J. Wiethoff, J. Wang, M. Spiller, T. J. McCurry and P. Caravan, *Inorg. Chem*., 2004, **43**, 6313; (*f*) B. Drahoš, M. Pniok, J. Havlíčková, J. Kotek, I. Císařová, P. Hermann, I. Lukeš and É. Tóth, *Dalton Trans*., 2011, **40**, 10131.
2. (*a*) S. K. Saxena, H. Sharma, M. Patel and D. Oreopoulos, *Int. Urol. Nephrol.*, 2008, **40**, 715; (*b*) P. Marckmann, L. Skov, K. Rossen, A. Dupont, M. Damholt, J. Heaf and H. Thomsen, *J. Am. Soc. Nephrol.*, 2006, **17**, 2359; (*c*) C. Thakral, J. Alhariri and J. Abraham, *Contrast Media Mol. Imaging 2*, 2007, 199; (*d*) M. Sieber, P. Lengsfeld, J. Walter, H. Schirmer, T. Frenzel, F. Siegmund, H. Weinmann and H. Pietsch, *J. Magn. Reson. Imaging*, 2008, **27**, 955.
3. (*a*) E. Kanal and M. F. Tweedle, *Radiology*, 2015, **275**, 630; (*b*) N. Karabulut, *Diagn. Interv. Radiol*., 2015, **21**, 269; (*c*) T. Kanda, K. Ishii, H. Kawaguchi, K. Kitajima and D. Takenaka, *Radiology*, 2014, **270**, 834; (*d*) T. Kanda, M. Osawa, H. Oba, K. Toyoda, J. Kotoku, T. Haruyama, K. Takeshita and S. Furui, *Radiology*, 2015, **275**, 803; (*e*) T. Kanda, T. T. Fukusato, M. Matsuda, K. Toyoda, H. Oba, J. Kotoku, T. Haruyama, K. Kitajima and S. Furui, *Radiology*, 2015, **276**, 228; (*f*) Y. Errante, V. Cirimele, C. A. Mallio, V. Di Lazzaro, B. B. Zobel and C. C. Quattrocchi, *Investig. Radiol*., 2014, **49**, 685; (*g*) R. J. McDonald, J. S. McDonald, D. F. Kallmes, M. E. Jentoft, D. L. Murray, K. R. Thielen, E. E. Williamson and L. J. Eckel, *Radiology*, 2015, **275**, 773.
4. (*a*) D. W. Christianson, *Prog. Biophys. Mol. Biol.*, 1997, **67**, 217; (*b*) J. Crossgrove and W. Zheng, *NMR Biomed.*, 2004, **17**, 544; (*c*) Y. Li, T. T. Huang, E. J. Carlson, S. Melov, P. C. Ursell, J. L. Olson, L. J. Noble, M. P. Yoshimura, C. Berger and P. H. Chan, *Nat. Genet.*, 1995, **11**, 376; (*d*) F. C. Wedler and Denman, R. B. *Curr. Top. Cell Regul*., 1984, **24**, 153.
5. (*a*) Z. Garda, A. Forgács, Q. N. Do, F. K. Kálmán, S. Timári, Z. Baranyai, L. Tei, I. Tótha, Z. Kovács and G. Tircsó, *J. Inorg. Biochem*., 2016, **163**, 206; (*b*) E. Brücher, G. Tircsó, Z. Baranyai, Z. Kovács and A. D. Sherry, in: A. Merbach, L. Helm and E. Tóth, *The Chemistry of Contrast Agents in Medical Magnetic Resonance Imaging*, Second Edition.

Wiley, New York, 2001; (*c*) E. Terreno, D. D. Castelli, A. Viale, S. Aime, *Chem. Rev.*, 2010, **110**, 3019; (*d*) S. Aime, D. D. Castelli, S. G. Crich, E. Gianolio, E. Terreno, *Acc. Chem. Res*., 2009, **42**, 822; (*e*) L. Tei, G. Gugliotta, M. Fekete, F. K. Kalman, M. Botta, *Dalton Trans*., 2011, **40**, 2025.

6. S. M. Rocklage, W. P. Cacheris, S. C. Quay, E. Hahn and K. N. Raymond, *Inorg. Chem*., 1989, **28**, 477.
7. J. T. Jørgensen, M. Rief, T. B. Brismar, M. Wagner and N. Albiin, *Acta Radiologica*, 2012, **53**, 707.
8. (*a*) M. A. Verity, *Neurotoxicology*, 1999, **20**, 489; (*b*) R. G. Lucchini, C. J. Martin and B. C. Doney, *Neuromol. Med*., 2009, **11**, 311.
9. (*a*) G. S. Loving, S. Mukherjee and P. Caravan, *J. Am. Chem. Soc*., 2013, 135, 4620; (*b*) B. Phukan, A. B. Patel and C. Mukherjee, *Dalton Trans*., 2015, **44**, 12990; (*c*) A. Forgács, M. Regueiro-Figueroa, J. L. Barriada, D. Esteban-Gómez, A. de Blas, T. Rodríguez-Blas, M. Botta and C. Platas-Iglesias, *Inorg. Chem*., 2015, **54**, 9576; (*d*) G. A. Rolla, C. Platas-Iglesias, M. Botta, L. Tei, L. Helm, *Inorg. Chem.*, 2013, **52**, 3268.
10. Some examples are: (*a*) D. M. J. Doble, M. Melchior, B. O'Sullivan, C. Siering, J. Xu, V. C. Pierre and K. N. Raymond, *Inorg. Chem*., 2003, **42**, 4930; (*b*) C. J. Jocher, E. G. Moore, J. Xu, S. Avedano, M. Botta, S. Aime and K. N. Raymond, *Inorg. Chem*., 2007**, 46**, 9182; (*c*) D. T. Puerta, M. Botta, C. J. Jocher, E. J. Werner, S. Avedano, K. N. Raymond and S. M. Cohen, *J. Am. Chem. Soc*., 2006, **128**, 2222; (*d*) E. M. Gale, N. Kenton and P. Caravan, *Chem. Commun*., 2013, **49**, 8060; (*e*) A. Datta and K. N. Raymond, *Acc. Chem. Res*., 2009, **42**, 938.
11. (*a*) B. Drahoš, J. Kotek, P. Hermann, I. Lukeš and Eva Tóth, *Inorg. Chem.*, 2010**, 49**, 3224; (*b*) A. Forgács, R. Pujales-Paradela, M. Regueiro-Figueroa, L. Valencia, D. Esteban-Gómez, M. Botta and C. Platas-Iglesias, *Dalton Trans*., 2017, **46**, 1546.
12. M. Regueiro-Figueroa, G. A. Rolla, D. Esteban-Gómez, A. de Blas, T. Rodríguez-Blas, M. Botta and C. Platas-Iglesias, *Chem. Eur. J*., 2014, **20**, 17300.
13. E. M. Gale, I. P. Atanasova, F. Blasi, I. Ay and P. Caravan, *J. Am. Chem. Soc*., 2015, **137**, 15548.
14. (*a*) Md. N. Khan, S. Pal, T. Parvinb, L. H. Choudhury, *RSC Adv*., 2012, **2**, 12305; (*b*) G. Bringmann, Y. Reichert, V. V. Kane, *Tetrahedron*, 2004, **60**, 3539; (*c*) B. B. Fredholm, A. P. Izerman, K. A. Jacobson, K. N. Klotz, J. Linden, *Pharmacol. Rev*. 2001, **53**, 527.

15. (*a*) V. Bala, S. Jangir, D. Mandalapu, S. Gupta, Y. S. Chhonker, N. Lal, B. Kushwaha, H. Chandasana, S. Krishna, K. Rawat, J. P. Maikhuri, R. S. Bhatta, M. I. Siddiqi, R. Tripathi, G. Gupta, V. L. Sharma, *Bioorg. Med. Chem. Lett*., 2015, **25**, 881;.(*b*) Yuan-Y. Zhu, Chang-W. Liu, J. Yin, Zhao-S. Meng, Q. Yang, J. Wang, T. Liu and S. Gao, *Dalton Trans*., 2015, **44**, 20906; (*c*) V. Chandrasekhar, S. Hossain, S. Das, S. Biswas and Jean-P. Sutter, *Inorg. Chem*., 2013, **52**, 6346; (*d*) E. W. Price, J. F. Cawthray, G. A. Bailey, C. L. Ferreira, E. Boros, M. J. Adam and C. Orvig, *J. Am. Chem. Soc.*, 2012, **134**, 8670.

16. (*a*) J. Wang, G. R. Gao, Z. H. Zhang, X. D. Zhang, X. Z. Liu, Y. M. Kong and Y. Li, *Russ. J. Coord. Chem*., 2007, **33**, 258; (*b*) E. S. G. Choo, X. Tang, Y. Sheng, B. Shuter and J. Xue, *J. Mater. Chem*., 2011, **21**, 2310; (*c*) J. Coates, *Interpretation of Infrared Spectra: A Practical Approach*, John Wiley & Sons Ltd, Chichester, 2000; (*d*) B. C. Smith, *Infrared Spectral Interpretation: A Systematic Approach*, CRC press, 1998.

17. M. J. Frisch *et al.* Gaussian09, Revision D.01, Gaussian, Inc., Wallingford CT, 2009.

18. Y. Zhao, N. E. Schultz and D. G. Truhlar, *J. Chem. Theo. Comp.*, 2006, **2**, 364.

19. Y. Zhao and D. G. Truhlar, *Theo. Chem. Acc.*, 2008, **120,** 215.

20. S. Miertuš, E. Scrocco and J. Tomasi, *Chem. Phys*., 1981, **55**, 117.

21. V. Barone and M. Cossi, *J. Phys. Chem. A*, 1998, **102**, 1995.

22. The formation energy was calculated as

$$\Delta E = [E_{(\text{overall complex})} - \{E_{(\text{complex without water})} + nE_{H_2O}\}]$$

here, n is the no of water molecules.

23. (*a*) Q. Zhang, J. D. Gorden, R. J. Beyers and C. R. Goldsmith, *Inorg. Chem.*, 2011, **50**, 9365; (*b*) E. Molnár, N. Camus, V. Patinec, G. A. Rolla, M. Botta, G. Tircsó, F. K. Kálmán, T. Fodor, R. Tripier and C. Platas-Iglesias, *Inorg. Chem.*, 2014, **53**, 5136; (*c*) B. Drahoš, J. Kotek, I. Císařová, P. Hermann, L. Helm, I. Lukeš and É. Tóth, *Inorg. Chem.*, 2011, **50**, 12785; (*d*) M. Zampakou, N. Rizeq, V. Tangoulis, A. N. Papadopoulos, F. Perdih, I. Turel and G. Psomas, *Inorg. Chem.*, 2014, **53**, 2040.

24. (*a*) C. J. Jocher, M. Botta, S. Avedano, E. G. Moore, J. Xu, S. Aime and K. N. Raymond, *Inorg. Chem.*, 2007, **46**, 4796; (*b*) E. J. Werner, J. Kozhukh, M. Botta, E. G. Moore, S. Avedano, S. Aime and K. N. Raymond, *Inorg. Chem.*, 2009, **48**, 277.

25. Z. Garda, A. Forgács, Q. N. Do, F. K. Kálmán, S. Timári, Z. Baranyai, L. Tei, I. Tóth, Z. Kovács and G. Tircsó, *J. Inorg. Biochem*., 2016, **163**, 206.

26. (*a*) V. C. Pierre, M. Botta, A. Silvio and K. N. Raymond, *Inorg. Chem.*, 2006, **45**, 8355; (*b*) J. I. Bruce, R. S. Dickens, L. J. Govenlock, T. Gunnlaugsson, S. Lopinski, M. P. Lowe, D.

Parker, R. D. Peacock, J. J. B. Perry, S. Aime and M. Botta, *J. Am. Chem. Soc*., 2000, **122**, 9674.

Thesis Conclusions and Perspectives

The main aim of this work has been the development of new, better and safer MRI contrast agents, compared to the existing contrast agents, that exhibit good water solubility, giving better contrast and reducing acquisition time; for the possible future applications in the field of MRI.

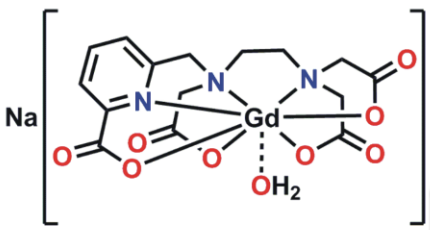

Complex **2A**

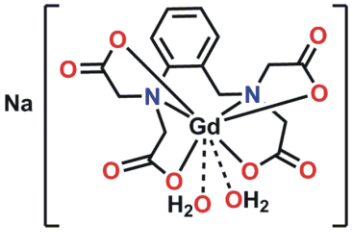

Complex **3A**

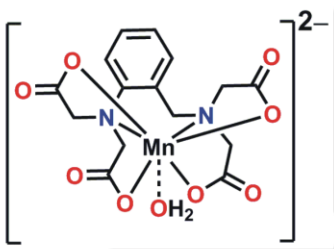

Complex **4A**

Complex **5B**

The water soluble, aquated Gd(III) complex of ligand H_4peada, **2A** showed r_1 realxivity value of 6.08 $mM^{-1}s^{-1}$ at 1.41 T, 25 °C and pH ~ 7.4. While the r_1 relaxivity values of the commercially available Gd(III)–based MRI contrast agents are in the range 4.4–5.2 $mM^{-1}s^{-1}$, with comparable thermodynamic and kinetic stability to that of commercially available $[Gd(DTPA)(H_2O)]^-$ complex, complex **2A** can be thought of as an alternative to the currently used MRI contrast agents with enhanced contrast.

In contrast to the current trend of decreasing the r_1 relaxivity values of the commercially available Gd(III)–based MRI contrast agents with increasing field strength, the Gd(III) complex of ligand H_4bedik, **3A** provided a higher r_1 realxivity value of 12.40 $mM^{-1}s^{-1}$ at 14.1 T, 25 °C and pH ~ 7.4. With better thermodynamic and kinetic stability than that of the commercially available $[Gd(DTPA)(H_2O)]^-$ complex, complex **3A** holds promise regarding the development of MRI imaging probes that can be used at higher magnetic fields.

Looking for a safer MRI contrast agent for patients having severe renal diseases or who underwent liver transplantation, Mn(II) complex of ligand H_4bedik, **4A** with one inner sphere water molecule provided the r_1 realxivity value of 3.11 $mM^{-1}s^{-1}$ at 1.41 T, 25 °C and pH ~ 7.4. In addition to this, at 14.1 T, the higher r_1 and r_2 realxivity values of the complex (r_1 = 6.29 mM^-

$^{1}s^{-1}$ and r_2 = 132.77 $mM^{-1}s^{-1}$, 25 °C and pH ~ 7.4) reinforce its candidature as a future T_1 and T_2 dual mode MRI contrast agent at higher magnetic field.

Next step towards safer and powerful imaging involved the synthesis of bis(aquated) Mn(II) complex of ligand H_2pmpa, **5B** with r_1 realxivity value of 5.88 $mM^{-1}s^{-1}$ at 1.41 T, 25 °C and pH ~ 7.4. The favourable relaxation properties and thermodynamic stability of the complex make it a promising candidate for the development of effective MRI contrast agents for safer and emerging applications in MRI.

The results included in this thesis suggest the possibility of new water soluble and water coordinated Gd(III) and Mn(II)–based candidates for clinically useful MRI contrast agents. Further study on solution dynamic properties and biocompatibility should be preferred. In addition to the reported complexes, the following organic ligands and their corresponding Gd(III), Mn(II) and Fe(III) complexes could be synthesised and studied as the next generation MRI contrast agents.

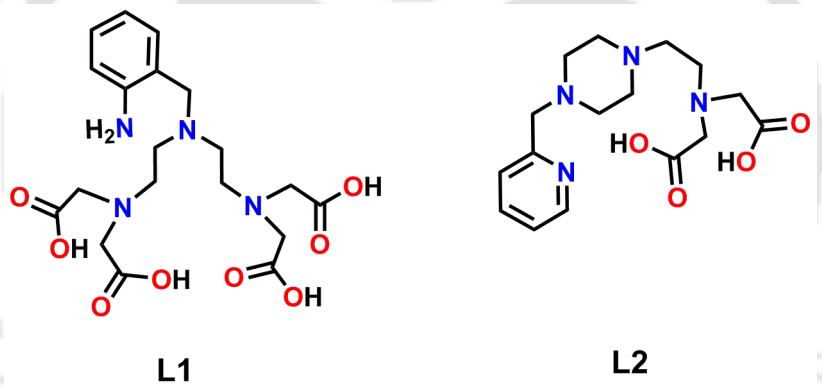

Scheme. Proposed ligands for synthesising new MRI contrast agents.

Chapter VI

Equipment and Experimental Section

6.1 Methods and Equipments

Chemicals and Solvents

All the chemicals and solvents were obtained from commercial sources and were used as supplied, unless noted otherwise.

Infrared Spectroscopy

Solid state FTIR spectra were recorded (4000–400 cm^{-1}) on 'Perkin Elmer Instrument' at room temperature. The pellet has been made by grinding the sample with IR grade KBr powder.

NMR Spectroscopy

^{1}H and ^{13}C NMR spectra were recorded by using 'Varian Mercury plus 400 MHz', 'Bruker AscendTm 600 MHz', and 'Bruker 300 MHz' nuclear magnetic resonance (NMR) spectrometer at 298 K. Chemical shifts, δ (in ppm), were reported relative to TMS [δ (^{1}H) 0.0 ppm, δ (^{13}C) 0.0 ppm] which was used as the internal standard. Otherwise, the solvent residual proton and carbon resonance were taken as references (For $CDCl_3$, δ (^{1}H) 7.26 ppm, and δ (^{13}C) 77.2 ppm; for CD_3OD, δ (^{1}H) 3.31, 4.87 ppm, and δ (^{13}C) 49.0 ppm). The resultant spectra were drawn by using 'MestReNova' NMR data processing software.

Mass Spectrometry

Mass spectra were recorded on QTOF–MS Spectrometer ('Waters, Model: Q–Tof Premier') or 'Agilent Accurate–Mass Q–TOF LC/MS 6520' spectrometer and peaks were given in *m*/*z* (% of basis peak). HPLC grade CH_3CN, CH_3OH and Mili Q water were used as solvents for taking the mass spectra.

Single Crystal X–ray Crystallography

Single crystal suitable for X–ray diffraction study was obtained from evaporation of water at room temperature (25 °C). X–ray crystallographic data were collected by using a 'Super Nova, Single source at offset, Eos diffractometer'. Structures were solved by direct methods using SHELXS–97 and refined with full–matrix least squares on F^2 using SHELXL–97. All the non–hydrogen atoms were refined anisotropically.

UV–Vis Spectroscopy

The electronic absorption spectrum of the sample(s) was recorded on a 'Perkin Elmer, Lamda 25, UV/VIS spectrometer' in Mili Q water using cuvette of 1 cm width.

Inversion Recovery Method

In this method, the intial magnetisation M_0 is first exposed to a 180 ° pulse which inverts the the magnetisation to its opposite direction and becomes antiparallel to the direction of applied magnetic field. An inversion time (TI) is given to the system during which the magnetisation starts to recover to its original position. After a certain inversion time, another 90 ° pulse is applied and the magnetisation is then measured in the *xy*–plane. A schematic representation of the method is shown in **Figure 6.1**.

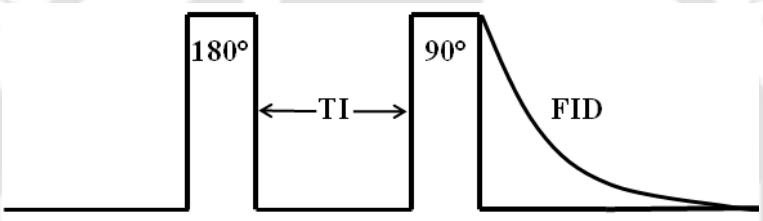

Figure 6.1. Pulse sequences in inversion recovery method.

Saturation Recovery Method

In this method, the intial magnetisation M_0 is first exposed to a 90 ° pulse. A repition time (TR) is allowed to the system during which the magnetisation in the *xy*–plane starts to return its original position. Then another 90 ° pulse is applied which again pushed the magnetisation to the *xy*–plane and then FID can be monitored. A schematic representation of the method is shown in **Figure 6.2**.

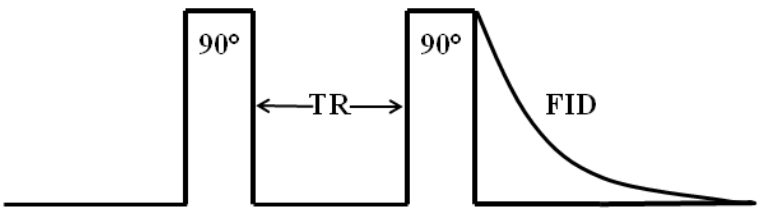

Figure 6.2. Pulse sequences in saturation recovery method.

Competition Batch Titration Method for Determination of pM

pM values of the ligands were determined at pH = 7.4, and 25 °C. The protonation equilibria of the ligands can be neglected under this constant pH and at equilibrium,

$M + L \longleftrightarrow ML$

$M + C \longleftrightarrow MC$

where M, L, and C represent the metal ion, ligand and competing ligand respectively.

The formation constants for the above reactions are given by,

$\beta_{ML} = [ML]/[M][L]$ and $\beta_{MC} = [MC]/[M][C]$

Since standard conditions are used at pH 7.4, these formation constants can be considered as conditional stability constants. The difference in the logarithimic values of formation constants will now equivalent to the difference in the pM values.

Now, $pM_{ML} - pM_{MC} = \log \beta_{ML} - \log \beta_{MC}$

$= \log ([ML]/[M][L]) - \log ([MC]/[M][C])$

$= \log ([ML][C] /[MC][L])$

$= \log ([ML]/[MC]) + \log ([C]/[L])$

This equation is primarily used to determine the pM value of the ligand and can be rearranged to:

$-\log ([ML]/[MC]) = \log ([C]/[L]) - (pM_{ML} - pM_{MC})$

or $\log ([MC]/[ML]) = \log ([C]/[L]) + \Delta pM$

where $\Delta pM = pM_{MC} - pM_{ML}$

Now the plot of log ([MC]/[ML]) *vs.* log ([C]/[L]) directly gives the difference in pM value between the ligand and the competing ligand (ΔpM), when log ([MC]/[ML]) = 0 or when the concentration of the competing ligand generates a equal partition of the metal between the ligand and the competing ligand.

EPR Spectroscopy

First derivative X–band EPR spectrum of the sample solution in water was measured by using 'JEOL JESFA200 ESR Spectrometer'. Spin–Hamiltonian simulation of the EPR spectrum was done by using a program which was developed from S = 5/2 routines of Gaffiney and Silverstone and it specially makes use of the resonance search procedure based on a Newton–Raphson algorithm as described therein.

6.2 Experimental Section

6.2.1 Synthesis of Ligand H_4peada

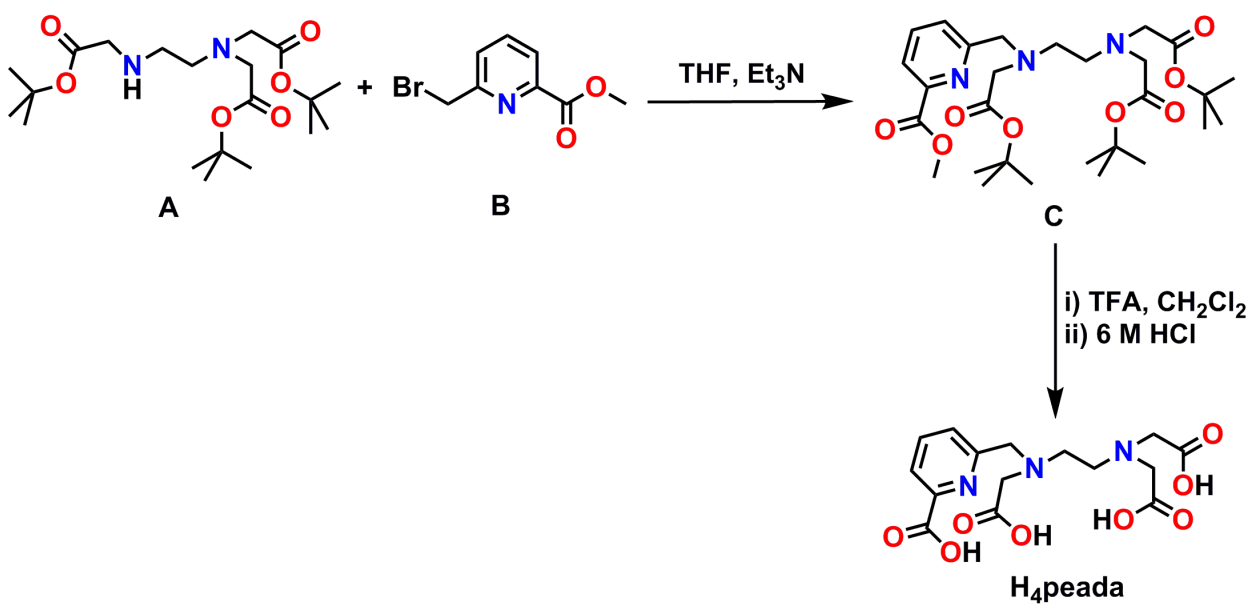

Scheme 6.1. Synthetic route of ligand H_4peada.

Synthesis of $[C_{20}H_{38}N_2O_6]$, (A): To a stirred solution of ethylenediamine (0.309 g, 5 mmol) in 10 mL THF, Et_3N (2.4 mL, 15 mmol) was added dropwise at 0 °C, followed by addition of *tert*–butylbromoacetate (1.953 g, 10 mmol). The reaction mixture was then stirred at room temperature (25 °C) for another 12 h. The solvent was removed completely *in vacuo* and water (10 mL) was added. The organic compound was then extracted from the aqueous phase with CH_2Cl_2 (3 × 30 mL). The combined organic extracts were dried over anhy. Na_2SO_4 and the crude product was obtained as a pale yellow liquid after concentrating the organic solvent. The pure compound was obtained as colourless oil by column chromatography on silica gel by using hexane/ethyl acetate (1:4) as eluent.

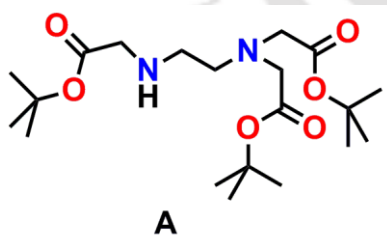

Yield: 0.316 g, 16 %.

FTIR (KBr, cm^{-1}): 3324, 2982, 2934, 1735, 1370, 1222, 1150, 843, 744.

^{1}H NMR ($CDCl_3$, 600.17 MHz): δ 3.43 (s, 4H), 3.32 (s, 2H), 2.88 (t, J = 6 Hz, 2H), 2.68 (t, J = 6 Hz, 2H), 1.45 (s, 9H), 1.44 (s, 18H) ppm.

ESI–MS (+) *m/z* for $[C_{20}H_{38}N_2O_6 + H]^+$: Calcd, 403.2802; Found, 403.2779.

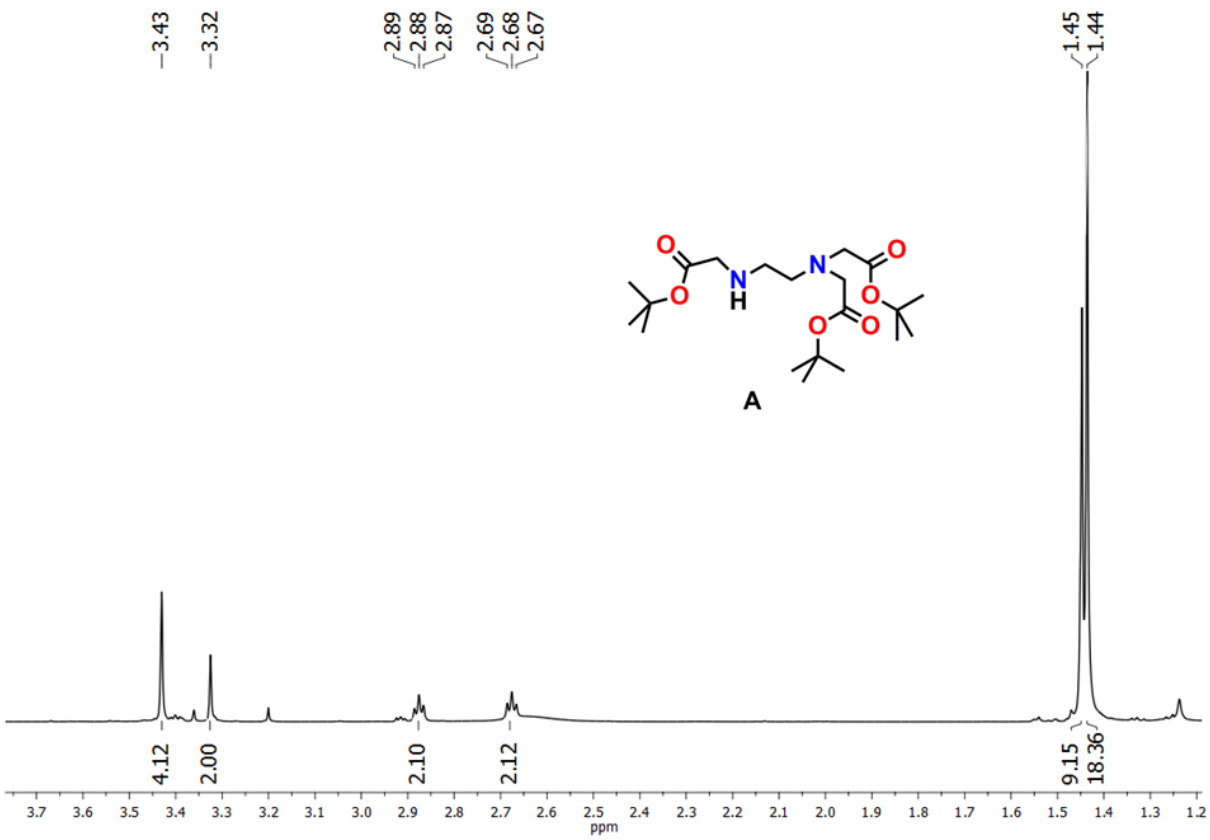

Figure 6.3. ^{1}H NMR spectrum of $[C_{20}H_{38}N_2O_6]$, (A).

Synthesis of [$C_8H_8BrNO_2$], (B): Synthesis of 6–(bromomethyl)pyridine–2–carboxylate, (B) involved the following steps:

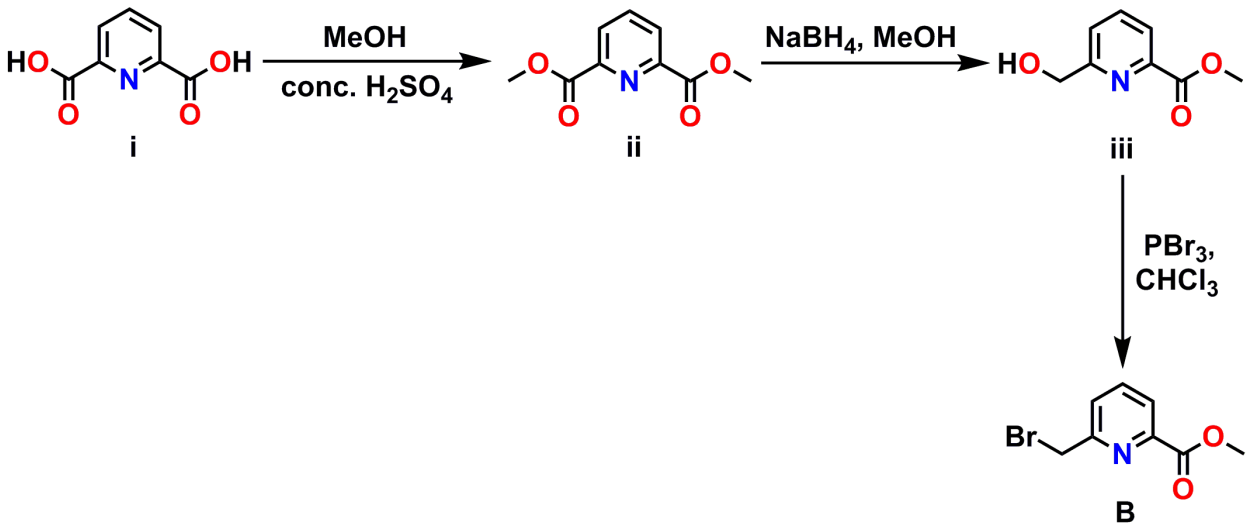

Scheme 6.2. Synthetic route of 6–(bromomethyl)pyridine–2–carboxylate, (B).

Synthesis of [$C_9H_9NO_4$], (ii): To a stirred solution of pyridine–2,6–dicarboxylic acid, (i) (3.34 g, 20 mmol) in methanol (20 mL), conc. H_2SO_4 (0.5 mL) was added dropwise at 0 °C under inert atmosphere. The reaction mixture was stirred at reflux condition for 48 h and the insoluble powder was completely dissolved under this condition. The reaction mixture was then cooled to room temperature (25 °C), and kept at room temperature for ~ 2 h. White crystalline solids were obtained from the solution, which were then filtered, and washed thoroughly with water.

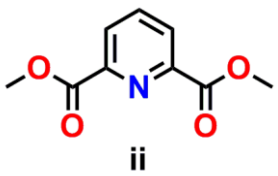

Yield: 3.31 g, 85 %.

FTIR (KBr, cm^{-1}): 3451, 3063, 2968, 2925, 2854, 1742, 1572, 1450, 1438, 1290, 1246, 1197, 1165, 1145, 1081, 997, 952, 813, 758, 723.

^1H NMR ($CDCl_3$, 399.85 MHz): δ 8.31 (d, J = 8 Hz, 2H), 8.02 (t, J = 8 Hz, 1H), 4.02 (s, 6H) ppm.

ESI–MS (+) *m/z* for $[C_9H_9NO_4 + H]^+$: Calcd, 196.0604; Found, 196.0619.

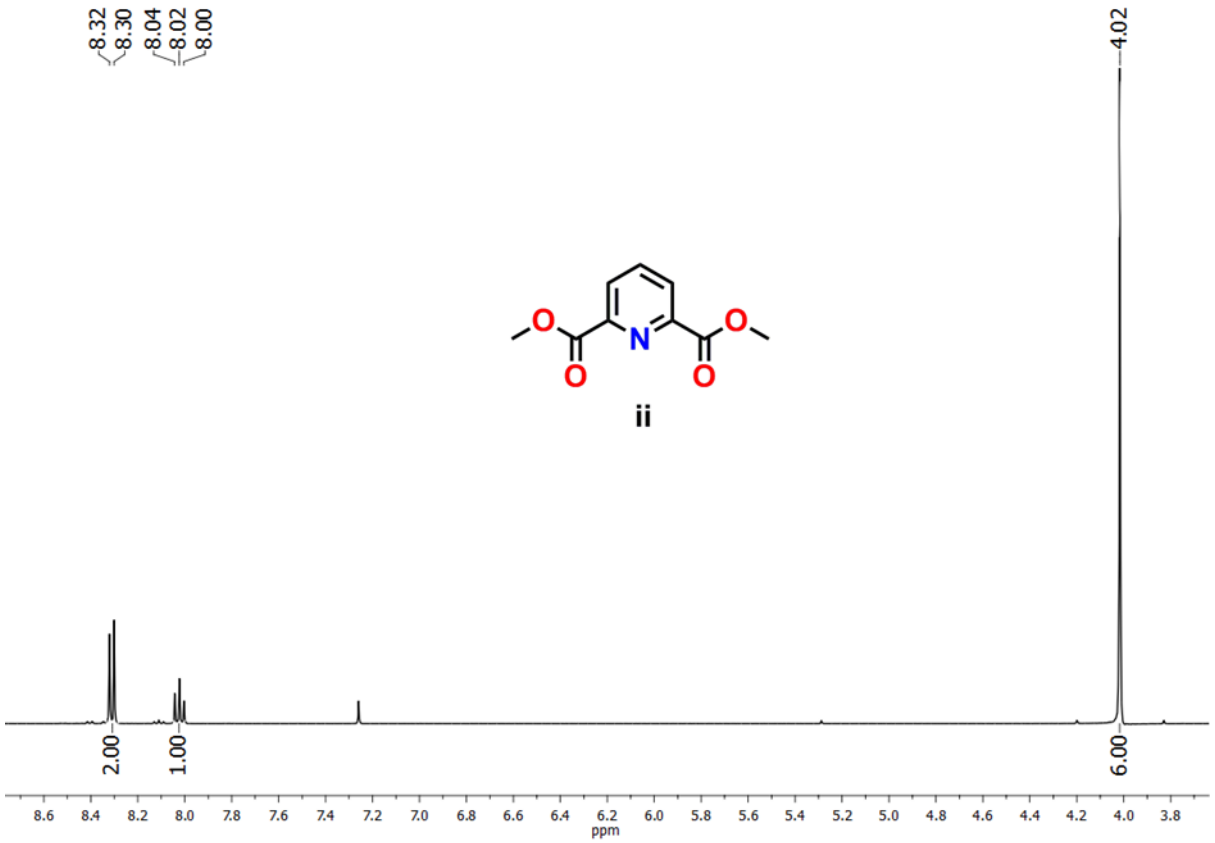

Figure 6.4. ^{1}H NMR spectrum of dimethylpyridine–2,6–dicarboxylate, (ii).

Synthesis of [$C_8H_9NO_3$], (iii): To a stirred suspension of dimethylpyridine–2,6–dicarboxylate, (ii) (1.96 g, 10 mmol) in methanol (15 mL) at 0 °C, $NaBH_4$ (0.58 g, 15 mmol, 1.5 equiv) was added in small portions over a period of 15 min. The reaction mixture was then stirred at room temperature (25 °C) for another 5 h. Methanol was removed completely in a rotavapor and a saturated aqueous solution of $NaHCO_3$ (20 mL) was added to the residue. The aqueous solution was then extracted with $CHCl_3$ (3 × 10 mL) and the combined organic layers were dried over anhy. Na_2SO_4. It was then filtered and concentrated the filtrate to dryness. The crude product was purified by column chromatography on silica gel by using hexane/ethyl acetate (1:1) as eluent.

iii

Yield: 1.17 g, 70 %.

FTIR (KBr, cm^{-1}): 3298, 2955, 2909, 1746, 1593, 1469, 1449, 1295, 1217, 1196, 1147, 1163, 1093, 1073, 1001, 985, 871, 826, 762, 714, 674.

^{1}H NMR ($CDCl_3$, 399.85 MHz): δ 8.03 (d, J = 8 Hz, 1H), 7.85 (t, J = 8 Hz, 1H), 7.53 (d, J = 8 Hz, 1H), 4.86 (s, 2H), 3.99 (s, 3H) ppm.

ESI–MS (+) *m/z* for $[C_8H_9NO_3 + H]^+$: Calcd, 168.0655; Found, 168.0657.

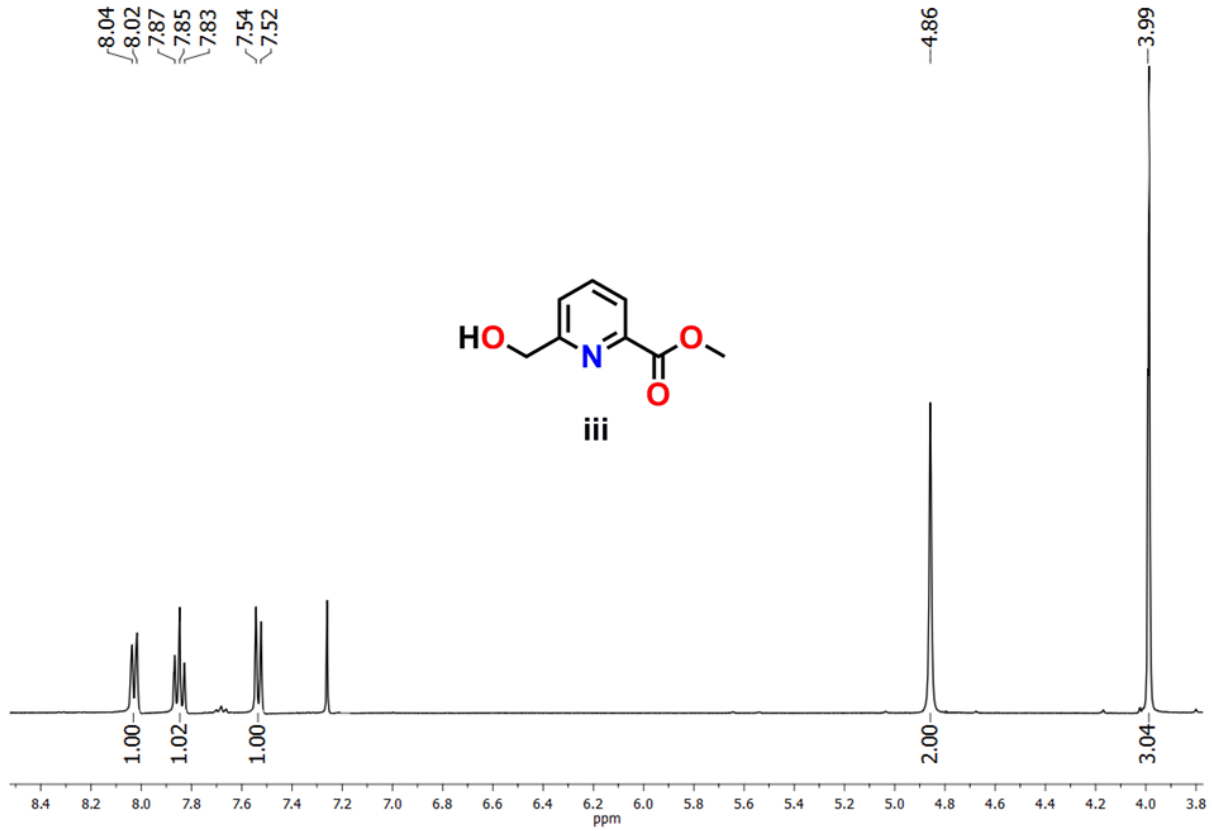

Figure 6.5. ^{1}H NMR spectrum of 6–(hydroxymethyl)pyridine–2–carboxylate, (iii).

Synthesis of $[C_8H_8BrNO_2]$, (B): To a stirred solution of 6–(hydroxymethyl)pyridine–2–carboxylate, (iii) (1.34 g, 8 mmol) in $CHCl_3$ (10 mL) under argon atmosphere and at 0 °C, PBr_3 (0.8 mL, 8.8 mmol) was added dropwise. A white precipitate was formed, and the solution became bright yellow. Stirring was continued at room temperature (25 °C) for another 6 h. The reaction mixture was then quenched using aqueous solution of $NaHCO_3$ (20 mL) and extracted with $CHCl_3$ (3 × 10 mL). The combined organic layers were dried over anhy. Na_2SO_4, filtered, and concentrated *in vacuo* to afford an off–white solid. The pure product was obtained as a white solid by column chromatography on silica gel by using hexane/ethyl acetate (7:3) as eluent.

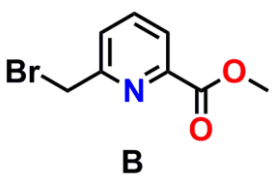

Yield: 1.27 g, 69 %.

FTIR (KBr, cm^{-1}): 3458, 3090, 3062, 3040, 3004, 2981, 2952, 1739, 1578, 1441, 1298, 1238, 1172, 1149, 1087, 1000, 993, 796, 770, 670, 627, 582.

^1H NMR ($CDCl_3$, 399.85 MHz): δ 8.06 (d, J = 8 Hz, 1H), 7.86 (t, J = 8 Hz, 1H), 7.68 (d, J = 8 Hz, 1H), 4.64 (s, 2H), 4.00 (s, 3H) ppm.

ESI–MS (+) *m/z* for $[C_8H_8BrNO_2 + H]^+$: Calcd, 229.9811; Found, 229.9815.

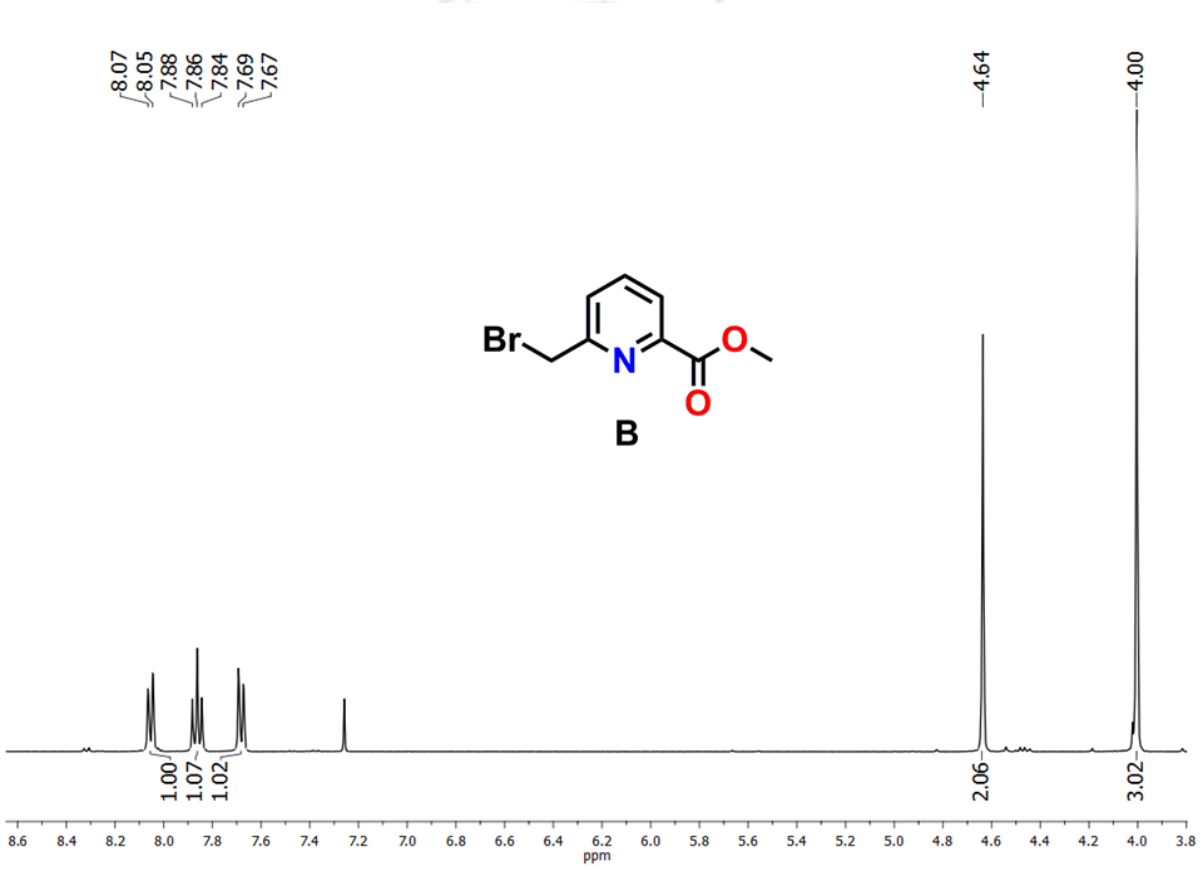

Figure 6.6. ^1H NMR spectrum of 6–(bromomethyl)pyridine–2–carboxylate, (B).

Synthesis of [$C_{28}H_{45}N_3O_8$], (C): To a stirred solution of compound **A** (0.536 g, 1.33 mmol) and Et_3N (0.37 ml, 2.66 mmol) in THF (10 mL) was added compound **B** (0.337 g, 1.46 mmol) and the reaction was stirred at room temperature (25 °C) for 24 h. The solvent was removed *in vacuo* and the residue was partitioned between CH_2Cl_2 (10 mL) and saturated aq. $NaHCO_3$ (10 mL) solution. The aqueous phase was then washed with CH_2Cl_2 (3×10 mL), and the combined organic extracts were dried over anhy. Na_2SO_4. The solvents were evaporated *in vacuo* and the crude compound was purified by column chromatography on silica gel (hexane/ ethyl acetate, 1:1), to afford the ester–protected precursor as a colourless oil.

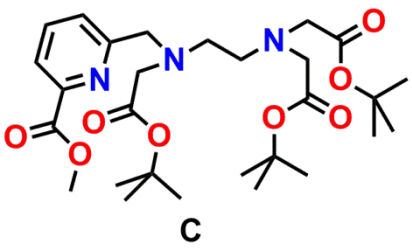

C

Yield = 0.506 g, 69 %.

FTIR (KBr, cm^{-1}): 3437, 2979, 2932, 2853, 1742, 1591, 1462, 1374, 1218, 1157, 995, 848, 764, 678.

^1H NMR ($CDCl_3$, 600.17 MHz): δ 7.99 (d, J = 6 Hz, 1H), 7.88 (d, J = 6 Hz, 1H), 7.80 (t, J = 6 Hz, 1H), 4.03 (s, 2H), 3.98 (s, 3H), 3.42 (s, 4H), 3.35 (s, 2H), 2.85 (t, J = 6 Hz, 2H), 2.81 (t, J = 6 Hz, 2H), 1.44 (s, 9H), 1.42 (s, 18H) ppm.

^{13}C NMR ($CDCl_3$, 100.55 MHz): δ 170.7, 166.0, 161.0, 147.2, 137.4, 126.2, 123.5, 81.0, 60.6, 56.4, 56.1, 52.9, 52.2, 28.3, 28.1 ppm.

ESI–MS (+) *m/z* for $[C_{28}H_{45}N_3O_8 + H]^+$: Calcd, 552.3279; Found, 552.3284.

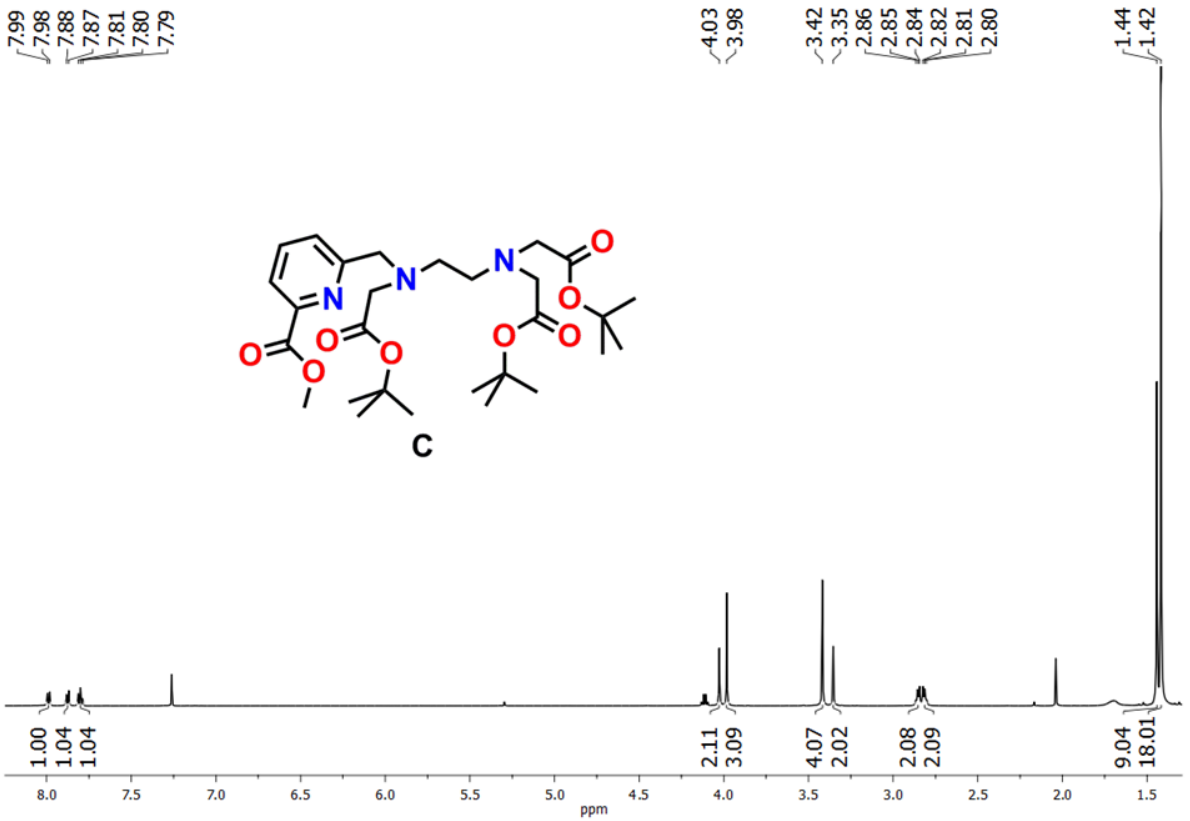

Figure 6.7. ^{1}H NMR spectrum of [$C_{28}H_{45}N_3O_8$], (C).

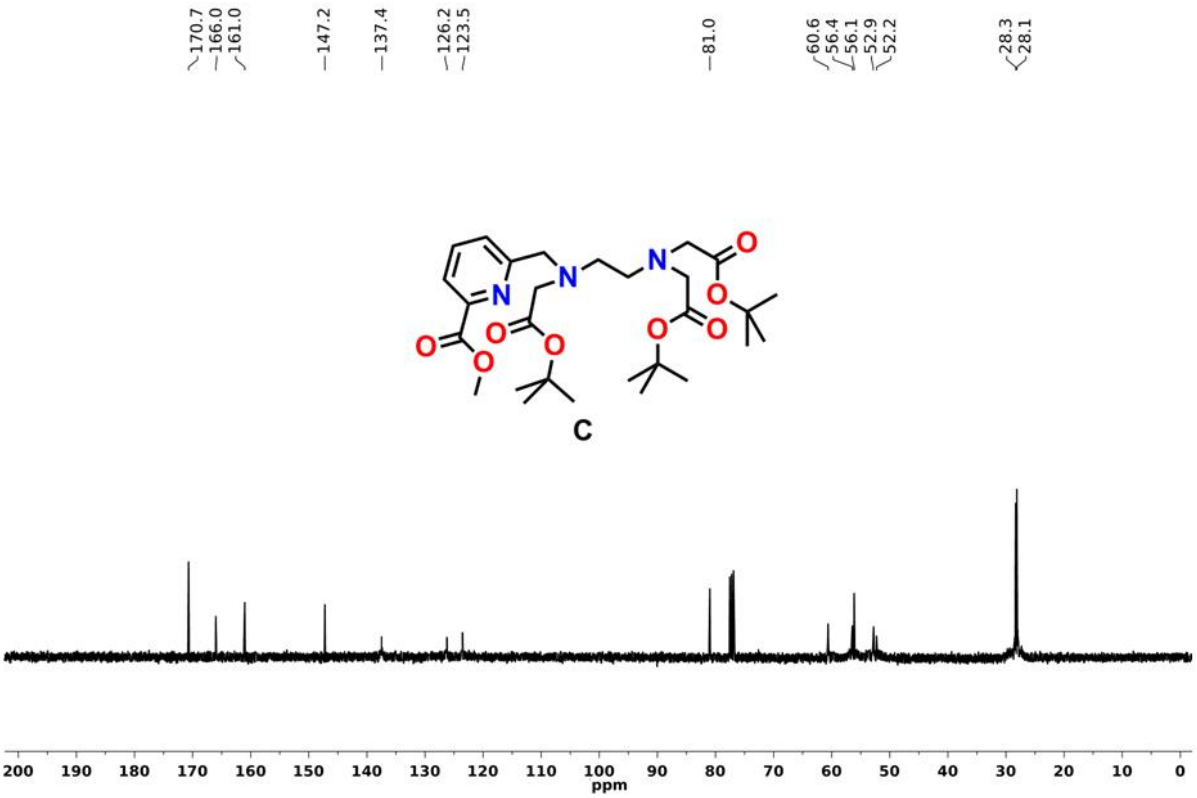

Figure 6.8. ^{13}C NMR spectrum of [$C_{28}H_{45}N_3O_8$], (C).

Synthesis of [$C_{15}H_{19}N_3O_8$], H_4peada: To Compound **C** (0.421g, 0.8 mmol), a solution of CH_2Cl_2/TFA (1:1, 4 mL) was added and stirred the reaction mixture at room temperature (25 °C) for 16 h. The solvent was then evaporated completely *in vacuo* and diethyl ether was added. A white solid was obtained which was again dissolved in 6 M HCl and refluxed for 48 h. The solvent was then completely evaporated to dryness and the ligand H_4peada was obtained as a pale yellow solid by adding excess diethyl ether. The ligand was then filtered, washed thoroughly with diethyl ether (3 × 5 mL) and dried under high vacuum.

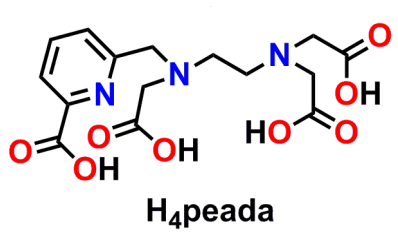

H_4peada

Yield = 0.195 g, 69 %.

FTIR (KBr, cm^{-1}): 3413, 3392, 2976, 2592, 1735, 1627, 1414, 1262, 1199, 764, 658.

^{1}H NMR (CD_3OD, 399.85 MHz): δ 8.39–8.32 (m, 2H), 8.06 (d, J = 4 Hz, 1H), 4.79 (s, 2 H), 4.42 (s, 4H), 4.18 (s, 2H), 4.00–3.97 (m, 2H), 3.82–3.79 (m, 2H) ppm.

^{13}C NMR (CD_3OD, 75.5 MHz): δ 172.6, 170.9, 166.7, 155.5, 148.4, 140.3, 128.8, 126.0, 58.9, 55.7, 55.4, 53.6, 53.1 ppm.

ESI–MS (+) *m/z* for $[C_{15}H_{19}N_3O_8 + H]^+$: Calcd, 370.1244; Found, 370.1258.

6.2.2 Synthesis of Ligand H_4bedik

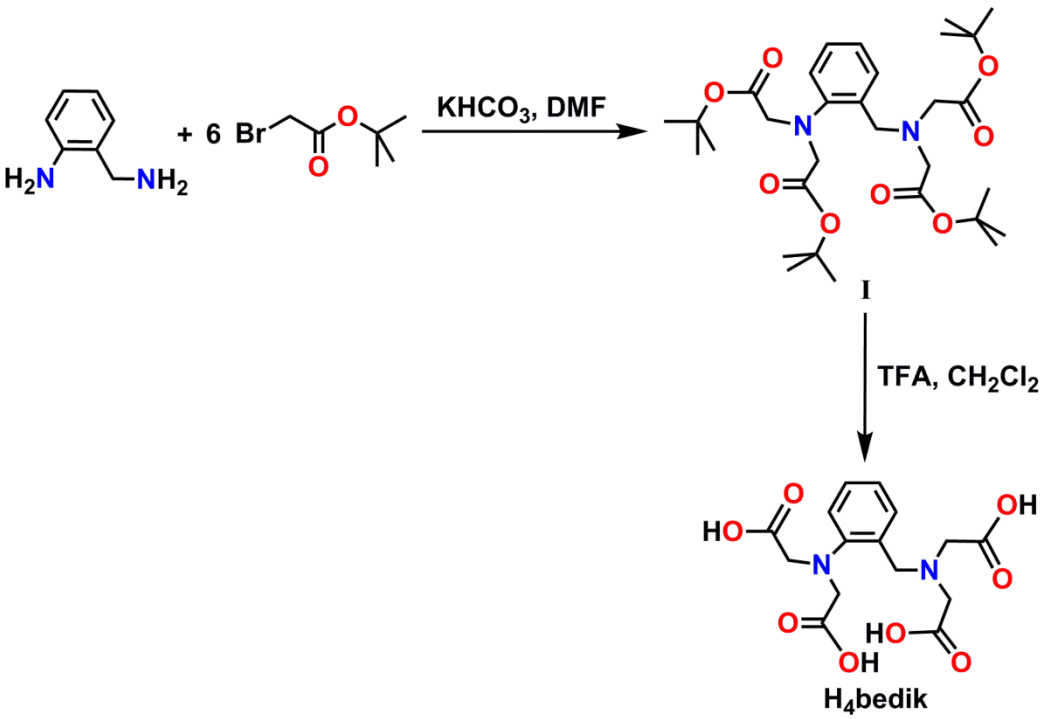

Scheme 6.3. Synthetic route of ligand H_4bedik.

Synthesis of $[C_{31}H_{50}N_2O_8]$, (I): To *tert*–butyl bromoacetate (11.70 g, 60 mmol) in DMF (15 mL), $KHCO_3$ (1.20 g, 120 mmol) was added and the suspension was cooled to 0 ºC. A solution of 2–aminobenzylamine (1.22 g, 10 mmol) in DMF (2 mL) was added dropwise to the stirred solution. The resulting reaction mixture was stirred at 0 ºC for 30 min. After that the stirring was continued further at room temperature (25 °C) for 22 h. A saturated $NaHCO_3$ solution was added to the reaction mixture, and the mixture was extracted with diethyl ether. The organic phase was dried over anhy. Na_2SO_4, filtered and then the solvent was removed completely to get the crude product as brown coloured oil. Trituration of the crude product with hexane afforded the pure compound as white solid.

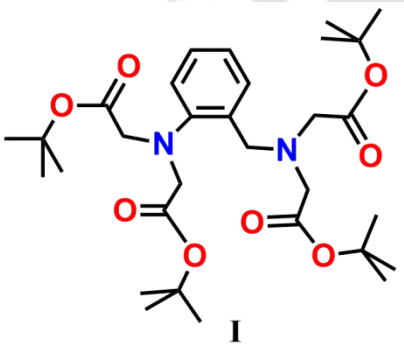

Yield = 2.76 g, 48 %.

FTIR (KBr, cm^{-1}): 3434, 2978, 2933, 2914, 1742, 1642, 1457, 1370, 1247, 1156, 971, 843, 750, 601.

^{1}H NMR ($CDCl_3$, 399.85 MHz): δ 7.81 (d, J = 8 Hz, 1H), 7.45 (d, J = 8 Hz, 1H), 7.39 (t, J = 8 Hz, 1H), 7.21 (t, J = 8 Hz, 1H), 5.16 (s, 2H), 4.87–4.83 (m, 2H), 4.29–4.25 (m, 2H), 3.88 (s, 4H), 1.41 (s, 18H), 1.37 (s, 18H) ppm.

^{13}C NMR ($CDCl_3$, 100.55 MHz): δ 170.9, 164.6, 149.9, 134.3, 131.6, 126.4, 125.4, 84.5, 82.4, 58.3, 56.6, 54.9, 27.9 ppm.

ESI–MS (+) *m/z* for $[C_{31}H_{50}N_2O_8 + H]^+$: Calcd, 579.3639; Found, 579.3734.

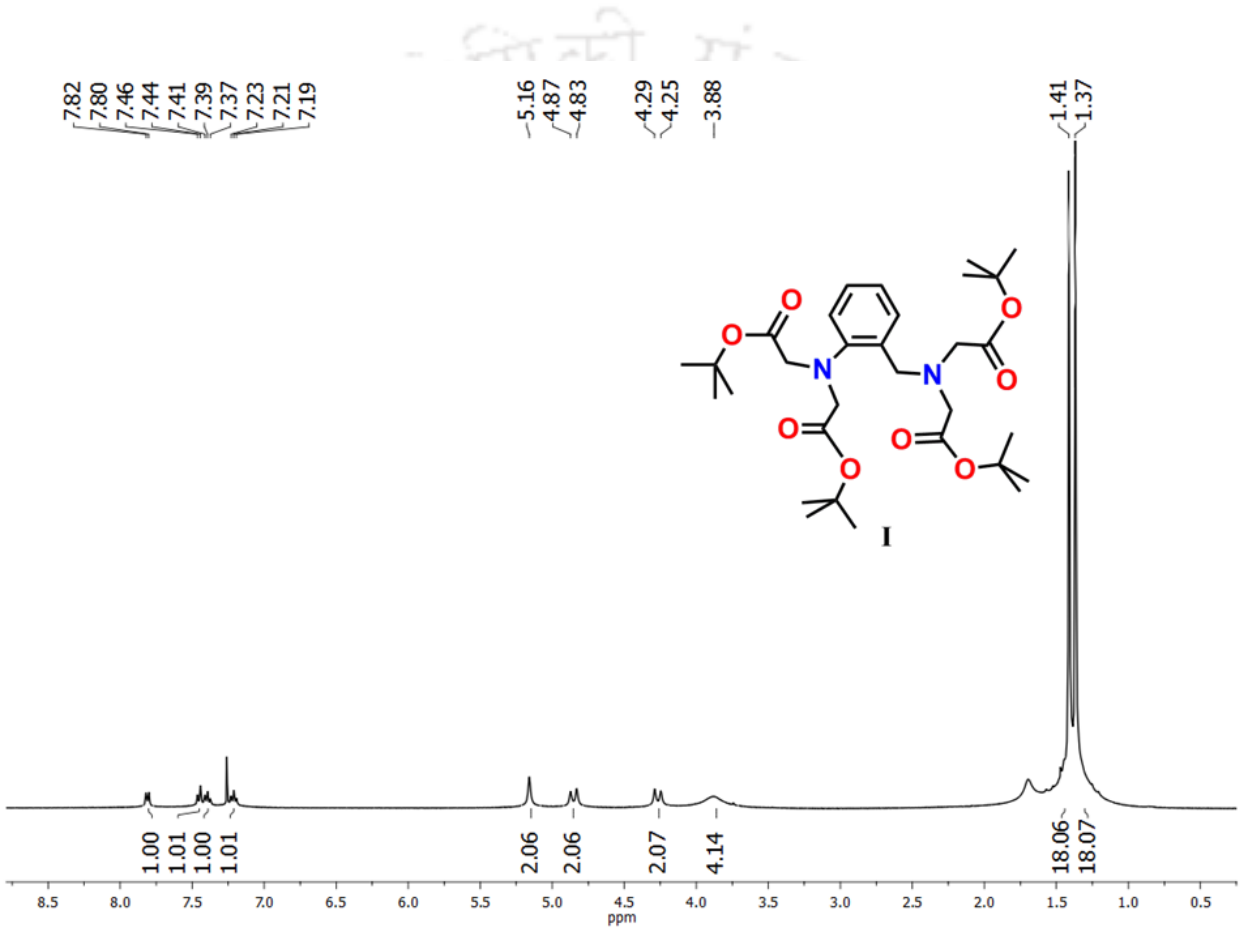

Figure 6.9. ^{1}H NMR spectrum of $[C_{31}H_{50}N_2O_8]$, (I).

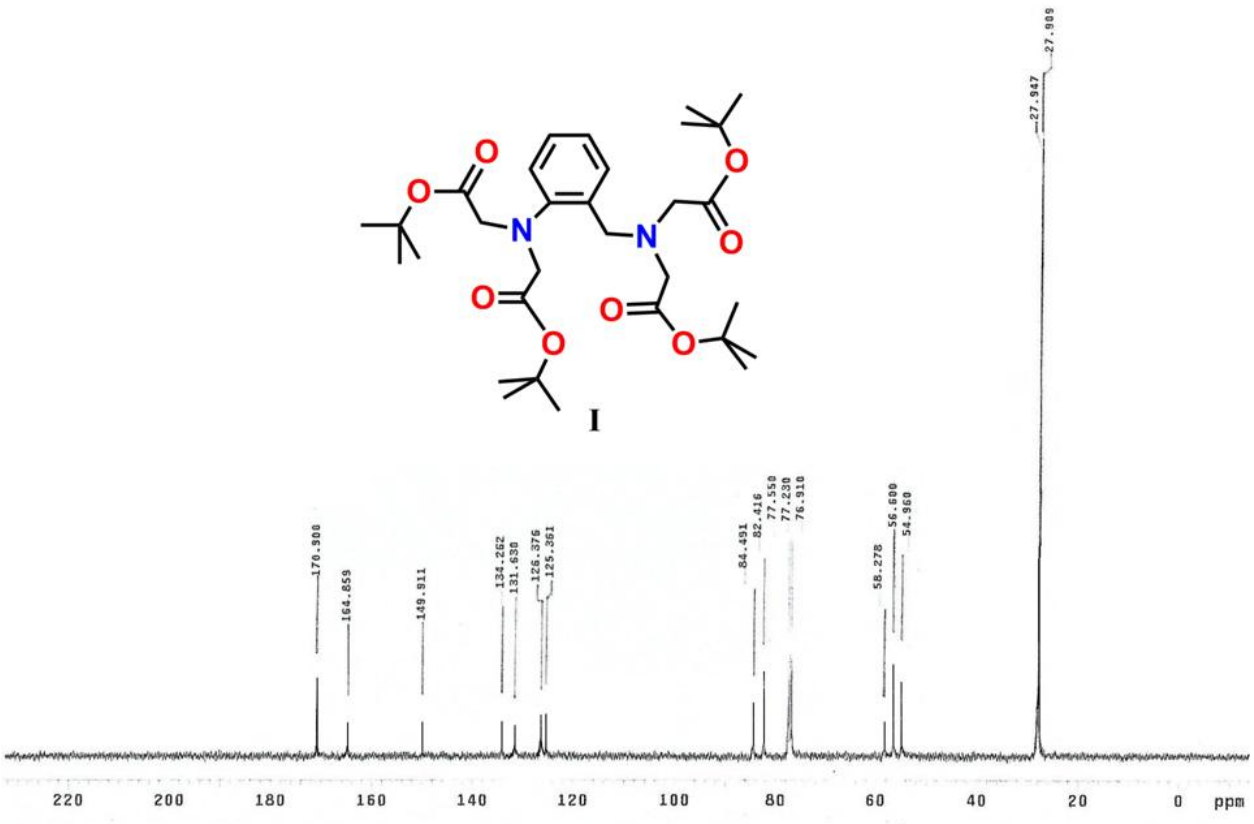

Figure 6.10. ^{13}C NMR spectrum of $[C_{31}H_{50}N_2O_8]$, (I).

Synthesis of $[C_{15}H_{18}N_2O_8]$, H_4bedik: Compound **A** (0.579 g, 1 mmol) in CH_2Cl_2/TFA (1:1, 4 mL) was stirred at room temperature (25 °C) for 16 h. The solvent was then evaporated *in vacuo* and the product was obtained as a white solid by adding excess diethyl ether. The solid was then filtered, washed with diethyl ether (10 mL) and dried under high vacuum.

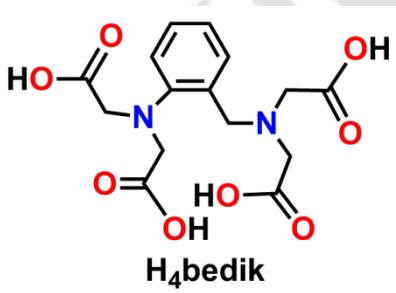

Yield = 0.339 g, 96 %.

FTIR (KBr, cm^{-1}): 3450, 3013, 2964, 2925, 2534, 1726, 1630, 1603, 1496, 1406, 1210, 968, 891, 782, 721, 601.

^1H NMR (CD_3OD, 600.17 MHz): δ 7.57 (d, J = 6 Hz, 1H), 7.47 (t, J = 6 Hz, 1H), 7.35 (d, J = 12 Hz, 1H), 7.25–7.22 (m, 1H), 4.72 (s, 2H), 4.10 (s, 4H), 4.06 (s, 4H) ppm.

^{13}C NMR (CD_3OD, 150.93 MHz): δ 174.5, 169.1, 151.2, 134.1, 132.5, 128.0, 127.2, 125.8, 58.2, 56.4, 55.3 ppm.

ESI–MS (+) *m/z* for $[C_{15}H_{18}N_2O_8 + H]^+$: Calcd, 355.1136; Found, 355.1175.

6.2.3 Synthesis of Ligand H_2pmpa

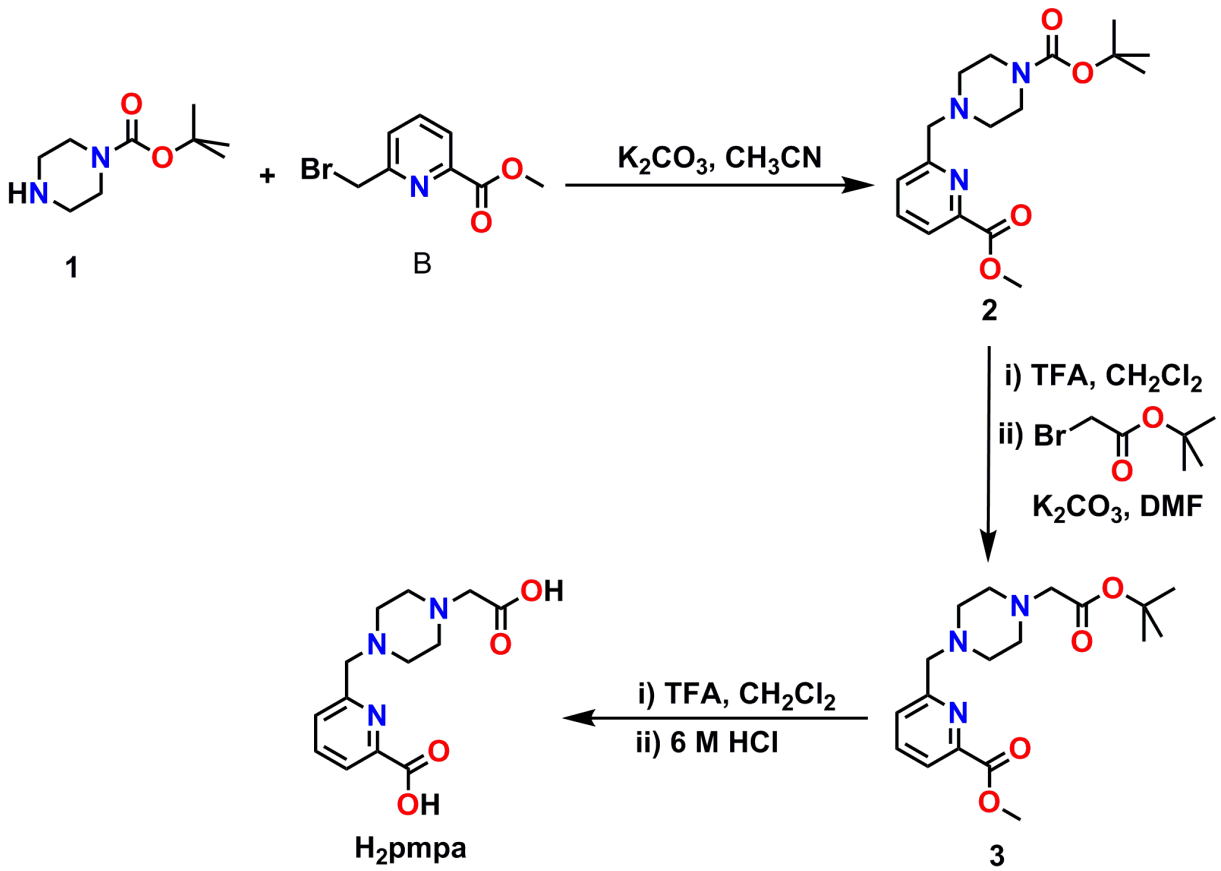

Scheme 6.4. Synthetic route of ligand H_2pmpa.

Synthesis of N–Boc piperazine, $[C_9H_{18}N_2O_2]$, (1): To a stirred solution of piperazine (1.72 g, 20 mmol) in methanol (10 mL), Et_3N (4.2 mL, 30 mmol) was added. Di–*tert*–butyl dicarbonate (1.74 g, 8 mmol) was then added dropwise and stirred the reaction mixture at room temperature (25 °C) for 4 h. Methanol was completely removed and ethyl acetate (20 mL) was added. The insoluble white solid was filtered off and the filtrate was washed with water (3 × 10

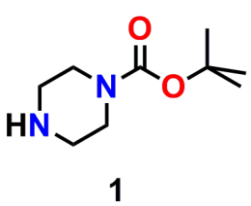
1

mL). The organic layer was dried over anhy. Na_2SO_4, filtered, and concentrated to get the desired product as a white solid.

Yield: 0.912 g, 62 %.

FTIR (KBr, cm^{-1}): 3343, 2977, 2930, 2868, 1692, 1428, 1363, 1246, 1176, 1104, 1007, 869, 767, 558.

^1H NMR ($CDCl_3$, 399.85 MHz): δ 3.38 (s, 4H), 2.80 (s, 2H), 1.75 (s, 2H), 1.45 (s, 9H) ppm.

ESI–MS (+) *m/z* for $[C_9H_{18}N_2O_2 + H]^+$: Calcd, 187.1441; Found, 187.1468.

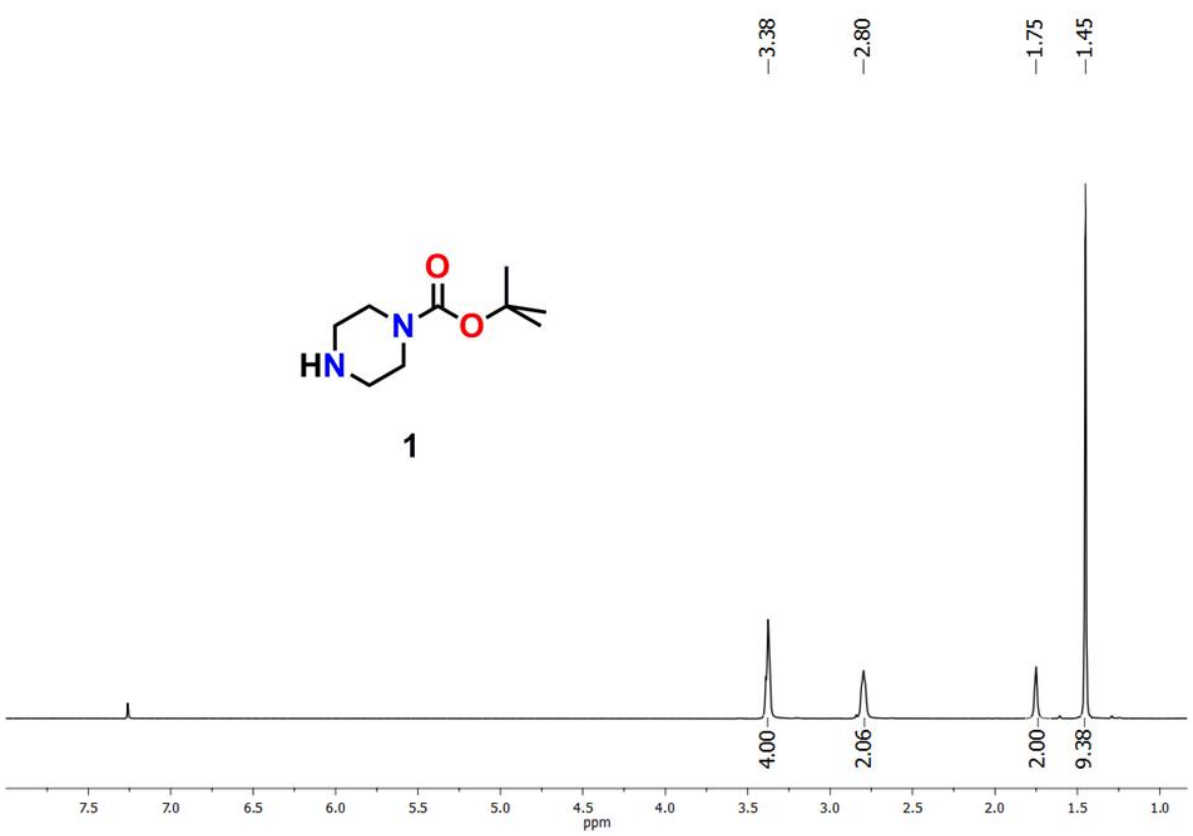

Figure 6.11. ^1H NMR spectrum of $[C_9H_{18}N_2O_2]$, (1).

Synthesis of [$C_{17}H_{25}N_3O_4$], (2): To N–Boc piperazine (0.375 g, 2 mmol) in 5 ml CH_3CN, K_2CO_3 (0.549 g, 4 mmol) was added and stirred the reaction mixture at room temperature for 10 min. A solution of B (0.465 g, 2 mmol) in 2 ml CH_3CN was then added drop wise to the stirred solution and stirring was continued at 50 °C for 48 h. The reaction mixture was then cooled to room temperature and filtered. The white precipitate obtained was washed thoroughly with CH_3CN (10 mL) and the filtrate was then concentrated to dryness to get the crude product as brown oil. The pure compound was obtained by column chromatography on silica gel by using hexane/ethyl acetate (2:3) as eluent.

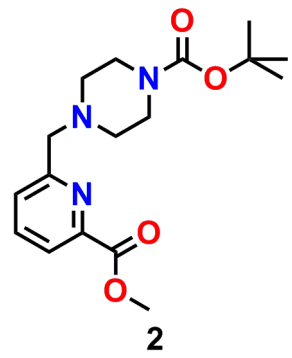

2

Yield: 0.341 g, 51 %.

FTIR (KBr, cm^{-1}): 3448, 2975, 2950, 2860, 2813, 1725, 1695, 1589, 1457, 1423, 1316, 1247, 1170, 1139, 1083, 1006, 866, 762, 678.

^{1}H NMR ($CDCl_3$, 399.85 MHz): δ 7.99(d, J = 8 Hz, 1H), 7.79 (t, J = 8 Hz, 1H), 7.06 (d, J = 8 Hz, 1H), 3.96 (s, 3H), 3.76 (s, 2H), 3.44–3.41 (m, 4H), 2.46–2.43 (m, 4H), 1.42 (s, 9H) ppm.

^{13}C NMR ($CDCl_3$, 100.55 MHz): δ 165.9, 159.4, 154.9, 147.6, 137.6, 126.3, 123.8, 79.8, 64.2, 53.1, 53.0, 29.6 ppm.

ESI–MS (+) *m/z* for $[C_{17}H_{25}N_3O_4 + H]^+$: Calcd, 336.1918; Found, 336.1926.

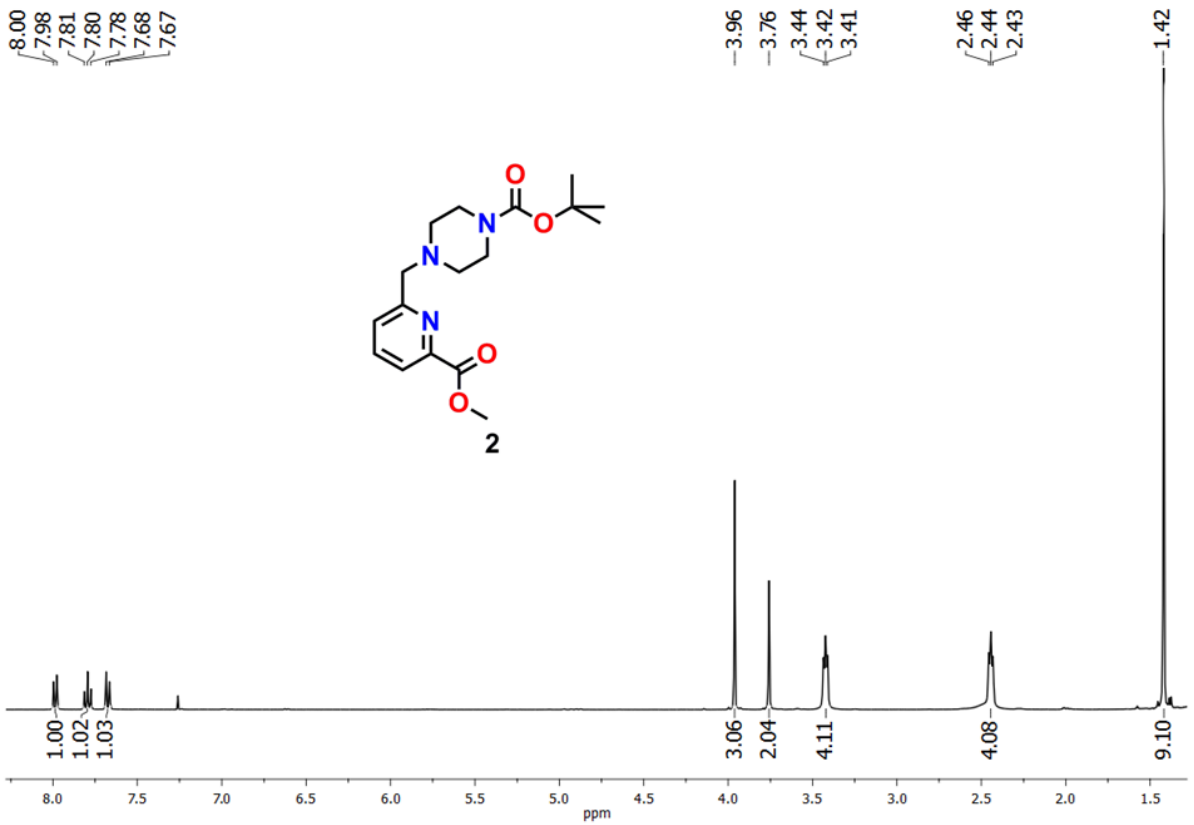

Figure 6.12. ^{1}H NMR spectrum of $[C_{17}H_{25}N_3O_4]$, (2).

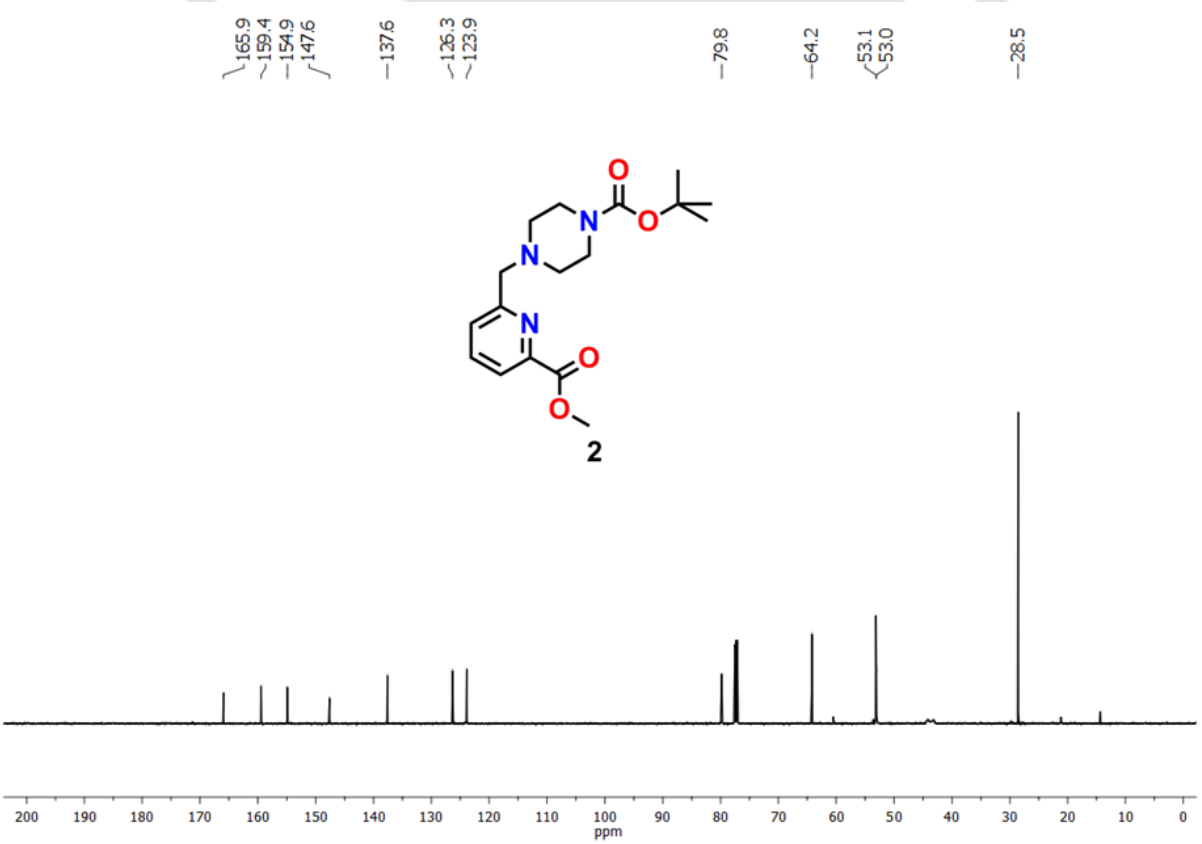

Figure 6.13. ^{13}C NMR spectrum of $[C_{17}H_{25}N_3O_4]$, (2).

Synthesis of [$C_{18}H_{27}N_3O_4$], (3): To Compound **2** (0.341 g, 1.0 mmol), CH_2Cl_2/TFA (1:1, 4 mL) solution was added dropwise and stirred at room temperature (25 °C) for 16 h. The solvent was then evaporated *in vacuo* and a white solid was obtained by adding excess diethyl ether. The white solid was then filtered, washed with diethyl ether (10 mL) and used in the next reaction without further purification. To this compound in 5 mL DMF, K_2CO_3 (0.423 g, 3 mmol) was added followed by dropwise addition of *tert*–butylbromoacetate (0.324 g, 1.7 mmol). The reaction was then stirred at 50 °C for 48 h, cooled the reaction mixture to room temperature and was concentrated to dryness. Water was added and the residue was then extracted by using $CHCl_3$ (3 × 30 mL). The organic phase was dried over anhy. Na_2SO_4, filtered and the solvent was evaporated to give an oily residue that was purified by column chromatography on silica gel by using hexane/ethyl acetate (2:3) as eluent.

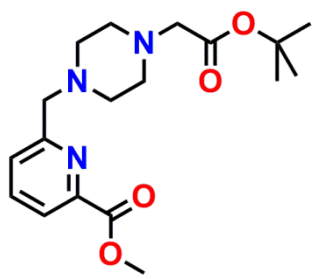

3

Yield: 0.243 g, 68 %.

FTIR (KBr, cm^{-1}): 3436, 2979, 2816, 1742, 1589, 1457, 1369, 1228, 1156, 1015, 839, 765.

^{1}H NMR ($CDCl_3$, 399.85 MHz): δ 7.99(d, J = 8 Hz, 1H), 7.79(t, J = 8 Hz, 1H), 7.68(d, J = 8 Hz, 1H), 3.98(s, 3H), 3.78(s, 2H), 3.11(s, 2H), 2.60(s, 8H), 1.44(s, 9H) ppm.

^{13}C NMR ($CDCl_3$, 100.55 MHz): δ 170.5, 165.0, 159.4, 147.1, 137.1, 126.0, 123.4, 80.6, 63.8, 57.0, 56.1, 52.9, 50.6, 27.9 ppm.

ESI–MS (+) *m/z* for $[C_{18}H_{27}N_3O_4 + H]^+$: Calcd, 350.2074; Found, 350.2079.

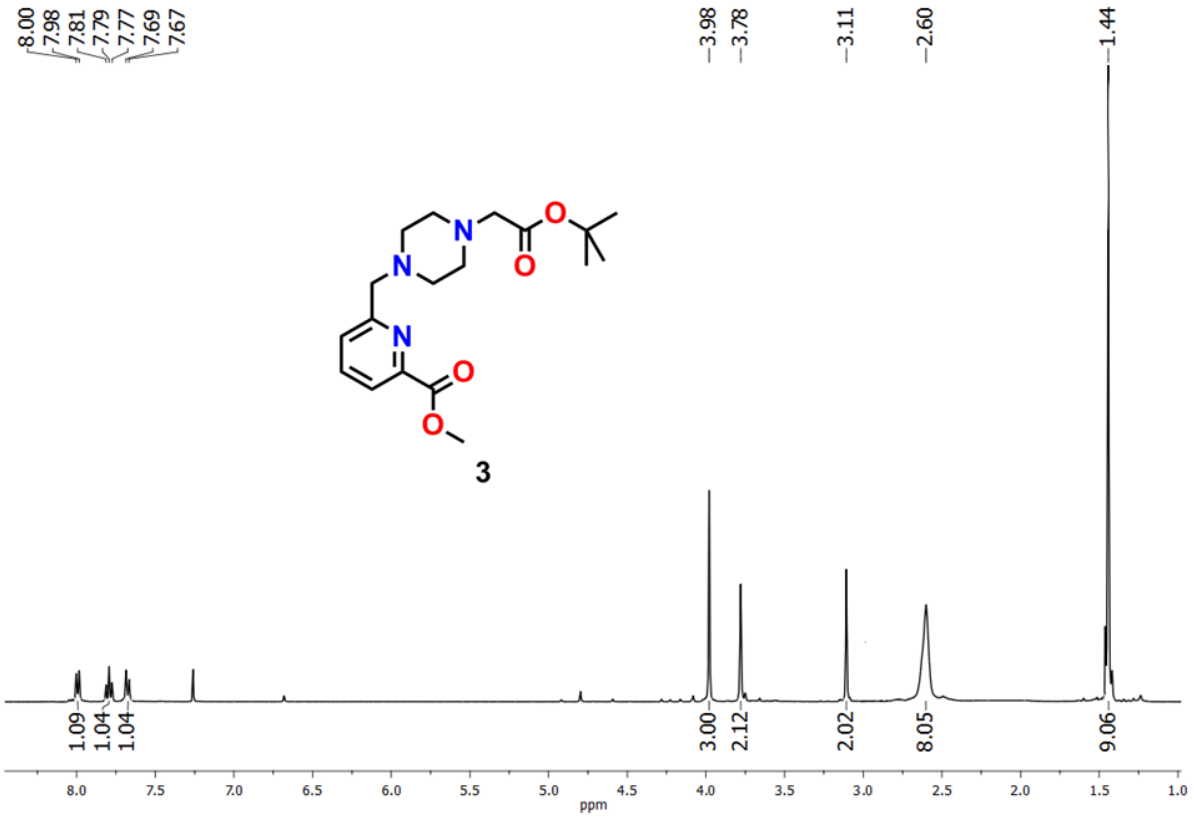

Figure 6.14. ^{1}H NMR spectrum of [$C_{18}H_{27}N_3O_4$], (3).

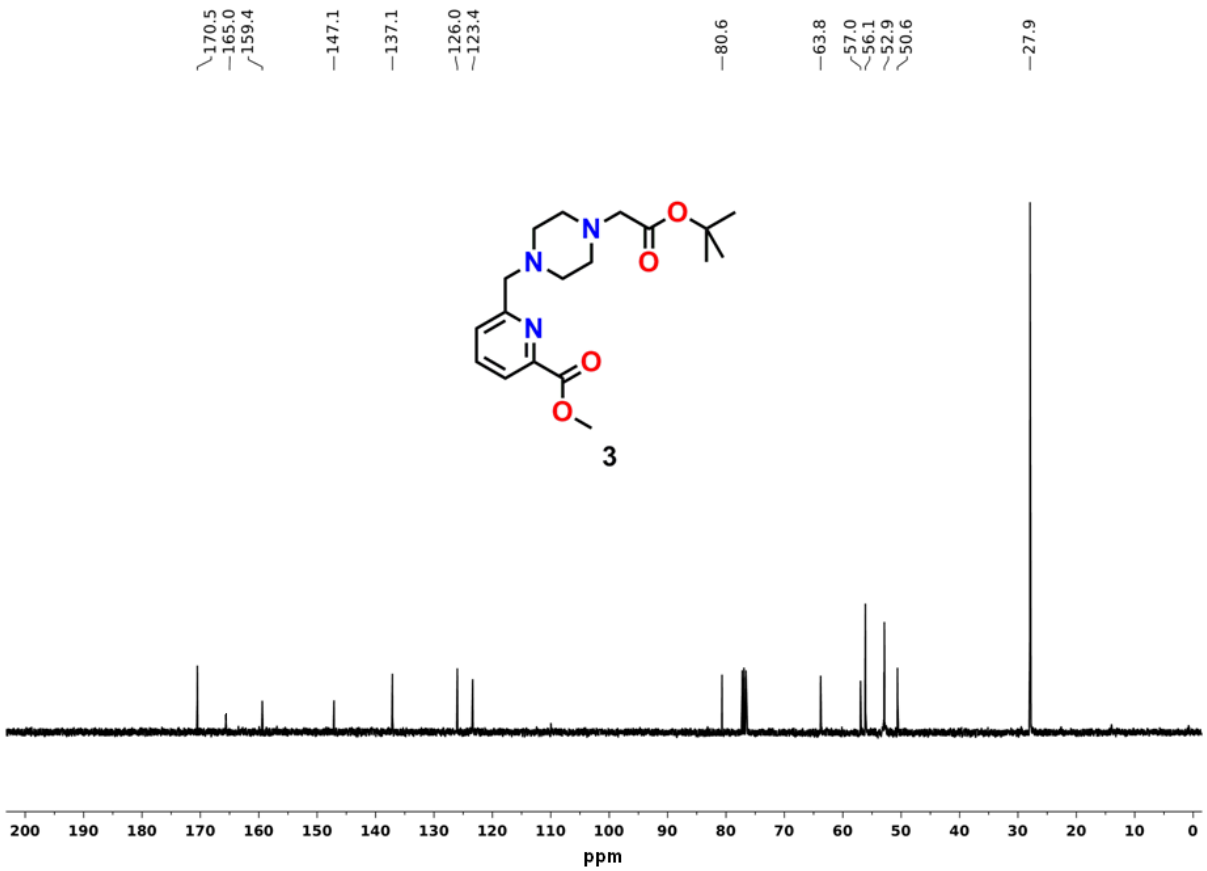

Figure 6.15. ^{13}C NMR spectrum of [$C_{18}H_{27}N_3O_4$], (3).

Synthesis of $[C_{13}H_{17}N_3O_4]$, H_2pmpa: To Compound **3** (0.309 g, 0.9 mmol), a solution of

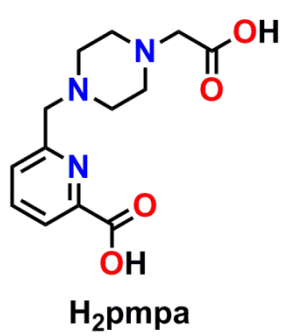

H_2pmpa

CH_2Cl_2/TFA (1:1, 4 mL) was added and stirred the reaction mixture at room temperature (25 °C) for 16 h. The solvent was then evaporated *in vacuo* and diethyl ether was added. A white solid was obtained which was again dissolved in 6 M HCl (4 mL) and refluxed for 24 h. The solvent was then completely evaporated to dryness and the ligand was obtained as a light brown coloured solid by adding excess diethyl ether. The ligand was then filtered, washed thoroughly with diethyl ether (3× 5 mL) and dried under high vacuum.

Yield = 0.184 g, 74 %.

FTIR (KBr, cm^{-1}): 3434, 2976, 2927, 2648, 2601, 2561, 2542, 1724, 1623, 1466, 1443, 1398, 1339, 1263, 1188, 1083, 1003, 967, 894, 853, 733, 715, 638.

^{1}H NMR (CD_3OD, 399.85 MHz): δ 8.25(d, J = 4 Hz, 1H), 8.17(t, J = 4 Hz, 1H), 7.82 (d, J = 8 Hz, 1H), 4.75 (s, 2H), 4.26 (s, 2H), 3.78–3.75 (m, 8H) ppm.

^{13}C NMR (CD_3OD, 100.55 MHz): δ 168.7, 165.3, 151.3, 147.2, 139.2, 127.7, 124.9, 59.2, 55.8, 52.3, 50.1 ppm.

ESI–MS (+) *m/z* for $[C_{13}H_{17}N_3O_4 + H]^+$: Calcd, 280.1292; Found, 280.1333.

6.2.4 Synthesis of Complex 2A

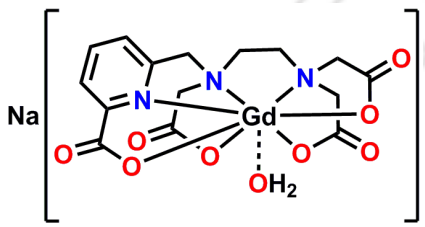

Na[Gd(peada)(H_2O]; **2A**

To a solution of H_4peada (0.112 g, 0.30 mmol) in water (3 mL) was added $GdCl_3$•xH_2O (0.075 g, 0.28 mmol) and stirred until the solution became transparent. The pH of the solution was adjusted to ~ 6.5 by adding aq. NaOH solution dropwise. Stirring was continued at room temperature (25 °C) for 24 h. The resulted clear solution was kept at room temperature for slow evaporation of water. The white solid obtained was washed thoroughly with MeOH.

Yield = 0.093g, 55 %.

FTIR (KBr, cm^{-1}): 3396, 1630, 1433, 1394, 1020, 924, 769, 666, 597.

ESI–MS (–) *m/z* for $[C_{15}H_{15}GdN_3O_8]^-$: Calcd, 523.0057; Found, 523.0028.

6.2.5 Synthesis of Complex 2B

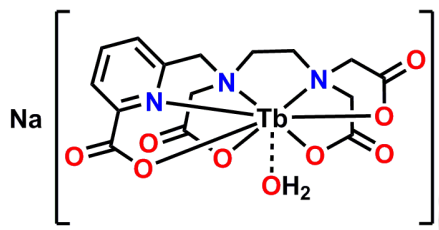

Na[Tb(peada)(H_2O)]; **2B**

To a solution of H_4peada (0.125 g, 0.34 mmol) in water (3 mL) was added $TbCl_3$•$6H_2O$ (0.118 g, 0.32 mmol) and stirred the solution for 5 min. The pH of the solution was adjusted to ~ 6.5 by adding aq. NaOH solution dropwise. The solution was refluxed for 24 hours and the resulted clear solution was kept at room temperature (25 °C) for slow evaporation of water. The white solid obtained was washed thoroughly with MeOH.

Yield = 0.105 g, 57 %.

FTIR (KBr, cm^{-1}): 3427, 1596, 1447, 1395, 1312, 1266, 1090, 990, 811, 717, 644.

ESI–MS (–) *m/z* for $[C_{15}H_{15}TbN_3O_8]^-$: Calcd, 524.0113; Found, 524.0112.

6.2.6 Synthesis of Complex 3A

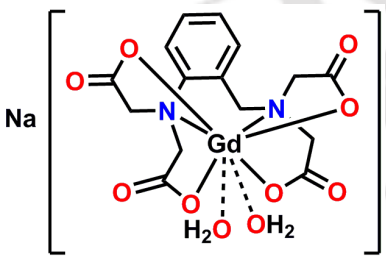

Na[Gd(bedik)(H_2O)$_2$]; **3A**

To a solution of H_4bedik (0.178 g, 0.50 mmol) in water (3 mL) was added $GdCl_3$•xH_2O (0.128 g, 0.48 mmol) and stirred until the solution became transparent. The pH of the solution was adjusted to ~ 6.5 by adding aq. NaOH solution dropwise. Stirring was continued at room temperature (25 °C) for 24 h. The resulted clear solution was kept at room temperature for slow evaporation of water. The white solid obtained was washed thoroughly with MeOH.

Yield = 0.195 g, 69 %.

FTIR (KBr, cm^{-1}): 3434, 2965, 2916, 2844, 1606, 1495, 1413, 1318, 1260, 1180, 1088, 1017, 908, 749, 546.

ESI–MS (–) *m/z* for $[C_{15}H_{14}GdN_2O_8]^-$: Calcd, 507.99; Found, 508.23.

6.2.7 Synthesis of Complex 3B

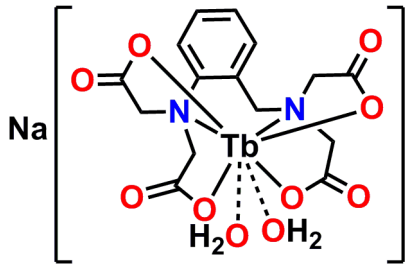

Na[Tb(bedik)(H_2O)$_2$]; **3B**

To a solution of H_4bedik (0.181 g, 0.51 mmol) in water (3 mL) was added $TbCl_3$•$6H_2O$ (0.178 g, 0.48 mmol) and stirred the solution for 5 min. The pH of the solution was adjusted to ~ 6.5 by adding aq. NaOH solution dropwise. The solution was refluxed for 24 h and the resulted clear solution was kept at room temperature (25 °C) for slow evaporation of water. The white solid obtained was washed thoroughly with MeOH.

Yield = 0.173 g, 62 %.

FTIR (KBr, cm^{-1}): 3437, 1622, 1493, 1411, 1317, 1132, 939, 908, 789, 620.

ESI–MS (–) *m/z* for $[C_{15}H_{14}TbN_2O_8]^-$: Calcd, 509.00; Found, 509.09.

6.2.8 Synthesis of Complex 4A

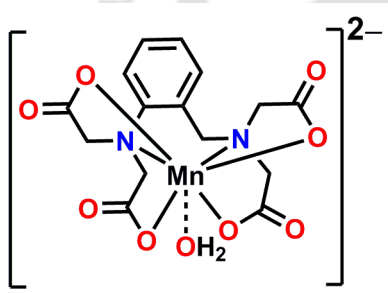

$[Mn(bedik)]^{2-}$; 4A

To a solution of H_4bedik (0.177 g, 0.5 mmol) in water (3 mL) was added $MnCl_2$•$4H_2O$ (0.082 g, 0.48 mmol) and stirred for 10 min. The solution became transparent and then the pH of the solution was adjusted to ~ 6.5 by adding aq. NaOH solution dropwise. Stirring was continued at room temperature (25 °C) for 24 h. The resulted clear solution was kept at room temperature for slow evaporation to obtain crystal. The appeared colourless crystals were then washed thoroughly with MeOH. The obtained crystals were suitable for single crystal X–ray diffraction study.

Yield = 0.098 g, 64 % (or 32% if it is considered that maximum yield would be 50 in percentage scale).

FTIR (KBr, cm^{-1}): 3391, 1591, 1496, 1412, 1316, 1102, 1010, 939, 905, 779, 748, 711, 618.

ESI–MS (–) *m/z* for $[C_{15}H_{14}MnN_2O_8 + H]^-$: Calcd, 406.0209; Found, 406.0095.

Anal. Calcd. for $C_{15}H_{32}Mn_2N_2O_{17}$: C, 28.94; H, 5.18 ; N, 4.50. Found: C, 28.80; H, 4.68; N, 4.38.

6.2.9 Synthesis of Complex 5B

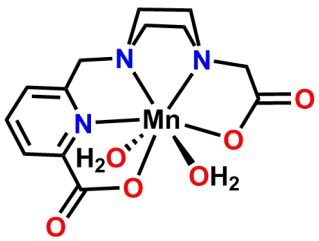

[Mn(pmpa)(H_2O)$_2$]; **5B**

To a solution of H_2pmpa (0.131 g, 0.47 mmol) in water (3 mL) was added $MnCl_2$•$4H_2O$ (0.076 g, 0.44 mmol) and stirred for 10 min. The solution became transparent and then the pH of the solution was adjusted to ~ 6.5 by adding aq. NaOH solution dropwise. Stirring was continued at room temperature (25 °C) for 24 h. The resulted clear solution was then kept at room temperature for slow evaporation. A pale brown coloured solid was obtained after complete evaporation of water which was then washed thoroughly with MeOH.

Yield = 0.073 g, 42 %.

FTIR (KBr, cm^{-1}): 3406, 2961, 2926, 2853, 1595, 1496, 1410, 1316, 1100, 1008, 936, 905, 777, 619.

ESI–MS (+) *m/z* for $[C_{13}H_{15}MnN_3O_4 + H]^+$: Calcd, 333.05; Found, 333.03.

Addendum

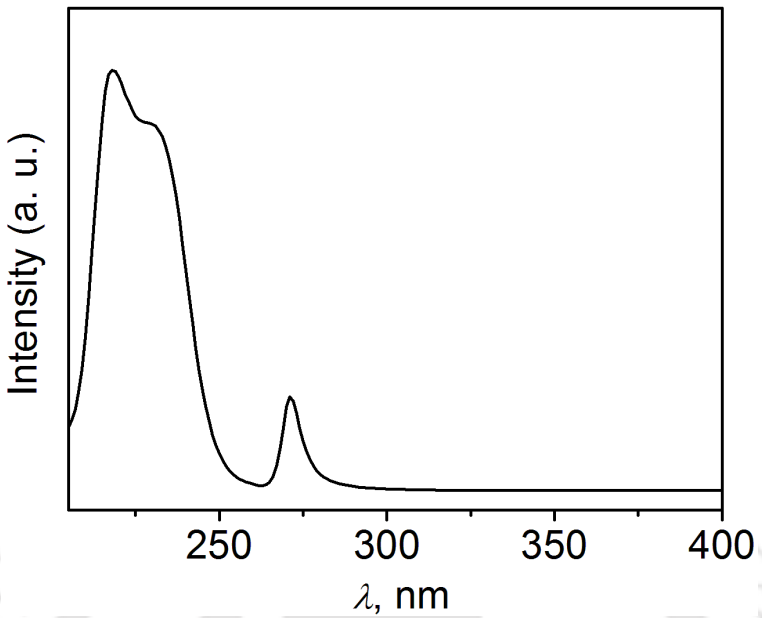

Figure 2.22. Excitation spectrum of complex **2B**.

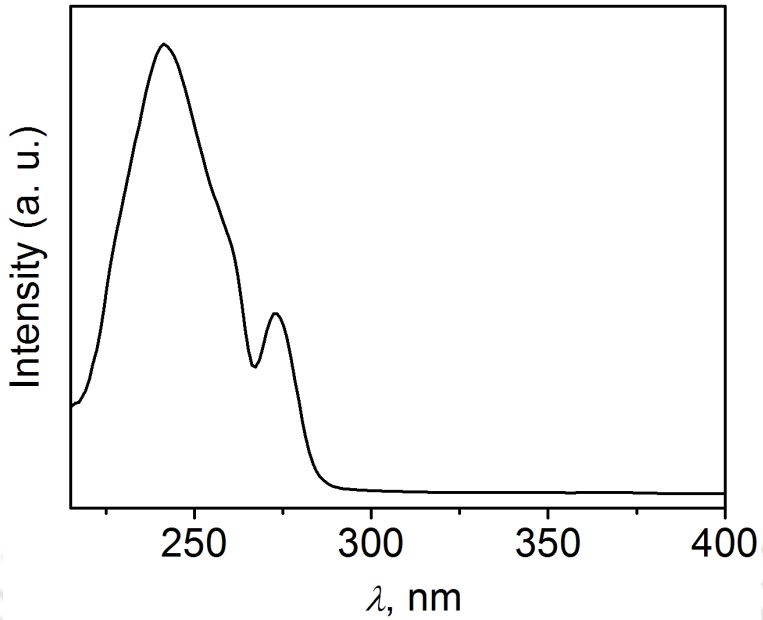

Figure 3.31. Excitation spectrum of complex **3B**.

^{1}H NMRD and ^{17}O NMR measurement of complex 3A

The higher relaxivity of complex **3A** even at very high field can be explained from the presence of two inner sphere water molecules along with its very fast water exchange rate (k_{ex}) of the complex. ^{1}H NMRD and ^{17}O NMR experiments were performed to determine different parameters responsible for high relaxivity value of the complex.

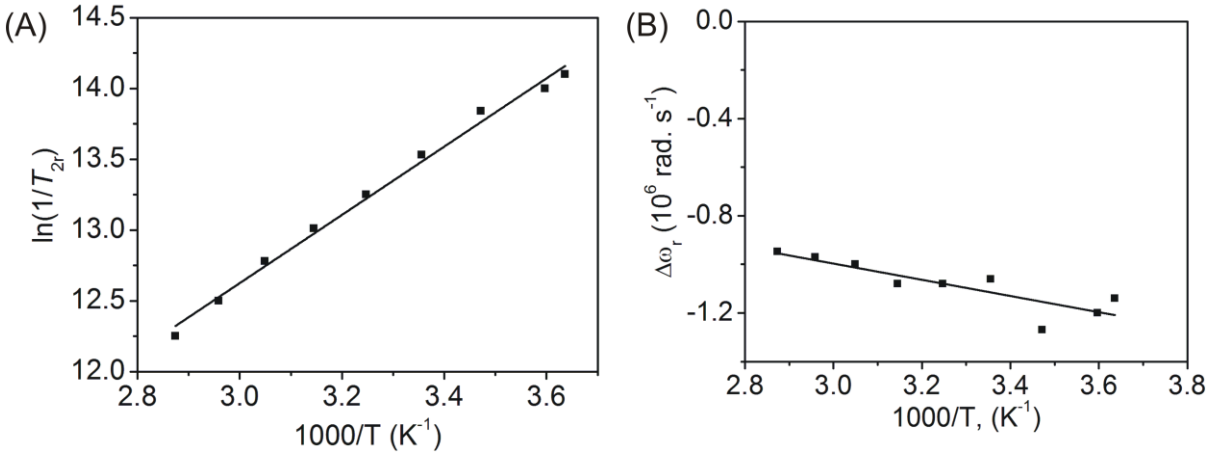

Figure 3.32. (A) Temperature dependence of the reduced ^{17}O transverse relaxation rates of complex **3A**, (B) Temperature dependence of the reduced ^{17}O chemical shifts of complex **3A**.

The transverse ^{17}O relaxation rates ($1/T_2$) and the chemical shifts were measured in aqueous solutions of complex **3A** (12.3 mM, pH = 6.98) in the temperature range 275–348K, on a Bruker Nanobay 400 (9.4 T, 54.3 MHz) spectrometer. The temperature was calculated according to previous calibration with ethylene glycol and methanol.[1] An acidified water solution ($HClO_4$, pH 3.3) was used as external reference. Transverse relaxation times (T_2) were obtained by the Carr-Purcell-Meiboom-Gill spin-echo technique.[2] The technique of the ^{17}O NMR measurements on Gd(III) complexes has been described elsewhere.[3] The samples were sealed in glass spheres fitted into 10 mm NMR tubes to avoid susceptibility corrections of the chemical shifts.[4] To improve the sensitivity, ^{17}O-enriched water (10% $H_2{}^{17}O$, CortectNet) was added to the solutions to reach around 1% enrichment. The least-squares fit of the ^1H NMRD data were performed using Visualiseur/Optimiseur running on a MATLAB 8.3.0 (R2014a) platform.[5] The variable temperature ^{17}O T_2 measurements give access to the water exchange rate, k_{ex}. The ^{17}O chemical shifts give indication of the number of water molecules directly coordinated to Gd(III), q. The results for complex **3A** are presented Figure 3.32. The experimental ^{17}O chemical shifts evidence bishydration of complex **3A**, which is consistent with the previous luminescence lifetime measurements. The reduced ^{17}O transverse relaxation rates decrease with increasing temperature indicating that the complex is in the fast exchange region on the whole temperature range studied.

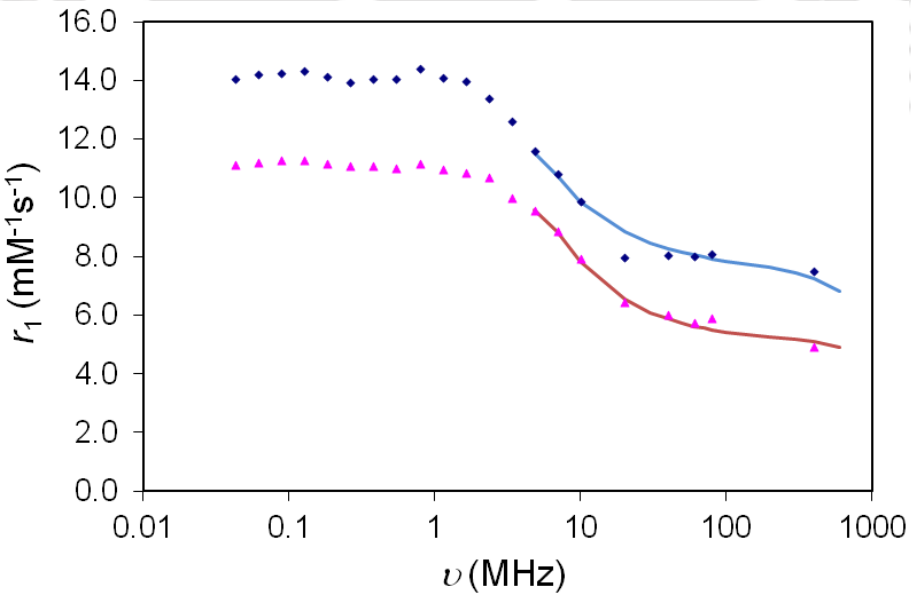

Figure 3.33. NMRD profiles of complex **3A** at 3.97 mM, pH = 6.98, at 25°C (◆) and 37 °C (▲).The lines represent the best fit to the SBM theory.

Proton NMRD profiles ([complex **3A**] = 3.97 mM, pH = 6.98;) were recorded on a Stelar SMARTracer Fast Field Cycling relaxometer (0.01-10 MHz) and a Bruker WP80 NMR electromagnet adapted to variable field measurements (20-80 MHz) and controlled by a SMARTracer PC-NMR console. The temperature was monitored by a VTC91 temperature control unit and maintained by a gas flow. The temperature was determined by previous calibration with a Pt resistance temperature probe. The longitudinal relaxation rates ($1/T_1$) were determined in water. The least-squares fit of the ^{1}H NMRD data were performed using Visualiseur/Optimiseur running on a MATLAB 8.3.0 (R2014a) platform.[5]

The NMRD profiles and ^{17}O NMR measurements were simultaneously analysed with the Solomon-Bloembergen and Morgan (SBM) theory to yield the microscopic parameters characterizing the complex. If we are not interested in detailed information about electron spin relaxation, the SBM approach can be applied to the analysis of the NMRD data at medium and high magnetic fields, and gives reliable information on dynamic processes like water exchange and rotational correlation times for small complexes.[7] Therefore we decided to include only relaxivity values above 4.8 MHz in the fitting. The number of water molecules directly coordinated to Gd(III), *q*, was fixed to 2, and several parameters have been fixed to common values. Among these, r_{GdO} has been fixed to 2.5 Å, based on available crystal structures and ENDOR results,[8] and the quadrupolar coupling constant, $\chi(1+\eta^2/3)^{1/2}$, has been set to the value for pure water, 7.58 MHz.[9] The diffusion coefficient Δ^t was fixed to $2.6.10^{-9}$ $m^2.s^{-1}$, and the corresponding activation energy E_{DGdH} was fitted. The Gd-water proton distance was fixed to r_{GdH} = 3.1Å, and the closest approach between the Gd(III) ion and the outer sphere protons to a_{GdH} = 3.5 Å. The following parameters have been adjusted: The water exchange rate k_{ex}^{298}, and its activation energy, the rotational correlation time, τ_R^{298}, and its activation energy, E_R, and the parameters describing electron spin relaxation, the mean square of the zero field splitting, Δ^2, the correlation time for the modulation of the zero field splitting, τ_V^{298}, while its activation energy, E_V has been fixed to 1 kJ.mol^{-1}. The empirical constant describing the outer-sphere contribution to the ^{17}O chemical shift, C_{OS}, was fitted to 0.25. The parameters resulting from the best fit are presented in Table 2.

Table 2. Parameters obtained from the simultaneous fitting of the NMRD profiles at 298 K and 310 K and ^{17}O NMR data. The number in brackets represent the error on the last digit, and the parameters fixed during the fitting procedure are underlined.

	Complex 3A	**GdHYD[a]**	**GdPy[b]**	**GdDTPA[c]**
q	2	2	2	1
k_{ex}^{298} **($10^6 s^{-1}$)**	116(9)	7.8	9.3	3.3
$\Delta H^{\neq}$ **(kJ.mol^{-1})**	18(1)	43.5	50.4	51.6
τ_R^{298} **(ps)**	96 (1)	93	92[d]	58
E_R **(kJ.mol^{-1})**	27 (3)	21.0	20.2	17.3
E_{DGdH} **(kJ.mol^{-1})**	17(5)	23.2		19.4
A/ħ (10^6rad.s^{-1})	-4.0(1)	-4.0	-3.7	-3.8
τ_V^{298}	65 (9)	2.1	2.8	25
Δ^2 **(10^{20} s^{-2})**	0.28 (2)	0.55	0.96	0.46

a. From ref 6; b. From ref 10; c. From ref 11; d. τ_R^{298}

The rotational correlation time found for complex **3A** was typical of those found for small molecular complexes of this size (τ_{RH}^{298} = 96(1) ps). However, a higher water exchange rate of the complex was found (k_{ex}^{298} = 116(9) × 10^6 s^{-1}), which is even higher for a bis(aquated) Gd(III) complexes. This fast water exchange rate of the complex along with its two inner sphere water molecules is responsible for the high relaxivity of the complex even at high field.

References:

1. D. S. Raiford, C. L. Fisk and E. D. Becker, *Anal. Chem*., 1979, **51**, 2050.
2. S. Meiboom and D. Gill, *Rev. Sci. Instrum*., 1958, **29**, 688..
3. K. Micskei, L. Helm, E. Brucher and A. E. Merbach, *Inorg. Chem*., 1993, **32**, 3844.
4. A. D. Hugi, L. Helm and A. E. Merbach, *Hel. Chim. Acta*., 1985, **68**, 508.
5. (a) F. Yerly, OPTIMISEUR 2.3.5 1999, Lausanne, Switzerland; (b) F. Yerly, VISUALISEUR 2.3.5 1999, Lausanne, Switzerland.
6. C. S. Bonnet, S. Laine, F. Buron, G. Tircso, A. Pallier, L. Helm, F. Suzenet and E. Toth, *Inorg. Chem*., 2015, **54**, 5991.
7. P. H. Fries and E. Belorizky, *J. Chem. Phy*., 2005, **123**, 124510.
8. P. Caravan, J. J. Ellison, T. J. McMurry and R. B. Lauffer, *Chem. Rev*., 1999, **99**, 2293.
9. B. Halle and H. Wennerstrom, *J. Chem. Phys*., 1981, **75**, 1928.
10. C. S. Bonnet, F. Buron, F. Caille, C. M. Shade, B. Drahos, L. Pellegatti, J. Zhang, S. Villette, L. Helm, C. Pichon, F. Suzenet, S. Petoud and E. Toth, *Chem. Eur. J*., 2012, **18**, 1419.
11. D. H. Powell, O. M. NiDhubhghaill, D. Pubanz, L. Helm, Y. S. Lebedev, W. Schlaepfer and A. E. Merbach, *J. Am. Chem. Soc*., 1996, **118**, 9333.

Dalton Transactions

COMMUNICATION

View Article Online
View Journal | View Issue

Cite this: *Dalton Trans.*, 2015, **44**, 12990

Received 12th May 2015,
Accepted 5th June 2015

DOI: 10.1039/c5dt01781e

www.rsc.org/dalton

A water-soluble and water-coordinated Mn(II) complex: synthesis, characterization and phantom MRI image study†‡

Bedika Phukan,[a] Anant B Patel[b] and Chandan Mukherjee*[a]

Ligand H_4bedik was reacted with $MnCl_2{\cdot}4H_2O$ at pH ~ 6.5 to give a highly water-soluble and water-coordinated Mn(II) complex (1). The complex was found to show r_1 = 3.11 mM^{-1} s^{-1} per Mn(II) at 1.4 T and 6.26 mM^{-1} s^{-1} per Mn(II) at 14.1 T at 25 °C, pH = 7.4. In addition to r_1, the r_2 at 14.1 T was found to be 132.78 mM^{-1} s^{-1} per Mn(II) at 25 °C, pH = 7.4.

Magnetic resonance imaging (MRI) is a non-invasive modern clinical technique that is widely used for the high resolution imaging of soft tissues.[1] In the technique, the protons' NMR signal, mainly from water, is measured as an image. The difference in relaxation time (T_1 = longitudinal relaxation time, T_2 = transverse relaxation time) causes a difference in the signal intensity and hence creates contrast in the image. This facilitates the differentiation between normal and pathological tissues.

Nowadays, ~30% of all MRI measurements are accompanied by paramagnetic metal complexes, called contrast agents (CAs), to enhance the image contrast.[1,2] Contrast agents (CAs; M) undergo coordination to nearby water molecules and increase the relaxation rate of bound water protons by several orders of magnitude by shortening the T_1 or T_2 of the bound-water protons. The efficiency of a CA is expressed by its relaxivity (r_1 = longitudinal relaxivity, r_2 = transverse relaxivity), which is defined as the enhancement of relaxation rate per millimolar concentration of the contrast agent; $r_1 = (\Delta 1/T_1)/[M]$, where [M] = the concentration of the CA.[1–3] In this regard, the synthesis of stable and water-soluble, as well as water-coordinated, metal complexes of paramagnetic metal ions with a large number of unpaired electrons such as Fe(III) [$3d^5$, S = 5/2], Mn(II) [$3d^5$, S = 5/2], and Gd(III) [$4f^7$, S = 7/2] has attracted special attention.[1,4] Among these complexes, Gd(III)-based CAs are the most widely studied because Gd(III) acquires seven unpaired electrons, a long electronic relaxation time, and forms stable water-soluble complexes.[5] However, some Gd(III)-based contrast agents are known to cause a disease called nephrogenic systemic fibrosis (NFS) in patients with severe kidney diseases or following liver transplantation.[6] Henceforth, Mn(II) with five unpaired electrons, slow electronic relaxation[1h] and a high water exchange rate on its complexes[1f] is an alternative to Gd(III). In addition, Mn(II) is an essential element in human biological systems and acts as a cofactor in enzymes such as manganese superoxide dismutase, arginase, and glutamine synthetase.[1p,7] Because large doses of Mn(II) ions can also cause neurological disorders in human, called manganism, the synthesis of stable and water-soluble Mn(II) complexes such as T_1-weighted CAs and T_2-weighted CAs have attracted considerable attention.[1f,h,q,8]

A good Mn(II)-based T_1–CA requires coordination of at least a water molecule to the Mn(II). However, stable and water-soluble seven-coordinated Mn(II)-based MRI CAs are very rare, because most of the stable Mn(II) complexes are mainly six-coordinated with no coordinated-water molecule. The employment of 15-membered pentadentate macrocyclic ligands are known to provide water-coordinated six-coordinated or seven-coordinated Mn(II) complexes.[1f,9] However, in these complexes, the water exchange rate is substantially decreased due to H-bonding.[1f,10]

Herein, in order to achieve a water-coordinated seven-coordinated Mn(II) complex, ligand H_4bedik (Scheme 1), which contains a 2-amidobenzylamide backbone, was synthesized. In this ligand, the presence of an sp^3 methylene unit in the backbone creates an asymmetric environment and a difference in the coordination capability of the two backbone-belonging nitrogen atoms. This asymmetric coordination environment favours the water molecule binding to the central Mn(II) metal

[a]*Department of Chemistry, Indian Institute of Technology, Guwahati, 781039, Assam, India. E-mail: cmukherjee@iitg.ernet.in; Fax: (+) 91-361-258-2349; Tel: (+) 91-361-258-2327*

[b]*CSIR–Center for Cellular and Molecular Biology, Uppal Road, Hyderabad, 500007, India*

†Dedicated to Prof. Dr Thorsten Glaser on the occasion of his 45th birthday.

‡Electronic supplementary information (ESI) available: Experimental methods, experimental procedures and characterization data, UV-Vis spectra for the ligand and the complex. ^1H and ^{13}C NMR data for ligand H_4bedik. $1/T_1$ *vs.* [Mn(II)] plot of complex **1**, measured at 1.41 T, 25 °C, and pH = 7.4. Crystallographic and structural refinement parameters. CCDC 1041650. For ESI and crystallographic data in CIF or other electronic format see DOI: 10.1039/c5dt01781e

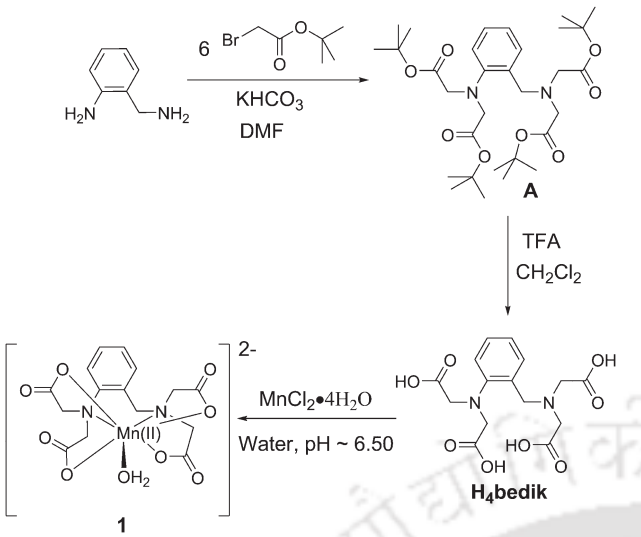

Scheme 1

ion and consequently a seven-coordinated Mn(II) complex can be obtained. In order to impose stability as well as water solubility on the ligand, all the amine H-atoms of the 2-aminobenzylamine backbone are substituted by four acetic acid units.

In this report, we present the synthesis of the ligand H_4bedik and the corresponding water-coordinated seven-coordinated Mn(II) complex. This water soluble complex has been found to show r_1 = 3.11 mM^{-1} s^{-1} per Mn(II) at 1.41 T and 6.26 mM^{-1} s^{-1} per Mn(II) at 14.1 T at 25 °C and pH = 7.4. In addition to r_1, the r_2 at 14.1 T was found to be 132.78 mM^{-1} s^{-1} per Mn(II) at 25 °C and pH = 7.4. This led us to investigate the efficiency of the complex as both a T_1-weighted and T_2-weighted contrast agent.

A schematic of the synthesis of ligand H_4bedik, and the corresponding Mn(II) complex (**1**) is given in Scheme 1. A reaction between a 1 : 6 2-aminobenzylamine and *tert*-butyl-bromoacetate mixture in DMF in the presence of $KHCO_3$ provided **A**, which upon reaction with trifluoroacetic acid provided ligand H_4bedik in a 48% yield. Complex **1** was synthesized in a 64% yield by reacting an equimolar amount of the ligand and $MnCl_2 \cdot 4H_2O$ in water at pH ~ 6.50. An X-ray quality single crystal of complex **1** was obtained by slow evaporation of the reaction mixture.

A single crystal X-ray diffraction measurement for complex **1** was performed at 293 K. The complex crystallized in the triclinic $P\bar{1}$ space group. The molecular structure (only the dinegative unit) is shown in Fig. 1A. Selected bond distances and bond angles are given in Table 1.

In the crystal structure, it was found that a unit cell was comprised of two neutral molecules (Fig. 1B). Each asymmetric unit, *i.e.*, each neutral molecule, was composed of two Mn(II) ion-containing units, which were different in terms of the coordination environment and formal charge. Mn1 was seven-coordinated and was encapsulated by the six-coordinated tetra-negative ligand, $[bedik]^{4-}$, and a neutral water molecule. This

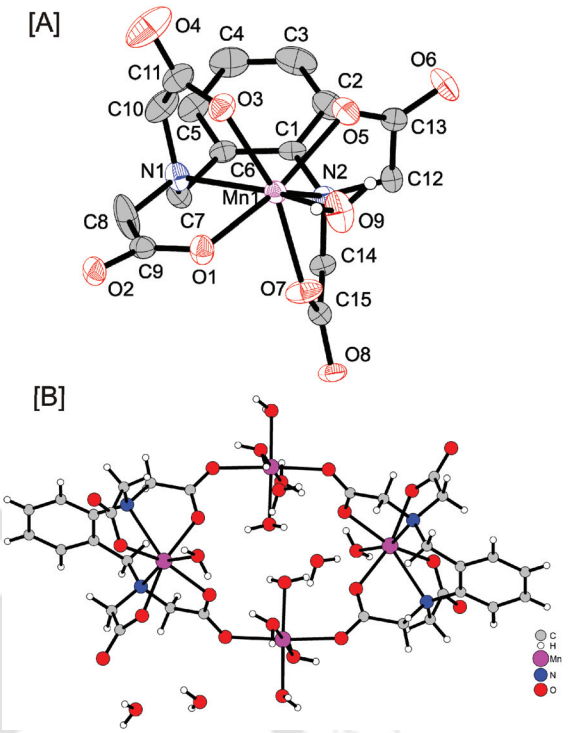

Fig. 1 A: ORTEP representation of **1** (dinegative unit); the ellipsoids are drawn at the 50% probability level, all the hydrogen atoms except those relating to the bound water and solvent molecules have been omitted for clarity. B: A unit cell in the crystal structure.

Table 1 Selected bond distances (Å) and bond angles (°) for complex **1**

Mn1–O1	2.228(2)	O1–Mn1–O3	81.19(10)
Mn1–O5	2.201(2)	O1–Mn1–N1	76.86(9)
Mn1–O3	2.257(3)	O5–Mn1–O1	155.67(10)
Mn1–O9	2.184(2)	O5–Mn1–O3	79.63(10)
Mn1–O7	2.197(3)	O5–Mn1–N1	111.36(10)
Mn1–N1	2.339(3)	O3–Mn1–N1	73.26(10)
Mn1–N2	2.650(3)	O9–Mn1–O1	83.33(9)
O8–C15	1.247(4)	O9–Mn1–O5	83.45(10)
O1–C9	1.257(4)	O9–Mn1–O3	94.68(10)
O4–C11	1.250(5)	O9–Mn1–O7	84.92(11)
O2–C9	1.265(4)	O9–Mn1–N1	158.08(10)
O6–C13	1.246(4)	O7–Mn1–O1	81.66(10)
O5–C13	1.260(4)	O7–Mn1–O5	117.33(10)
O3–C11	1.253(4)	O7–Mn1–O3	62.78(9)
O7–C15	1.258(4)	O7–Mn1–N1	101.19(11)

unit was formally dinegative. The other Mn(II) centre, Mn2, was octahedrally coordinated by four water molecules and two neutral keto oxygen atoms (O2, and O8) from two dinegative units; hence, the overall dipositive formal charge prevailed in this unit.

In the dinegatively charged unit, the Mn1–O1 = 2.228(2), Mn2–O3 = 2.257(3), Mn–O5 = 2.201(2), Mn–O7 = 2.197(2), Mn1–N1 = 2.339(3), and Mn1–N2 = 2.650(3) Å bond distances indicated that the geometry around the Mn1 centre was asymmetric, and the asymmetric environment was mainly caused

by Mn–N coordination linkages. The presence of the sp^3 methylene unit (C7) between C6 and N1 promoted more flexibility in the C6–C7–N1 arm than that of the C1–N2 arm. Hence, N1 experienced a closer exposure to Mn1 than that of N2. The coordinated water molecule was tightly bound with the Mn(II) centre with a Mn–O bond distance of 2.184(2) Å.

A spectrophotometric titration method was used to determine the conditional stability constant, pM,[11] of the ligand with metal Mn. pM is defined as pM = $-\log[M^{n+}]_{free}$, *i.e.*, –log of the concentration of free metal ion, typically at the condition when the metal ion concentration [M] = 1 μM and the ligand concentration [L] = 10 μM at pH = 7.4 at 25 °C. A competitive batch titration was performed with EDTA as the competing ligand to determine the pMn value of the ligand at 25 °C. In this method, different volumes of EDTA stock solutions were added to solutions of constant concentrations of the ligand H_4bedik and Mn(II). The pH was kept constant at 7.4 using HEPES buffer. The concentrations of the free and the complexed ligand in each solution were determined from the corresponding absorption spectra (Fig. 1 and 2, S4–S5‡). From the slope of the plot log([MnEDTA]/[Mnbedik]) *versus* log([EDTA]/[H_4bedik]), the difference in pMn between the ligand and EDTA was obtained (Fig. 2). This difference was the value of log([EDTA]/[H_4bedik]) when log([MnEDTA]/[Mnbedik]) = 0 or when the concentration of EDTA generated an equal partition of Mn(II) between the ligand and EDTA. Using the value 11.42 for the pMn of EDTA, the pMn of the ligand was found to be 10.16.

The longitudinal relaxation time (T_1) of the water proton with and without complex **1** were measured using inversion recovery and saturation recovery methods in BRUKER 1.41 T and 14.1 T NMR machines at 25 °C with pH = 7.4. T_1 was measured at four different concentrations, and the slope of the plot of the longitudinal relaxation rate ($R_1 = 1/T_1$) *versus* [Mn(II)] provided the longitudinal relaxivity, r_1 (Fig. 5, S6‡). It was observed that with the increase in the concentration of complex **1**, R_1 increased linearly (Fig. 5, S6‡). The r_1 value of complex **1** was found to be 3.11 mM^{-1} s^{-1} per Mn(II) at 1.41 T, which is significantly higher than that of the commercially available Mn(II)-based MRI contrast agent, Teslascan® (r_1 = 2.10 mM^{-1} s^{-1}, at 1.5 T).[8e]

Imaging at high-fields is essential to reduce the image acquisition-time and to achieve a higher signal-to-noise ratio.

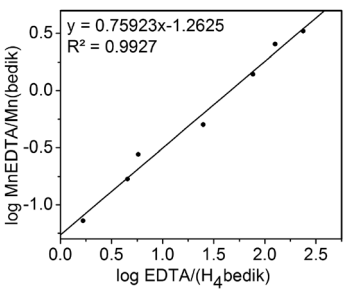

Fig. 2 A competitive titration of the ligand against EDTA.

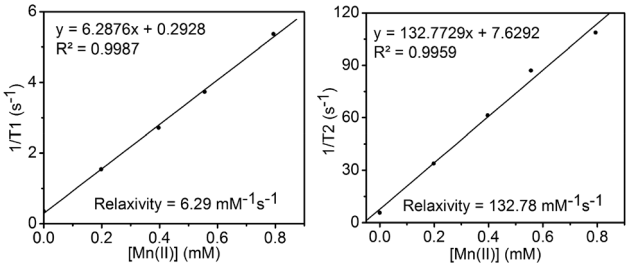

Fig. 3 Left: $1/T_1$ *vs.* [Mn(II)]; right: $1/T_2$ *vs.* [Mn(II)] plot. The measurements were performed using complex **1** at 14.1 T, 25 °C, and pH = 7.4.

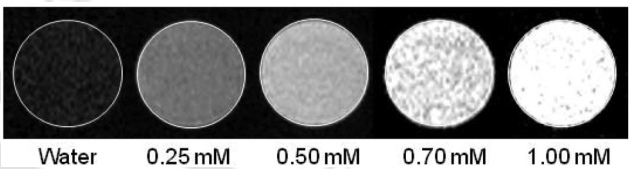

Fig. 4 T_1-weighted MR images of a micro-centrifuge tube (phantom images) containing the complex in water at concentrations of 0, 0.25, 0.50, 0.70, and 1.00 mM.

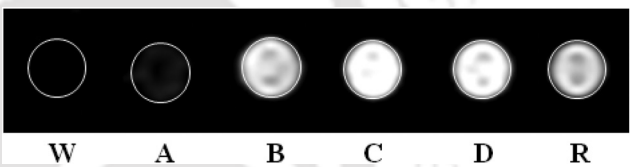

Fig. 5 Phantom T_1-weighted MR images of complex **1** measured at different concentrations (W = Water only, A = 0.25 mM, B = 0.50 mM, C = 0.70 mM, D = 1.00 mM, R = Reference = MultiHance®, 0.5 M) in water at 1.5 T, 25 °C, and pH = 7.4.

In this regard, relaxivity measurements were performed at a high field (14.1 T). It is noteworthy that a higher r_1 = 6.29 mM^{-1} s^{-1} per Mn(II) was found at 14.1 T (Fig. 3). This indicated that r_1 was field dependent and unconventionally increases with increase in the field strength. The multimeric nature of CA and the intermediate correlation time (0.5–4 ns) have been suggested as being responsible for such behaviour.[12] However, special attention will be given to this in the near future for this system.

Transverse relaxation rate measurements at four different concentrations of complex **1** at 14.1 T and thereafter transverse relaxivity (r_2) calculations provided r_2 = 132.78 mM^{-1} s^{-1} at 25 °C with pH = 7.4 (Fig. 3). This indicated that the complex, in addition to the T_1 contrast property, also possesses an excellent T_2 contrast property. Therefore, using the complex, both T_1-weighted and T_2-weighted images of the phantom images were examined.

T_1-weighted phantom MR images of an aqueous solution of complex **1** were measured at 14.1 and 1.5 T by maintaining the concentrations of 0.25, 0.50, 0.70, and 1.00 mM (Fig. 4 and 5).

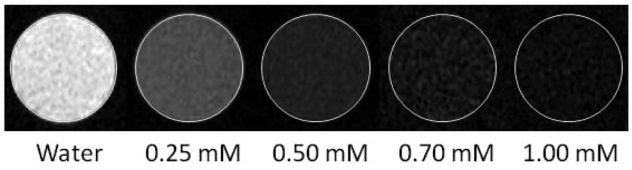

Fig. 6 T_2-weighted MR images of a micro centrifuge tube (phantom images) containing the complex in water with concentrations of 0, 0.25, 0.50, 0.70, 1.00 mM at 14.1 T, 25 °C, and pH = 7.4.

It was found that with the increase in concentration, the MR image intensity of the corresponding image also increases. A comparative MR image intensity with respect to commercially available MultiHance® was performed at 1.5 T using a clinical imager. It should be noted that the T_1-weighted MR image intensity with 0.5 mM of complex **1** [Fig. 5(B)] was similar to that of 0.5 M MultiHance® [Fig. 5(R)].

It was observed that with the increase in concentration of the complex from 0.25 mM to 1.00 mM, the T_2-weighted MR image signal intensity decreases gradually and becomes almost nil at 1.00 mM concentration (Fig. 6). These phenomena bolster the candidature of the complex as a T_2–CA.

To conclude, a hexadentate asymmetric water soluble ligand H_4bedik was synthesized. The ligand reacted with $MnCl_2{\cdot}4H_2O$ at pH ~ 6.50 and provided complex **1**, which showed comparable stability to the Mn(II)–EDTA complex. The complex exhibited high longitudinal relaxivity = 3.11 mM^{-1} s^{-1} at 1.41 T and 6.29 mM^{-1} s^{-1} at 14.1 T per Mn(II), as well as a high transverse relaxivity of 132.78 mM^{-1} s^{-1} per Mn(II) at 14.1 T at 25 °C and at physiological pH = 7.4. These data indicate that the complex can be employed as a contrast agent for a dual-mode (T_1 = brightening and T_2 = darkening) MRI measurement. Hence, the complex opens up an alternative of using nanomaterials[13] for dual-mode imaging. Phantom MR images employing the complex measured at 1.5 T consolidated its potential use as an MRI contrast agent. Field-dependent studies and *in vivo* imaging will be performed in the near future. Ligand H_4bedik will also be further employed for the synthesis of the corresponding Gd(III) complex.

This project is funded by DST (SR/FT/CS-86/2011), Govt. of India. BP thanks IIT Guwahati for doctoral fellowship. CM is indebted to Dr Baijayanta Saharia, Director, Department of Radiology and Imaging, GNRC Hospital, Guwahati, India for MRI image measurements at 1.5 T. Relaxivity measurements were performed on the Bruker minispec mq60 NMR Analyzer, Chemical Biology Laboratory, Tata Institute of Fundamental Research. BP acknowledges Mr. Samsuzzoha Mondal, for his help in relaxivity measurements. CM is thankful to Dr Ankona Datta, TIFR, Mumbai, India, for her immense support.

Notes and references

1 (*a*) P. Caravan, J. J. Ellison, T. J. McMurry and R. B. Lauffer, *Chem. Rev.*, 1999, **99**, 2293; (*b*) R. B. Lauffer, *Chem. Rev.*, 1987, **87**, 901; (*c*) P. Caravan, *Chem. Soc. Rev.*, 2006, **35**, 512; (*d*) P. Hermann, J. Kotek, V. Kubíček and I. Lukeš, *Dalton Trans.*, 2008, 3027; (*e*) S. Laus, R. Ruloff, E. Tóth and A. E. Merbach, *Chem. – Eur. J.*, 2003, **9**, 3555; (*f*) B. Drahoš, I. Lukeš and E. Tóth, *Eur. J. Inorg. Chem.*, 2012, 1975; (*g*) K. N. Raymond and V. C. Pierre, *Bioconjugate Chem.*, 2005, **16**, 3; (*h*) J. S. Troughton, M. T. Greenfield, J. M. Greenwood, S. Dumas, A. J. Wiethoff, J. Wang, M. Spiller, T. J. McCurry and P. Caravan, *Inorg. Chem.*, 2004, **43**, 6313; (*i*) S. M. Rocklage, W. P. Cacheris, S. C. Quay, F. E. Hahn and K. N. Raymond, *Inorg. Chem.*, 1989, **28**, 477; (*j*) S. Wang and T. D. Westmoreland, *Inorg. Chem.*, 2009, **48**, 719; (*k*) P. Caravan, *Acc. Chem. Res.*, 2009, **42**, 851; (*l*) J. Oakes and E. G. Smith, *J. Chem. Soc., Faraday Trans. 2*, 1981, **77**, 299; (*m*) D. J. Mastarone, V. S. R. Harrison, A. L. Eckermann, G. Parigi and T. J. Meade, *J. Am. Chem. Soc.*, 2011, **133**, 5329; (*n*) E. Terreno, D. D. Castelli, A. Viale and S. Aime, *Chem. Rev.*, 2010, **110**, 3019; (*o*) E. Boros, M. Polasek, Z. Zhang and P. Caravan, *J. Am. Chem. Soc.*, 2012, **134**, 19858; (*p*) D. W. Christianson, *Prog. Biophys. Mol. Biol.*, 1997, **67**, 217; (*q*) M. G. Cersosimo and W. C. Koller, *NeuroToxicology*, 2006, **27**, 340.

2 (*a*) J. M. Major and T. J. Meade, *Acc. Chem. Res.*, 2009, **42**, 893; (*b*) E. J. Werner, A. Datta, C. J. Jocher and K. N. Raymond, *Angew. Chem., Int. Ed.*, 2008, **47**, 8568; (*c*) E. L. Que and C. J. Chang, *Chem. Soc. Rev.*, 2010, **39**, 51.

3 A. J. L. Villaraja, A. Bumb and M. W. Brechbiel, *Chem. Rev.*, 2010, **110**, 2921.

4 (*a*) A. Datta and K. N. Raymond, *Acc. Chem. Res.*, 2009, **42**, 938; (*b*) S. Aime, M. Botta, M. Fasano and E. Terreno, *Chem. Soc. Rev.*, 1998, **27**, 19.

5 (*a*) M. T. Vlaardingerbroek and J. A. den Boer, *Magnetic Resonance Imaging. Theory and Practice*, Springer Verlag, Germany, 1996; (*b*) L. Banci, I. Bertini and C. Luchinat, *Nuclear and Electron relaxation*, VCH, Weinheim, 1991.

6 (*a*) P. Marckmann, L. Skov, K. Rossen, A. Dupont, M. Damholt, J. Heaf and H. Thomsen, *J. Am. Soc. Nephrol.*, 2006, **17**, 2359; (*b*) C. Thakral, J. Alhariri and J. Abraham, *Contrast Media Mol. Imaging 2*, 2007, 199; (*c*) M. Sieber, P. Lengsfeld, J. Walter, H. Schirmer, T. Frenzel, F. Siegmund, H. Weinmann and H. Pietsch, *J. Magn. Reson. Imaging*, 2008, **27**, 955.

7 S. Mukhopadhyay, S. K. Mandal, S. Bhaduri and W. H. Armstrong, *Chem. Rev.*, 2004, **104**, 3981.

8 For some examples: (*a*) S. Aime, P. L. Anelli, M. Botta, M. Brocchetta, S. Canton, F. Fedeli, E. Gianolio and E. Terreno, *J. Biol. Inorg. Chem.*, 2002, **7**, 58; (*b*) Q. Zhang, J. D. Gorden, R. J. Beyers and C. R. Goldsmith, *Inorg. Chem.*, 2011, **50**, 9365; (*c*) H. Su, C. Wu, J. Zhu, T. Miao, D. Wang, C. Xia, X. Zhao, Q. Gong, B. Song and H. Ai, *Dalton Trans.*, 2012, **41**, 14480; (*d*) E. Molnár, N. Camus, V. Patinec, G. A. Rolla, M. Botta, G. Tircsó, F. K. Kálmán, T. Fodor, R. Tripier and C. P. Iglesias, *Inorg. Chem.*, 2014, **53**, 5136; (*e*) E. Wiener, K. Woertler, G. Weirich, E. J. Rummeny and M. Settles, *Eur. J. Radiol.*, 2007, **63**, 110; (*f*) B. Sana, C. L. Poh and S. Lim, *Chem. Commun.*, 2012,

48, 862; (*g*) A. Bertin, J. Steibel, A. I. Michou-Gallani, J. L. Gallani and D. Felder-Flesch, *Bioconjugate Chem.*, 2009, **20**, 760; (*h*) K. H. Chuang, A. P. Koretsky and C. H. Sotak, *Magn. Reson. Med.*, 2009, **61**, 1528.

9 (*a*) S. Wang and T. Westmoreland, *Inorg. Chem.*, 2009, **48**, 719; (*b*) A. Bertin, J. Steibel, A. Michou–Gallani, J. Gallani and D. Felder–Flesch, *Bioconjugate Chem.*, 2009, **20**, 760; (*c*) A. Bianchi, L. Calabi, C. Giorgi, P. Losi, P. Mariani, D. Palano, P. Paoli, P. Rossi and B. Valtancoli, *J. Chem. Soc., Dalton Trans.*, 2001, 917; (*d*) S. Aime, P. Anelli, M. Botta, M. Brocchetta, S. Canton, F. Fedeli, E. Gianolio and E. Terreno, *J. Biol. Inorg. Chem.*, 2002, **7**, 58.

10 (*a*) B. K. Wagnont and S. C. Jackels, *Inorg. Chem.*, 1989, **28**, 1923; (*b*) B. Drahoš, J. Kotek, P. Hermann, I. Lukeš and E. Tóth, *Inorg. Chem.*, 2010, **49**, 3224.

11 (*a*) C. J. Jocher, E. G. Moore, J. Xu, S. Avedano, M. Botta, S. Aime and K. N. Raymond, *Inorg. Chem.*, 2007, **46**, 9182; (*b*) E. J. Werner, J. Kozhukh, M. Botta, E. G. Moore, S. Avedano, S. Aime and K. N. Raymond, *Inorg. Chem.*, 2009, **48**, 277; (*c*) K. N. Raymond and V. C. Pierre, *Bioconjugate Chem.*, 2005, **16**, 3; (*d*) D. M. J. Doble, M. Melchior, B. O'Sullivan, C. Siering, J. Xu, V. C. Pierre and K. N. Raymond, *Inorg. Chem.*, 2003, **42**, 4930; (*e*) V. C. Pierre, M. Botta, S. Aime and K. N. Raymond, *Inorg. Chem.*, 2006, **45**, 8355.

12 P. Caravan, C. T. Farrar, L. Frullano and R. Uppal, *Contrast Media Mol. Imaging*, 2009, **4**, 89.

13 (*a*) T. Courant, V. G. Roullin, C. Cadiou, M. Callewaert, M. C. Andry, C. Protefaix, C. Hoeffel, M. C. de. Goltstein, M. Port, S. Laurent, L. V. Elst, R. Muller, M. Molinari and F. Chuburu, *Angew. Chem., Int. Ed.*, 2012, **51**, 9119 and references therein; (*b*) T. H. Sin, J. S. Choi, S. Yun, I. S. Kim, H. T. Song, Y. Kim, K. I. Park and J. Cheon, *ACS Nano*, 2014, **8**, 3393.

CRYSTAL GROWTH & DESIGN

Article

Cite This: *Cryst. Growth Des.* 2018, 18, 531−539

pubs.acs.org/crystal

Interactions of Alkali and Alkaline-Earth Metals in Water-Soluble Heterometallic Fe^{III}/M (M = Na^+, K^+, Ca^{2+})-Type Coordination Complex

Bedika Phukan,[†] Samir Ghorai,[†] Kashmiri Deka,[‡] Pritam Deb,[‡] and Chandan Mukherjee*[,†]

[†]Department of Chemistry, Indian Institute of Technology Guwahati, Guwahati 781039, Assam, India

[‡]Advanced Functional Material Laboratory, Tezpur University, Napaam, Tezpur 784028, Assam, India

Supporting Information

ABSTRACT: A water-soluble hexadentate ligand H_4bedik was reproduced and employed to synthesize the corresponding mononegative $[Fe^{III}bedik]^-$ complex core. In the complex formation process, NaOH, KOH, and $Ca(OH)_2$ bases were used in order to have the corresponding cations as the counterpart of the mononegative complex core. Thus, formed complexes were designated as complex **1**·H_2O, Na^+ ion as the countercation; complex **2**, K^+ ion as the countercation; and complex **3**·H_2O, 1/2 Ca^{2+} ion as the countercation. Complexes were characterized by IR and mass spectrometric techniques. Additionally, the complexes were structurally characterized by single crystal X-ray diffraction analysis. In complex **1**·H_2O, where the Na^+ ion was present as a countercation, a two-dimensional (2D) zigzag layer structure was formed along the *bc* plane. The two adjacent layers were parallel to each other and propagated along the same direction, and the adjacent layers were connected to each other by H-bonding. Thus, a three-dimensional (3D) network was found. A K^+ ion-containing complex **2** formed a one-dimensional (1D) linear network that propagated along the *b* axis. H-bonding driven 3D layers were also found in complex **2**. Akin to complex **1**·H_2O, complex **3**·H_2O also formed a 2D layers structure; however, the structure was planar and not zigzag as observed in complex **1**·H_2O. In complex **3**·H_2O, two adjacent parallel layers were propagated along two opposite directions. Thermogravimetric analyses indicated that the stability of the complexes and the $[Fe^{III}bedik]^-$ complex core depended on the nature of the countercation. Longitudinal (r_1) and transverse relaxivity (r_2) measurements of aqueous solutions of the complexes have been performed. The value was cation-dependent and thus emphasized different interactions between $[Fe^{III}bedik]^-$ units in the presence of different cations.

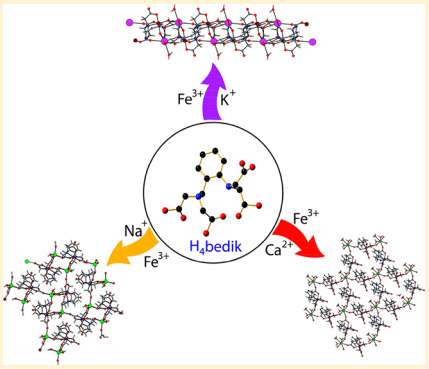

INTRODUCTION

Supramolecular chemistry and crystal engineering have achieved a special attention for the design of metal coordination polymers (MCPs), which can also be termed as metal−organic frameworks (MOFs).[1−6] MCPs have earned their importance for the design of fascinating and diverse network topologies. In addition, MCPs have potentially been applied as heterogeneous catalysts, magnetic materials, sensors, adsorbents, gas-storage materials, electrical conductors, luminescence materials, and biologically active molecules.[7−28] While transition and non-transition MCPs have been widely investigated for their purposes, use of alkali or alkaline earth metal ions are relatively rare due to their lack of preferred geometrical orientation as well as coordination number. Despite the fact that construction of these polymers based on alkali or alkaline earth metal ions remains a challenge, they do provide the advantages of structurally interesting and diverse materials with potentially interesting properties. Moreover, being oxophilic in nature, these cations are attractive candidates for coordinating with O-donor ligands.[29−38]

Water-soluble paramagnetic transition and lanthanide metal complexes with a large number of unpaired-electrons have received significance interest for the design of contrast agents for magnetic resonance imaging (MRI).[39] On this note, high−spin Fe(III) complexes have received special attention as Fe(III) is economically benign, abundant, and the metal ion acquires five unpaired electrons ($3d^5$).[40−46]

Among all alkali and alkaline-earth metals, Na^+, K^+, and Ca^{2+} ions are the most essential and abundant. Herein, the interactions between these ions and the employed water-soluble high-spin Fe(III) complex of ligand H_4bedik, which is comprised of four carboxylic acid groups, will be investigated (Scheme 1A). The carboxylic acid group is polar and hence will be supportive for the water solubility of the corresponding Fe(III) complex. Furthermore, the coordinated acetate group is capable of forming diverse multidimensional networks owing to the variety in coordination motifs (Scheme 1B). Therefore, different types of possible architectures formation centering the

Received: November 13, 2017
Published: November 22, 2017

DOI: 10.1021/acs.cgd.7b01588
Cryst. Growth Des. 2018, 18, 531−539

Scheme 1[a]

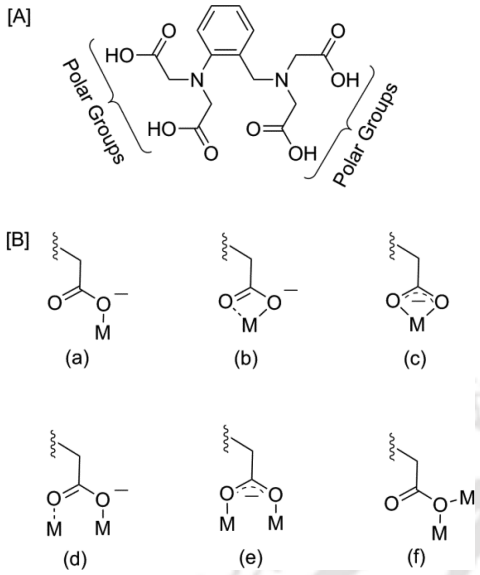

[a]M stands for the same or different metal ions.

Fe(III) complex in the presence of alkali and alkaline-earth metals can be explored. It is noteworthy that Na^+ ($r_{Na}{}^+$ = 116 pm) and Ca^{2+} ($r_{Ca}{}^{2+}$ = 114 pm) have almost the same ionic radii, while K^+ is bigger in size ($r_K{}^+$ = 152 pm) than Na^+. Therefore, the effect of charge as well as size can be studied for the architectures.

The ligand upon losing four carboxylic protons will be in $[bedik]^{4-}$ form, and the corresponding mononuclear Fe(III) complex core will be mononegative in nature. Hence, the introduction of individual Na^+, K^+, and Ca^{2+}-salts during the complex formation will allow the cation to associate with the ionic $[Fe^{III}bedik]^-$ unit. Consequently, the interaction of $[Fe^{III}bedik]^-$ unit with the cations can be studied.

In the present report, the synthesis, characterization, stability, and relaxivity (r_1 and r_2) of the Fe(III) complexes formed by employing ligand H_4bedik, $FeCl_3$, and NaOH or KOH or $Ca(OH)_2$ will be described. In addition, the cationic size and charge dependent Fe(III)-coordination polymer formation and thus constructed supramolecular architecture will also be described.

RESULTS AND DISCUSSION

Ligand H_4bedik was synthesized by following the method as previously reported.[44] A schematic to the synthesis of Fe(III) complexes employing ligand H_4bedik is shown in Scheme 2. A 1:6 reaction between 2-aminobenzylamine and *tert*-butylbromoacetate in DMF in the presence of $KHCO_3$ provided compound **A**, which upon reaction with trifluoroacetic acid provided ligand H_4bedik. The complexes were synthesized by reacting equimolar amounts of the ligand and $FeCl_3$ in water at pH ≈ 6.5 by using NaOH, or KOH, or $Ca(OH)_2$. X-ray quality single crystals of the complexes were obtained by slow evaporation of the reaction mixtures.

The molecular structures of complex **1**·H_2O, **2**, and **3**·H_2O have been established by single crystal X-ray diffraction measurements at 296(2) K. Complex **1**·H_2O, **2**, and **3**·H_2O crystallized in the monoclinic space group $P2_1/n$, triclinic space group $P\bar{1}$, and monoclinic space group $C2/c$, respectively. In all the complexes the asymmetric unit was comprised of a hetero-

Scheme 2

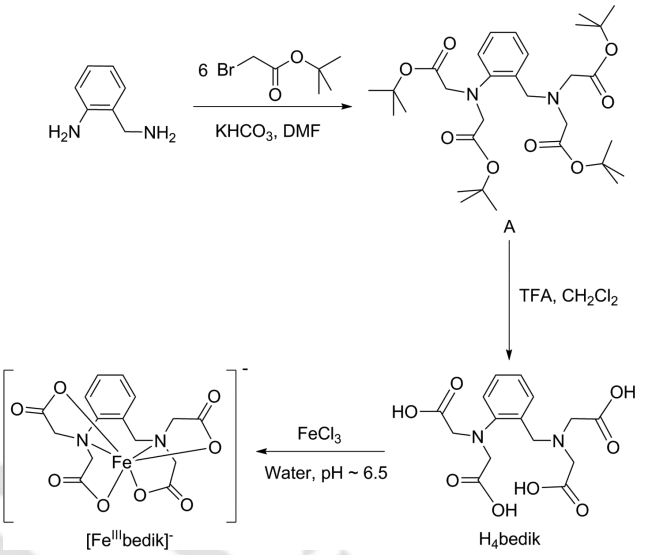

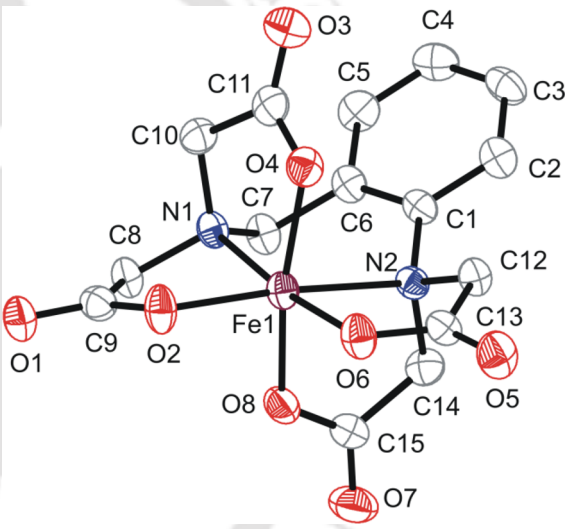

Figure 1. ORTEP presentation of coordination environment of Fe atom; ellipsoids are drawn at the 50% probability level.

bimetallic coordination sphere, where the monoanionic unit was mononuclear $[Fe^{III}bedik]^-$ unit and the cationic part was hydrated $-Na^+$, $-K^+$, or $-1/2Ca^{2+}$ unit. Molecular structures of $[Fe^{III}bedik]^-$ core in the complexes are shown in Figure 1. Selected bond distances and bond angles are listed in Table 1.

The geometry around the six-coordinated Fe atom was found as distorted octahedral. The $[bedik]^{4-}$ unit was composed of two $N(CH_2COO)_2$ arms bridged by a benzyl group. Both the $N(CH_2COO)_2$ groups coordinated to the central Fe atom in *cis*-N facial order in all the three complexes. The coordination constructed four five-member N−C−C−O−Fe chelate rings and one six-member N−C−C−C−N−Fe chelate ring. The six-member chelate ring was present in boat form.

In the complexes the Fe1−N1 and Fe1−N2 bond distances were 2.146(3) [**1**·H_2O], 2.132(3) [**2**], 2.145(2) [**3**·H_2O] Å and 2.254(3) [**1**·H_2O], 2.223(2) [**2**], 2.248(2) [**3**·H_2O] Å, respectively. The bond distances indicated that the Fe1−N2 bond was ∼0.10 Å longer compared to the Fe1−N1 bond. The elongation was because of the angle strain that originated from the boat conformation of the six-member chelate ring. The Fe−

DOI: 10.1021/acs.cgd.7b01588
Cryst. Growth Des. 2018, 18, 531−539

Table 1. Selected Bond Distances (Å) and Bond Angles (deg)

	1·H_2O	2	3·H_2O
Fe1−O2	1.955(2)	1.9719(19)	1.9375(18)
Fe1−O4	1.973(3)	1.950(2)	1.9766(17)
Fe1−O6	1.952(3)	1.948(2)	1.9452(17)
Fe1−O8	2.001(3)	2.011(2)	2.0043(17)
Fe1−N1	2.146(3)	2.132(3)	2.145(2)
Fe1−N2	2.254(3)	2.223(2)	2.248(2)
O1−C9	1.230(4)	1.222(3)	1.217(3)
O2−C9	1.284(4)	1.293(4)	1.291(3)
O3−C11	1.214(5)	1.209(4)	1.228(3)
O4−C11	1.286(5)	1.307(4)	1.285(3)
O5−C13	1.211(4)	1.206(4)	1.224(3)
O6−C13	1.297(4)	1.305(4)	1.284(3)
O7−C15	1.220(4)	1.222(3)	1.237(3)
O8−C15	1.300(4)	1.298(4)	1.272(3)
O4−Fe1−O8	161.89(11)	90.49(8)	162.56(8)
O6−Fe1−N1	172.55(11)	173.84(8)	173.84(8)
O2−Fe1−N2	167.44(11)	86.01(8)	167.15(8)

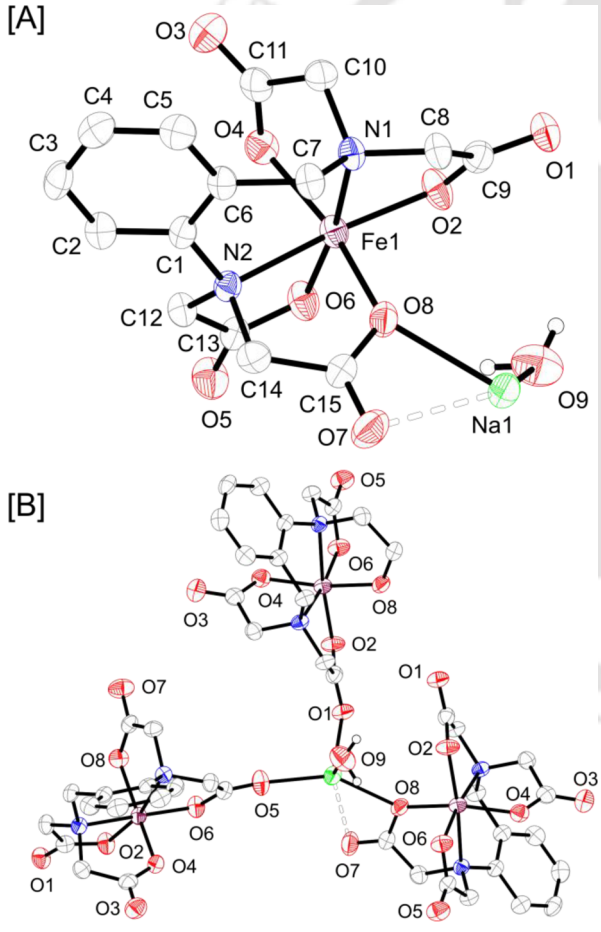

Figure 2. [A] ORTEP presentation of the asymmetric unit of complex 1·H_2O and [B] coordination environment of Na^+; thermal ellipsoid drawn at the 50% probability level. H atoms except lattice water molecules were omitted.

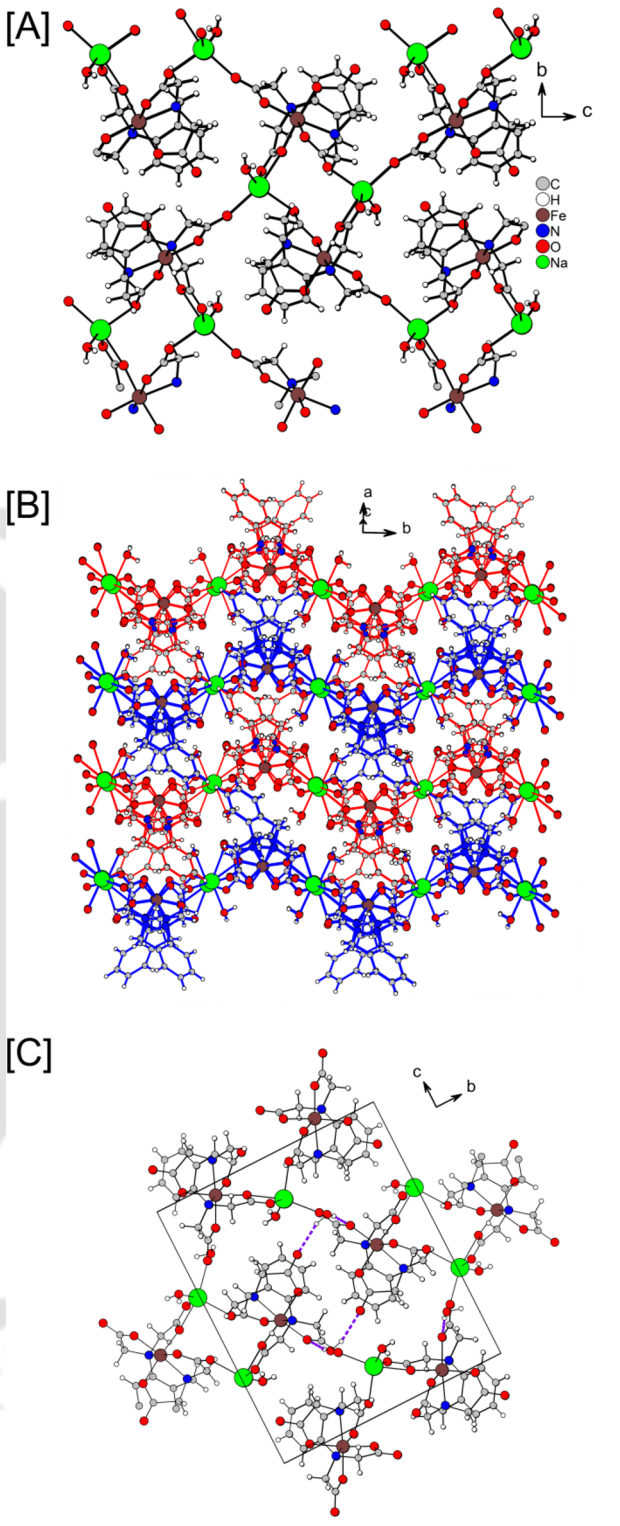

Figure 3. [A] Zigzag like 2D layer structure of complex 1·H_2O. [B] Orientation between two adjacent layers (different in color red and blue). [C] Showing H-bonds between crystalline water molecule and [Fe^{III}bedik]$^-$ units. H atoms, except water-belonging H atoms, were not shown.

O bond distances were within the range of 1.937−2.010 Å in all three complexes. The Fe−O bonds *trans*- to the Fe−N bonds were found shorter compared to the other Fe−O bonds. However, Fe−O/N bond distances were in good agreement with the high-spin Fe(III) complexes.[47] The C−O bond distances in each acetate unit were not the same (Table 1), which indicated that the negative charge was localized on one of the two acetate-belonging O atoms.

DOI: 10.1021/acs.cgd.7b01588
Cryst. Growth Des. 2018, 18, 531−539

Table 2. Selected H-Bond Distances (Å) in the Complexes[a]

1·H_2O		2		3·H_2O	
O3−H10D	2.155	O1−H10C	1.991	O1−H11B	1.929
O3−H9B	2.084	O1−H12A	3.184	O5−H11A	1.991
O7−H9A	2.432	O4−H9A	2.228	O11−H10C	1.882
O6−H10C	1.910	O7−H9B	2.186	O11−H9B	2.437

[a]Suffixes A, B, C, and D represent the H number.

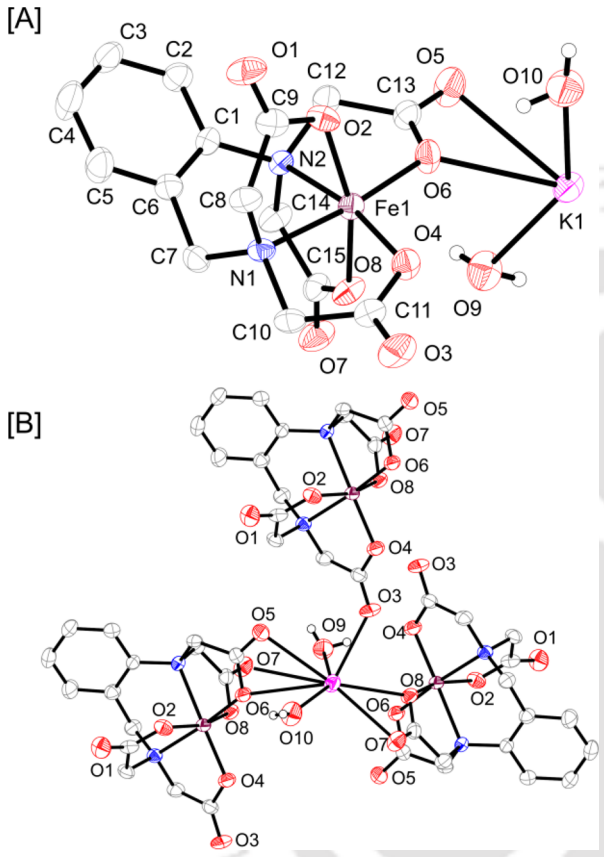

Figure 4. [A] ORTEP presentation of the asymmetric unit of complex **2** and [B] coordination environment of K^+; thermal ellipsoid drawn at 50% probability level. H atoms except lattice water molecules were omitted.

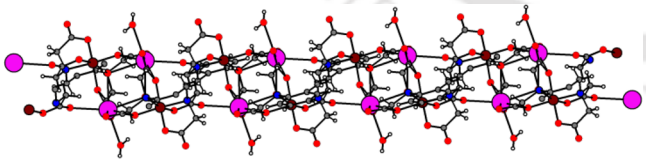

Figure 5. 1D network formed by the coordination of $[Fe^{III}bedik]^-$ and K^+ ions along the *b* axis. K = pink; Fe = brown.

In complex **1**·H_2O, the asymmetric unit was comprised of a six-coordinate monoanionic $[Fe^{III}bedik]^-$ unit and a monohydrated monocationic Na^+ unit (Figure 2). The Na^+ unit was four-coordinate and in this four-coordinate complex the other three coordination sites were occupied by two keto-oxygen atoms (O1 and O5) from two different $[Fe^{III}bedik]^-$ units and one carboxylate oxygen atom O8 (Figure 2B), while Na1−O1 = 2.303(3); Na1−O5 = 2.269(3); Na1−O8 = 2.391(4); Na1−O9 = 2.298(5) Å bond distances were within the expected Na−O bond.[48−51] A comparatively long Na1−O7 = 2.734(3) Å bond was also observed. This bond can be considered as weak

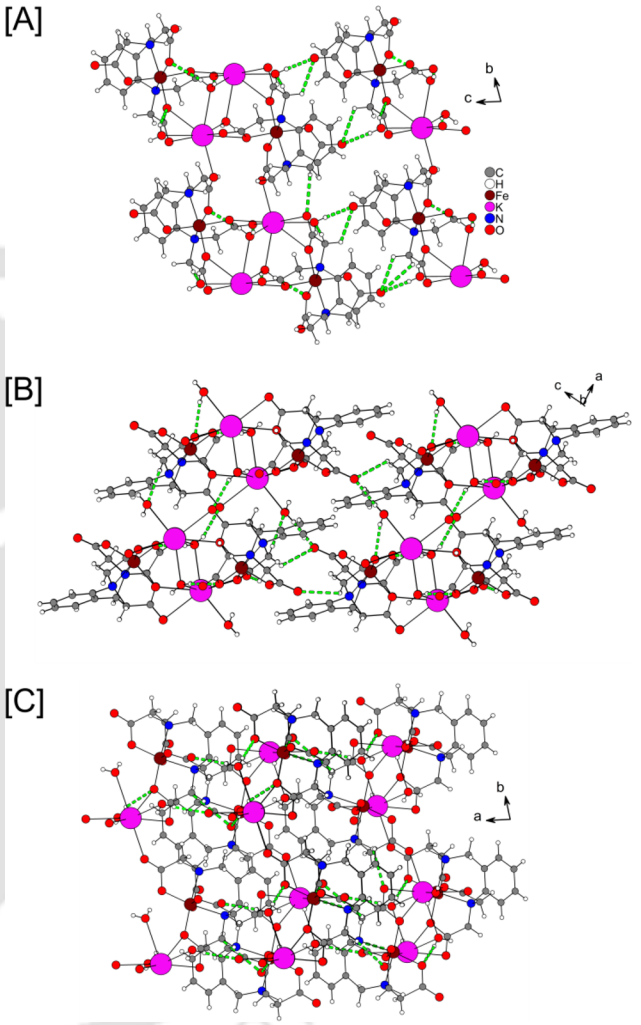

Figure 6. Inter- and Intramolecular H-bonding between 1D layers of complex **2** along; [A] *a* axis, [B] *b* axis, and [C] *c* axis. H-bonds are green in color.

Na···O interaction (Figure 2). The τ_4 value for the Na^+ coordination environment was 0.77 which indicated a distorted tetrahedral environment.

The coordination of two separate $[Fe^{III}bedik]^-$ units with a Na^+ cation formed a zigzag 2D parallel layers along the *bc* plane (Figure 3A). The 2D layers were propagated in a parallel way, i.e., toward the same direction (Figure 3B). The Na-coordinated water molecule was strongly H-bonded with the acetate O atom of another 2D layer. The O9−H9A···O7 bond distance was 2.432 Å, and O−H···O bond angle was 149°. Thus, the zig-zag-like 2D coordination polymer constituted a 3D supramolecular architecture via extended intermolecular H-bonding with the Na-coordinated water molecules. In addition, each unit cell contained four free water molecules, which were strongly H-bonded to the two $[Fe^{III}bedik]^-$ units via acetate

DOI: 10.1021/acs.cgd.7b01588
Cryst. Growth Des. 2018, 18, 531−539

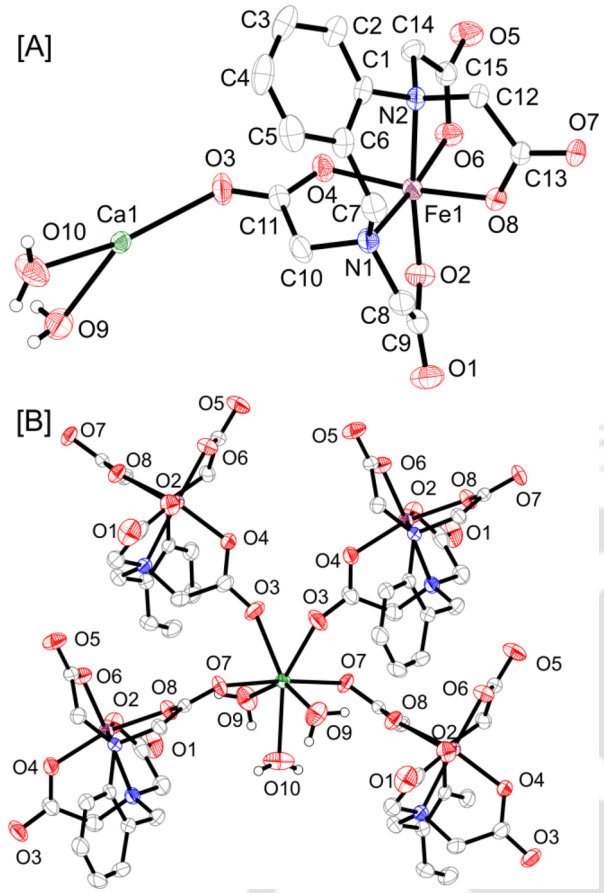

Figure 7. [A] ORTEP presentation of the asymmetric unit of complex **3**·H_2O and [B] coordination environment of Ca^{2+}; thermal ellipsoid drawn at 50% probability level. H atoms except lattice water molecules were omitted.

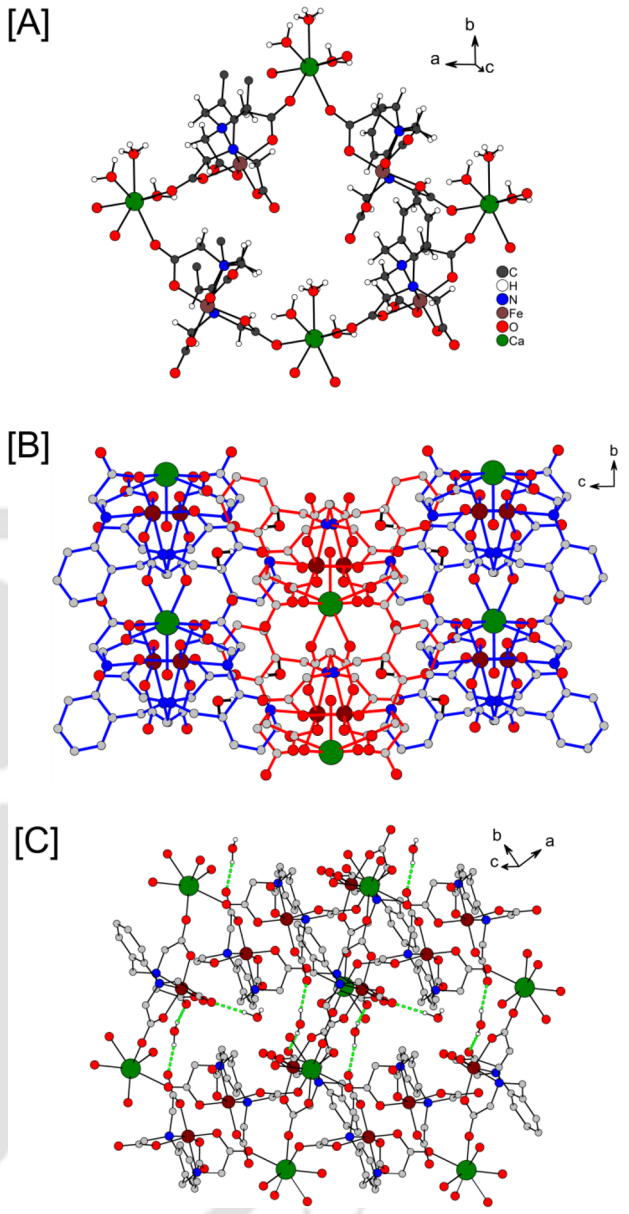

Figure 8. [A] 2D layer structure of complex **3**·H_2O. [B] antiparallel orientation between two adjacent layers (different in color red and blue) along the *a* axis and [C] H-bonds between two adjacent layers along the *c* axis. H atoms, except water H atom involved in H-bondings, were not shown for panel [B] and [C] for clarity. H-bonds are shown in green.

groups. The O10—H10C···O6, O9—H9B···O3, and O10—H10D···O3 bond distances were 1.910, 2.084, and 2.155 Å, respectively (Table 2), and the O—H···O bond angles were 172°, 172° and 149°, respectively.

In complex **2**, the asymmetric unit was comprised of a $[Fe^{III}bedik]^-$ unit and a dihydrated K^+ cation (Figure 4A). The K^+ ion was attached to the $[Fe^{III}bedik]^-$ unit through both oxygen atoms (O5 and O6) of a acetate unit. A close inspection to the crystal structure of complex **2** revealed that the coordination number of the K center was eight that was made by coordination of acetate groups belonging O from three individual $[Fe^{III}bedik]^-$ units and three water molecules [Figure 6A]. Among the three water molecules, two water molecules (O9) acted as bridging units between two K centers. Acetate groups from two $[Fe^{III}bedik]^-$ units coordinated to the K center in η^2-fashion (O5, O6; O7, O8), while the third one was coordinated in η^1-fashion (O3) that involved in building a 1D coordination polymeric-layer along the *b* axis (Figure 5). To note, the 1D coordination layers were connected to each other through 1.991 and 3.184 Å H-bonds. In addition to intralayer H-bonds, bridging water molecule belonging H-atoms formed intra- as well as intermolecular H-bonds (Table 2) with acetate oxygen atoms (O1, O4, O7) of 2.228 and 2.186 Å, respectively (Figure 6).

A $[Fe^{III}bedik]^-$ unit and a dihydrated 1/2 Ca^{2+} cation unit were present in the asymmetric unit of complex **3**·H_2O (Figure 7A). The $[Fe^{III}bedik]^-$ unit was attached to 1/2 Ca^{2+} ion by the keto O3 oxygen atom. In the crystal structure, the Ca atom was seven-coordinate and formed pentagonal bipyramidal geometry around the metal center (Figure 7B). The coordination sphere was constituted by four acetate O atoms coming from four individual monoanionic $[Fe^{III}bedik]^-$ subunits and three water-belonging O atoms (Figure 7B). The Ca—O bond distances (from water molecules attached to the cation) were 2.428, 2.440, 2.413, 2.428 Å, respectively. The bond distances were accord with the previously reported Ca^{2+}—O bonds.[49,52−54]

In complex **3**·H_2O, a sheet like 2D coordination polymer was formed through coordination of Ca atom and acetate O atoms of the monoanionic subunit $[Fe^{III}bedik]^-$ having the repeating unit of $[Fe^{III}bedik]$-Ca-$[Fe^{III}bedik]$ (Figure 8A). In the complex, among four acetate groups of the monoanionic

DOI: 10.1021/acs.cgd.7b01588
Cryst. Growth Des. 2018, 18, 531−539

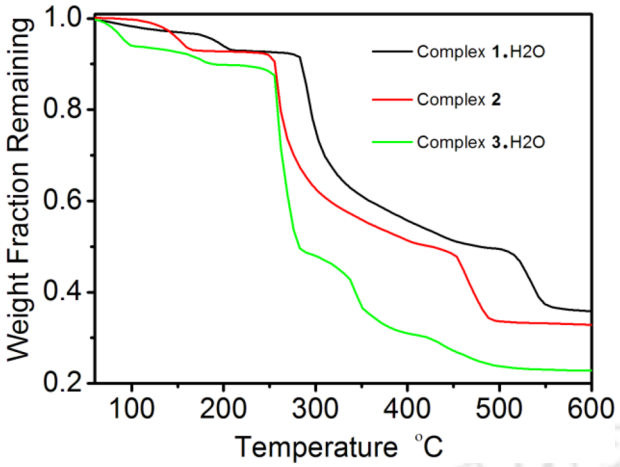

Figure 9. TGA plots for the complexes.

subunit, two acetate groups employed only one O atom for the coordination with the central Fe atom, while other two acetate groups used both oxygen atoms to coordinate to both Fe and Ca metal centers in η^1-fashion. In complex **3**·H_2O, unlike complex **1**·H_2O, two adjacent 2D layers propagated in two opposite directions (Figure 8B,C). Each neighboring layers were further linked into a 3D supramolecular architecture via interlayer strong H-bonding with free water molecules and acetate O atom of adjacent layer. The O11−H11B···O1, O10−H10C···O11 bond distances and O−H···O bond angles were 1.928 Å, 1.880 Å and 172°, 163°, respectively. The free water molecules were also involved in forming of intralayer H-bonding; intralayer O11−H11A···O5, O9−H9B···O11 bond distances were 1.991 Å, 2.437 Å and O−H···O bond angles were 171°, 139°, respectively (Figure 8C).

The thermogravimetric analysis (TGA) on complexes **1**−**3** was performed in order to get into the stability of the complexes and shown in Figure 9. All the complexes lost 8−10% weight upon heating within 140−200 °C. The weight loss corresponded to the removal of alkali or alkaline-earth metal-coordinated water molecule(s) and lattice water molecule upon heating. The temperature required for the removal of all the water molecules follows the order, complex **1**·H_2O (190 °C) > complex **3**·H_2O (176 °C) > complex **2** (143 °C). A higher M−water bond distance (2.76−3.00 Å) could be attributed to the easy removal for water molecule in complex **2** compared to the other two complexes (Na−water = 2.299 Å in complex **1**·H_2O; Ca−water = 2.413−2.428 Å in complex **3**·H_2O). Upon further heating a sharp change in weight, 43−45%, occurred. This decrease in weight was related to the loss of ligand-centered carboxylate groups and hence, implied the decomposition of $[Fe^{III}bedik]^-$ unit. Interestingly, it was observed that the stability of the unit was also governed by the nature of cation present in the crystal lattice (Figure 9).

MRI contrast agents (CAs) enhance the image contrast by catalytically reducing longitudinal (T_1) and transverse (T_2) relaxation times of nearby water protons.[39] In the case of T_1-weighted images, a brighter signal is observed in the region where the longitudinal relaxation rate ($1/T_1$) is fast, whereas in the case of T_2-weighted images, a darker signal is observed in the region where the transverse relaxation rate ($1/T_2$) is fast. Gd(III) based MRI CAs are the most widely used because of its seven unpaired electrons, long electronic relaxation time, and fast water exchange rate.[55,56] However, recent concerns

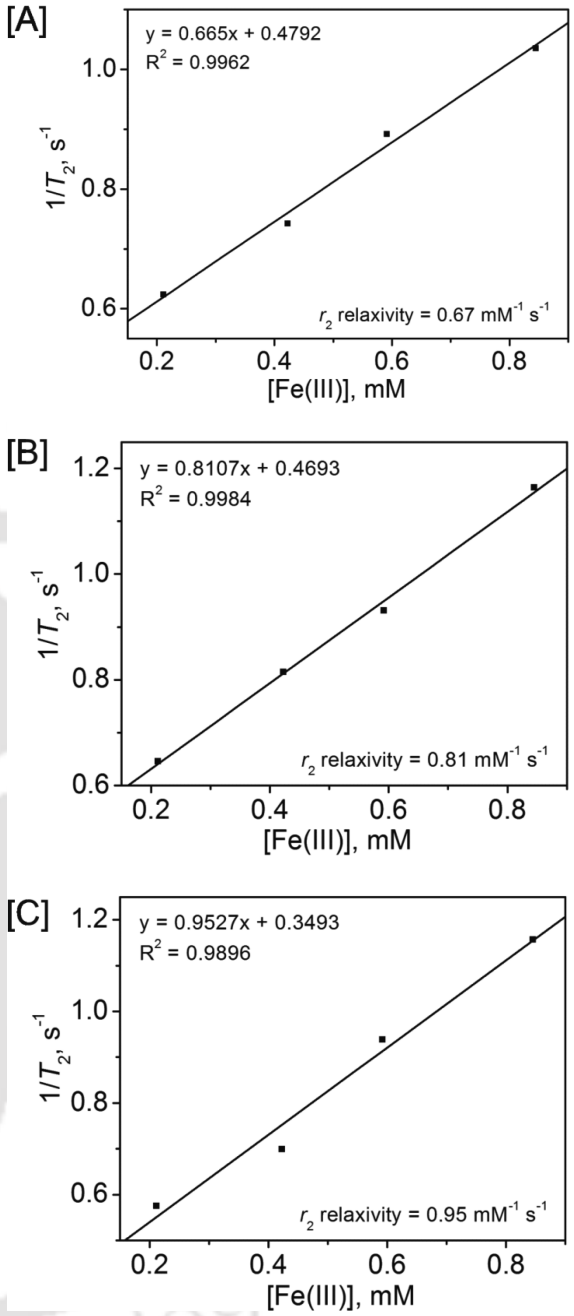

Figure 10. $1/T_2$ versus [Fe(III)] plots for complexes **1**·H_2O, **2**, and **3**·H_2O.

regarding in vivo release and accumulation of free Gd(III) ion in patients having severe renal diseases or who underwent liver transplantation led to design and synthesis of less toxic MRI CA from endogenous metal ions.[57−59] In this regard, the high spin d^5 Fe(III) metal center is an attractive less toxic alternative to Gd(III) based MRI CA.[60,62] Fe(III) based contrast agents are very appealing as several small molecule Fe(III) complexes are known to show biocompatibility as well as high stability under physiological conditions.[63,64]

To investigate the potential utility of complexes **1**−**3** as MRI contrast agents, longitudinal relaxivity (r_1) of the complexes was measured at 1.41 T, 25 °C, and pH 7.4. The r_1 relaxivity values per Fe(III) ion of the complexes were found to be 0.68 mM^{-1} s^{-1}, 0.53 mM^{-1} s^{-1}, and 0.59 mM^{-1} s^{-1} for complex **1**·H_2O, **2**, and **3**·H_2O respectively. The lower longitudinal

DOI: 10.1021/acs.cgd.7b01588
Cryst. Growth Des. 2018, 18, 531−539

relaxivity values were due to the absence of inner sphere water molecules in the complexes, and the observed relaxivity values were attributed to a contribution from outer sphere water molecules. Similarly, at 1.41 T, 37 °C, and pH 7.4, the transverse relaxivity (r_2) values of complexes **1**−**3** were measured, and r_2 relaxivity values per Fe(III) ion were found to be 0.67 mM^{-1} s^{-1}, 0.81 mM^{-1} s^{-1}, and 0.95 mM^{-1} s^{-1} for complex **1**·H_2O, **2**, and **3**·H_2O, respectively (Figure 10). The exact Fe(III) ion concentration in each complex was determined by the ICP−AES method. For coordination polymers of Fe(III), it was expected to have a high r_2 value. The observed r_2 values indicated that in solution phase the polymeric nature of the complexes collapsed, and the observed relaxivity values were due to $[Fe^{III}bedik]^-$ unit only. However, the different r_2 values, exhibited by the complexes, implied the cation-dependent interaction between $[Fe^{III}bedik]^-$ units in solution. The interaction was highest for Ca^{2+} and lowest for Na^+. The Ca^{2+} and Na^+ ions are almost the same in size; thus, the difference in interaction in solution was governed by a higher charge density.

CONCLUSION

To conclude, herein, we have documented $[Fe^{III}bedik)/M^{n+}]$ type complexes. In complex **1**·H_2O, where the Na^+ ion was present as a countercation, a two-dimensional (2D) zigzag layer structure was formed along the *bc* plane. The two adjacent layers were parallel to each other and propagated along the same direction, and the adjacent layers were connected to each other by H−bonding. Thus, a three-dimensional (3D) network was found. K^+ ion−containing complex **2** formed a one-dimensional (1D) linear network that propagated along the *b* axis. H-bonding driven 3D layers were also found in complex **2**. Akin to complex **1**·H_2O, complex **3**·H_2O also formed a 2D layers structure; however, the structure was planar and not zigzag as observed in complex **1**·H_2O. In complex **3**·H_2O, two adjacent parallel layers were propagated along the two opposite directions.

The size of the cations has been found to play a vital role in decorating coordination network in the crystalline phase. The K^+ cation being larger in size compared to both Na^+ and Ca^{2+} ions formed 1D layers, while the latter two cations formed 2D layers due to the facilitation of closure arrangements of $[Fe^{III}bedik]^-$ units and either Na^+ or Ca^{2+} ions via metal-carboxylate linkages. In the solution phase, the polymeric nature of the complexes collapsed and interaction between $[Fe^{III}bedik]^-$ units were found as cationic charge-density dependent. A higher r_2 value, shown by the aqueous solution complex **3**·H_2O compared to complexes **1**·H_2O and **2**, demonstrated the fact.

EXPERIMENTAL SECTION

Materials. All the chemicals and solvents were obtained from commercial sources and were used as supplied, unless noted otherwise. Solvents were obtained from Merck (India). Mass spectra were measured in MiliQ water.

Physical Methods. X-ray crystallographic data were collected using Super Nova, Single source at offset, Eos diffractometer. Structures were solved by direct methods using SHELXS-97 and refined by the full matrix least-squares method using SHELXL−97. All the non-hydrogen atoms were refined anisotropically. IR spectra were recorded on a PerkinElmer Instrument at normal temperature with KBr pellet by grinding the sample with KBr (IR grade).

Synthesis of H_4bedik, $[C_{14}H_{18}N_2O_8]$: As reported previously.[44]

Synthesis of Complex 1·H_2O. To a solution of H_4bedik (0.177 g, 0.5 mmol) in water (3 mL) was added $FeCl_3$ (0.077 g, 0.48 mmol), and the mixture was stirred until the solution became transparent. The pH of the solution then was adjusted to ∼6.5 by adding aq. NaOH solution dropwise. Stirring was continued at room temperature (25 °C) for 24 h. The resulted solution was kept at room temperature (25 °C). Yellow colored crystals were obtained after slow evaporation of the solution, which were washed thoroughly with MeOH and used for single crystal X-ray diffraction study. Yield = 0.096 g, 41%. FTIR (KBr, cm^{-1}): 3611, 3485, 3387, 2958, 2926, 1642, 1363, 1335, 1248, 1178, 1111, 1079, 1042, 1007, 966, 930, 908, 812, 789, 760,750, 725, 651. ESI−MS (−) *m*/*z* for $[C_{15}H_{14}FeN_2O_8]^-$: Calcd, 406.01; Found, 406.83. Anal. Calcd for $C_{15}H_{18}FeN_2O_{10}Na$: C, 38.71; H, 3.90; N, 6.02. Found: C, 38.53; H, 3.63; N, 5.96.

Synthesis of Complex 2. To a solution of H_4bedik (0.177 g, 0.5 mmol) in water (3 mL) was added $FeCl_3$ (0.077 g, 0.48 mmol), and the mixture was stirred until the solution became transparent. The pH of the solution then was adjusted to ∼6.5 by adding aq. KOH solution dropwise. Stirring was continued at room temperature (25 °C) for 24 h. The resulted solution was kept at room temperature (25 °C) for slow evaporation to obtain crystals. The appeared yellow crystals were washed thoroughly with MeOH and were suitable for single crystal X-ray diffraction study. Yield = 0.108 g, 45%. FTIR (KBr, cm^{-1}): 3537, 3417, 2964, 2934, 1675, 1627, 1348, 1281, 1239, 1180, 1118, 1079, 1042, 1005, 969, 934, 910, 811, 775, 759, 744, 723, 652. ESI−MS (−) *m*/*z* for $[C_{15}H_{14}FeN_2O_8]^-$: Calcd, 406.01; Found, 406.83. Anal. Calcd for $C_{15}H_{18}FeN_2O_{10}K$: C, 37.42; H, 3.77; N, 5.82. Found: C, 36.51; H, 3.54; N, 5.69.

Synthesis of Complex 3·H_2O. To a solution of H_4bedik (0.177 g, 0.5 mmol) in water (3 mL) was added $FeCl_3$ (0.077 g, 0.48 mmol), and the mixture was stirred until the solution became transparent. The pH of the solution then was adjusted to ∼6.5 by adding aq. $Ca(OH)_2$ solution dropwise. Stirring was continued at room temperature (25 °C) for 24 h during which a brown colored precipitate was formed. This precipitate was filtered off and washed with water, and the filtrate was kept at room temperature (25 °C) for slow evaporation to obtain crystals. The appeared yellow crystals were washed thoroughly with MeOH and were suitable for single crystal X-ray diffraction study. Yield = 0.114 g, 46%. FTIR (KBr, cm^{-1}): 3439, 3275, 2953, 1653, 1362, 1333, 1254, 1241, 1175, 1118, 1078, 1041, 1008, 968, 939, 930, 813, 783, 756, 720, 653. ESI−MS (−) *m*/*z* for $[C_{15}H_{14}FeN_2O_8]^-$: Calcd, 406.01; Found, 406.81. Anal. Calcd for $C_{30}H_{40}Fe_2N_4O_{21}Ca$: C, 37.49; H, 4.19; N, 5.83. Found: C, 37.96; H, 3.72; N, 5.87.

ASSOCIATED CONTENT

Supporting Information

The Supporting Information is available free of charge on the ACS Publications website at DOI: 10.1021/acs.cgd.7b01588.

Infrared and mass spectra of the complexes (PDF)

Accession Codes

CCDC 1439426, 1439428, and 952727 contain the supplementary crystallographic data for this paper. These data can be obtained free of charge via www.ccdc.cam.ac.uk/data_request/cif, or by emailing data_request@ccdc.cam.ac.uk, or by contacting The Cambridge Crystallographic Data Centre, 12 Union Road, Cambridge CB2 1EZ, UK; fax: +44 1223 336033.

AUTHOR INFORMATION

Corresponding Author

*E-mail: cmukherjee@iitg.ernet.in.

ORCID

Chandan Mukherjee: 0000-0002-2771-2468

Funding

Science and Engineering Research Board (SERB), India.

DOI: 10.1021/acs.cgd.7b01588
Cryst. Growth Des. 2018, 18, 531−539

Notes

The authors declare no competing financial interest.

■ ACKNOWLEDGMENTS

This project is supported by SERB [EMR/2015/002491], India. B.P. thanks Indian Institute of Technology Guwahati (IITG) for her doctoral fellowship. The Department of Chemistry and CIF, IIT Guwahati, are thankfully acknowledged for instrumental facility.

■ ABBREVIATIONS

H_4bedik: 2,2′-((2-(bis(carboxymethyl)amino)benzyl) azanediyl)diacetic acid

■ REFERENCES

(1) Robin, A. Y.; Fromm, K. M. Coordination polymer networks with O- and N-donors: What they are, why and how they are made. *Coord. Chem. Rev.* **2006**, *250*, 2127−2157.
(2) Rowsell, J. L. C.; Yaghi, O. M. Effects of Functionalization, Catenation, and Variation of the Metal Oxide and Organic Linking Units on the Low-Pressure Hydrogen Adsorption Properties of Metal-Organic Frameworks. *J. Am. Chem. Soc.* **2006**, *128*, 1304−1315.
(3) Zhu, X.; Zhao, J. W.; Li, B. L.; Song, Y.; Zhang, Y. M.; Zhang, Y. A Two-Dimensional Metal-Organic Framework Based on a Ferromagnetic Pentanuclear Copper(II). *Inorg. Chem.* **2010**, *49*, 1266−1270.
(4) Wang, M.; Xie, M. H.; Wu, C. D.; Wang, Y. G. From one to three: a serine derivate manipulated homochiral metal-organic framework. *Chem. Commun.* **2009**, 2396−2398.
(5) Jackson, S. L.; Rananaware, A.; Rix, C.; Bhosale, S. V.; Latham, K. Highly Fluorescent Metal−Organic Framework for the Sensing of Volatile Organic Compounds. *Cryst. Growth Des.* **2016**, *16*, 3067−3071.
(6) Fujita, M.; Kwon, Y. J.; Washizu, S.; Ogura, K. Preparation, Clathration Ability, and Catalysis of a Two-Dimensional Square Network Material Composed of Cadmium(II) and 4,4′-Bipyridine. *J. Am. Chem. Soc.* **1994**, *116*, 1151−1152.
(7) Carlucci, L.; Ciani, G.; Proserpio, D. M. Polycatenation, polythreading and polyknotting in coordination network chemistry. *Coord. Chem. Rev.* **2003**, *246*, 247−289.
(8) Verma, G.; Kumar, S.; Pham, T.; Niu, Z.; Wojtas, L.; Perman, J. A.; Chen, Y.-S.; Ma, S. Partially Interpenetrated NbO Topology Metal−Organic Framework Exhibiting Selective Gas Adsorption. *Cryst. Growth Des.* **2017**, *17*, 2711−2717.
(9) Wang, L.; Han, Y.; Feng, X.; Zhou, J.; Qi, P.; Wang, B. Metal−organic frameworks for energy storage: Batteries and supercapacitors. *Coord. Chem. Rev.* **2016**, *307*, 361−381.
(10) Custelcean, R.; Haverlock, T. J.; Moyer, B. A. Anion Separation by Selective Crystallization of Metal−Organic Frameworks. *Inorg. Chem.* **2006**, *45*, 6446−6452.
(11) Oar-Arteta, L.; Wezendonk, T.; Sun, X.; Kapteijn, F.; Gascon, J. Metal organic frameworks as precursors for the manufacture of advanced catalytic materials. *Mater. Chem. Front.* **2017**, *1*, 1709−1745.
(12) Eddaoudi, M.; Kim, J.; Rosi, N.; Vodak, D. T.; Wachter, J.; O'Keeffe, M.; Yaghi, O. M. Systematic Design of Pore Size and Functionality in Isoreticular MOFs and Their Application in Methane Storage. *Science* **2002**, *295*, 469−472.
(13) Noro, S.; Kitaura, R.; Kondo, M.; Kitagawa, S.; Ishii, T.; Matsuzaka, H.; Yamashita, M. Framework Engineering by Anions and Porous Functionalities of Cu(II)/4,4′-bpy Coordination Polymers. *J. Am. Chem. Soc.* **2002**, *124*, 2568−2583.
(14) Liu, R.; Yu, T.; Shi, Z.; Wang, Z. The preparation of metal−organic frameworks and their biomedical application. *Int. J. Nanomed.* **2016**, 1187−1200.
(15) Sudik, A. C.; Millward, A. R.; Ockwig, N. W.; Côté, A. P.; Kim, J.; Yaghi, O. M. Design, Synthesis, Structure, and Gas (N_2, Ar, CO_2, CH_4, and H_2) Sorption Properties of Porous Metal-Organic Tetrahedral and Heterocuboidal Polyhedra. *J. Am. Chem. Soc.* **2005**, *127*, 7110−7118.
(16) Brammer, L. Developments in inorganic crystal engineering. *Chem. Soc. Rev.* **2004**, *33*, 476−489.
(17) Smith, S. J. D.; Konstas, K.; Lau, C. H.; Gozukara, Y. M.; Easton, C. D.; Mulder, R. J.; Ladewig, B. P.; Hill, M. R. Post-Synthetic Annealing: Linker Self-Exchange in UiO-66 and Its Effect on Polymer−Metal Organic Framework Interaction. *Cryst. Growth Des.* **2017**, *17*, 4384−4392.
(18) Zhang, H.; Sheng, T.; Hu, S.; Zhuo, C.; Li, H.; Fu, R.; Wen, Y.; Wu, X. Stitching 2D Polymeric Layers into Flexible 3D Metal−Organic Frameworks via a Sequential Self-Assembly Approach. *Cryst. Growth Des.* **2016**, *16*, 3154−3162.
(19) Mukherjee, S.; Babarao, R.; Desai, A. V.; Manna, B.; Ghosh, S. K. Polar Pore Surface Guided Selective CO_2 Adsorption in a Prefunctionalized Metal−Organic Framework. *Cryst. Growth Des.* **2017**, *17*, 3581−3587.
(20) Matsuda, R.; Kitaura, R.; Kitagawa, S.; Kubota, Y.; Belosludov, R. V.; Kobayashi, T. C.; Sakamoto, H.; Chiba, T.; Takata, M.; Kawazoe, Y.; Mita, Y. Highly controlled acetylene accommodation in a metal−organic microporous material. *Nature* **2005**, *436*, 238−241.
(21) Liu, D. H.; Liu, T. F.; Chen, Y. P.; Zou, L. F.; Feng, D. W.; Wang, K. C.; Zhang, Q.; Yuan, S.; Zhong, C. L.; Zhou, H. C. A Reversible Crystallinity-Preserving Phase Transition in Metal−Organic Frameworks: Discovery, Mechanistic Studies, and Potential Applications. *J. Am. Chem. Soc.* **2015**, *137*, 7740−7746.
(22) Hu, Z.; Huang, G.; Lustig, W. P.; Wang, F.; Wang, H.; Teat, S. J.; Banerjee, D.; Zhang, D.; Li, J. Achieving exceptionally high luminescence quantum efficiency by immobilizing an AIE molecular chromophore into a metal−organic framework. *Chem. Commun.* **2015**, *51*, 3045−3048.
(23) Grancha, T.; Ferrando-Soria, J.; Zhou, H. C.; Gascon, J.; Seoane, B.; Pasan, J.; Fabelo, O.; Julve, M.; Pardo, E. Postsynthetic Improvement of the Physical Properties in a Metal−Organic Framework through a Single Crystal to Single Crystal Trans-metallation. *Angew. Chem., Int. Ed.* **2015**, *54*, 6521−6525.
(24) Ke, F. S.; Wu, Y. S.; Deng, H. X. Metal-organic frameworks for lithium ion batteries and supercapacitors. *J. Solid State Chem.* **2015**, *223*, 109−121.
(25) Sun, L.; Hendon, C. H.; Minier, M. A.; Walsh, A.; Dincă, M. Million-Fold Electrical Conductivity Enhancement in Fe_2(DEBDC) versus Mn_2(DEBDC) (E = S, O). *J. Am. Chem. Soc.* **2015**, *137*, 6164−6167.
(26) Pramanik, S.; Zheng, C.; Zhang, X.; Emge, T. J.; Li, J. New Microporous Metal−Organic Framework Demonstrating Unique Selectivity for Detection of High Explosives and Aromatic Compounds. *J. Am. Chem. Soc.* **2011**, *133*, 4153−4155.
(27) Banerjee, D.; Hu, Z. C.; Li, J. Luminescent metal−organic frameworks as explosive sensors. *Dalton Trans.* **2014**, *43*, 10668−10685.
(28) Duan, L. N.; Dang, Q. Q.; Han, C. Y.; Zhang, X. M. An interpenetrated bioactive nonlinear optical MOF containing a coordinated quinolone-like drug and Zn(II) for pH-responsive release. *Dalton Trans.* **2015**, *44*, 1800−1804.
(29) Pan, L.; Woodlock, E. B.; Wang, X.; Zheng, C. A New Porous Three-Dimensional Lanthanide Coordination Polymer. *Inorg. Chem.* **2000**, *39*, 4174−4178.
(30) Kelly, N. R.; Goetz, S.; Batten, S. R.; Kruger, P. E. Coordination behaviour and network formation with 4,4′,6,6′-tetracarboxy-2,2′-bipyridine and 4,4′-dicarboxy-2,2′-bipyridine ligands with rare and alkaline earth metals. *CrystEngComm* **2008**, *10*, 68−78.
(31) Xiao, X.; Tao, Z.; Xue, S. F.; Zhang, Y. Q.; Zhu, Q. J.; Liu, J. X.; Wei, G. Coordination polymers constructed from alkali metal ions and $(HO)_{10}$cucurbit[5]uril. *CrystEngComm* **2011**, *13*, 3794−3800.
(32) Gao, H. L.; Yi, L.; Ding, B.; Wang, H. S.; Cheng, P.; Liao, D. Z.; Yan, S. P. First 3D Pr(III)−Ni(II)−Na(I) Polymer and A 3D Pr(III) Open Network Based on Pyridine-2,4,6-tricarboxylic Acid. *Inorg. Chem.* **2006**, *45*, 481−483.

DOI: 10.1021/acs.cgd.7b01588
Cryst. Growth Des. 2018, 18, 531−539

(33) Han, L.; Bu, X.; Zhang, Q.; Feng, P. Solvothermal in Situ Ligand Synthesis through Disulfide Cleavage: 3D (3,4)-Connected and 2D Square-Grid-Type Coordination Polymers. *Inorg. Chem.* **2006**, *45*, 5736−5738.
(34) Karmakar, A.; Goldberg, I. Coordination polymers of flexible tetracarboxylic acids with metal ions. I. Synthesis of CH_2- and $(CH_2)_2$-spaced bis(oxy)isophthalic acid ligands, and structural characterization of their polymeric adducts with lanthanoid ions. *CrystEngComm* **2011**, *13*, 339−349.
(35) Lazarescu, A.; Shova, S.; Bartolome, J.; Alonso, P.; Arauzo, A.; Balu, A. M.; Simonov, Y. A.; Gdaniec, M.; Turta, C.; Filoti, G.; Luque, R. Heteronuclear (Co−Ca, Co−Ba) 2,3-pyridinedicarboxylate complexes: synthesis, structure and physico-chemical properties. *Dalton Trans.* **2011**, *40*, 463−471.
(36) Cao, R.; Sun, D.; Liang, Y.; Hong, M.; Tatsumi, K.; Shi, Q. Syntheses and Characterizations of Three-Dimensional Channel-like Polymeric Lanthanide Complexes Constructed by 1,2,4,5-Benzenetetracarboxylic Acid. *Inorg. Chem.* **2002**, *41*, 2087−2094.
(37) Argent, S. P.; Adams, H.; Riis-Johannessen, T.; Jeffrey, J. C.; Harding, L. P.; Ward, M. D. High-nuclearity Homoleptic and Heteroleptic Coordination Cages Based on Tetra-Capped Truncated Tetrahedral and Cuboctahedral Metal Frameworks. *J. Am. Chem. Soc.* **2006**, *128*, 72−73.
(38) Leonard, J. P.; Jensen, P.; McCabe, T.; O'Brien, J. E.; Peacock, R. D.; Kruger, P. E.; Gunnlaugsson, T. Self-Assembly of Chiral Luminescent Lanthanide Coordination Bundles. *J. Am. Chem. Soc.* **2007**, *129*, 10986−10987.
(39) Lauffer, R. B. Paramagnetic Metal Complexes as Water Proton Relaxation Agents for NMR Imaging: Theory and Design. *Chem. Rev.* **1987**, *87*, 901−927.
(40) Dorazio, S. J.; Tsitovich, P. B.; Siters, K. E.; Spernyak, J. A.; Morrow, J. R. Iron(II) PARACEST MRI Contrast Agents. *J. Am. Chem. Soc.* **2011**, *133*, 14154−14156.
(41) Szpak, A.; Fiejdasz, S.; Prendota, W.; Straczek, T.; Kapusta, C.; Szmyd, J.; Nowakowska, M.; Zapotoczny, S. T_1−T_2 Dual-modal MRI contrast agents based on superparamagnetic iron oxide nanoparticles with surface attached gadolinium complexes. *J. Nanopart. Res.* **2014**, *16*, 2678.
(42) White, D. L.; Aicher, K. P.; Tzika, A. A.; Kucharczyk, J.; Engelstad, B. L.; Moseley, M. E. Iron-dextran as a magnetic susceptibility contrast agent: flow-related contrast effects in the T2-weighted spin-echo MRI of normal rat and cat brain. *Magn. Reson. Med.* **1992**, *24*, 14−28.
(43) Dorazio, S. J.; Morrow, J. R. The Development of Iron(II) Complexes as ParaCEST MRI Contrast Agents. *Eur. J. Inorg. Chem.* **2012**, *2012*, 2006−2014.
(44) Phukan, B.; Patel, A. B.; Mukherjee, C. A water-soluble and water-coordinated Mn(II) complex: synthesis, characterization and phantom MRI image study. *Dalton. Trans.* **2015**, *44*, 12990−12994.
(45) Jha, D. K.; Saikia, K.; Chakrabarti, S.; Bhattacharya, K.; Varadarajan, K. S.; Patel, A. B.; Goyary, D.; Chattopadhyay, P.; Deb, P. Direct one-pot synthesis of glutathione capped hydrophilic FePt-CdS nanoprobe for efficient bimodal imaging application. *Mater. Sci. Eng., C* **2017**, *72*, 415−424.
(46) Jha, D. K.; Shameem, M.; Patel, A. B.; Kostka, A.; Schneider, P.; Erbe, A.; Deb, P. Simple synthesis of superparamagnetic magnetite nanoparticles as highly efficient contrast agent. *Mater. Lett.* **2013**, *95*, 186−189.
(47) Shin, J. W.; Bae, J.; Kim, C.; Min, K. S. Catalysis and molecular magnetism of dinuclear iron(III) complexes with N-(2-pyridylmethyl)-iminodiethanol/-ate. *Dalton Trans.* **2014**, *43*, 3999−4008.
(48) Mähler, J.; Persson, I. A Study of the Hydration of the Alkali Metal Ions in Aqueous Solution. *Inorg. Chem.* **2012**, *51*, 425−438.
(49) Fromm, K. M. Coordination polymer networks with s-block metal ions. *Coord. Chem. Rev.* **2008**, *252*, 856−885.
(50) Mai, J.; Gong, S.; Li, N.; Luo, Q.; Li, Z. A novel class of compounds—superalkalides: $M^+(en)_3M_3'O^-$ (M, M′ = Li, Na, and K; en = ethylenediamine)—with excellent nonlinear optical properties and high stabilities. *Phys. Chem. Chem. Phys.* **2015**, *17*, 28754−28764.
(51) Kottalanka, R. K.; Harinath, A.; Rej, S.; Panda, T. K. Group 1 and group 2 metal complexes supported by a bidentate bulky iminopyrrolyl ligand: synthesis, structural diversity, and ε-caprolactone polymerization study. *Dalton Trans.* **2015**, *44*, 19865−19879.
(52) Kashima, A.; Sakate, M.; Ota, H.; Fuyuhiro, A.; Sunatsukia, Y.; Suzuki, T. Thyminate(2−)-bridged cyclic tetranuclear rhodium(III) complexes formed by a template of a sodium, calcium or lanthanoid ion. *Chem. Commun.* **2015**, *51*, 1889−1892.
(53) Xu, F.; Wang, H.; Teat, S. J.; Liu, W.; Xia, Q.; Li, Z.; Li, J. Synthesis, structure and enhanced photoluminescence properties of two robust, water stable calcium and magnesium coordination networks. *Dalton Trans.* **2015**, *44*, 20459−20463.
(54) Gerey, B.; Gennari, M.; Gouré, E.; Pécaut, J.; Blackman, A.; Pantazis, D. A.; Neese, F.; Molton, F.; Fortage, J.; Duboc, C.; Collomb, M. N. Calcium and heterometallic manganese−calcium complexes supported by tripodal pyridine-carboxylate ligands: structural, EPR and theoretical investigations. *Dalton Trans.* **2015**, *44*, 12757−12770.
(55) Hermann, P.; Kotek, J.; Kubíček, V.; Lukeš, I. Gadolinium(III) complexes as MRI contrast agents: ligand design and properties of the complexes. *Dalton Trans.* **2008**, 3027−3047.
(56) Merbach, A.; Helm, L.; Toth, É. The Chemistry of Contrast Agents in Medical Magnetic Resonance Imaging, 2nd ed.; Wiley: New York, 2001.
(57) Saxena, S. K.; Sharma, H.; Patel, M.; Oreopoulos, D. Nephrogenic systemic fibrosis: an emerging entity. *Int. Urol. Nephrol.* **2008**, *40*, 715−724.
(58) Thakral, C.; Alhariri, J.; Abraham, J. Long-term retention of gadolinium in tissues from nephrogenic systemic fibrosis patient after multiple gadolinium-enhanced MRI scans: case report and implications. *Contrast Media Mol. Imaging* **2007**, *2*, 199−205.
(59) Marckmann, P.; Skov, L.; Rossen, K.; Dupont, A.; Damholt, M.; Heaf, J.; Thomsen, H. Nephrogenic Systemic Fibrosis: Suspected Causative Role of Gadodiamide Used for Contrast-Enhanced Magnetic Resonance Imaging. *J. Am. Soc. Nephrol.* **2006**, *17*, 2359−2362.
(60) Bertini, I.; Capozzi, F.; Luchinat, C.; Xia, Z. Nuclear and electron relaxation of hexaaquairon(3+). *J. Phys. Chem.* **1993**, *97*, 1134−1137.
(61) Bertini, I.; Luchinat, C.; Parigi, G. ^{1}H NMRD Profiles of paramagnetic complexes and metalloproteins. *Adv. Inorg. Chem.* **2005**, *57*, 105−172.
(62) Auerbach, M.; Coyne, D.; Ballard, H. Intravenous iron: From anathema to standard of care. *Am. J. Hematol.* **2008**, *83*, 580−588.
(63) Yi, P.; Chen, G.; Zhang, H.; Tian, F.; Tan, B.; Dai, J.; Wang, Q.; Deng, Z. Magnetic resonance imaging of Fe_3O_4@$SiO_2$$^-$labeled human mesenchymal stem cells in mice at 11.7 T. *Biomaterials* **2013**, *34*, 3010−3019.
(64) Mahmoudi, M.; Hosseinkhani, H.; Hosseinkhani, M.; Boutry, S.; Simchi, A.; Journeay, W. S.; Subramani, K.; Laurent, S. Magnetic Resonance Imaging Tracking of Stem Cells in Vivo Using Iron Oxide Nanoparticles as a Tool for the Advancement of Clinical Regenerative Medicine. *Chem. Rev.* **2011**, *111*, 253−280.

DOI: 10.1021/acs.cgd.7b01588
Cryst. Growth Des. 2018, 18, 531−539

Dalton Transactions

PAPER

View Article Online
View Journal | View Issue

Check for updates

Cite this: *Dalton Trans.*, 2018, **47**, 135

A new heptadentate picolinate-based ligand and its corresponding Gd(III) complex: the effect of pendant picolinate *versus* acetate on complex properties†

Bedika Phukan,[a] Chandan Mukherjee *[a] and Raunak Varshney[b]

Received 3rd November 2017,
Accepted 30th November 2017

DOI: 10.1039/c7dt04150k

rsc.li/dalton

To attain high relaxivity as well as stability, a new water-soluble, water-coordinated Gd(III) complex, which was synthesised by reacting equimolar amounts of picolinate-based ligand **H_4peada** and $GdCl_3{\cdot}xH_2O$ at pH ~ 6.5, was examined. The number of inner sphere water molecules (q) in the complex was found to be 1.7 ± 0.1 from luminescence lifetime measurements of its Tb(III) congener, complex **2**. At 1.41 T, 25 °C, and pH = 7.4, the longitudinal relaxivity (r_1) value of the complex was found to be 6.08 mM^{-1} s^{-1}, which remained almost constant in the pH range 4–10. The r_1 relaxivity value has not been affected in the presence of a 100 fold excess of bicarbonate and phosphate anions, whereas in the case of fluoride ions, the value dropped to 4.6 mM^{-1} s^{-1} due to a binding interaction of fluoride ions by replacing inner sphere water molecules of the complex. From the potentiometric titration method, the stability constant of the complex was found to be log K_{GdL} = 17.0 ± 0.08 (in 0.15 M KCl and 25 °C). At pH = 7.4, the pGd value of ligand **H_4peada** was found to be 14.01 which was comparable to the commercially available MRI contrast agent Omniscan®. Phantom MR images of the complex under a clinical MR scanner at 1.5 T also demonstrated the usefulness of complex **1** as a potential MRI contrast agent.

Introduction

Magnetic resonance imaging (MRI) is one of the most widely used non-invasive modern modalities for imaging anatomical details. It does not involve any ionising radiation and images are obtained by utilising the ^{1}H NMR signals of water molecules present inside the body.[1] The normal contrast in MR images is obtained from the differences in longitudinal (T_1) and transverse (T_2) relaxation times developed in the different environments of the tissues. Nevertheless, in the case of many pathological conditions, the differences in the relaxation times between normal and diseased tissues are not sufficient to contrast them well. Under these circumstances, the contrast can be improved by using an MRI contrast agent (CA) that locally accelerates the relaxation rates of the tissues.[2] On the basis of two types of relaxation processes, contrast agents are divided into two categories: one is the T_1 contrast agent that mainly reduces the longitudinal relaxation time of nearby water molecules resulting in brighter images; and the other is the T_2 contrast agent, which increases the transverse relaxation time and produces darker images. The increase in signal intensities due to the MRI CA is measured in terms of relaxivity, which is defined as the paramagnetic enhancement of the relaxation rate of water protons in the presence of a 1 mM paramagnetic metal ion concentration. A number of paramagnetic metal ions, such as Fe(III) [$3d^5$, S = 5/2], Mn(II) [$3d^5$, S = 5/2], Gd(III) [$4f^7$, S = 7/2], and other lanthanides such as Eu(III), Tb(III), Dy(III) *etc.*, have been employed successfully for the development of MRI CAs.[3]

The unique properties of the Gd(III) ion with its high magnetic moment (S = 7/2), slow electronic relaxation, and high water exchange rate make it ideal for enhancing the image contrast by significantly decreasing the T_1 relaxation time.[4] Currently, ~50% of all MRI scans are made after the administration of a Gd(III)-based CA. To date, monoaquated-Gd(III) complexes of poly(aminocarboxylate) based ligands such as DTPA (diethylenetriaminepentaacetic acid) and DOTA (1,4,7,10-tetraazacyclododecane-1,4,7,10-tetraacetic acid) are most widely used.[5] However, relative to the theoretically attainable maximum, these CAs show lower relaxivity values due to the difference in real and optimal values of the relaxivity-governing parameters such as the number of Gd-coordinated water molecules (q), water exchange rate ($1/\tau_M$), molecular

[a]*Department of Chemistry, Indian Institute of Technology Guwahati, Guwahati-781039, Assam, India. E-mail: cmukherjee@iitg.ernet.in*
[b]*Institute of Nuclear Medicine and Allied Sciences, Brig S. K. Majumdar Road, Delhi-100054, India*

†Electronic supplementary information (ESI) available: NMR spectra of ligand **H_4peada**, IR and mass spectra of complexes **1** and **2**, and the xylenol orange test. See DOI: 10.1039/c7dt04150k

tumbling rate ($1/\tau_R$), and electronic relaxation of the metal centre ($1/T_i$).[6] Therefore, an incessant quest is on going for the development of new and better high relaxivity MRI contrast agents. In this regard, ligands containing picolinate group(s) (Scheme 1) and their corresponding Gd(III) complexes have been investigated as potential MRI CAs.[7] The presence of picolinate group(s) in the ligand backbone plays a pivotal role in elevating the relaxivity value of the corresponding Gd(III) complexes as well as in targeting biological molecules due to its easy functionalization.[8] It has been established that the Gd(III) complexes of picolinate-based ligands have a very high water exchange rate, which in turn is responsible for the high relaxivity value of the complexes. This higher water exchange rate is related to the presence of a very flexible inner coordination sphere around the metal centre.[9]

The Gd(III) complex of octadentate ligand H_4bpeda (Scheme 1) having ethylene diamine as the ligand backbone contains two picolinate groups in it and shows a longitudinal relaxivity value of 5.0 mM^{-1} s^{-1} at 20 MHz, and 25 °C.[10] This value is relatively higher than the commercially available Gd(III) complexes of ligands DOTA and DTPA (r_1 values for $[Gd(DOTA)(H_2O)]^-$ and $[Gd(DTPA)(H_2O)]^{2-}$ are 4.7 and 4.8 mM^{-1} s^{-1}, respectively).[4] However, in spite of the presence of two pyridine units in octadentate ligand H_4bpeda, the stability of its corresponding Gd(III) complex is found to be lower than that of the hexadentate ligand H_4edta. Similarly, the bis(aquated) Gd(III) complex ($[Gd(tpaa)(H_2O)_2]^0$) of heptadentate tripodal ligand H_3tpaa, which is comprised of three picolinate groups (Scheme 1), shows very high relaxivity (13.3 mM^{-1} s^{-1} at 1.41 T, 25 °C), albeit low in stability.[11] When one of the picolinate groups was replaced by a carboxylate group (ligand H_3dpaa, Scheme 1), its corresponding tris(aquated) Gd(III) complex was obtained with high relaxivity at high-field (11.93 mM^{-1} s^{-1} at 4.7 T, 25 °C) as well as higher stability than $[Gd(tpaa)(H_2O)_2]$, despite of a lower coordination number of the employed ligand.[8a] The lower stability of the Gd(III) complexes with an increased number of pyridine units is conjectured as the lower contribution of a metal–nitrogen bond to complex stability.[8g]

Considering the aforementioned facts, herein, in order to attain higher relaxivity as well as better stability, heptadentate ligand **H_4peada** has been designed and synthesised (Scheme 1). The ligand was based on the ethylene diamine backbone where four amine H-atoms were substituted by one picolinate group and three carboxylate pendants. On account of the known oxophilic nature of Gd(III), it was expected that Gd(III) would coordinate more strongly with the four carboxylate oxygen atoms and the picolinate group would assist in a fast water exchange rate. Since Gd(III) can form either eight- or nine-coordinate complexes, ligand **H_4peada**, being heptadentate, might allow two inner sphere water molecules to bind to the metal centre, and consequently higher relaxivity could be achieved as the relaxivity increases with an increase in the number of inner sphere water molecules [hydration state (q)] irrespective of the magnetic field strength.[12] Ligand **H_4peada** upon reacting with $GdCl_3 \cdot xH_2O$ at pH ~ 6.5 provided complex **1**. The thermodynamic stability of the complex was found to be relatively higher compared to the previously reported acyclic picolinate-based analogues.[8f] The hydration state of complex **1** was being determined as 1.7 ± 0.1 by using a surrogate Tb(III) complex (**2**) of the ligand. The water soluble and water coordinated complex **1** showed a high longitudinal relaxivity (r_1) value of 6.08 mM^{-1} s^{-1} at 1.41 T, 25 °C and pH = 7.4, which remained almost unaltered in the pH range 4–10. The effects of physiological anions on complex **1** were also examined by measuring the r_1 relaxivity of the complex in the presence of a 100 fold excess of different anions and included in this study.

Results and discussion

A schematic diagram for the synthesis of ligand **H_4peada** and its corresponding Gd(III) complex (**1**) is given in Scheme 2. *N*,*N*′,*N*′-Tris(*tert*-butyloxycarbonylmethyl)ethylenediamine (**A**)

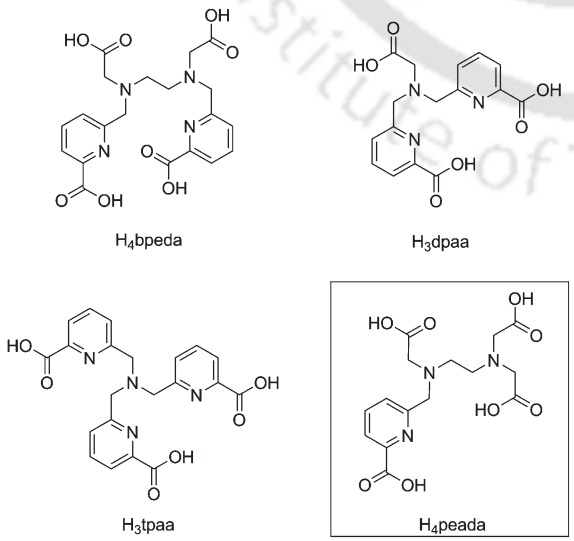

Scheme 1 Structure of picolinate-based ligands discussed in the text.

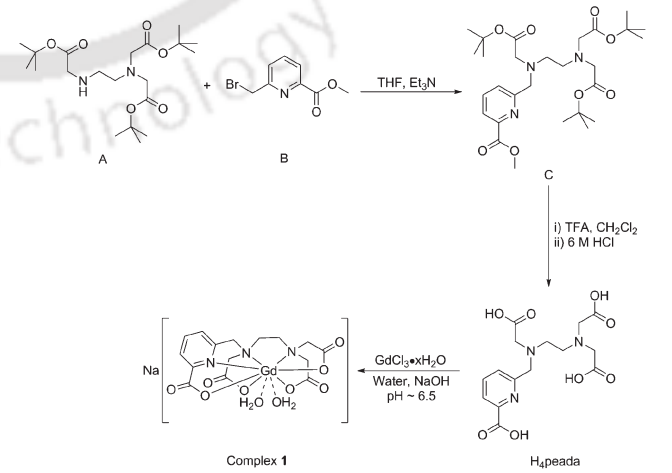

Scheme 2 A schematic representation for the syntheses of **H_4peada** and complex **1**.

and 6-(bromomethyl)pyridine-2-carboxylate (**B**) were prepared according to the reported methods.[13] A reaction between equimolar amounts of **A** and **B** in the presence of Et_3N provided O-protected ligand **C** in 69% yield. The ligand **H_4peada** was obtained as a pale yellow solid in 69% yield after the successive treatment of **C** with trifluoroacetic acid and 6 M HCl. The synthesis of complex **1** was carried out by reacting the ligand with an equivalent amount of $GdCl_3{\cdot}xH_2O$ in water followed by the adjustment of pH ~ 6.5 with aq. NaOH. Slow evaporation of the reaction mixture at room temperature (25 °C) provided the complex as a white solid.

Crystallization of complex **1** from pure water or various other organic solvent mixtures did not provide single crystals suitable for XRD analysis. Thus, to find out the number of inner sphere water molecules (q) in complex **1**, its Tb(III) congener (complex **2**) with luminescence properties was synthesised by reacting 1 : 1 ligand **H_4peada** and $TbCl_3{\cdot}6H_2O$ in water at pH ~ 6.5 under refluxing conditions. The $^7F_6 \rightarrow {}^5D_4$ transition in the Tb(III) congener of the Gd(III) chelates permits the determination of the number of coordinated water molecules (q) *via* time dependent luminescence lifetime decay.[14] O–H oscillators are found to be the most efficient quenchers of metal-centred luminescence both in solution and in the solid state. When the O–H oscillator is replaced by O–D in a deuterated solvent, it results in less efficient quenching of the lanthanide excited states. Hence, in D_2O, the luminescence lifetimes of lanthanides are much longer than those in H_2O.

The number of inner sphere water molecules in complex **1** was confirmed by measuring the luminescence lifetime of complex **2** in H_2O and D_2O (at pH = 7.4 and 25 °C). Both the solutions were excited at 270 nm and the luminescence decay curves were recorded at the emission intensity of 544 nm. The luminescence lifetimes (τ) of complex **2** in H_2O (τ_{H_2O} = 1.21 ms) and D_2O (τ_{D_2O} = 2.31 ms) were obtained by exponential-decay fitting of the experimental curves (Fig. 1). By using modified Horrock's equation for the Tb(III) complex:[15]

$$q = 5(1/\tau_{H_2O} - 1/\tau_{D_2O} - 0.06)$$

the number of inner sphere water molecules in complex **1** was found to be 1.7 ± 0.1, which implied that about 70% of the complex existed in the solution in its bis(aquated) form. Herein, it is worth noting that the Gd(III)-complex of the analogous ligand with a cyclohexane backbone[12a] has been reported to exist in solution in a fully bis(aquated) form. The coexistence of both mono(aquated) and bis(aquated) forms might be because of the lower energy barrier for the conversion of the complex from its nine-coordinate to eight-coordinate form and the phenomenon was supported by the flexible ligand-coordination environment.[10,16]

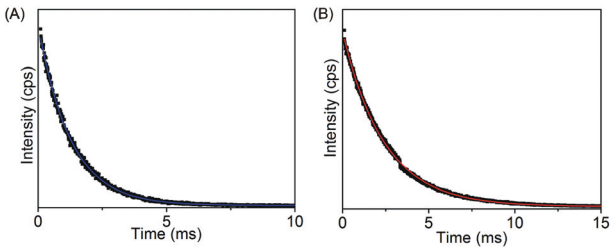

Fig. 1 Luminescence lifetime measurements of complex **2** in (A) H_2O and (B) D_2O.

To ensure thermodynamic stability, stepwise protonation constants of ligand **H_4peada** as well as the stability of its corresponding Gd(III) complex (complex **1**) were determined by pH potentiometric titration in 0.15 M KCl at 25 °C. The protonation constants of ligand **H_4peada** are defined by the equation:

$$K_i^H = [H_iL]/[H_{i-1}L][H^+] \quad i = 1, 2, 3, 4, ...$$

The protonation constants of the ligand were determined to be $\log K_1^H$ = 2.9, $\log K_2^H$ = 5.6, $\log K_3^H$ = 8.5, and $\log K_4^H$ = 10.2 (Table 1). Comparing these values to the previously reported ligand H_4edta and picolinate based analogues of ligand **H_4peada** (Table 1), the protonation constants at 10.2, 8.5 and 5.6 could be assigned to the protonation of N-atoms present in the ligand backbone (Table 1 and references therein). The lowest value of the protonation constant at 2.9 could be due to the protonation of the carboxylate group of the picolinate

Table 1 Protonation constants, stability constants and pGd values for **H_4peada** and its analogues

Ligand	$\log K_i^H$	$\sum \log K_i^H$	$\log K_{GdL}$	pGd[b]
H_4peada[a]	10.2, 8.5, 5.6, 2.9	27.20	17.0	14.0
H_4edta[c]	10.08, 6.42, 3.11, 2.33	21.94	17.7	15.3
H_4bpeda[d]	8.5, 5.2, 3.5, 2.9	20.10	15.1	14.9
H_3dpaa[e]	7.33, 3.8, 2.9	14.03	10.6	12.3
H_3tpaa[e]	4.11, 3.3, 2.5	9.91	10.2	11.2
H_3mpatcn[f]	10.4, 5.57, 3.89, 2.95, 2.20	25.01	13.9	11.8
H_4dpaba[f]	7.13, 4.38, 3.83, 3.2	18.54	12.5	13.3
H_3ebpatcn[g]	10.40, 5.60, 4.25, $\sum \log K_{1,2}^H$ = 5.0	25.25	15.10	13.1
H_3tpatcn[f]	10.8, 5.7, 3.8, 3.0, 2.5	25.8	17.4	14.9
H_3bpatcn[h]	10.5, 5.42, 3.71, 2.3, 2.2	24.12	15.8	13.6
H_5dtpa(bma)[c]	9.37, 4.38, 3.31, 1.43	18.49	16.85	15.8

[a] This work (I = 0.15 M KCl and 25 °C). [b] pGd values were defined as $-\log[Gd(III)]_{free}$ at pH = 7.4 and 25 °C having [Gd(III)] = 1 μM and $[ligand]_{total}$ = 10 μM. [c] From ref. 17. [d] From ref. 8*g*. [e] From ref. 8*a*. [f] From ref. 8*f*. [g] From ref. 8*d*. [h] From ref. 18.

moiety. However, protonation of the other three acetate groups occurs at a much lower pH and could not be determined.

The stability constant of complex **1** was also determined under the same conditions as those for protonation constant determination which is defined by the equation:

$$K_{GdL} = [GdL]/[Gd][L]$$

In 0.15 M KCl at 25 °C, the stability constant of the complex ($\log K_{GdL}$) was found to be 17.0 ± 0.08. The value, which is higher than that of ligand H_4bpeda and comparable to that of ligand H_4edta (Table 1), consolidated that in the case of Gd(III) complexes of picolinate based ligands, an increase in picolinate group(s) in the ligand backbone do not impart any contribution to the stability, rather it gets decreased. The increase in the total basicity ($\sum \log K_i^H$) of ligand **H_4peada** was about 7 $\log K$ units higher compared to ligand H_4bpeda and could be argued as the factor for the higher stability of complex **1**. A comparison of the stability constant values of Gd(III) complexes of ligands H_3dpaa ($\log K_{GdL}$ = 10.6(2)) and H_3tpaa ($\log K_{GdL}$ = 10.2(2)) also revealed a lack of contribution of the pyridyl group to the stability of the complexes. The species distribution diagram of Gd(III) : **H_4peada** (1 : 1) solution, in 0.15 M KCl and 25 °C is shown in Fig. 2.

When used under physiological conditions, the pM value of a metal–ligand complex is considered to be more precise for describing the stability of a complex, where pM is $-\log[M^{n+}]_{free}$ at pH = 7.4, 25 °C having [M] = 1 μM and $[L]_{total}$ = 10 μM.[19] The pGd value for ligand **H_4peada** was found to be 14.01, which was although slightly lower than the pGd value of ligands H_4bpeda and H_4edta, but higher than most of the previously reported picolinate based Gd(III) complexes, except for the nine-coordinated Gd(III) complex of ligand H_3tpatcn (Table 1). Additionally, the pGd and the $\log K_{GdL}$ of complex **1** implied a good physiological stability while compared with the commercially available MRI contrast agent Omniscan® ([Gddtpa(bma)$(H_2O)]^-$, pGd = 15.8 and $\log K_{GdL}$ = 16.85).[17]

The longitudinal relaxivity (r_1) of complex **1** was measured at 1.41 T, 25 °C, and pH = 7.4 using a BRUKER minispec mq60 NMR analyzer. By using the inversion recovery method, at four

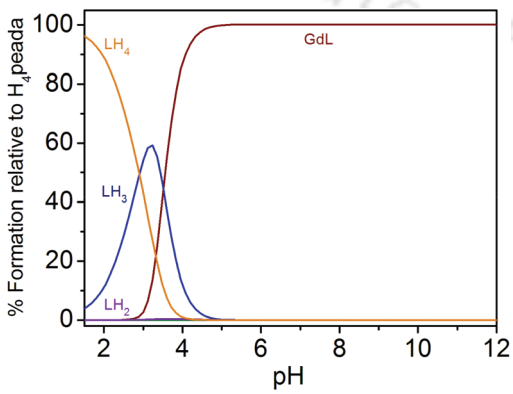

Fig. 2 Species distribution diagram of Gd(III) : **H_4peada** (1 : 1) solution, [ligand] = [Gd(III)] = 10^{-3} M (L in the figure refers to ligand **H_4peada**).

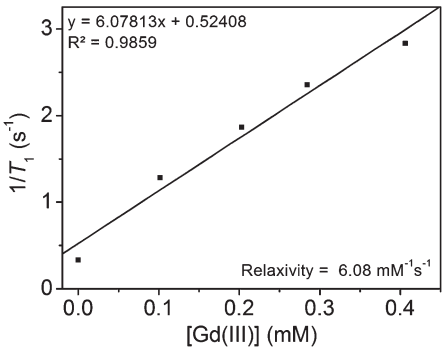

Fig. 3 $1/T_1$ *vs.* [Gd(III)] plot. Measurements were performed using complex **1** at 1.41 T, 25 °C, and pH = 7.4.

different concentrations of the complex, the longitudinal relaxation times (T_1) were recorded. The r_1 relaxivity of the complex was found to be 6.08 mM^{-1} s^{-1} per Gd(III) ion (Fig. 3) from the slope of the longitudinal relaxation rate (*i.e.*, $R1 = 1/T_1$) *vs.* [Gd(III)] plot. The exact concentration of Gd(III) ions in the solutions was determined by the ICP-AES method. In accordance with the expectation, the relaxivity value of complex **1** with q = 1.7 ± 0.1 was higher compared to the reported mono(aquated), monomeric Gd(III)-based MRI CAs (r_1 = 2.9–5.2 mM^{-1} s^{-1})[4,12a] and almost the same or comparable with the bis(aquated) monomeric Gd(III)-based MRI CAs (r_1 = 5.7–7.5 mM^{-1} s^{-1}).[4,12a]

In the pH range 4–10, the r_1 relaxivity values of complex **1** were measured at 1.41 T and 25 °C (Fig. 4(A)). A negligible increase in the r_1 relaxivity value was observed towards lower pH (at pH = 4, Δr_1 = +0.16 mM^{-1} s^{-1}, 2.6%), while at pH 10, the r_1 relaxivity value decreased to 5.17 mM^{-1} s^{-1} from 6.08 mM^{-1} s^{-1}. This 15% decrease in relaxivity could be due to the formation of hydroxy species at higher pH by replacing inner sphere water molecules.[8a]

In the history of MRI CAs, the Gd(III) complex of the H_4edta ligand was one of the prime candidates to be explored as a potential MRI CA. Although, structural modifications on the H_4edta ligand backbone overcame the drawbacks related to its lower denticity, the formation of ternary complexes upon exposure to biological matrices could not be eliminated by these modifications.[4] The replacement of coordinated water molecules by various endogenous anions, which are present in blood serum in non-negligible amounts, results in a sharp

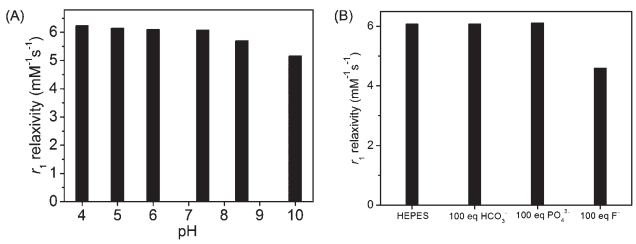

Fig. 4 (A) r_1 relaxivity changes of complex **1** in the pH range 4–10, at 1.41 T and 25 °C. (B) Relaxivity measurements of complex **1** in the presence of 100 equivalents of different anions (at 1.41 T, 25 °C, pH ~ 7.4, [complex **1**] = 0.5 mM, and [physiological anions] = 50 mM).

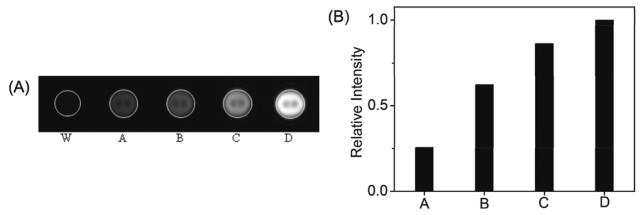

Fig. 5 (A) T_1-Weighted phantom MR images of complex **1** at 1.5 T, 25 °C, pH ~ 7.4 (W = water, *A* = 0.25 mM, *B* = 0.50 mM, *C* = 0.70 mM, *D* = 1.00 mM); (B) comparison of MR image intensity by ImageJ software.

decrease in the relaxivity value with the formation of these ternary adducts. Therefore, it is very important for the Gd(III) complexes to have less affinity towards these anions to use them in a biological setting. Thus, the affinity of complex **1** for PO_4^{3-}, HCO_3^-, and F^- ions was investigated by measuring r_1 relaxivity values of the complex in the presence of 100 fold excess of the respective anions (experimental conditions: 1.41 T, 25 °C, pH ~ 7.4, [complex **1**] = 0.5 mM, [physiological anions] = 50 mM). While the respective concentrations of PO_4^{3-} and HCO_3^- ions in blood serum are 0.38 mM and 24.5 mM, because of the strong affinity of serum F^- ions for lanthanides and the formation of a stable complex,[20] the F^- ions were also included in this study. The results are depicted as a bar diagram in Fig. 4(B). The r_1 relaxivity values remained almost unaltered in the case of PO_4^{3-} and HCO_3^- ions, whereas in the case of F^- ions, the value dropped to 4.60 mM^{-1} s^{-1} (Δr_1 = 1.48 mM^{-1} s^{-1}; 24%). The mononegative charge of the metal-coordination unit in complex **1** restricted the approach of bulky anions to the metal centre, however, the small F^- ion interacted with the metal ion and refrained water molecules to coordinate to the Gd(III) centre.

The effectiveness of complex **1** as a T_1 MRI CA was further evaluated by obtaining MR images of the complex under a clinical MRI scanner. At 1.5 T, 25 °C, pH ~ 7.4, under a BRIVO MR355 MR scanner, at four different concentrations of the complex, T_1-weighted phantom MR images were obtained and are depicted in Fig. 5(A). The image intensities increased with the increase in complex concentration. A comparison of the image intensities under the same area of the images was done by using ImageJ software and is shown in Fig. 5(B).

Conclusions

To study the effect of picolinate *vs.* acetate pendant on the stability of Gd(III) complexes of ligands having ethylene diamine as the backbone, we have reported a new heptadentate, mono(picolinate)-based ligand **H_4peada** and its corresponding Gd(III) complex, (**1**). The stability constant measurement showed that complex **1** was more stable compared to the previously reported Gd(III) complex of the octadentate, bis(picolinate) H_4bpeda ligand. The finding implied that a strong interaction prevailed between the carboxylate oxygen atom and highly oxophilic Gd(III) centre compared to the picolinate to Gd(III) interactions. The number of inner sphere water molecules in the complex was found to be 1.7 ± 0.1 from luminescence lifetime measurements of its Tb(III) congener (complex **2**). This implied the presence of 70% bis(aquated) complex **1** in the solution state at pH = 7.4 and 25 °C.

At 1.41 T, 25 °C and pH = 7.4, the complex showed an r_1 relaxivity value of 6.08 mM^{-1} s^{-1}, which was almost constant in the pH range 4–10. While the formation of ternary adducts restricted the use of Gd(III) complexes of the H_4etda ligand as potential MRI contrast agents, the replacement of one acetate group with one picolinate group in **H_4peada** overcame these limitations with almost constant r_1 relaxivity values of complex **1** even in the presence of a 100 fold excess of physiological anions. To make the system more biocompatible by elevating the stability of the complex, investigation of the pyridine-*N*-oxide derivative of the ligand and its corresponding Gd(III) complex is currently in progress in our laboratory.

Experimental

Materials and methods

All the chemicals and solvents were obtained from commercial sources and were used as supplied, unless noted otherwise. Ethylenediamine, *tert*-butylbromoacetate and TFA were purchased from Spectrochem. $KHCO_3$, Et_3N and solvents were obtained from Merck (India). HEPES buffer was purchased from SRL. $GdCl_3{\cdot}xH_2O$, $TbCl_3{\cdot}6H_2O$ and 2,6-pyridinedicarboxylic acid were purchased from Sigma-Aldrich. Water used for the experiments was purified by using a Millipore-water purifier, Milli-Q, Merck.

FT-IR spectra were recorded on a PerkinElmer Instrument at normal temperature using a KBr pellet prepared by grinding the sample with KBr (IR Grade). UV–vis spectra were recorded on a PerkinElmer, Lambda 25, UV/VIS spectrometer. Mass spectral data were obtained using a HRMS Spectrometer. ^1H and ^{13}C NMR analyses were carried out using Varian Mercury Plus 400 MHz, BRUKER 600 MHz and 300 MHz NMR machines. The longitudinal (r_1) relaxivity at 1.41 T was measured using a BRUKER minispec mq60 NMR Analyzer. MRI images at 1.5 T were collected using a BRIVO MR355 MRI Scanner.

Luminescence lifetime measurements in H_2O and D_2O

A 10 μM solution of complex **2** in 10 mM HEPES buffer (pH 7.4), 25 °C was used for the lifetime measurements. The solution was excited at 270 nm with a pulsed xenon lamp having a pulse width of ~3 μs and time per pulse 61 ms. Emission at 544 nm was recorded and a luminescence decay curve was generated by the 'decay by delay' method with an initial delay of 0.1 ms and a maximum delay of 10 ms. The decay curve was fitted with a single exponential model using the non-linear least squares method and goodness of the fits were determined by minimizing the reduced chi^2 values. The above solution was then evaporated completely by spin concentration under reduced pressure and kept overnight in a vacuum desiccator. The addition of equal volume of D_2O to

the completely dry residue resulted in a solution of the same concentration as that of the complex **2** in D_2O buffer. All transfers of the D_2O containing sample were performed inside a glove bag under an argon atmosphere to avoid the contamination of moisture (H_2O) and lifetime measurements were done in a cuvette, sealed under argon using the identical instrument parameters as previously described (maximum delay in the case of D_2O measurement was 15 ms).

Potentiometric measurements

$GdCl_3$ stock solution was prepared in the range 0.01–0.001 M by dissolving $GdCl_3{\cdot}xH_2O$ in double distilled water, and their concentration was determined by complexometric titration with standardized Na_2H_2edta and xylenol orange as the indicator. A 0.001 M stock solution of ligand **H_4peada** and the corresponding Gd(III) complex were prepared for kinetics. 0.1 M tetra-butyl ammonium hydroxide (TBAOH) and 0.15 M KCl were also prepared for titration. The protonation constants and stability constant were determined using pH potentiometry by titrating 0.1 mM ligand solution with standardized tetra-butyl ammonium hydroxide (TBAOH) solution at 25 °C using a Metrohm Dosimat 713 pH meter equipped with a Metrohm glass electrode, 800 Dosino autoburet. Titrations were performed in the pH range 1.5–12.5 for all equilibrium measurements (direct titrations) which were carried out in 20 mL sample volumes with magnetic stirring after the calibration of the electrode was done using standard buffers (pH 4, 7 and 9). The stability constant of complex **1** was determined under the same conditions as those for the protonation constant calculations. The protonation and stability constant were evaluated from the titration data using the program TIAMO 2.0 by Metrohm India Ltd.

Synthesis of $[C_{28}H_{45}N_3O_8]$, (C)

N,*N*′,*N*′-Tris(*tert*-butyloxycarbonylmethyl)ethylenediamine (**A**) and 6-(bromomethyl)pyridine-2-carboxylate (**B**) were prepared by using reported procedures. To a stirred solution of compound **A** (0.536 g, 1.33 mmol) and Et_3N (0.37 ml, 2.66 mmol) in THF (10 mL) was added compound **B** (0.337 g, 1.46 mmol) and the reaction mixture was stirred at room temperature (25 °C) for 24 h. The solvent was then removed *in vacuo* and the residue was partitioned between CH_2Cl_2 (10 mL) and aq. $NaHCO_3$ (10 mL) solution. The aqueous phase was washed with CH_2Cl_2 (3 × 10 mL), and the combined organic extracts were dried over anhydrous Na_2SO_4. The solvents were evaporated *in vacuo* and the crude compound was purified by column chromatography on silica gel (hexane/ethyl acetate, 1 : 1) to afford the ester-protected precursor as a colourless oil. Yield = 0.506 g, 69%. FTIR (KBr, cm^{-1}): 3437, 2979, 2932, 2853, 1742, 1591, 1462, 1374, 1218, 1157, 995, 848, 764, 678. ^{1}H NMR ($CDCl_3$, 600.17 MHz): δ 7.99 (d, J = 6 Hz, 1H), 7.88 (d, J = 6 Hz, 1H), 7.80 (t, J = 6 Hz, 1H), 4.03 (s, 2H), 3.98 (s, 3H), 3.42 (s, 4H), 3.35 (s, 2H), 2.85 (t, J = 6 Hz, 2H), 2.81 (t, J = 6 Hz, 2H), 1.44 (s, 9H), 1.42 (s, 18H) ppm. ^{13}C NMR ($CDCl_3$, 100.55 MHz): δ 170.7, 166.0, 161.0, 147.2, 137.4, 126.2, 123.5, 81.0, 60.6, 56.4, 56.1, 52.9, 52.2, 28.3, 28.1 ppm. ESI-MS (+) m/z for $[C_{28}H_{45}N_3O_8 + H]^+$: calcd, 552.3279; found, 552.3284.

Synthesis of $[C_{15}H_{19}N_3O_8]$, H_4peada

To compound **C** (0.421 g, 0.76 mmol), a solution of CH_2Cl_2/TFA (1 : 1, 4 mL) was added and the reaction mixture was stirred at room temperature (25 °C) for 16 h. The solvent was then evaporated completely *in vacuo* and diethyl ether was added. A white solid was obtained which was again dissolved in 6 M HCl and refluxed for 48 h. The solvent was then completely evaporated to dryness and the ligand **H_4peada** was obtained as a pale yellow solid by adding excess diethyl ether. The ligand was then filtered, washed thoroughly with diethyl ether and dried under high vacuum. Yield = 0.195 g, 69%. FTIR (KBr, cm^{-1}): 3413, 3392, 2976, 2592, 1735, 1627, 1414, 1262, 1199, 764, 658. ^{1}H NMR (CD_3OD, 399.85 MHz): δ 8.39–8.32 (m, 2H), 8.06 (d, J = 4 Hz, 1H), 4.79 (s, 2 H), 4.42 (s, 4H), 4.18 (s, 2H), 4.00–3.97 (m, 2H), 3.82–3.79 (m, 2H) ppm. ^{13}C NMR (CD_3OD, 75.5 MHz): δ 172.6, 170.9, 166.7, 155.5, 148.4, 140.3, 128.8, 126.0, 58.9, 55.7, 55.4, 53.6, 53.1 ppm. ESI-MS (+) m/z for $[C_{15}H_{19}N_3O_8 + H]^+$: calcd, 370.1244; found, 370.1258.

Synthesis of $[C_{15}H_{18}GdN_3O_{10}]$, complex 1

To a solution of **H_4peada** (0.112 g, 0.30 mmol) in water (3 mL) was added $GdCl_3{\cdot}xH_2O$ (0.075 g, 0.28 mmol) and stirred until the solution became transparent. The pH of the solution was adjusted to ~6.5 by adding aq. NaOH solution dropwise. Stirring was continued at room temperature (25 °C) for 24 h. The resulting clear solution was kept at room temperature for slow evaporation of water. The white solid obtained was washed thoroughly with MeOH and the absence of free Gd(III) ions was confirmed by the xylenol orange test. Yield = 0.093 g, 53%. FTIR (KBr, cm^{-1}): 3396, 1630, 1433, 1394, 1020, 924, 769, 666, 597. ESI-MS (−) m/z for $[C_{15}H_{15}GdN_3O_8]^-$: calcd, 523.0057; found, 523.0028.

Synthesis of $[C_{15}H_{18}TbN_3O_{10}]$, complex 2

To a solution of **H_4peada** (0.125 g, 0.34 mmol) in water (3 mL) was added $TbCl_3{\cdot}6H_2O$ (0.118 g, 0.32 mmol) and the solution was stirred for 5 min. The pH of the solution was adjusted to ~6.5 by adding aq. NaOH solution dropwise. The solution was refluxed for 24 h and the resulting clear solution was kept at room temperature (25 °C) for slow evaporation of water. The white solid obtained was washed thoroughly with MeOH. Yield = 0.109 g, 55%. FTIR (KBr, cm^{-1}): 3427, 1596, 1447, 1395, 1312, 1266, 1090, 990, 811, 717, 644. ESI-MS (−) m/z for $[C_{15}H_{15}TbN_3O_8]^-$: calcd, 524.0113; found, 524.0112.

Conflicts of interest

There are no conflicts to declare.

Acknowledgements

This project is funded by the Department of Biotechnology and the Department of Science & Technology Govt. of India.

BP thanks IIT Guwahati, India for doctoral fellowship. CM is indebted to Dr Baijayanta Saharia, Director, Department of Radiology and Imaging, GNRC Hospital, Guwahati, India for MRI image measurements at 1.5 T and Dr Anjani Tiwari, INMAS, Delhi, India, for potentiometric measurements. BP and CM thankfully acknowledge the Department of Chemistry, IIT Guwahati and CIF, IIT Guwahati for the instrumental facilities.

Notes and references

1 (*a*) P. Caravan, *Chem. Soc. Rev.*, 2006, **35**, 512; (*b*) P. Caravan, J. J. Ellison, T. J. McMurry and R. B. Lauffer, *Chem. Rev.*, 1999, **99**, 2293; (*c*) R. B. Lauffer, *Chem. Rev.*, 1987, **87**, 901; (*d*) K. N. Raymond and V. C. Pierre, *Bioconjugate Chem.*, 2005, **16**, 3; (*e*) P. Hermann, J. Kotek, V. Kubíček and I. Lukeš, *Dalton Trans.*, 2008, **23**, 3027; (*f*) S. Laus, R. Ruloff, E. Tóth and A. E. Merbach, *Chem. – Eur. J.*, 2003, **9**, 3555; (*g*) P. Caravan, *Acc. Chem. Res.*, 2009, **42**, 851; (*h*) D. J. Mastarone, V. S. R. Harrison, A. L. Eckermann, G. Parigi and T. J. Meade, *J. Am. Chem. Soc.*, 2011, **133**, 5329; (*i*) E. Terreno, D. D. Castelli, A. Viale and S. Aime, *Chem. Rev.*, 2010, **110**, 3019; (*j*) E. Boros, M. Polasek, Z. Zhang and P. Caravan, *J. Am. Chem. Soc.*, 2012, **134**, 19858; (*k*) A. Datta and K. N. Raymond, *Acc. Chem. Res.*, 2009, **42**, 938; (*l*) N. Rastogi, N. Tyagi, O. Singh, B. S. H. Kumar, U. P. Singh, K. Ghosh and R. Roy, *J. Inorg. Biochem.*, 2017, **117**, 76; (*m*) D. Messeri, M. P. Lowe, D. Parker and M. Botta, *Chem. Commun.*, 2001, 2742.

2 (*a*) M. H. Mendonça-Dias, E. Gaggelli and P. C. Lauterbur, *Semin. Nucl. Med.*, 1983, **13**, 364; (*b*) J. M. Major and T. J. Meade, *Acc. Chem. Res.*, 2009, **42**, 893; (*c*) S. Aime, M. Botta, M. Fasano and E. Terreno, *Chem. Soc. Rev.*, 1998, **27**, 19.

3 (*a*) B. Drahoš, I. Lukeš and É. Tóth, *Eur. J. Inorg. Chem.*, 2012, 1975; (*b*) S. Aime, M. Botta, M. Fasano and E. Terreno, *Chem. Soc. Rev.*, 1998, **27**, 19; (*c*) A. J. L. Villaraja, A. Bumb and M. W. Brechbiel, *Chem. Rev.*, 2010, **110**, 2921; (*d*) S. Aime, A. Barge, D. D. Castelli, F. Fedeli, A. Mortillaro, F. U. Nielsen and E. Terreno, *Magn. Reson. Med.*, 2002, **47**, 639; (*e*) G. Han, Y. Deng, J. Sun, J. Ling and Z. Shen, *Exp. Ther. Med.*, 2015, **9**, 1561; (*f*) G. Liu, Y. Li and M. D. Pagel, *Magn. Reson. Med.*, 2007, **58**, 1249; (*g*) S. M. Rocklage and A. D. Watson, *J. Magn. Reson. Imaging*, 1993, **3**, 167.

4 A. Merbach, L. Helm and É. Tóth, *The Chemistry of Contrast Agents in Medical Magnetic Resonance Imaging*, Wiley, New York, 2nd edn, 2001.

5 (*a*) K. W.-Y. Chan, S. Barra, M. Botta and W.-T. Wong, *J. Inorg. Biochem.*, 2004, **98**, 677; (*b*) S. Gu, H.-K. Kim, G. H. Lee, B.-S. Kang, Y. Chang and T.-J. Kim, *J. Med. Chem.*, 2011, **54**, 143.

6 (*a*) E. Boros, E. M. Gale and P. Caravan, *Dalton Trans.*, 2005, **44**, 4804; (*b*) V. C. Pierre, M. J. Allen and P. Caravan, *J. Biol. Inorg. Chem.*, 2014, **19**, 127; (*c*) E. Boros and P. Caravan, *Inorg. Chem.*, 2015, **54**, 2403.

7 (*a*) J. Costa, É. Tóth, L. Helm and A. E. Merbach, *Inorg. Chem.*, 2005, **44**, 4747; (*b*) P. Verwilst, S. Park, B. Yoon and J. S. Kim, *Chem. Soc. Rev.*, 2015, **44**, 1791; (*c*) Z. Zhang, M. T. Greenfield, M. Spiller, T. J. McMurry, R. B. Lauffer and P. Caravan, *Angew. Chem., Int. Ed.*, 2005, **44**, 6766.

8 (*a*) A. Nonat, P. H. Fries, J. Pècaut and M. Mazzanti, *Chem. – Eur. J.*, 2007, **13**, 8489; (*b*) A. Nonat, C. Gateau, P. H. Fries and M. Mazzanti, *Chem. – Eur. J.*, 2006, **12**, 7133; (*c*) M. Mato-Iglesias, C. Platas-Iglesias, K. Djanashvili, J. A. Peters, É. Toth, E. Balogh, R. N. Muller, L. V. Elst, A. de Blas and T. Rodríguez-Blas, *Chem. Commun.*, 2005, 4729; (*d*) A. Nonat, M. Giraud, C. Gauteau, P. H. Fries, L. Helm and M. Mazzanti, *Dalton Trans.*, 2009, 8033; (*e*) C. Platas-Iglesias, M. Mato-Iglesias, K. Djanashvili, R. N. Muller, L. V. Elst, J. A. Peters, A. de Blas and T. Rodríguez-Blas, *Chem. – Eur. J.*, 2004, **10**, 3579; (*f*) A. Nonat, C. Gateau, P. H. Fries, L. Helm and M. Mazzanti, *Eur. J. Inorg. Chem.*, 2012, 2049; (*g*) N. Chatterton, C. Gateau, M. Mazzanti, J. Pècaut, A. Borel, L. Helm and A. Merbach, *Dalton Trans.*, 2005, 1129.

9 (*a*) Md. N. Khan, S. Pal, T. Parvinb and L. H. Choudhury, *RSC Adv.*, 2012, **2**, 12305; (*b*) G. Bringmann, Y. Reichert and V. V. Kane, *Tetrahedron*, 2004, **60**, 3539; (*c*) B. B. Fredholm, A. P. Izerman, K. A. Jacobson, K. N. Klotz and J. Linden, *Pharmacol. Rev.*, 2001, **53**, 527.

10 E. Balogh, M. Mato-Iglesias, C. Plates-Iglesias, É. Tóth, K. Djanashvili, J. A. Peters, A. de Blas and T. Rodríguez-Blas, *Inorg. Chem.*, 2006, **45**, 8719.

11 Y. Bretonniere, M. Mazzanti, J. Pecaut, F. A. Dunand and A. E. Merbach, *Chem. Commun.*, 2001, 621.

12 (*a*) E. M. Gale, N. Kenton and P. Caravan, *Chem. Commun.*, 2013, **49**, 8060; (*b*) E. J. Werner, J. Kozhukh, M. Botta, E. G. Moore, S. Avedano, S. Aime and K. N. Raymond, *Inorg. Chem.*, 2009, **48**, 277; (*c*) J. Xu, S. J. Franklin, D. W. Whisenhunt Jr. and K. N. Raymond, *J. Am. Chem. Soc.*, 1995, **117**, 7245; (*d*) C. J. Jocher, M. Botta, S. Avedano, E. G. Moore, J. Xu, S. Aime and K. N. Raymond, *Inorg. Chem.*, 2007, **46**, 4796; (*e*) E. J. Werner, S. Avedano, M. Botta, B. P. Hay, E. G. Moore, S. Aime and K. N. Raymond, *J. Am. Chem. Soc.*, 2007, **129**, 1870.

13 (*a*) T. Storr, B. R. Cameron, R. A. Gossage, H. Yee, R. T. Skerlj, M. C. Darkes, S. P. Fricker, G. J. Bridger, N. A. Davis, M. T. Wilson, K. P. Maresca and J. Zubieta, *Eur. J. Inorg. Chem.*, 2005, 2685; (*b*) Y.-Y. Zhu, C.-W. Liu, J. Yin, Z.-S. Meng, Q. Yang, J. Wang, T. Liu and S. Gao, *Dalton Trans.*, 2015, 20906; (*c*) V. Chandrasekhar, S. Hossain, S. Das, S. Biswas and J.-P. Sutter, *Inorg. Chem.*, 2013, **52**, 6346; (*d*) E. W. Price, J. F. Cawthray, G. A. Bailey, C. L. Ferreira, E. Boros, M. J. Adam and C. Orvig, *J. Am. Chem. Soc.*, 2012, **134**, 8670.

14 (*a*) G. R. Choppin and D. R. Peterman, *Coord. Chem. Rev.*, 1998, **174**, 283; (*b*) J. G. Bünzli and C. Piguet, *Chem. Soc. Rev.*, 2005, **34**, 1048; (*c*) W. D. Horrocks Jr. and D. R. Sudnick, *Acc. Chem. Res.*, 1981, **14**, 384; (*d*) L. M. Manus, R. C. Strauch, A. H. Hung, A. L. Eckermann and T. J. Meade, *Anal. Chem.*, 2012, **84**,

6278; (*e*) S. Faulkner, S. J. A. Pope and B. P. Burton-Pye, *Appl. Spectrosc. Rev.*, 2005, **40**, 1.

15 A. Beeby, I. M. Clarkson, R. S. Dickins, S. Faulkner, D. Parker, L. Royle, A. S. de Sousa, J. A. G. Williams and M. Woods, *J. Chem. Soc., Perkin Trans. 2*, 1999, 493.

16 V. C. Pierre, M. Botta, S. Aime and K. N. Raymond, *J. Am. Chem. Soc.*, 2006, **128**, 5344.

17 L. Moriggi, C. Cannizzo, C. Prestinari, F. Berrière and L. Helm, *Inorg. Chem.*, 2008, **18**, 8357.

18 G. Nocton, A. Nonat, C. Gateau and M. Mazzanti, *Helv. Chim. Acta*, 2009, **92**, 2257.

19 (*a*) D. M. J. Doble, M. Melchior, B. O'Sullivan, C. Siering, J. Xu, V. C. Pierre and K. N. Raymond, *Inorg. Chem.*, 2003, **42**, 4930; (*b*) C. J. Jocher, M. Botta, S. Avedano, E. G. Moore, J. Xu, S. Aime and K. N. Raymond, *Inorg. Chem.*, 2007, **46**, 4796; (*c*) C. J. Jocher, E. G. Moore, J. Xu, S. Avedano, M. Botta, S. Aime and K. N. Raymond, *Inorg. Chem.*, 2007, **46**, 9182; (*d*) E. J. Werner, J. Kozhukh, M. Botta, E. G. Moore, S. Avedano, S. Aime and K. N. Raymond, *Inorg. Chem.*, 2009, **48**, 277; (*e*) D. T. Puerta, M. Botta, C. J. Jocher, E. J. Werner, S. Avedano, K. N. Raymond and S. M. Cohen, *J. Am. Chem. Soc.*, 2006, **128**, 2222; (*f*) V. C. Pierre, M. Botta, S. Aime and K. N. Raymond, *Inorg. Chem.*, 2006, **45**, 8355.

20 M. Botta, S. Aime, A. Barge, G. Bobba, R. S. Dickins, D. Parker and E. Terreno, *Chem. – Eur. J.*, 2003, **9**, 2102.

Inorganic Chemistry
Cite This: Inorg. Chem. XXXX, XXX, XXX−XXX
Article
pubs.acs.org/IC

A New Bis(aquated) High Relaxivity Mn(II) Complex as an Alternative to Gd(III)-Based MRI Contrast Agent

Bedika Phukan,[†] Chandan Mukherjee,*[,†] Upashi Goswami,[#] Amrit Sarmah,[‡] Subhajit Mukherjee,[§] Suban K. Sahoo,[⊥] and Sankar Ch. Moi[§]

[†]Department of Chemistry, Indian Institute of Technology Guwahati, Guwahati 781039, Assam, India
[#]Centre for Nanotechnology, Indian Institute of Technology Guwahati, Guwahati 781039, Assam, India
[‡]Department of Molecular Modelling, Institute of Organic Chemistry and Biochemistry ASCR, Flemingovo nám. 2, CZ-166 10 Prague 6, Czech Republic
[§]Department of Chemistry, National Institute of Technology, Durgapur 713209, West Bengal, India
[⊥]Department of Applied Chemistry, S.V. National Institute of Technology, Surat 395007, Gujarat, India

Supporting Information

ABSTRACT: Disclosed here are a piperazine, a pyridine, and two carboxylate groups containing pentadentate ligand H_2pmpa and its corresponding water-soluble Mn(II) complex (**1**). DFT-based structural optimization implied that the complex had pentagonal bipyramidal geometry where the axial positions were occupied by two water molecules, and the equatorial plane was constituted by the ligand ON_3O donor set. Thus, a bis(aquated) disc-like Mn(II) complex has been synthesized. The complex showed higher stability compared with Mn(II)−EDTA complex [$\log K_{MnL}$ = 14.29(3)] and showed a very high r_1 relaxivity value of 5.88 mM^{-1} s^{-1} at 1.41 T, 25 °C, and pH = 7.4. The relaxivity value remained almost unaffected by the pH of the medium in the range of 6−10. Although the presence of 200 equiv of fluoride and bicarbonate anions did not affect the relaxivity value appreciably, an increase in the value was noticed in the presence of phosphate anion due to slow tumbling of the complex. Cell viability measurements, as well as phantom MR images using clinical MRI imager, consolidated the possible candidature of complex **1** as a positive contrast agent.

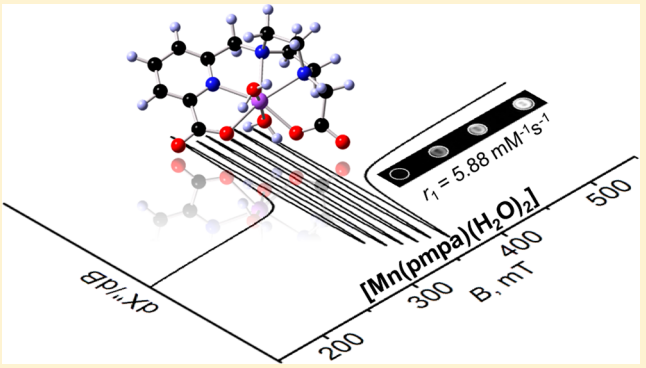

INTRODUCTION

Magnetic resonance imaging (MRI) is a crucial diagnostic tool in medical science for anatomical tissue imaging. The technique is based on NMR principle and provides high-resolution images of soft tissues by monitoring the differences in the relaxation rates ($1/T_1$ = longitudinal relaxation rate and $1/T_2$ = transverse relaxation rate) of water protons present in the tissues.[1] However, the sensitivity and prolonged-examination time are the constraints of the technique. To deal with the issues, MRI measurements are often carried out in the presence of external agents, called MRI contrast agents (CAs).[2] These agents are mainly paramagnetic metal complexes (e.g., Fe(III) [$3d^5$, S = 5/2], Mn(II) [$3d^5$, S = 5/2], Gd(III) [$4f^7$, S = 7/2], etc.) endowed with high stability, high relaxivity, and good water solubility. CAs shorten the relaxation times of the proximal water-protons to a great extent and consequently enhance the contrast between the located-tissue and the peripheral tissues. The efficacy of a CA is expressed in terms of relaxivity (r_i, i = 1, 2), defined as the enhancement of the relaxation rate of water protons in the presence of 1 mM paramagnetic metal ion.[1,2]

The majority of the clinically used CAs are based on Gd(III) ion because of its seven unpaired electrons; long electronic relaxation time; and formation of stable, water-coordinated, and water-soluble complexes.[3] However, recent detection of nephrogenic systemic fibrosis (NSF), a fatal disease related to Gd(III) deposition in patients who suffer from severe renal failure or underwent liver transplantation, restricts the use of Gd-based contrast agents.[4] Thus, finding of alternatives has achieved special attention. In this context, Mn(II)-based complexes have become the paramount members for investigations as Mn(II) ion is an essential element in human biological system; it contains five-unpaired electrons, and it has slow electronic relaxation rate and fast water exchange rate.[5]

The effect of fewer unpaired electrons in the Mn(II) ion as compared with Gd(III) ion is reflected in the r_1 (brightening effect) relaxivity value. At 0.47 T and 25 °C, although one water molecule-coordinated Gd(III)-based commercially available MRI CAs have the relaxivity (r_1) value in the range 4.4−5.2

Received: December 1, 2017

DOI: 10.1021/acs.inorgchem.7b03039
Inorg. Chem. XXXX, XXX, XXX−XXX

mM^{-1} s^{-1}, the reported relaxivity of Mn(II)-based complexes is only 2.44−3.7 mM^{-1} s^{-1}.[6] Therefore, improvement in the relaxivity value is the main aim. It is well established that the r_1 relaxivity value, irrespective of field strength, increases with increase in the number of coordinated-water molecule (q).[7] Thus, a higher relaxivity value in Mn(II)-based CAs can be attained by increasing the number of coordinated-water molecules.

In order to accommodate more numbers of water molecule in a thermodynamically stable Mn(II) complex, the coordination number needs to be high. However, because of small ionic charge and small ionic radius of Mn(II) ion, five- and six-coordinate Mn(II) complexes are very common, whereas seven-coordinate complexes are indeed scarce and remained as intriguing and challenging quests. Tóth and co-workers have reported Mn(II) complexes—which are based on 15-membered triaza−dioxa−crown (15-pyN_3O_2) and pentaaza-crown ether (15-pyN_5) macrocycles—that contain two coordinated water molecules.[8] The complexes showed modest r_1 relaxivity (3.5−4.5 mM^{-1} s^{-1} at 20 MHz and 25 °C); however, they are low in stability. Recently, a series of dipicolinic acid-based ligands have been employed to the synthesis of mono-, di- and trinuclear Mn(II) complexes, which contain two coordinated water molecules per Mn(II) ions. These complexes showed modarate to high r_1 relaxivity values (3.8−5.3 mM^{-1} s^{-1} per Mn(II) center at 20 MHz and 25 °C).[9]

Herein, we report a pentadentate ligand H_2pmpa for the synthesis of a bis(aquated) Mn(II) complex. In the ligand backbone, a piperazine unit has been introduced. It was envisaged that to achieve chelate-stability, the unit would be in boat form and two N atoms would be in *cis*- positions; thus, in the corresponding Mn(II) complex, both the N atoms would be at the equatorial sites as well as *cis*- to each other. The more electronegative carboxylate oxygen atoms would prefer the axial positions. However, due to cyclic structure and boat form of piperizine, the N-substituted groups will be in the same plane as that of two N atoms of the piperizine moiety. Therefore, a disc-shaped five-coordinate Mn(II) complex could be synthesized. Both the axial positions would thus be available for the coordination of water molecules to the Mn(II) center. As the carboxylate units would reside at the equatorial positions, H-bonding of the units with the axially interacting water molecules would be minimized and hence, H-bonding-promoted decrease in water exchange rate could be avoided. The existence of a π-accepting pyridine unit and two strong σ-donating carboxylate units were expected to elevate the thermodynamic stability of the corresponding Mn(II) complex. The ligand upon reacting with $MnCl_2{\cdot}4H_2O$ at pH ∼ 6.5 provided complex **1**. DFT-based geometry-optimized structure of complex **1** revealed pentagonal bipyramidal geometry as expected. Complex **1** showed r_1 relaxivity 5.88 mM^{-1} s^{-1} at 1.41 T, 25 °C, and pH = 7.4. The thermodynamic stability of the mononuclear, bis-(aquated) complex **1** was higher compared with reported analogous Mn(II) complexes.[8,9] Gratifyingly, the r_1 relaxivity value of the complex remained almost indifferent to physiological anions (phosphate, bicarbonate, and fluoride). The efficiency of the complex as a contrast agent was further investigated by acquiring phantom MR images and presented here.

RESULTS AND DISCUSSION

A schematic diagram for the syntheses of ligand H_2pmpa and complex **1** is presented in Scheme 1. A reaction between 1:1 N-

Scheme 1. Schematic Representation for the Syntheses of H_2pmpa and Complex 1[a]

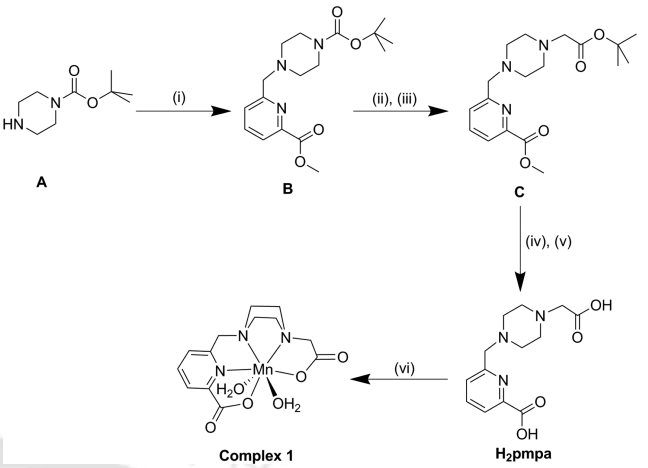

[a](i) methyl 6-(bromomethyl)pyridine-2-carboxylate, CH_3CN, K_2CO_3; (ii) TFA, CH_2Cl_2; (iii) *tert*-butylbromoacetate, DMF, K_2CO_3; (iv) TFA, CH_2Cl_2; (v) 6 M HCl; (vi) $MnCl_2{\cdot}4H_2O$, water, pH ∼ 6.5.

Boc protected piperazine[10] with methyl 6-(bromomethyl)-pyridine-2-carboxylate[11] in CH_3CN in the presence of K_2CO_3 gave **B** in 51% yield. Deprotection of **B** with trifluoroacetic acid (TFA) followed by addition of *tert*-butyl bromoacetate in DMF in the presence of K_2CO_3 produced the O-protected ligand **C**. The ligand H_2pmpa was obtained in 74% yield by successive deprotection of **C** using TFA and 6 M HCl. The synthesis of complex **1** was carried out by reacting the ligand with an equivalent amount of $MnCl_2{\cdot}4H_2O$ in water followed by the adjustment of the pH ∼ 6.5 with aq NaOH. Slow evaporation of the reaction solution provided the complex as a pale brown solid. Recrystallization of the solid from pure water or various other solvent mixtures did not provide single crystal suitable for XRD analysis. Thus, DFT-based calculations have been performed to optimize the most favorable structure of the complex (Figure 1).

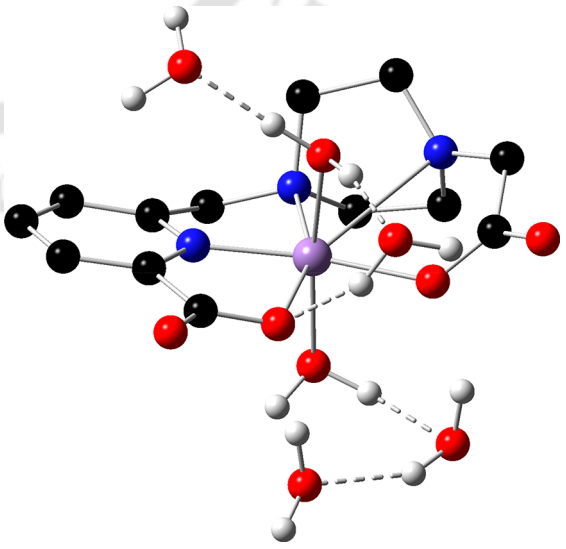

Figure 1. Optimized structure of bis(aquated) complex **1**. Optimized at B3LYP/6-31G(d,p) level. Red = oxygen, blue = nitrogen, black = carbon, purple = manganese, and white = hydrogen.

DOI: 10.1021/acs.inorgchem.7b03039
Inorg. Chem. XXXX, XXX, XXX−XXX

For Mn(II) complexes to behave as T_1 CAs, it is very important to have at least one water coordination site. Mn(II) ion can form six or seven coordinated mono- and bis(aquated) complexes. The ligand H_2pmpa being pentadentate, can form either a six-coordinate Mn(II) complex with one coordinated-water molecule or a seven-coordinate Mn(II) complex with two coordinated-water molecules.

We performed density functional theory (DFT)-based calculations to understand the coordination environment around the central metal (Mn (II)) atom. There was a strong possibility that the complex would contain more than one coordinated water molecule; where two water molecules could accommodate in the primary coordination sphere and the others could complete the secondary coordination of the complex through hydrogen bonding interactions. This particular theoretical approach with the hybrid cluster/continuum model to treat the noncovalently bonded water molecules around the metal atom was well documented in the literature.[12] In this study, we performed theoretical calculations on different systems containing a different number of water molecules in the complex framework. The set of optimized structures along with the computed water molecule binding energies and selected average bond distances are included in Table S1. It was observed that the optimized ligand coordinations around the Mn(II) center took a planner arrangement. Subsequently, the greater possibility of water coordination through above and below the ligand mean plane was wide open. We systematically screened different structural orientations of the complex by gradually adding single water molecule in each step. The substantial improvement in the thermodynamic stability of the complex with the addition of Mn−OH_2 coordination was evident from the computed binding energy data. In the process, different orientation of the water molecules in the vicinity of the central Mn(II) ion was tested and a preferential water−coordination through above and below the molecular plane of the complex was attributed from our calculations. It is important to note that the coordination of water molecule at the axial position with respect to the molecular plane induced significant modulation to the thermodynamic stability of the system. In principle, a stronger coordination of the water molecules to the metal center is directly proportional to Mn−O_{water} bond distance. The most preferable structural orientation predicted from the DFT simulations was pentagonal bipyramidal, where coordinated water molecules occupied the axial positions. It was also observed that four second-sphere water molecules were also weakly interacting with the two carboxylic oxygens and the two coordinated water molecule through hydrogen bonding interactions (Figure 1). In this particular structural orientation, the average Mn−O_{water} bond length was found to be 2.073 Å, which was shortest among all the possible screened orientations. It is worth mentioning here that a strong hydrogen bonding network due to the presence of water molecules in the vicinity of complex coordination sphere was also accounted for the enhanced stability of the complex (as depicted in Figure 1). As the number of water molecules increase, the higher amount of possible hydrogen bonding interactions improves the overall stability of the complex.

Thus, the most favorable optimized structure showed that complex **1** acquired pentagonal bipyramidal geometry where the two axial positions were occupied by two water molecules and the basal plane was constituted by two N atoms from the piperazine unit, one pyridine N atom, and two O atoms from the two carboxylate groups. Thus, the ligand moiety generated a disc-like geometry around the central Mn(II) ion. The Mn(II) center could then feasibly interact with the nearby water molecules from the both side of the disc. The Mn−N(Py) = 1.920, Mn−N(piperazine) = 2.284, 2.934, Mn−O(carboxylate) = 2.025, 2.084, and Mn−O(water) = 2.065, 2.081 Å bond distances corroborated with the previously reported similar Mn(II) complexes.[13]

The oxidation state of the central manganese ion was verified by measuring X-band EPR spectrum at room temperature (Figure 2). A six-line spectrum, which is a signature spectrum

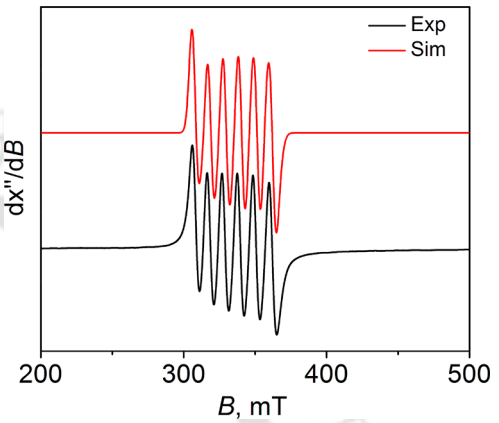

Figure 2. X-band EPR spectrum (9.44 GHz) of aqueous solution of complex **1** measured at room temperature, power = 0.995 mW, modulation frequency = 100 kHz and amplitude = 30 G.

for Mn(II) species, was obtained. Simulation to the experimental spectrum provided the following parameters: g_1 = 2.010, g_2 = 1.988, g_3 = 2.022, g_{av} = 2.007; $^{Mn}(A_x, A_y, A_z)$ = (103, 94, 94) × 10^{-4} cm^{-1}. The simulated parameters implied +2 oxidation state of the manganese ion in complex **1**.

Stepwise protonation constants of ligand H_2pmpa (H_2L) and stability constant of its corresponding Mn(II) complex were determined by pH potentiometric titration in 0.1 M KCl solution at 25 °C. The protonation constants obtained for the ligand were defined by the following equation:

$$K_i^H = [H_iL]/[H_{i-1}L][H^+] \qquad i = 1, 2, ...$$

The protonation constants for the ligand were found to be log K_1^H = 9.89(2), log K_2^H = 7.97(2), log K_3^H = 4.73(4), and log K_4^H = 2.64(3). On the basis of prior reports,[14] the protonation constants at 9.89, 7.97, and 4.73 could be assigned to the protonation of N-atoms present in the ligand backbone. The protonation constant at 2.64 corresponded to the carboxylate groups of the picolinate moiety. The protonation of the remaining carboxylic group from acetate pendant might occur at lower pH and could not be determined.[14c] The stability constant of complex **1** was also determined under the same experimental conditions as that for protonation constant determination and is defined by the equation:

$$K_{MnL} = [MnL]/[Mn][L]$$

In 0.1 M KCl and at 25 °C, the stability constant of the complex was found to be 14.29(3), which supports using complex **1** as an efficient contrast agent. A comparison of the pronation constants and stability constant of ligand H_2pmpa with other reported ligands is shown in Table 1. The species distribution of complex **1** is shown in Figure 3. The dissociation of the complex occurred below pH ∼ 6, whereas it was the

DOI: 10.1021/acs.inorgchem.7b03039
Inorg. Chem. XXXX, XXX, XXX−XXX

Table 1. Ligand Protonation Constants and Stability Constants of Their Corresponding Mn(II) Complexes Determined by Potentiometric Titration Method

ligand	$\log K_1^H$	$\log K_2^H$	$\log K_3^H$	$\log K_4^H$	$\log K_{MnL}$
15-pyN_3O_2[a]	8.82	7.80			7.18
15−pyN_5[a]	9.40	8.54	5.28		10.89
DPAPhA[b]	5.48	4.51	4.28	2.70	9.55
DPAMeA[b]	7.82	3.71	2.61		10.13
EDTA[c]	10.26	6.42	3.11	2.33	13.88
H_2pmpa[d]	9.89(2)	7.97(2)	4.73(4)	2.64(3)	14.29(3)

[a]ref 8 (25 °C, I = 0.1 M NMe_4Cl), [b]ref 9b (25 °C, I = 0.15 M NaCl), [c]refs 15 and 16b (25 °C, I = 0.1 M KCl), [d]This work (25 °C, I = 0.1 M KCl).

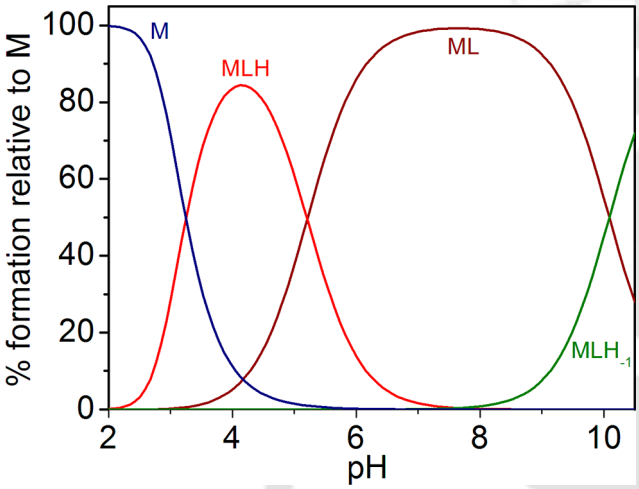

Figure 3. Species distribution diagram of complex **1** having [M] = [L] = 1 mM, ionic strength, I = 0.1 M KCl and 25 °C. (M and H_2L represent Mn(II) and ligand H_2pmpa respectively).

predominant species in solution up to pH ∼ 9. However, above pH ∼ 8, deprotonation of the complex started probably due to the coordination of a OH^- anion to the central Mn(II) ion.[9a]

At physiological pH, the thermodynamic stability of the complex with other reported complexes can be best understood by pM values of the ligand as it allows a direct comparison of complex stability at that condition. pM is defined as $-\log[M]_{free}$ at pH = 7.4; [M] = [L] = 10 μM, where, M and L represent the metal and the ligand, respectively.[8] The pMn of ligand was found to be 8.06, which was higher compared with the previously reported aquated Mn(II) complexes, e.g., (I) mono(aquated): [Mn(EDTA)] (pMn = 8.01; [M] = [L] = 10 μM, I = 0.1 M KCl, and 25 °C); (II) bis(aquated): [Mn(15−pyN_3O_2)] (pMn = 5.28; [M] = [L] = 10 μM, I = 0.1 M NMe_4Cl, and 25 °C), [Mn(15−pyN_5)] (pMn = 6.37; [M] = [L] = 10 μM, I = 0.1 M NMe_4Cl, and 25 °C), [Mn(DPAPhA)] (pMn = 7.37; [M] = [L] = 10 μM, I = 0.15 M NaCl, and 25 °C), and [Mn(DPAMeA)] (pMn = 7.38; [M] = [L] = 10 μM, I = 0.15 M NaCl, and 25 °C).[8,9]

At pH = 7.4, an equilibrium constant (K_{comp}) can also be deduced by using eq 1,[7b] where M = Mn(II), L = H_2pmpa and L′ = EDTA. EDTA serves as a reference in case of potential MRI contrast agents and $[Mn(EDTA)]^{2-}$ derivatives have been successfully used in in vivo MRI studies.[16]

$$[ML] + L' \rightleftharpoons [ML'] + L;$$
$$K_{comp} = ([ML][L'])/([ML'][L]) \quad (1)$$

We found a K_{comp} value of 1.41 at pH 7.4 for ligand H_2pmpa. In other words, the affinity of H_2pmpa for Mn(II) was found to be higher than EDTA at pH 7.4.

To understand the efficiency of complex **1** as a positive contrast agent (brightening agent), relaxivity measurements at 1.41 T, 25 °C, and pH ∼ 7.4 were performed. Using the inversion recovery method, at four different concentrations of the complex, the longitudinal relaxation time (T_1) was measured, and from the slope of the plot of longitudinal relaxation rate (R1 = $1/T_1$) versus Mn(II) ion concentration, the r_1 relaxivity value was found to be 5.88 mM^{-1} s^{-1} (at 25 °C and pH ∼ 7.4) per Mn(II) (Figure 4A). The concentration of

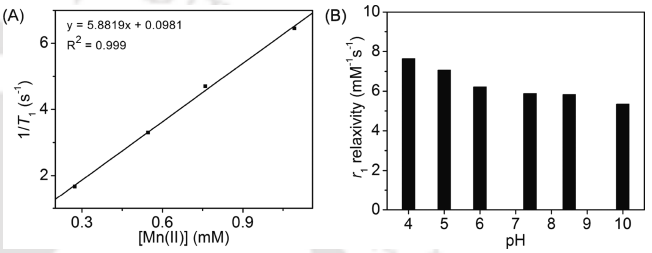

Figure 4. (A) $1/T_1$ versus [Mn(II)] plot at 1.41 T, 25 °C, and pH = 7.4. (B) r_1 relaxivity changes in the pH range 4−10; at 1.41 T and 25 °C.

Mn(II) ion was determined by the ICP-AES method. The r_1 value was significantly higher compared with the previously reported value per bis(aquated) Mn(II) species.[8,9] Notably, the r_1 relaxivity value of $Mn(H_2O)_6$ at 1.41 T, 25 °C, and pH ∼ 7.4 was found to be 7.4 mM^{-1} s^{-1}. Along with the disc-like geometry of the bis(aquated) complex as well as the steric compression, exerted by the piperazine moiety, the higher r_1 relaxivity value was probably due to a faster water exchange rate of its inner sphere water molecules. Such higher water exchange rates have been observed in the case of previously reported bis(aquated) Mn(II) complexes having picolinate moiety in the ligand backbone.[8,9,12a] Moreover, Gd(III) complexes having picolinate moiety in their ligand backbone are well-known for their very fast water exchange rate in their complexes imparting higher r_1 relavity values.[14] The higher water exchange rate for these complexes was related to the presence of a very flexible inner coordination sphere around the metal center.

The pH dependent-stability of complex **1** and its efficiency as a contrast agent were further examined by measuring r_1 relaxivity value in the pH range 4−10 at 1.41 T, 25 °C. The r_1 relaxivity of the complex was found to be almost constant in the range of 6−9. However, at pH ∼ 4, approximately 31% increase in the relaxivity value was observed. This was attributed to the dissociation of the complex at lower pH and formation of aqua complex of the metal ion (Figure 4B). At higher pH ∼ 10, the relaxivity value was dropped by approximately 9%, which could be due to coordination of a OH^- ion to the Mn(II) ion.

Physiological anions play an important role while using a complex as MRI contrast agent in vivo. The anions can replace the coordinated-water molecules of the complex forming stable ternary complexes.[17] Consequently, the r_1 relaxivity value sharply decreases. Thus, the interaction and the influence of

DOI: 10.1021/acs.inorgchem.7b03039
Inorg. Chem. XXXX, XXX, XXX−XXX

physiological anions to complex **1** were examined. In this context, the affinity of the complex toward phosphate (PO_4^{3-}), bicarbonate (HCO_3^-), and fluoride (F^-) ions was investigated by relaxivity measurements in the presence of 200 equiv of the respective anions (experimental conditions: 1.41 T, 25 °C, pH ∼ 7.4, [complex **1**] = 0.5 mM, [physiological anions] = 100 mM). The r_1 relaxivity values are presented as a bar diagram in Figure 5A. The results implied no significant decrease in r_1

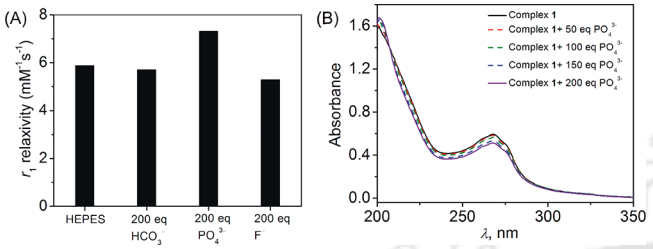

Figure 5. (A) Relaxivity measurements of complex **1** in the presence of 200 equiv of different anions (at 1.41 T, 25 °C, pH ∼ 7.4, [Complex **1**] = 0.5 mM, and [oxyanions] = 100 mM). (B) UV−vis spectra of complex **1** in the presence of up to 200 equiv of phosphate anion.

relaxivity value in case of fluoride and bicarbonate ions, (Δr_1 = −0.17 for HCO_3^- and Δr_1 = −0.59 for F^-) (Figure 5A). However, in the case of phosphate ions, about 24% increase in realxivity value was observed. The increment may be either due to release of free Mn(II) in solution or due to formation of a slowly tumbling system. To confirm this fact, UV−vis spectra of complex **1** were measured in the presence of various concentrations of phosphate anion at pH ∼ 7.4, 25 °C (Figure 5B). No significant change in the spectral features overruled the decomposition of the complex and indicated the formation of a slowly tumbling system by presumable intermolecular interactions in the presence of phosphate anion and/or complex-phosphate interaction. However, a contribution from the outer sphere water molecules to the relaxivity cannot be ignored following the formation of ion-pairing interactions.[8,17a] A detailed investigation will be carried out in the near future to better understand the phenomenon.

The cytotoxicity of complex **1** was examined by measuring cell viability using the MTT [3-(4,5-dimethylthiazol-2-yl)-2,5-diphenyltetrazolium bromide] assay on HeLa cell line (human cervical carcinoma).[18] The cells were incubated with different concentrations of the complex (0−1 mM) for 36 h at 37 °C. It was observed that even at the concentration of 1 mM, the cell viability remained ∼80% (Figure 6). When comparing the cell viability of the complex with that of free ligand H_2pmpa and $MnCl_2{\cdot}4H_2O$, at the concentration of 1 mM, cell viability of the ligand remained ∼90% and that of $MnCl_2{\cdot}4H_2O$ was found to be considerably lower at ∼46%. For further improvement in the toxicity profile to use the complex in biological systems, incorporation of the complex to biological macromolecules is currently under progress.

To evaluate the efficiency of complex **1** as a brightening contrast agent, the T_1-weighted phantom MR images of the complex at four different concentrations (0.25, 0.50, 0.70, and 1.00 mM) were measured at 1.5 T by using clinical MRI imager BRIVO MR355 and depicted in Figure 7. Gratifyingly, the image intensity was found to increase with increase in concentration of complex **1**. A comparison of the image intensities was also done by using ImageJ Software under the same area of the images and presented in Figure S12.

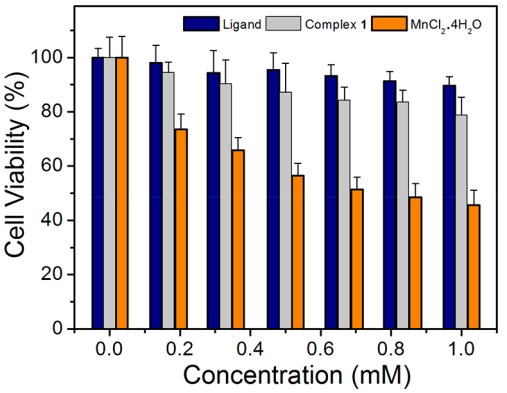

Figure 6. Showing % cell viability of HeLa cells incubated with different concentrations of complex **1**, ligand H_2pmpa, and $MnCl_2{\cdot}4H_2O$.

Figure 7. T_1-weighted phantom MR images of the complex **1** at different concentrations (*A* = 0.25 mM, *B* = 0.50 mM, *C* = 0.70 mM, *D* = 1.00 mM) at 1.5 T, 25 °C, and pH ∼ 7.4.

CONCLUSION

To conclude, we have reported here a pentadentate water-soluble ligand H_2pmpa, which upon reacting with $MnCl_2{\bullet}4H_2O$ at pH ∼ 6.5 provided complex **1**. DFT-based structural optimization implied that the complex acquired a pentagonal bipyramidal geometry where the coordinating ligand resided at the equatorial positions and the two axial positions were occupied by two water molecules. The stability of complex **1** was found to be higher compared to the previously reported bis(aquated) Mn(II) complexes. The complex exhibits high r_1 relaxivity value of 5.88 mM^{-1} s^{-1} at 1.41 T, 25 °C, and pH = 7.4, even better than clinically used Gd(III) complexes. This higher relaxivity value was due to the presence of two coordinated water molecules. This result indicated the usefulness of the complex as an alternative to the Gd(III) based MRI CAs. Finally, cell viability and phantom MR images of the complex at 1.5 T also consolidated its potential use as a safer MRI probe. In the near future in vivo study will be carried out employing the complex.

EXPERIMENTAL SECTION

Materials. All the chemicals and solvents were obtained from commercial sources and were used as supplied, unless noted otherwise. Piperazine, di-*tert*-butyldicarbonate, *tert*-butylbromoacetate and TFA were purchased from Spectrochem. $MnCl_2{\cdot}4H_2O$, $KHCO_3$, and solvents were obtained from Merck (India). HEPES buffer was purchased from SRL. 2,6-Dipicolinic acid was purchased from Sigma-Aldrich. HeLa cells (human cervical carcinoma) were procured from National Center for Cell Sciences (NCCS), Pune, India. Water used for the experiments was purified by using a Millipore water purifier (Milli-Q, Merck).

Physical Methods. FTIR spectra were recorded on PerkinElmer Instrument at normal temperature making KBr pellet grinding the sample with KBr (IR grade). UV−vis spectra were recorded on PerkinElmer, Lamda 25, UV/vis Spectrometer. Mass spectral data were obtained from either HRMS or QTOF MS Spectrometer. EPR spectrum was recorded on X-band microwave unit, JESFA200 ESR spectrometer. ^1H and ^{13}C NMR analyses were carried out using Varian

DOI: 10.1021/acs.inorgchem.7b03039
Inorg. Chem. XXXX, XXX, XXX−XXX

Mercury plus 400 MHz NMR machine. The longitudinal (r_1) relaxivity at 1.41 T was measured using BRUKER minispec mq60 NMR Analyzer. MRI images at 1.5 T were collected using BRIVO MR355 MRI Scanner.

Computational Details. All the calculations were done using Gaussian09 package.[19] The initial geometries of the complexes were optimized at B3LYP[20,21]/6-31G(d,p) level with an energy correction at B3LYP/6-311+G(d,p) level. The solvent effect was taken care through SCRF (self-consistent reaction field)[22] approach using CPCM[23] (polarizable conductor calculation model) formalism for water, as implemented in Gaussian09. Subsequent frequency calculations were performed (on the optimized structures) to ensure the complete optimization.

Potentiometric Measurements. Potentiometric titrations were carried out at a 1:1 metal-to-ligand molar ratio, at 25 °C ± 0.1 °C, and an ionic strength of I = 0.1 M KCl. Stock solution of ligand and Mn(II) were prepared using double distilled water, and an inert atmosphere was maintained by a constant passage of argon in the solution. The protonation constants and stability constant were determined using pH−potentiometry by titrating 1 mM ligand solution with standardized 0.15 M KOH solution using a Metrohm Titrando-888 titro-processor equipped with a Metrohm glass electrode. Titrations were performed in the pH range of 1.6−10.5 for all equilibrium measurements (direct titrations) with an extra HCl added to the starting solution. The stability constant of the ligand with Mn(II) was determined under same experimental conditions as for the protonation constant determination. The protonation and stability constant were evaluated from the titration data using the program *Hyperquad2008*.

MTT Assay of Complex 1. The HeLa cells were cultivated in Dulbecco's modified Eagle's medium supplemented with L-glutamine (4 mM), penicillin (10^4 units/mL), streptomycin (10 mg/mL), and 10% (v/v) fetal bovine serum (obtained from PAA Laboratories, Austria) in a 5% CO_2 humidified incubator at 37 °C. To perform the MTT based cell viability assay, 1×10^4 HeLa cells/well were seeded in a 96-well microtiter plate and grown overnight by maintaining the same medium and conditions as mentioned above. Then, different concentrations of complex **1** were added into it and incubated for 36 h prior to the addition of MTT dye to find out the number of viable cells. The absorbance was read at 570 nm which is the measure of viable cells.

Synthesis of $[C_{17}H_{25}N_3O_4]$, (B). N-Boc-protected piperazine (**A**) and 6-(bromomethyl)pyridine-2-carboxylate were prepared by using the reported procedure. To N-Boc-protected piperazine (0.375 g, 2 mmol) in 5 mL of CH_3CN, K_2CO_3 (0.549 g, 4 mmol) was added and stirred the reaction mixture at room temperature (25 °C) for 10 min. A solution of 6-(bromomethyl)pyridine−2-carboxylate (0.465 g, 2 mmol) in 2 mL of CH_3CN was added dropwise to the stirred solution, and stirring was continued at 50 °C for 48 h. The reaction mixture was then cooled to room temperature and filtered. The white precipitate obtained was washed thoroughly with CH_3CN (10 mL), and the filtrate was then concentrated to dryness to get the crude product as brown oil. The pure compound was obtained as colorless oil by column chromatography on silica gel by using hexane/ethyl acetate (2:3) as eluent. Yield: 0.341 g, 51%. FTIR (KBr, cm^{-1}): 3448, 2975, 2950, 2860, 2813, 1725, 1695, 1589, 1457, 1423, 1316, 1247, 1170, 1139, 1083, 1006, 866, 762, 678. ^{1}H NMR ($CDCl_3$, 399.85 MHz): δ 7.99 (d, J = 8 Hz, 1H), 7.79 (t, J = 8 Hz, 1H), 7.06 (d, J = 8 Hz, 1H), 3.96 (s, 3H), 3.76 (s, 2 H), 3.44−3.41 (m, 4H), 2.46−2.43 (m, 4H), 1.42 (s, 9H) ppm. ^{13}C NMR ($CDCl_3$, 100.55 MHz): δ 165.9, 159.4, 154.9, 147.6, 137.6, 126.3, 123.8, 79.8, 64.2, 53.1, 53.0, 29.6 ppm. ESI−MS (+) m/z for $[C_{17}H_{25}N_3O_4 + H]^+$: Calcd, 336.1918; Found, 336.1926.

Synthesis of $[C_{18}H_{27}N_3O_4]$, (C). To compound **B** (0.341 g, 1.0 mmol), CH_2Cl_2/TFA (1:1, 4 mL) solution was added dropwise, and the reaction mixture was stirred at room temperature (25 °C) for 16 h. The solvent was then evaporated in vacuo, and a white solid was obtained by adding excess diethyl ether. The white solid was then filtered, washed with diethyl ether (10 mL), and used in the next reaction without further purification. To this deprotected compound in 5 mL of DMF, K_2CO_3 (0.423 g, 3 mmol) was added followed by dropwise addition of *tert*-butylbromoacetate (0.324 g, 1.7 mmol). The reaction was then stirred at 50 °C for 48 h. The reaction mixture was cooled to room temperature and concentrated to dryness. Water was added, and the residue was then extracted by using $CHCl_3$ (3 × 30 mL). The organic phase was dried over Na_2SO_4, filtered, and the solvent was evaporated to give an oily residue that was purified by column chromatography on silica gel by using hexane/ethyl acetate (2:3) as eluent. Yield: 0.243 g, 68%. FTIR (KBr, cm^{-1}): 3436, 2979, 2816, 1742, 1589, 1457, 1369, 1228, 1156, 1015, 839, 765. ^{1}H NMR ($CDCl_3$, 399.85 MHz): δ 8.00 (d, J = 4 Hz, 1H), 7.81 (t, J = 4 Hz, 1H), 7.69 (d, J = 4 Hz, 1H), 3.98 (s, 3H), 3.78 (s, 2 H), 3.44 (s, 4H), 2.46 (s, 4H), 1.44 (s, 9H) ppm. ^{13}C NMR ($CDCl_3$, 100.55 MHz): δ 170.5, 165.6, 159.4, 147.1, 137.1, 126.0, 123.4, 80.7, 63.8, 57.0, 56.1, 52.9, 50.6, 27.9 ppm. ESI−MS (+) m/z for $[C_{18}H_{27}N_3O_4 + H]^+$: Calcd, 350.2074; Found, 350.2079.

Synthesis of $[C_{13}H_{17}N_3O_4]$, H_2pmpa. To compound **C** (0.309 g, 0.9 mmol), a solution of CH_2Cl_2/TFA (1:1, 4 mL) was added, and the reaction mixture was stirred at room temperature (25 °C) for 16 h. The solvent was then evaporated in vacuo, and diethyl ether was added. A white solid was obtained which was again dissolved in 6 M HCl and refluxed for 24 h. The solvent was then completely evaporated to dryness, and the ligand was obtained as a light brown colored solid by adding excess diethyl ether. The ligand was then filtered, washed thoroughly with diethyl ether (3 × 5 mL), and dried under high vacuum. Yield = 0.184 g, 74%. FTIR (KBr, cm^{-1}): 3434, 2976, 2927, 2648, 2601, 2561, 2542, 1724, 1623, 1466, 1443, 1398, 1339, 1263, 1188, 1083, 1003, 967, 894, 853, 733, 715, 638. ^{1}H NMR (CD_3OD, 399.85 MHz): δ 8.25 (d, J = 4 Hz, 1H), 8.18 (t, J = 4 Hz, 1H), 7.82 (d, J = 8 Hz, 1H), 4.75 (s, 2H), 4.26 (s, 2H), 3.78−3.75 (m, 8H) ppm. ^{13}C NMR (CD_3OD, 100.55 MHz): δ 168.7, 165.3, 151.3, 147.2, 139.2, 127.7, 124.9, 59.2, 55.8, 52.3, 50.1 ppm. ESI−MS (+) m/z for $[C_{13}H_{17}N_3O_4 + H]^+$: Calcd, 280.1291; Found, 280.1333.

Synthesis of Complex 1, $[C_{13}H_{19}MnN_3O_6]$. To a solution of H_2pmpa (0.131 g, 0.47 mmol) in water (3 mL) was added $MnCl_2 \cdot 4H_2O$ (0.076 g, 0.44 mmol) and stirred for 10 min. The solution became transparent, and then the pH of the solution was adjusted to ∼6.5 by adding aq. NaOH solution dropwise. Stirring was continued at room temperature (25 °C) for 24 h. The resulting clear solution was then kept at room temperature for slow evaporation. A pale brown colored solid was obtained after complete evaporation of water which was then washed thoroughly with MeOH. Yield = 0.073 g, 42%. FTIR (KBr, cm^{-1}): 3409, 2961, 2926, 2853, 1595, 1496, 1410, 1316, 1100, 1008, 936, 905, 777, 619. ESI−MS (+) m/z for $[C_{13}H_{15}MnN_3O_4 + H]^+$: Calcd, 333.05; Found, 333.03.

■ ASSOCIATED CONTENT

Ⓢ Supporting Information

The Supporting Information is available free of charge on the ACS Publications website at DOI: 10.1021/acs.inorgchem.7b03039.

^{1}H and ^{13}C NMR spectra of ligand H_2pmpa. IR and mass spectra of the ligand and complex **1**; comparison of phantom MR images of complex **1**; and coordinates for geometrically optimized structures of bis(aquated) complex (PDF)

■ AUTHOR INFORMATION

Corresponding Author

*E-mail: cmukherjee@iitg.ernet.in.

ORCID

Chandan Mukherjee: 0000-0002-2771-2468

Suban K. Sahoo: 0000-0003-1751-5310

Funding

This project is funded by Department of Biotechnology (BT/PR23622/NNT/281294/2017), Govt. of India.

DOI: 10.1021/acs.inorgchem.7b03039
Inorg. Chem. XXXX, XXX, XXX−XXX

Notes

The authors declare no competing financial interest.

■ ACKNOWLEDGMENTS

B.P. and C.M. are indebted to Dr. Ankona Datta, Prof. Siddhartha Sankar Ghosh and Dr. Baijayanta Saharia, for helpful discussions and instrumental facilities. C.M. is indebted to the referees for the improvement of the manuscript. The Department of Chemistry and CIF, IIT Guwahati are also thankfully acknowledged for instrumental facilities.

■ REFERENCES

(1) (a) Caravan, P. Strategies for increasing the sensitivity of gadolinium based MRI contrast agents. *Chem. Soc. Rev.* **2006**, *35*, 512−523. (b) Caravan, P.; Ellison, J. J.; McMurry, T. J.; Lauffer, R. B. Gadolinium(III) Chelates as MRI Contrast Agents: Structure, Dynamics, and Applications. *Chem. Rev.* **1999**, *99*, 2293−2352. (c) Lauffer, R. B. Paramagnetic Metal Complexes as Water Proton Relaxation Agents for NMR Imaging: Theory and Design. *Chem. Rev.* **1987**, *87*, 901−927. (d) Caravan, P. Protein-Targeted Gadolinium-Based Magnetic Resonance Imaging (MRI) Contrast Agents: Design and Mechanism of Action. *Acc. Chem. Res.* **2009**, *42*, 851−862. (e) Raymond, K. N.; Pierre, V. C. Next Generation, High Relaxivity Gadolinium MRI Agents. *Bioconjugate Chem.* **2005**, *16*, 3−8. (f) Terreno, E.; Castelli, D. D.; Viale, A.; Aime, S. Challenges for Molecular Magnetic Resonance Imaging. *Chem. Rev.* **2010**, *110*, 3019−3042.

(2) (a) Hermann, P.; Kotek, J.; Kubíček, V.; Lukeš, I. Gadolinium(III) complexes as MRI contrast agents: ligand design and properties of the complexes. *Dalton Trans.* **2008**, 3027−3047. (b) Boros, E.; Gale, E. M.; Caravan, P. MR imaging probes: design and applications. *Dalton Trans.* **2015**, *44*, 4804−4818. (c) Aime, S.; Botta, M.; Fasano, M.; Terreno, E. Lanthanide(III) chelates for NMR biomedical applications. *Chem. Soc. Rev.* **1998**, *27*, 19−29. (d) Que, E. L.; Chang, C. J. Responsive magnetic resonance imaging contrast agents as chemical sensors for metals in biology and medicine. *Chem. Soc. Rev.* **2010**, *39*, 51−60. (e) Major, J. M.; Meade, T. J. Bioresponsive, Cell-Penetrating, and Multimeric MR Contrast Agents. *Acc. Chem. Res.* **2009**, *42*, 893−903. (f) Villaraja, A. J. L.; Bumb, A.; Brechbiel, M. W. Macromolecules, Dendrimers, and Nanomaterials in Magnetic Resonance Imaging: The Interplay between Size, Function, and Pharmacokinetics. *Chem. Rev.* **2010**, *110*, 2921−2959. (g) Heffern, M. C.; Matosziuk, L. M.; Meade, T. J. Lanthanide Probes for Bioresponsive Imaging. *Chem. Rev.* **2014**, *114*, 4496−4539. (h) Runge, V. M.; Foster, M. A.; Clanton, J. A.; Jones, M. M.; Lukehart, C. M.; Hutchison, J. M.; Mallard, J. R.; Smith, F. W.; Partain, C. L.; James, A. E., Jr. Contrast enhancement of magnetic resonance images by chromium EDTA: an experimental study. *Radiology* **1984**, *152*, 123−126.

(3) (a) Verwilst, P.; Park, S.; Yoon, B.; Kim, J. S. Recent advances in Gd-chelate based bimodal optical/MRI contrast agents. *Chem. Soc. Rev.* **2015**, *44*, 1791−1806. (b) Bianchi, A.; Calabi, L.; Corana, F.; Fontana, S.; Losi, P.; Maiocchi, A.; Paleari, L.; Valtancoli, B. Thermodynamic and structural properties of Gd(III) complexes with polyamino-polycarboxylic ligands: basic compounds for the development of MRI contrast agents. *Coord. Chem. Rev.* **2000**, *204*, 309−393. (c) Boros, E.; Polasek, M.; Zhang, Z.; Caravan, P. Gd(DOTAla): A Single Amino Acid Gd-complex as a Modular Tool for High Relaxivity MR Contrast Agent Development. *J. Am. Chem. Soc.* **2012**, *134*, 19858−19868. (d) Messeri, D.; Lowe, M. P.; Parker, D.; Botta, M. A stable, high relaxivity, diaqua gadolinium complex that suppresses anion and protein binding. *Chem. Commun.* **2001**, 2742−2743. (e) Boros, E.; Karimi, S.; Kenton, N.; Helm, L.; Caravan, P. Gd(DOTAlaP): Exploring the Boundaries of Fast Water Exchange in Gadolinium-Based Magnetic Resonance Imaging Contrast Agents. *Inorg. Chem.* **2014**, *53*, 6985−6994.

(4) (a) Thakral, C.; Alhariri, J.; Abraham, J. L. Long-term retention of gadolinium in tissues from nephrogenic systemic fibrosis patient after multiple gadolinium-enhanced MRI scans: case report and implications. *Contrast Media Mol. Imaging* **2007**, *2*, 199−205. (b) Saxena, S. K.; Sharma, M.; Patel, M.; Oreopoulos, D. Nephrogenic systemic fibrosis: an emerging entity. *Int. Urol. Nephrol.* **2008**, *40*, 715−724. (c) Marckmann, P.; Skov, L.; Rossen, K.; Dupont, A.; Damholt, M.; Heaf, J.; Thomsen, H. Nephrogenic Systemic Fibrosis: Suspected Causative Role of Gadodiamide Used for Contrast-Enhanced Magnetic Resonance Imaging. *J. Am. Soc. Nephrol.* **2006**, *17*, 2359−2362.

(5) (a) Drahoš, B.; Lukeš, I.; Tóth, É. Manganese(II) Complexes as Potential Contrast Agents for MRI. *Eur. J. Inorg. Chem.* **2012**, *2012*, 1975−1986. (b) Rocklage, S. M.; Cacheris, W. P.; Quay, S. C.; Hahn, F. E.; Raymond, K. N. Manganese(II) *N*,*N*′-Dipyridoxylethylenediamine-*N*,*N*′-diacetate 5,5′-Bis(phosphate). Synthesis and Characterization of a Paramagnetic Chelate for Magnetic Resonance Imaging Enhancement. *Inorg. Chem.* **1989**, *28*, 477−485. (c) Wagnon, B. K.; Jackels, S. C. Synthesis, Characterization, and Aqueous Proton Relaxation Enhancement of a Manganese(II) Heptaaza Macrocyclic Complex Having Pendant Arms. *Inorg. Chem.* **1989**, *28*, 1923−1927. (d) Gale, E. M.; Mukherjee, S.; Liu, C.; Loving, G. S.; Caravan, P. Structure−Redox−Relaxivity Relationships for Redox Responsive Manganese-Based Magnetic Resonance Imaging Probes. *Inorg. Chem.* **2014**, *53*, 10748−10761. (e) Tei, L.; Gugliotta, G.; Fekete, M.; Kálmán, F. K.; Botta, M. Mn(II) complexes of novel hexadentate AAZTA-like chelators: a solution thermodynamics and relaxometric study. *Dalton Trans.* **2011**, *40*, 2025−2032. (f) Wang, S.; Westmoreland, T. D. Correlation of Relaxivity with Coordination Number in Six-, Seven-, and Eight-Coordinate Mn(II) Complexes of Pendant-Arm Derivatives. *Inorg. Chem.* **2009**, *48*, 719−727. (g) Tan, M.; Ye, Z.; Jeong, E.K.; Wu, X.; Parker, D. L.; Lu, Z.-R. Synthesis and Evaluation of Nanoglobular Macrocyclic Mn(II) Chelate Conjugates as Non-Gadolinium(III) MRI Contrast Agents. *Bioconjugate Chem.* **2011**, *22*, 931−937. (h) Su, H.; Wu, C.; Zhu, J.; Miao, T.; Wang, D.; Xia, C.; Zhao, X.; Gong, Q.; Song, B.; Ai, H. Rigid Mn(II) chelate as efficient MRI contrast agent for vascular imaging. *Dalton Trans.* **2012**, *41*, 14480−14483. (i) Drahoš, B.; Pniok, M.; Havlíčková, J.; Kotek, J.; Císařová, I.; Hermann, P.; Lukeš, I.; Tóth, É. Mn^{2+} complexes of 1-oxa-4,7-diazacyclononane based ligands with acetic, phosphonic and phosphinic acid pendant arms: Stability and relaxation studies. *Dalton Trans.* **2011**, *40*, 10131−10146.

(6) (a) Rolla, G. A.; Platas-Iglesias, C.; Botta, M.; Tei, L.; Helm, L. ^{1}H and ^{17}O NMR Relaxometric and Computational Study on Macrocyclic Mn(II) Complexes. *Inorg. Chem.* **2013**, *52*, 3268−3279. (b) *The Chemistry of Contrast Agent in Medical Magnetic Resonance Imaging*, 2nd ed.; Merbach, A. E., Helm, L., Tóth, E., Eds.; John Wiley & Sons Ltd.: Chichester, U.K., 2013.

(7) (a) Datta, A.; Raymond, K. N. Gd-Hydroxypyridinone (HOPO)-Based High-Relaxivity Magnetic Resonance Imaging (MRI) Contrast Agents. *Acc. Chem. Res.* **2009**, *42*, 938−947. (b) Gale, E. M.; Kenton, N.; Caravan, P. $[Gd(CyPic3A)(H_2O)_2]^-$: a stable, bis(aquated) and high-relaxivity Gd(III) complex. *Chem. Commun.* **2013**, *49*, 8060−8062. (c) Xu, J.; Churchill, D. G.; Botta, M.; Raymond, K. N. Gadolinium(III) 1,2-Hydroxypyridonate-Based Complexes: Toward MRI Contrast Agents of High Relaxivity. *Inorg. Chem.* **2004**, *43*, 5492−5494. (d) Bretonnière, Y.; Mazzanti, M.; Dunand, F. A.; Merbach, A. E.; Pècaut, J. A new heptadentate tripodal ligand leading to a gadolinium complex with an improved relaxtion efficiency. *Chem. Commun.* **2001**, 621−622.

(8) Drahoš, B.; Kotek, J.; Hermann, P.; Lukeš, I.; Tóth, É. Mn^{2+} Complexes with Pyridine-Containing 15-Membered Macrocycles: Thermodynamic, Kinetic, Crystallographic, and $^{1}H/^{17}O$ Relaxation Studies. *Inorg. Chem.* **2010**, *49*, 3224−3238.

(9) (a) Forgács, A.; Regueiro-Figueroa, M.; Barriada, J. L.; Esteban-Gómez, D.; de Blas, A.; Rodríguez-Blas, T.; Botta, M.; Platas-Iglesias, C. Mono-, Bi-, and Trinuclear Bis-Hydrated Mn^{2+} Complexes as Potential MRI Contrast Agents. *Inorg. Chem.* **2015**, *54*, 9576−9587. (b) Forgács, A.; Pujales-Paradela, R.; Regueiro-Figueroa, M.; Valencia, L.; Esteban-Gómez, D.; Botta, M.; Platas-Iglesias, C. Developing the family of piconilate ligands for Mn^{2+} complexation. *Dalton Trans.* **2017**, *46*, 1546−1558.

DOI: 10.1021/acs.inorgchem.7b03039
Inorg. Chem. XXXX, XXX, XXX−XXX

(10) Bala, V.; Jangir, S.; Mandalapu, D.; Gupta, S.; Chhonker, Y. S.; Lal, N.; Kushwaha, B.; Chandasana, H.; Krishna, S.; Rawat, K.; Maikhuri, J. P.; Bhatta, R. S.; Siddiqi, M. I.; Tripathi, R.; Gupta, G.; Sharma, V. L. Dithiocarbamate−thiourea hybrids useful as vaginal microbicides also show reverse transcriptase inhibition: Design, synthesis, docking and pharmacokinetic studies. *Bioorg. Med. Chem. Lett.* **2015**, *25*, 881−886.

(11) (a) Zhu, Y.-Y.; Liu, C.-W.; Yin, J.; Meng, Z.-S.; Yang, Q.; Wang, J.; Liu, T.; Gao, S. Structural phase transition in a multi-induced mononuclear Fe^{II} spin−crossover complex. *Dalton Trans.* **2015**, *44*, 20906−20912. (b) Chandrasekhar, V.; Hossain, S.; Das, S.; Biswas, S.; Sutter, J.-P. Rhombus-Shaped Tetranuclear $[Ln_4]$ Complexes [Ln = Dy(III) and Ho(III)]: Synthesis, Structure, and SMM Behavior. *Inorg. Chem.* **2013**, *52*, 6346−6353. (c) Price, E. W.; Cawthray, J. F.; Bailey, G. A.; Ferreira, C. L.; Boros, E.; Adam, M. J.; Orvig, C. H_4octapa: An Acyclic Chelator for ^{111}In Radiopharmaceuticals. *J. Am. Chem. Soc.* **2012**, *134*, 8670−8683.

(12) (a) Molnár, E.; Camus, N.; Patinec, V.; Rolla, G. A.; Botta, M.; Tircsó, G.; Kálmán, F. K.; Fodor, T.; Tripier, R.; Platas-Iglesias, C. Picolinate-Containing Macrocyclic Mn2+ Complexes as Potential MRI Contrast Agents. *Inorg. Chem.* **2014**, *53*, 5136−5149. (b) Baranyai, Z.; Botta, M.; Fekete, M.; Giovenzana, G. B.; Negri, R.; Tei, L.; Platas-Iglesias, C. Lower Ligand Denticity Leading to Improved Thermodynamic and Kinetic Stability of the Gd^{3+} Complex: The Strange Case of OBETA. *Chem. - Eur. J.* **2012**, *18*, 7680−7685.

(13) (a) Zhang, Q.; Gorden, J. D.; Beyers, R. J.; Goldsmith, C. R. Manganese(II)-Containing MRI Contrast Agent Employing a Neutral and Non-Macrocyclic Ligand. *Inorg. Chem.* **2011**, *50*, 9365−9373. (b) Molnár, E.; Camus, N.; Patinec, V.; Rolla, G. A.; Botta, M.; Tircsó, G.; Kálmán, F. K.; Fodor, T.; Tripier, R.; Platas-Iglesias, C. Picolinate-Containing Macrocyclic Mn^{2+} Complexes as Potential MRI Contrast Agents. *Inorg. Chem.* **2014**, *53*, 5136−5149. (c) Drahoš, B.; Kotek, J.; Císařová, I.; Hermann, P.; Helm, L.; Lukeš, I.; Tóth, É. Mn^{2+} Complexes with 12-Membered Pyridine Based Macrocycles Bearing Carboxylate or Phosphonate Pendant Arm: Crystallographic, Thermodynamic, Kinetic, Redox, and $^{1}H/^{17}O$ Relaxation Studies. *Inorg. Chem.* **2011**, *50*, 12785−12801. (d) Zampakou, M.; Rizeq, N.; Tangoulis, V.; Papadopoulos, A. N.; Perdih, F.; Turel, I.; Psomas, G. Manganese(II) Complexes with the Non-steroidal Anti-Inflammatory Drug Tolfenamic Acid: Structure and Biological Perspectives. *Inorg. Chem.* **2014**, *53*, 2040−2052. (e) Phukan, B.; Patel, A. B.; Mukherjee, C. A water-soluble and water-coordinated Mn(II) complex: synthesis, characterization and phantom MRI image study. *Dalton Trans.* **2015**, *44*, 12990−12994. (f) Ratilainen, J.; Airola, K.; Fröhlich, R.; Nieger, M.; Rissanen, K. Synthesis of a tetradentate piperazine ligand and a structural study of its coordination compounds. *Polyhedron* **1999**, *18*, 2265−2273. (g) Geiger, R. A.; Chattopadhyay, S.; Day, V. W.; Jackson, T. A. Nucleophilic reactivity of a series of peroxomanganese(III) complexes supported by tetradentate aminopyridyl ligands. *Dalton Trans.* **2011**, *40*, 1707−1715. (h) Geiger, R. A.; Chattopadhyay, S.; Day, V. W.; Jackson, T. A. A Series of Peroxomanganese(III) Complexes Supported by Tetradentate Aminopyridyl Ligands: Detailed Spectroscopic and Computational Studies. *J. Am. Chem. Soc.* **2010**, *132*, 2821−2831. (i) Khannam, M.; Weyhermüller, T.; Goswami, U.; Mukherjee, C. A highly stable L-alanine-based mono(aquated) Mn(II) complex as a T_1-weighted MRI contrast agent. *Dalton Trans.* **2017**, *46*, 10426−10432.

(14) (a) Nonat, A.; Fries, P. H.; Pécaut, J.; Mazzanti, M. Structure, Stability, Dynamics, High-Field Relaxivity and Ternary-complex Formation of a New Tris(aquo) Gadolinium Complex. *Chem. - Eur. J.* **2007**, *13*, 8489−8506. (b) Nonat, A. M.; Gateau, C.; Fries, P. H.; Helm, L.; Mazzanti, M. New Bisaqua Picolinate-Based Gadolinium Complexes as MRI Contrast Agents with Substantial High-Field Realxivities. *Eur. J. Inorg. Chem.* **2012**, *2012*, 2049−2061. (c) Chatterton, N.; Gateau, C.; Mazzanti, M.; Pécaut, J.; Borel, A.; Helm, L.; Merbach, A. The effect of pyridinecarboxylate chelating groups on the stability and electronic relaxation of gadolinium complexes. *Dalton Trans.* **2005**, 1129−1135. (d) Mato-Iglesias, M.; Platas-Iglesias, C.; Djanashvili, K.; Peters, J. A.; Tóth, É.; Balogh, E.; Muller, R. N.; Elst, L. V.; de Blas, A. de; Rodríguez-Blas, T. The highest water exchange rate ever measured for a Gd(III) chelate. *Chem. Commun.* **2005**, *46*, 4729−4731.

(15) Bianchi, A.; Calabi, L.; Corana, F.; Fontana, S.; Losi, P.; Maiocchi, A.; Paleari, L.; Valtancoli, B. Thermodynamic and structural properties of Gd(III) complexes with polyamino-polycarboxylic ligands: basic compounds for the development of MRI contrast agents. *Coord. Chem. Rev.* **2000**, *204*, 309−393.

(16) (a) Troughton, J. S.; Greenfield, M. T.; Greenwood, J. M.; Dumas, S.; Wiethoff, A. J.; Wang, J.; Spiller, M.; McMurry, T. J.; Caravan, P. Synthesis and Evaluation of a High Relaxivity Manganese(II)-Based MRI Contrast Agent. *Inorg. Chem.* **2004**, *43*, 6313−6323. (b) Aime, S.; Anelli, P. L.; Botta, M.; Brocchetta, M.; Canton, S.; Fedeli, F.; Gianolio, E.; Terreno, E. Relaxometric evaluation of novel Manganese(II) complexes for application as contrast agents in magnetic resonance imaging. *JBIC, J. Biol. Inorg. Chem.* **2002**, *7*, 58−67.

(17) (a) Pierre, V. C.; Botta, M.; Aime, S.; Raymond, K. N. Substituent Effects on Gd(III)-Based MRI Contrast Agents: Optimizing the Stability and Selectivity of the Complex and the Number of Coordinated Water Molecules. *Inorg. Chem.* **2006**, *45*, 8355−8364. (b) Aime, S.; Botta, M.; Bruce, J. I.; Mainero, V.; Parker, D.; Terreno, E. Modulation of the water exchange rates in [Gd−DO3A] complex by formation of ternary complexes with carboxylate ligands. *Chem. Commun.* **2001**, 115−116. (c) Bruce, J. I.; Dickins, R. S.; Govenlock, L. J.; Gunnlaugsson, T.; Lopinski, S.; Lowe, M. P.; Parker, D.; Peacock, R. D.; Perry, J. J. B.; Aime, S.; Botta, M. The Selectivity of Reversible Oxy-Anion Binding in Aqueous Solution at a Chiral Europium and Terbium Center: Signaling of Carbonate Chelation by Changes in the Form and Circular Polarization of Luminescence Emission. *J. Am. Chem. Soc.* **2000**, *122*, 9674−9684.

(18) (a) Yang, H.; Zhuang, Y.; Sun, Y.; Dai, A.; Shi, X.; Wu, D.; Li, F.; Hu, H.; Yang, S. Targeted dual-contrast T1- and T2-weighted magnetic resonance imaging of tumors using multifunctional gadolinium-labeled superparamagnetic iron oxide nanoparticles. *Biomaterials* **2011**, *32*, 4584−4593. (b) Wei, L.; Li, S.; Yang, J.; Ye, Y.; Zou, J.; Wang, L.; Long, R.; Zurkiya, O.; Zhao, T.; Johnson, J.; Qiao, J.; Zhou, W.; Castiblanco, A.; Maor, N.; Chen, Y.; Mao, H.; Hu, X.; Yang, J. J.; Liu, Zhi-R. Protein-Based MRI Contrast Agents for Molecular Imaging of Prostate Cancer. *Mol. Imaging Biol.* **2011**, *13*, 416−423.

(19) Frisch, M. J.; Trucks, G. W.; Schlegel, H. B.; Scuseria, G. E.; Robb, M. A.; Cheeseman, J. R.; Scalmani, G.; Barone, V.; Mennucci, B.; Petersson, G. A.; Nakatsuji, H.; Caricato, M.; Li, X.; Hratchian, H. P.; Izmaylov, A. F.; Bloino, J.; Zheng, G.; Sonnenberg, J. L.; Hada, M.; Ehara, M.; Toyota, K.; Fukuda, R.; Hasegawa, J.; Ishida, M.; Nakajima, T.; Honda, Y.; Kitao, O.; Nakai, H.; Vreven, T.; Montgomery, J. A., Jr.; Peralta, J. E.; Ogliaro, F.; Bearpark, M.; Heyd, J. J.; Brothers, E.; Kudin, K. N.; Staroverov, V. N.; Kobayashi, R.; Normand, J.; Raghavachari, K.; Rendell, A.; Burant, J. C.; Iyengar, S. S.; Tomasi, J.; Cossi, M.; Rega, N.; Millam, J. M.; Klene, M.; Knox, J. E.; Cross, J. B.; Bakken, V.; Adamo, C.; Jaramillo, J.; Gomperts, R.; Stratmann, R. E.; Yazyev, O.; Austin, A. J.; Cammi, R.; Pomelli, C.; Ochterski, J. W.; Martin, R. L.; Morokuma, K.; Zakrzewski, V. G.; Voth, G. A.; Salvador, P.; Dannenberg, J. J.; Dapprich, S.; Daniels, A. D.; Farkas, O.; Foresman, J. B.; Ortiz, J. V.; Cioslowski, J.; Fox, D. J. *Gaussian 09*, Revision D.01; Gaussian, Inc.: Wallingford, CT, 2009.

(20) Becke, A. D. Density-functional exchange-energy approximation with correct asymptotic behavior. *Phys. Rev. A: At., Mol., Opt. Phys.* **1988**, *38* (6), 3098−3100.

(21) Lee, C.; Yang, W.; Parr, R. G. Development of the Colle-Salvetti correlation-energy formula into a functional of the electron density. *Phys. Rev. B: Condens. Matter Mater. Phys.* **1988**, *37* (2), 785−789.

(22) Miertuš, S.; Scrocco, E.; Tomasi, J. Electrostatic Interaction of a Solute with a Continuum, a Direct Utilization of ab initio Molecular Potentials. *Chem. Phys.* **1981**, *55*, 117−129.

(23) Barone, V.; Cossi, M. Quantum Calculation of Molecular Energies and Energy Gradients in Solution by a Conductor Solvent Model. *J. Phys. Chem. A* **1998**, *102*, 1995−2001.

DOI: 10.1021/acs.inorgchem.7b03039
Inorg. Chem. XXXX, XXX, XXX−XXX